Synthesis and Characterization of Novel Discotic Liquid Crystals for Potential Applications in Optoelectronic Devices

Monika Gupta

A Thesis Submitted for the Degree of
DOCTOR OF PHILOSOPHY

Department of Chemical Sciences
Indian Institute of Science Education and Research (IISER) Mohali
Sector 81, Knowledge City, S. A. S. Nagar, Mohali, 140306
Punjab, India

September 2017

Dedicated to

My Beloved Parents

DECLARATION

The work presented in this thesis entitled "***Synthesis and Characterization of Novel Discotic Liquid Crystals for Potential Applications in Optoelectronic Devices***" has been carried out by me under the supervision of **Dr. Santanu Kumar Pal** in the Department of Chemical Sciences, Indian Institute of Science Education and Research (IISER) Mohali, Mohali.

This work has not been submitted in part or full for a degree, diploma or a fellowship to any other university or institute.

Whenever contributions of others are involved, every effort is made to indicate this clearly with due acknowledgements of collaborative work and discussions. This thesis is a bonafide record of original work done by me and all sources listed within have been detailed in the bibliography.

Monika Gupta

Date:

Place:

In my capacity as the supervisor of the candidate's thesis work, I certify that the above statements by the candidate are true to the best of my knowledge.

Dr. Santanu Kumar Pal

Associate Professor

Department of Chemical Sciences

Indian Institute of Science Education and Research Mohali

Date:

Place:

ACKNOWLEDGEMENTS

At the end of my doctoral research, I would like to convey my heartfelt thanks to all those who supported and assisted in various ways. Foremost, I would like to express my profound gratitude to my research supervisor ***Dr. Santanu Kumar Pal*** *for his guidance, patience, valuable discussions and continuous help during my research work. I find myself privileged to have worked under his kind guidance. It was one of the best decisions I have ever made to join him for my doctoral research.*

I also thank ***Dr. Sugumar Venkataramani*** *and* ***Dr. Sabyasachi Rakshit****, members of my doctoral committee for their valuable suggestions during the yearly assessment of my work.*

I would like to acknowledge our former director, ***Prof. N. Sathyamurthy****, for providing the research and infrastructural facilities. I also acknowledge our director* ***Prof. Debi Sarkar****. I am thankful to our former HOD, Department of Chemical Sciences,* ***Prof. K. S. Viswanathan*** *for permitting the use of various departmental facilities. I am grateful to him and all the faculties of IISER for their motivation and encouragement. I also acknowledge our present HOD,* ***Dr. S. Arulananda Babu****.*

I acknowledge IISER Mohali for central NMR, HRMS, SAXS/WAXS, AFM, SEM and Raman facilities. I would like to thank Department of Chemical Sciences for providing various departmental facilities like UV-vis-NIR, FTIR spectrophotometers, TGA, DSC, Fluorimeter etc. I also acknowledge the training received from ***Dr. Kavita Dorai*** *to operate the NMR instrument.*

I am highly thankful to ***Dr. Santosh Prasad Gupta*** *for helping in X-ray diffraction analysis. I have spent countless hours discussing the various aspects of X-ray diffraction studies with him. His keen interest in the work has always been a source of motivation for me. I acknowledge* ***Ms. M. V. Rasna*** *and* ***Mr. Subhransu Sekhar Mohapatra****, University of Hyderabad for helping in opto-electronic studies. I would also like to express my sincere gratitude to* ***Prof. Surajit Dhara****, University of Hyderabad for helping in opto-electronic analysis and* ***Prof. Sandeep Kumar****, RRI, Bangalore for helping in Brewster Angle Microscopy studies. I am thankful to* ***Dr. A. S. Achalkumar****, IIT Guwahati for various useful discussions. I sincerely thank* ***Dr. Goutam Sheet*** *and* ***Dr. Debashis Adhikari****, IISER Mohali for helping in AFM and DFT studies, respectively.*

*I am thankful to **Ms. Nishtha Agarwal** (former MS-project student), **Mr. Vaibhav Pal**, **Mr. Priya Banerjee** and **Ms. Ananya Ashim** (former summer students) for helping in various ways in the work reported in this thesis. I really had very interesting scientific discussions with Nishtha.*

*I express my deep sense of gratitude to my current and former lab-mates **Dr. Sumyra Sidiq**, **Dr. Shilpa Setia**, **Dibyendu Das**, **Harpreet Singh**, **Indu Verma**, **Indu Bala**, **Joydip De**, **Vidhika Punjani**, **Supreet Kaur**, **Varsha Jain**, **Ipsita Pani**, **Musthafa Iqbal**, **Shruti Singh**, **Nitya**, **Lisha**, **Vaishnavi**, **Neelima**, **Swathy**, **Aneeshma**, **Manmohan**, **Ayush** for making a comfortable working atmosphere in the lab. I would like to thank post-doctoral fellows **Dr. Golam Mohiuddin**, **Dr. Rajib Kumar Nandi** and **Dr. Manish Thakur** for sharing their experiences. I had extremely enjoyable time with Indu Verma, Harpreet, Vidhika and Supreet.*

*I was lucky to have **Kanupriya**, **Abhijeet**, **Sandeep**, **Biswajit**, **Ginny**, **Hemaswasthi** and **Kavita** as my batchmates. I especially thank Kanupriya for her companionship and concern. A special vote of thanks to my friends **Raju**, **Pooja**, **Komal** and **Swati** for always being there for me. I also thank **Balaram**, **Ravindra** and **Ashwath** for useful discussions. I would like to acknowledge my cousins **Vivek**, **Shilpi**, **Swati**, **Vipul** and **Priyanka** for their support and encouragement.*

*I am thankful to all the staff members of stores, purchase office, administrative office, account section, library and computing facility of IISER Mohali for their help and co-operation during the course of time. I also acknowledge **Mr. Satvinder**, **Mr. Bahadur**, **Mr. Mangat** and **Mr. Prahlad**, lab assistants of chemistry teaching lab for their timely help.*

*I am thankful to **IISER Mohali** for a timely dispersal of research fellowship. I acknowledge DST for providing travel grant to attend 26th International Liquid Crystal Conference held in Ohio, USA and financial assistance from IUCr and IISER Mohali to attend 4th International Soft Matter Conference held in Grenoble, France.*

Finally, my Ph.D. endeavor could not have been completed without the unending support, endless love and support from my family members and relatives. I deeply express my sincere gratitude to my parents and brother for their constant motivation and belief in me. At last, I thank God for always being there for me in a way no one else can.

Contents

Page No.

Chapter 1: Introduction: Discotic Liquid Crystals & their applications in optoelectronic devices 1

1.1 Overview 3

1.2 Liquid crystals 4

1.3 History of liquid crystals 5

1.4 Classification of liquid crystals 7

1.5 Discotic liquid crystals 8

1.6 Design of discotic liquid crystals and their structure-property relationships 11

1.7 Characterization of liquid crystalline phases 12

1.8 Applications of discotic liquid crystals 17

1.9 Outline of thesis 22

References 25

Chapter 2: Rod-disc and disc-disc oligomers based on azobenzene tetracarboxylic acid core 33

2.1 Synthesis and characterization of novel azobenzene-based mesogens and their organization at the air-water and air-solid interface 35

2.1.1 Introduction 35

2.1.2 Objective 36

2.1.3 Results and Discussion 37

2.1.3.1 Synthesis and characterization 37

2.1.3.2 Thermal behavior 37

2.1.3.3 X-ray diffraction studies 40

2.1.3.4 Thin-Film Studies 41

2.1.4 Conclusions 46

2.2 A new class of triphenylene-based room temperature discotic oligomers exhibiting TNF induced switching of columnar rectangular to hexagonal assemblies 47

2.2.1 Introduction 47

2.2.2 Objective 48

2.2.3 Results and Discussion 49

2.2.3.1 Synthesis and characterization 49

2.2.3.2 Thermal behavior 49

2.2.3.3 X-ray diffraction studies 50

2.2.3.4 Charge-transfer complexes 56

2.2.3.5 Photophysical and electrochemical studies 62

2.2.4 Conclusions 64

2.3 Experimental Section 64

References 69

Appendix I 77

Chapter 3: Disc-disc and disc-rod dimers based on pentakis(phenylethynyl)benzene core 89

3.1 A room temperature discotic mesogenic dyad based-on triphenylene and pentaalkynylbenzene 91

3.1.1 Introduction 91

3.1.2 Objective 92

3.1.3 Results and Discussion 93

3.1.3.1 Synthesis and characterization 93

3.1.3.2 Thermal behavior 93

3.1.3.3 X-ray diffraction studies 96

3.1.3.4 Charge-transfer complexes 98

3.1.3.5 Photophysical studies 100

3.1.4 Conclusions 101

3.2 The first examples of room temperature liquid crystal dimers based-on cholesterol and pentaalkynylbenzene 102

3.2.1 Introduction 102

3.2.2 Objective 104

3.2.3 Results and discussion 105

3.2.3.1 Synthesis and characterization 105

3.2.3.2 Thermal behavior 105

3.2.3.3 X-ray diffraction studies 107

3.2.3.4 Photophysical properties 109

3.2.4 Conclusion 110

3.5 Experimental Section 110

References 113

Appendix II 119

Chapter 4: Multialkynylbenzene bridged discotic triads 127

4.1 Triphenylene-based room-temperature discotic liquid crystals: A new class of blue-light emitting materials with long-range columnar self-assembly 129

4.1.1 Introduction 129

4.1.2 Objective 131

4.1.3 Results and Discussion 131

4.1.3.1 Synthesis and Characterization 131

4.1.3.2 Thermal behavior 133

4.1.3.3 X-ray diffraction studies 136

4.1.3.4 Photophysical studies 144

4.1.4 Conclusion 147

4.2 Structure property relationships in lath-shaped triads based on multialkynylbenzene 148

4.2.1 Introduction 148

4.2.2 Objective 149

4.2.3 Results and Discussion 149

4.2.3.1 Synthesis and characterization 149

4.2.3.2 Thermal behavior 150

4.2.3.3 X-ray diffraction studies 152

4.2.4 Conclusions 154

4.3 Experimental Section 154

References 158

Appendix III 165

Chapter 5: New design strategies towards the synthesis of room-temperature discotic nematic liquid crystals 175

5.1 Design, synthesis and characterization of room-temperature discotic nematic liquid crystals by employing pentaalkynylbenzene units 179

5.1.1 Introduction 179

5.1.2 Objective 181

5.1.3 Design-I 183

5.1.3.1 Synthesis and characterization 183

5.1.3.2 Thermal behavior 184

5.1.3.3 X-ray diffraction studies 185

5.1.3.4 Dielectric and birefringence studies 187

5.1.4 Design-II 190

5.1.4.1 Synthesis and characterization 190

5.1.4.2 Thermal behavior 190

5.1.4.3 X-ray diffraction studies 192

5.1.4.4 Dielectric and birefringence studies 196

5.1.5 Conclusions 199

5.2 Room-temperature discotic nematic gold nanoparticles decorated with pentaalkynylbenzene units 200

5.2.1 Introduction 200

5.2.2 Objective 201

5.2.3 Results and discussion 202

5.2.3.1 Synthesis and characterization 202

5.2.3.2 Thermal behavior 203

5.2.3.3 X-ray diffraction studies 204

5.2.3.4 Preparation of GNPs decorated with thiol terminated PA units 206

5.3 Experimental section 212

References 220

Appendix IV 229

Chapter 6: Summary 259

List of Publications 265

General Remarks

Chemicals and solvents were all of AR quality and were used without further purification. Column chromatographic separations were performed on silica gel (60-120, 100-200 & 230-400 mesh). Thin layer chromatography (TLC) was performed on aluminium sheets pre-coated with silica gel (Merck, Kieselgel 60, F254). Structural characterization of the synthesized compounds was carried out through a combination of infrared spectroscopy (Perkin Elmer Spectrum AX3), ^{1}H NMR and ^{13}C NMR (Bruker Biospin Switzerland Avance-iii 400 MHz spectrometer), UV-vis-NIR spectrophotometers (Perkin Elmer Lambda 900 and Agilent Technologies UV-vis-NIR Spectrophotometer), MALDI (Waters synapt G2-S) and elemental analysis (Carlo-Erba 1106 analyser). ^{1}H NMR spectra were recorded using deuterated chloroform ($CDCl_3$) as solvent and tetramethylsilane (TMS) as an internal standard. The transition temperatures and associated enthalpy values were determined using a differential scanning calorimeter (DSC, Perkin-Elmer, Model Pyris 1D) which was operated at a scanning rate of 5 °C min^{-1} both on heating and cooling. The apparatus was calibrated using indium as a standard. Textural observations of the mesophase were performed with Nikon Eclipse LV100POL polarising microscope provided with a Linkam heating stage (LTS 420). All images were captured using a Q-imaging camera. Small-angle/Wide-angle X-ray scattering (SAXS/WAXS) studies were carried out on powder samples using Cu-K_α (λ = 1.54 Å) radiation from a source (GeniX 3D, Xenocs) operating at 50 kV and 0.6 mA. The diffraction patterns were collected on a two module Pilatus detector. Fluorescence emission spectra and steady state anisotropy experiments were performed on Horiba scientific fluoromax spectrofluorometer 4. Time resolved lifetime measurements were done on time correlated single photon counter from Horiba Jobin Yvon. For time resolved experiments, excitation was done by 375 nm laser diode. Langmuir monolayers were studied using surface manometry, Brewster angle microscopy (BAM) and atomic force microscopy (AFM). The surface manometry experiments were carried out using an APEX LB-2007 and a NIMA 611M trough. The subphase used was ultrapure deionized water obtained from Millipore Milli-Q system. The stock solutions were prepared using chloroform (HPLC grade, Merck). After spreading it on the air-water interface, the film was left for 20 min, allowing the solvent to evaporate. The π-A_m isotherms were obtained by symmetric compression of the barriers

with a constant compression rate of 10 cm^2/min. The surface pressure (π) was measured using the standard Wilhelmy plate technique. A Brewster angle microscope (BAM), MiniBAM (NFT, Nanotech, Germany) was employed to observe the films at the air-water interface. LB technique was employed to transfer various layers of the films onto hydrophilic and hydrophobic substrates at target surface pressure (π_t) with a dipping speed of 1 mm/min. For hydrophilic surfaces, freshly cleaved mica was used. To obtain hydrophobic surfaces, freshly etched silicon wafers were dipped in hexamethyldisilazane (HMDS) for 12 h and then rinsed with HPLC grade chloroform. Silicon wafers were etched by treating polished silicon wafers for about 5 min. in hot acidic piranha solution (3:1 ratio) which were then rinsed in ultrapure deionized water and then dried. The AFM studies on these LB films were performed using Asylum Research MFP 3D. We used silicon tips (radius: 9 ± 2 nm) with spring constant of 42 N/m and resonance frequency of 300 kHz. Non-contact mode was used to obtain the topography of the film. Surface manometry, BAM and depositions were carried out at room temperature (25 ±0.5 °C). AFM was carried out at different temperatures. For the dielectric and electro-optic measurements, the LC cells were made of two indium-tin-oxide (ITO) coated glass plates with patterned electrodes. These plates were cleaned thoroughly and spin coated with polyimide AL-1254. Subsequently they were cured at 180 °C for 1 hour and rubbed in an antiparallel way. Such cells usually provide planar alignment of the calamitic LCs. However, it gives uniform and homeotropic alignment of the N_D LCs. A typical cell thickness used in the experiment was about 8μm. The empty cell was heated by using a temperature controller (Mettler FP 90) and the sample was filled in the isotropic phase. Birefringence was measured using a phase modulation technique. The sample retardation was measured by using two crossed Glan–Thompson polarizers, Helium-Neon laser (λ = 632.8 nm), photo-elastic modulator (PEM) and a lock-in amplifier. A photo-detector collected the light transmitted through the LC, lock-in amplifier measured the first and second harmonics of the AC signal. Using a function generator (Tektronix-AFG 3102) and voltage amplifier (TEGAM- 2350), a sinusoidal voltage of frequency 1 kHz and amplitude up to 23 V was applied. At this high voltage the director was completely reoriented to the homogeneous or planar state. This was further verified by the optical polarising microscope. The birefringence was measured as a function of temperature and voltage. The dielectric constant as a function of voltage was measured using a LCR meter

(Agilent, E4980A). All the instruments were interfaced with a computer and a suitable computer program written in Lab View was used to control the experiments.

Chapter 1

Introduction: Discotic liquid crystals & their applications in optoelectronic devices

Discotic liquid crystals (LCs) discovered in 1977 by S. Chandrasekhar & co-workers have become the smart materials of modern era. They have gained increasing interest due to their applications in organic semiconductor devices. The organic semiconductors are advantageous over inorganic semiconductors in terms of cost, mechanical flexibility and fabrication in a flexible substrate. Further, the use of small organic molecules is preferable over polymers due to their easy solubility, high purity and stability. In this direction, the organic molecules such as discotic LCs are of high importance due to their columnar self-assembly which leads to their increased charge carrier mobilities. Several molecular electronic applications such as OLEDs, OFETs and OPVCs have been realized from these discotic systems. In addition, discotic LCs have revolutionized the display devices by acting as optical compensation films to widen viewing angle of the commonly used twisted nematic displays.

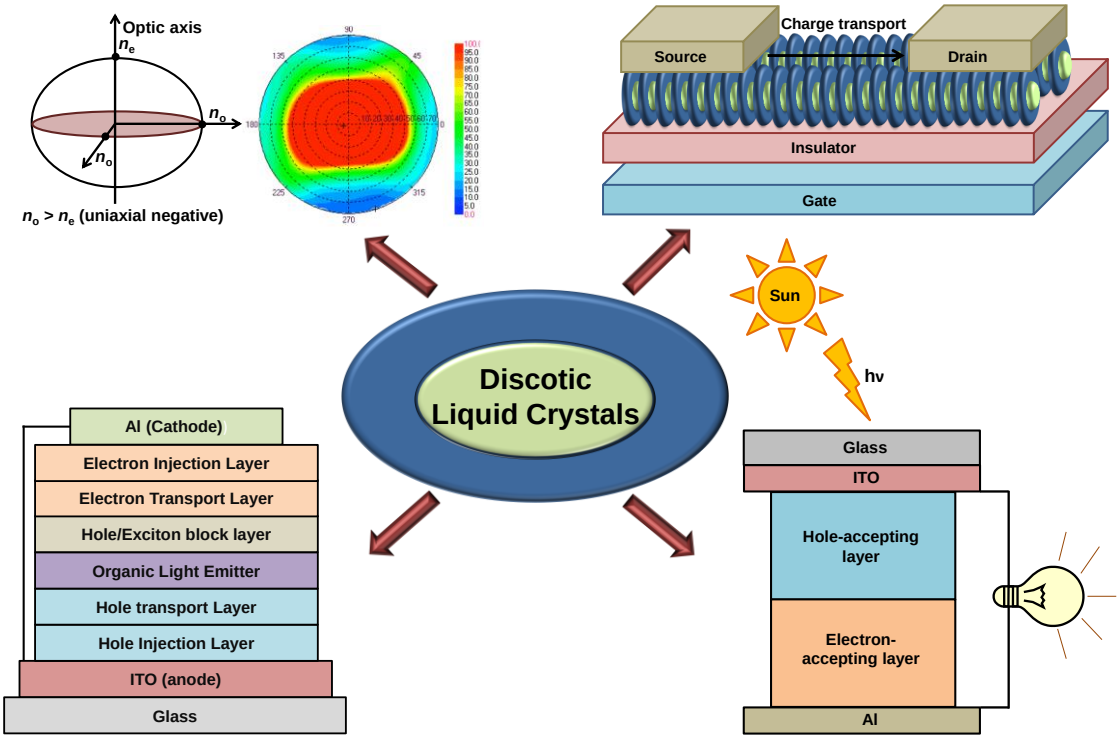

1.1 Overview

Molecular self-assembly is one of the nature's effective tools to form the dynamic functional materials of life for accomplishing the desired biological functions. Several supramolecular interactions such as hydrogen bonding, π-π stacking, polar-nonpolar interactions, metal coordination, charge-transfer complex, ionic interactions, etc. are utilized by nature at different molecular levels to build dynamic functional soft materials. Similarly, supramolecular systems are scientifically intriguing as they represent the complex systems found in nature. Among various supramolecular systems, liquid crystals (LCs) can be considered as quintessential self-organizing molecular materials of today. LCs can be associated with our lives due to their everyday use in laptops, computers, smart phones, digital cameras, MP3 players, flat panel TVs and other electronic devices. Numerous perspectives on LCs have been explored to scale down the cost, space, energy, raw materials and to increase the efficiency and stability of these LC materials for their easy commercialization.

LCs are mainly classified into rod-like (calamitic) and disc-like (discotic) mesogens. The discotic LCs which were discovered in 1977 by Chandrasekhar & co-workers, differ from their calamitic counterparts in their molecular shape, phase symmetry, the dimensionality of their charge transport, exciton migration and in the extent of their orbital overlap.[1-5] These discotic systems mainly consist of rigid aromatic units which are stacked on the top of each other to form columns which function as nano-wires. As a very high degree of conjugation is present in these discotic LCs, therefore the electrons are also highly delocalized which results into reduced band gap and thus these materials act as organic semiconductors.[6, 7] The band width values for discotic LCs have been found to be as low as 1.1 eV which is very close to that of graphite (1.0–1.4 eV).[8] They have also shown very high values of the charge carrier mobility 0.2–1.3 cm^2 V^{-1} s^{-1} arising from the extended orbital overlap between the π-π stacked units.[9-12] Moreover, the diffusion length of excitons in discotic systems has even exceeded 70 nm.[13] They have been realized as functional soft materials in many device applications through a combination of good solubility in organic solvents, facile processability, self-healing capability and aligned directional conduction of either charge or

energy.[14] All these unique structural and electronic properties makes them ideal candidates for use in various optical and electronic devices such as field effect transistors (FETs), photovoltaic cells (PVCs), light emitting diodes (LEDs), holographic data storage etc.[15-18] In addition, these columnar discotic LCs are superior to inorganic materials due to their easier processability, self-healing tendency and possible alignment by shear forces or electrical field which can be associated with their better film-forming ability over large area that is devoid of grain boundaries and crystallites between the domains.

In addition to the formation of columns, the discotic units can also self-assemble in an orientationally ordered manner to form the discotic nematic (N_D) phase. However, these N_D mesogens are very rare as these conjugated discs generally tend to stack on the top of each other due to π-π stacking interactions. The negative birefringence films formed by the N_D LCs have been commercialized as compensation foils to enlarge the viewing angle of commonly used twisted nematic LC displays.[19-21] Moreover, a LC display device with wide and symmetrical viewing angle has also been demonstrated by using N_D LCs.[22, 23]

In this thesis, synthesis and characterization of novel room-temperature discotic LCs for the possibility of creating, (i) a new generation of organic semiconductors for various opto-electronic applications and (ii) optical compensation films for display devices, is presented. Moreover, the thesis mainly focuses on the synthesis of non-conventional low molar mass LCs i.e. dimers and oligomers because of their fascinating mesomorphic properties due to restricted molecular motions and combination of desirable properties of monomers with those of the polymers.

1.2 Liquid Crystals

LCs represents a state of matter which has properties intermediate to that between liquids and crystals. In liquid state, the molecules are mobile and have no orientational or positional order, whereas, crystals possess long-range orientational and positional order where the molecules are positioned at regular repeated intervals and have no mobility. However, LCs exhibit intermediate properties i.e. a combination of both order and mobility (Figure 1.1). In the LC state, the molecules can slide over each other while preserving the parallelism and

thus show optical birefringence and dielectric anisotropy. For this reason, they are also called as mesophases (intermediate phases) and the constituent molecules that display mesophase are called mesogens. However, this mesophase formation is a very complex process. For exhibiting LC phase, a molecule should possess a rigid core as well as flexible alkyl chains. Not only that, a subtle balance between the interactions of the rigid and flexible parts leads to mesophase formation. Shape anisotropy, molecular segregation etc. are various other factors

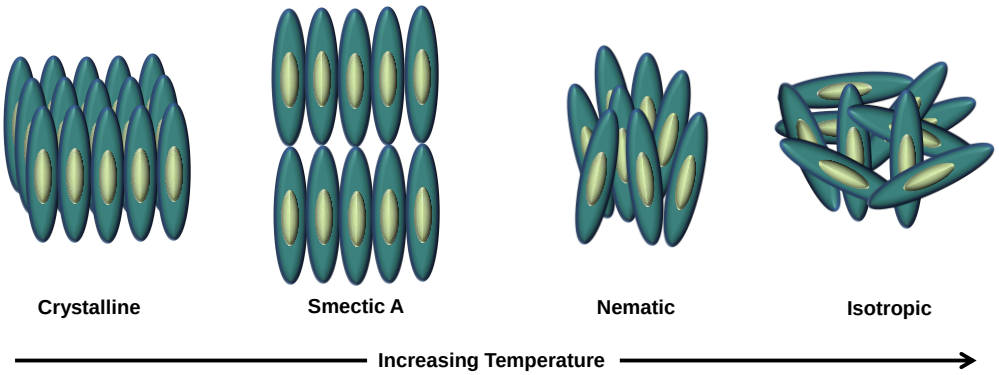

Figure 1.1 Schematic of the molecular ordering present in various phases.

which are involved in the mesophase formation. LCs can thus be regarded as unique functional soft materials having both order and mobility on a molecular, supramolecular and macroscopic level.[24-31]

1.3 History of Liquid Crystals

In 1888, Friedrich Reinitzer, a botanist-cum-chemist, observed an unusual 'double melting' behaviour of cholesteryl benzoate. He noticed that the crystals of this compound melted at 145.5 °C to form an opaque liquid which turned into a transparent liquid at 178.5 °C.[32] Otto Lehmann, a German physicist, further investigated that unusual phenomenon using a polarized optical microscope.[33] He first referred them as 'soft crystals' which was later replaced by the term 'crystalline fluids'. As the opaque liquid was showing the properties of both liquid as well as crystals, he later coined the term 'liquid crystals'. Soon after the discovery of LCs, the scientists started to synthesize new LC compounds. Daniel Vorlander, a German chemist, made an important contribution in this direction. He and his co-workers synthesized nearly 1100 LCs based-on which they laid down the foundation of molecular

structure-property relationship of LCs.[34] He also suggested that LC phase is mainly exhibited by the linear (rod) shaped compounds which are now called as calamitic molecules.[35]

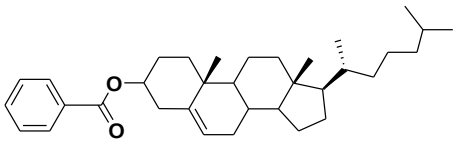

Cholesteryl Benzoate

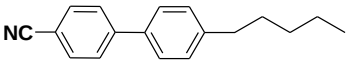

4'-Pentyl-4-Cyanobiphenyl

Georges Freidel, in 1922, first classified LCs into nematic, smectic and cholestric. He further observed that LCs can be re-oriented by an electric field.[36] Onsager and Flory in late 1950s proposed a theory explaining the molecular structure and property of the LC phase which promoted further research in the field of LCs.[37, 38] The introduction of stable room-temperature LCs which consists of 4-alkyl and 4-alkoxy-4'-cyanobiphenyl derivatives by Gray and co-workers in 1973 was the most important discovery which further provided a secure basis for LC research for the development of liquid crystal displays (LCDs).[39]

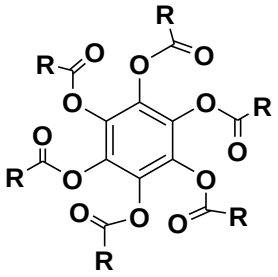

Benzene hexa-n-alkanoates

In 1977, when the calamitic LCs have revolutionalized the display technology, Chandrasekhar and co-workers reported that in-addition to rod-shaped molecules, disc-shaped molecules can also form LC phase.[40] They synthesized a series of benzene hexa-n-alkanoates and confirmed the presence of LC phase from optical, thermodynamic and X-ray studies. They stated that these materials which mainly consist of disc-like units stack on the top of each other to form columns which were further arranged in a hexagonal fashion. Before this discovery Vorlander also indicated the columnar packing behaviour in leaf-shaped flat molecules. However, he failed to demonstrate the LC behaviour as those molecules were devoid of alkyl chains.[41]

Later on, the similar leaf-shaped molecules surrounded by the flexible alkyl chains were found to exhibit columnar mesophases. Further, in 1996, Niori and co-workers discovered ferroelectricity in non-chiral bent shaped molecules which consisted of an angular central unit and two linear rigid cores with terminal alkyl chains.[42] Before this discovery it was known that chiral molecules can form both chiral and achiral mesophases, however, achiral molecules were not known to form chiral mesophase. This was in contrary to the above observation and thus it led to very intense research activity in the field of bent-shaped molecules. These bent-shaped molecules form mesophases with polar order and supramolecular chirality and have proved their applicability in various molecular electronic applications.[43-48]

1.4 Classification of Liquid Crystals

The detailed classification of LCs is shown in Figure 1.2.

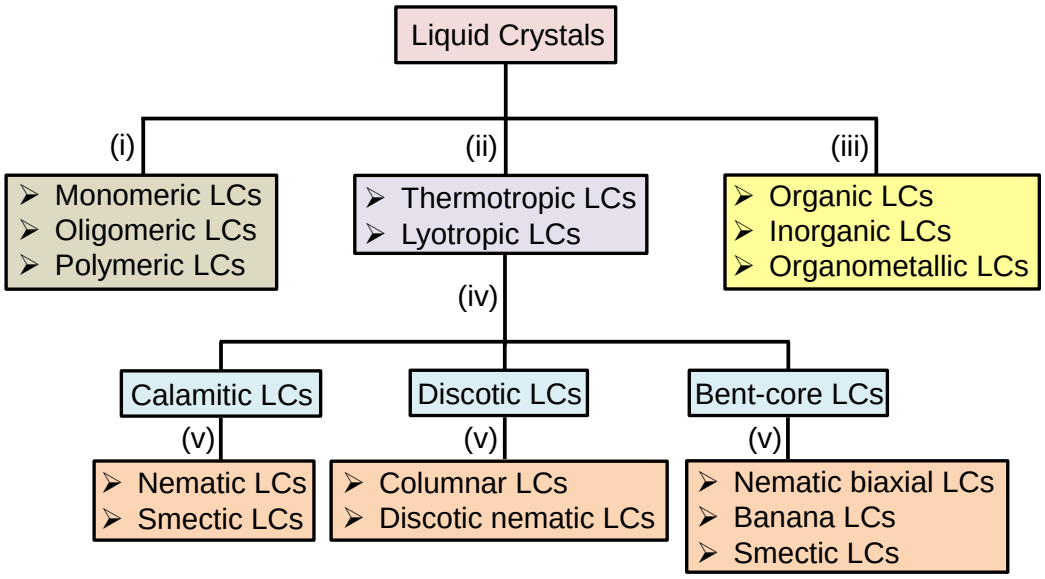

Figure 1.2 Classification of LCs based on various factors as described in the text.

LCs can be classified based-on:

(i) Molar mass of the constituent units (i.e. monomeric, oligomeric and polymeric LCs)

(ii) Method of achieving LC phase such as addition of solvent or varying the temperature (i.e. lyotropic and thermotropic LCs)

(iii) Nature of constituent molecules (organic, inorganic and organometallic LCs)

(iv) Shape of the mesogen (calamitic, discotic and bent-core LCs)

(v) Organization of molecules (nematic, smectic, columnar, helical, B phases etc.)

Since this thesis mainly deals with the discotic LCs, they are discussed in details in the next section.

1.5 Discotic Liquid crystals

Self-organization of disc-like molecules to form discotic LCs as discovered by Chandrasekhar *et. al*. in 1977 were an entirely new class of LCs and were completely different from their rod-like counterparts which were discovered in 1888. A typical discotic mesogen consists of a rigid π-conjugated aromatic core surrounded by flexible alkyl side chains. These discogens stack on the top of each other due to π-π stacking interactions to form one-dimensional columns. These columns then further self-organize on various two-dimensional (2D) lattices such as hexagonal, rectangular etc.

Discotic mesogens mainly forms four types of mesophase: nematic, smectic, columnar and cubic phase. In the nematic phase of discotic LCs i.e. N_D mesophase, molecules possess orientational order similar to that observed in nematic phases of calamitic LCs. In addition to that, discotic mesogens can also stack themselves into short columns which do not display any two dimensional positional order but rather these short columns are orientationally ordered. This means that discogens in such kind of self-assembly possess short range positional order and long-range orientational order. This mesophase is termed as nematic columnar (N_{Col}) mesophase. In addition to N_D and N_{Col} phase, one more variant of nematic phases exhibited by discs is observed where the disc-shaped molecules self-assemble in superstructures. These superstructures further exhibit an orientationally ordered arrangement similar to that observed in a nematic phase. This phase is known as nematic lateral phase (N_L) due to presence of strong lateral interactions. Similarity of mesophase formation of discotic LCs with calamitic mesogens is not only limited to nematic phases, but these discotic units can also exhibit smectic phases in a similar way. In discotic smectic phase, the discs are arranged in layers which are separated by sublayers of peripheral chains. However, the molecules do not form any columnar aggregates (Figure 1.3). These smectic phases are rarely observed in discotic LCs and have not been much explored.

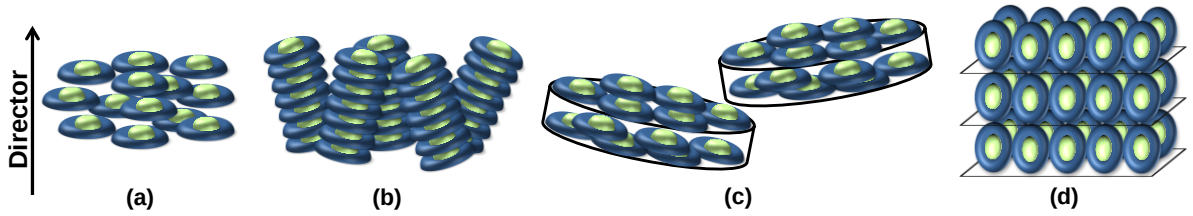

Figure 1.3 Schematic representing the (a) nematic discotic (N_D), (b) nematic columnar (N_{Col}), (c) nematic lateral (N_L) and (d) smectic phases formed by discotic LCs.

Out of the different variants of mesophases formed by discotic LCs, columnar mesophase is most commonly observed. This is also evident from the fact that discogens mainly consists of π-conjugated units which prefer to form columns due to π-π interactions among the discotics. Columnar mesophases are distinguished on the basis of different 2D lattices formed by one-dimensional columns. The formation of these different 2D lattices depends on various factors such as degree of the order in the molecular stacking, orientation of the molecules along the columnar axis, dynamics of the molecules within the columns etc. These columnar LCs are mainly classified into seven categories namely: (i) columnar hexagonal, (ii) columnar rectangular, (iii) columnar oblique, (iv) columnar plastic, (v) columnar helical, (vi) columnar square (tetragonal) and (vii) columnar lamellar mesophases (Figure 1.4).

In case of columnar hexagonal (Col_h) phase, the columns are arranged in a 2D hexagonal lattice, the constituent discs within the columns can be ordered or disordered which is reflected in the different values of their correlation lengths. In case of columnar rectangular (Col_r) mesophase, the columns are tilted with respect to the columnar axis which results into their elliptical cross-section. These columns are arranged on a rectangular lattice. For the formation of Col_r phase, strong core-core interactions are required as the cores of a column should be tilted with respect to the cores of neighbouring columns. Due to this reason, on increasing temperature or length of side chains, which leads to reduced core-core interactions a transition from Col_r to Col_h phase is generally observed. Analogous to Col_r phase, in case of columnar oblique (Col_{ob}) mesophase, the constituent columns are arranged on a 2D oblique lattice. Columnar plastic (Col_p) phase mainly consists of a three dimensional order in any of the above described columnar lattices (Col_h, Col_r and Col_{ob}). In case of Col_p phase, the discs are only allowed to rotate along the columnar axis and the motional freedom of discs (which is otherwise observed in the above mentioned columnar phases) is restricted.

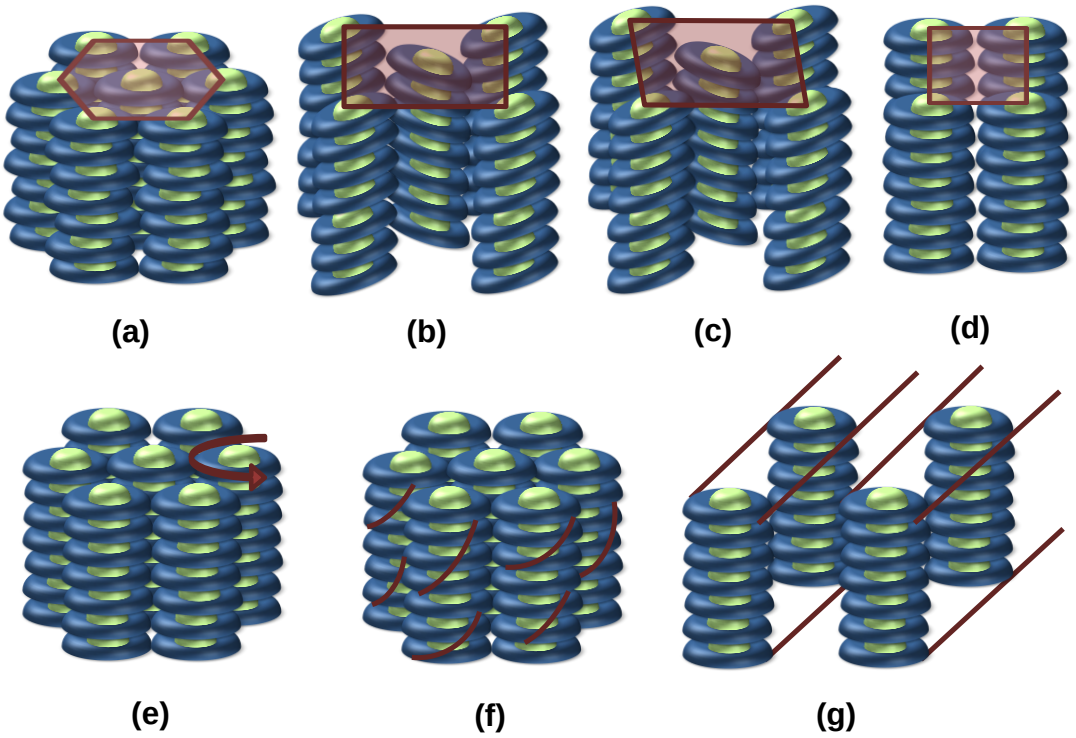

Figure 1.4 Schematic representing columnar phases formed by discotic LCs: (a) columnar hexagonal (Col_h); columnar rectangular (Col_r); columnar oblique (Col_{ob}); columnar tetragonal (Col_{tet}); columnar plastic (Col_p); columnar helical (H) and columnar lamellar (Col_L) phase.

Columnar helical (H) mesophase is characterized by the presence of helical columns where the discotic stacks interdigitate in the group of three. Both Col_p and H mesophase are generally considered as high order phases and display high values of correlation lengths as compared to the other columnar LCs. Columnar square or tetragonal (Col_{tet}) represent the mesophase where columns are upright and arranged on a square lattice. These mesogen show facile homeotropic alignment of columns. In case of columnar lamellar (Col_L) mesophase, the columns consisting of stacked discotic mesogens are arranged in layers. The columns in layers are allowed to slide and there is absence of any positional correlation between the columns of different layers. The last variation of the mesophase exhibited by discotic LCs is cubic phase. Cubic phase consists of branched interwoven columns of discotic mesogens arranged in a cubic lattice. This phase is rarely observed in discotic LCs.

1.6 Design of discotic liquid crystals and their structure-property relationships

Discotic LCs mainly consists of a conjugated disc-shaped central core which promotes the crystalline character and peripheral flexible alkyl chains which facilitates the liquid character (Figure 1.5). The discotic LCs with different mesophase morphologies can be obtained by varying the size, shape and nature of the central discotic core as well as the kind of flexible side chains. The linkage of these side chains to the central core can also be varied e.g. they can be connected via ether, ester, thioether, amide, alkanoyloxy, alkynyl and other such type of linkages.[49-62] It has been observed that a larger discotic core results in extended overlap leading to reduced band gap and thus an enhancement in the charge carrier mobility. Further, the increase in length, number and branching of alkyl chains leads to reduction in the transition temperature of discotic LCs due to increased steric hinderance.

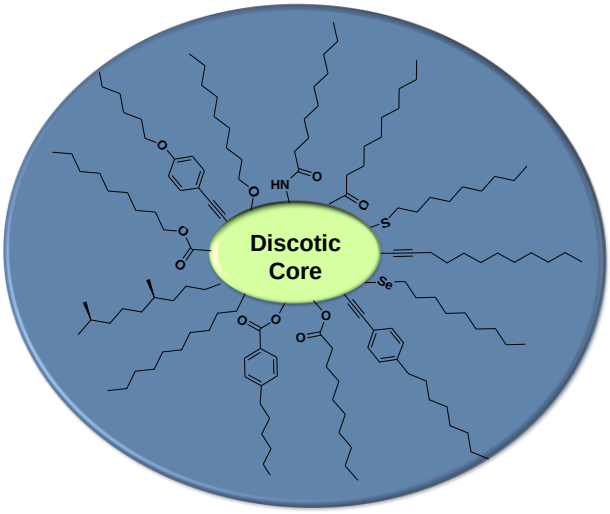

Figure 1.5 General design of discotic LCs.

Till now, more than 50 discotic cores have been explored to afford these discotic LC systems, which are mainly benzene, triphenylene, perylene, anthraquinone, truxene, pyrene, hexabenzocoronene, phenanthrene, phthalocyanines, tricycloquinazolines, thiatruxenes etc.[51] As explained in the earlier sections, the columnar phases formed by discotic LCs act as organic semiconductors and also find their applications in various devices e.g. FETs, LEDs, PVCs, xerographic processes, gas sensors etc. On the other hand, discogens showing nematic phase display interesting applications in display devices. They have been employed in the

optical compensation films to widen the viewing angle of LC displays. These N_D LCs have also been commercialized by Fuji Film Company which has further created enormous research interest in this area.[63, 64]

1.7 Characterization of liquid crystalline phases

LC mesophases are generally characterized by employing a combination of various techniques such as polarized optical microscopy (POM), differential scanning Calorimetry (DSC), small- and wide-angle X-ray scattering (SAXS/WAXS). The thermal behaviour of a LC compound is generally investigated by DSC whereas the mesophase behaviour is explored by POM and X-ray scattering studies. The thermal transitions occurring in the compounds are first investigated by DSC. The POM textures are then obtained in the corresponding phases using a polarized optical microscope with a heating and cooling stage. The quantitative analysis of these mesophases is carried out through X-ray scattering studies. Thus, for characterizing different mesophases formed by LCs, the analysis from all these techniques is required and the mesophase cannot be confirmed solely from any of these techniques.

1.7.1 Polarized Optical Microscopy (POM)

POM is a preliminary technique to characterize a mesophase. In a polarized optical microscope, a pair of crossed polarizers is employed and the compound is placed in between those polarizers. When crystalline samples are placed in between these crossed polarizers, the light is not completely blocked and birefringence from the sample is observed. However, due to restricted mobility of molecules the birefringent textures are not shearable.

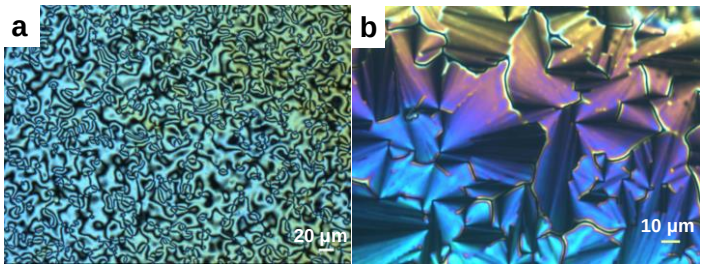

Figure 1.6 Polarized optical micrograph showing (a) Schlieren texture for a nematic phase and (b) focal conic texture for a columnar hexagonal phase.

On placing an isotropic liquid, the light is completely extinguished and a black or dark appearance is noticed. However, when a LC compound is placed in between the crossed polarizers, it displays a characteristic texture due to defects present in the mesophase. Further, these textures show shearability due to the presence of rotational motion of molecules. The presence of a LC phase is confirmed from the optical birefringence allied with shearability of the optical textures. Nematic phases generally show Schlieren textures whereas the columnar phases display focal conic, mosaic and dendritic textures under POM (Figure 1.6).

1.7.2 Differential Scanning Calorimetry (DSC)

The technique of DSC gives an idea of the phase transitions occurring in a compound with respect to variation in temperature and also their associated enthalpies (Figure 1.7). For these measurements, the sample and a blank are both heated with a constant heating rate. Upon a thermal transition, e.g. a melting (endothermic) transition, some of the heat is utilized by the sample and thus the system has to provide more heat to the sample to maintain it at a similar temperature to that of the blank.

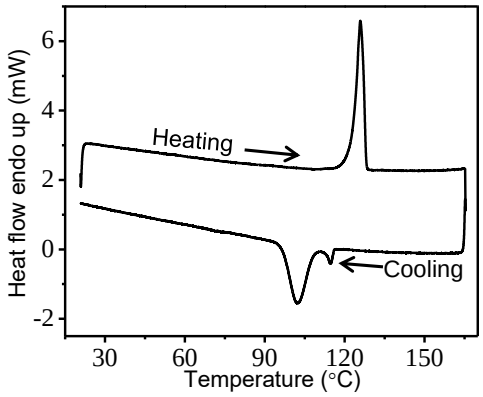

Heating Scan	Cr 125.9 (131.5) I
Cooling Scan	I 114.6 (6.5) N 102 (98.3) Cr

Figure 1.7 DSC thermogram of a monotropic nematic LC obtained on heating and cooling cycles. The table in the bottom shows phase transition temperatures in °C and latent heat values in kJ mol^{-1} (in parentheses). The phase assignments are, Cr = crystal, N = nematic phase, I = isotropic.

This additional amount of heat is represented in the form of a peak in the DSC thermogram. For calculation of exact transition temperatures and associated enthalpy changes, the instrument is generally calibrated with pure indium standard sample. The values of transition enthalpies obtained from DSC provide an indication of the order present in the mesophase. Further, mesophase-mesophase transitions can also be analysed from DSC which is otherwise difficult to study from POM alone.

1.7.3 Small- and wide-angle X-ray scattering (SAXS/WAXS)

The detailed mesophase morphology is quantified by X-ray analysis which leads to an understanding of supramolecular organization and the corresponding packing parameters in the mesophase. The larger *d*-spacings are visualized at the small-angle whereas the smaller *d*-spacings can be observed at wide-angle. Detailed X-ray analysis allows one to distinguish various nematic phases (e.g. N_D and N_{Col}) which otherwise show similar Schlieren textures under POM. Similarly, the different 2D lattices formed by columnar LCs can also be identified from the X-ray Studies (Figure 1.8). The various 2D lattices formed by columnar LCs and the corresponding relation between *d*-spacings (d_{hk}) & (hk) for indexing and space groups are given in Table 1.1. Proper indexing of the diffraction peaks provides the details about the lattice of the mesophase structure and corresponding symmetries. Moreover, the reconstructed electron density map by using the indexing details and intensities of the diffractions peaks further gives a clear idea of arrangement of molecules in the lattice. The degree of arrangement is expressed by correlation length which can be calculated by using Scherrer's equation.

Electron density maps can be reconstructed with the Miller indices and intensities of the reflections. The electron density ρ(x,y) of a LC is linked to its structure factor F(hk) by inverse Fourier transformation as follows:

$$\rho(x,y) = \sum_{hk} F(hk)\, e^{2\pi i(hx+ky)}$$

In this formula (h,k) are the Miller Indices and x, y are the fractional coordinates in the unit cell.

Table 1.1 Two dimensional space groups of columnar LCs with relation between *d*-spacings (d_{hk}) & (*hk*) for calculating inter-planar distance.

Type of columnar organization	Schematic representation of unit cell	Equation for indexing	Space group	Extinction rules	Area	No. of discoids in a unit cell
Columnar hexagonal (Col_h)	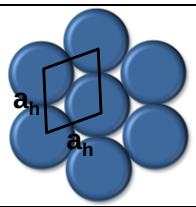	$\frac{1}{{d_{cal}}^2} = \frac{4}{3}\left(\frac{h^2 + h\,k + k^2}{{a_h}^2}\right)$	*p6mm*	-	$S_h = {a^2}_h 3^{1/2}/2$	1
Columnar tetragonal (Col_t)	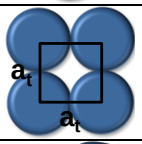	$\frac{1}{{d_{cal}}^2} = \left(\frac{h^2 + k^2}{{a_t}^2}\right)$	*p4mm*	-	$S_t = {a^2}_t$	1
Columnar rectangular (Col_r)	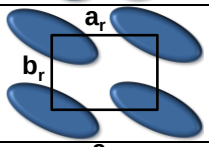	$\frac{1}{{d_{cal}}^2} = \frac{h^2}{{a_r}^2} + \frac{k^2}{{b_r}^2}$	*p2mm*	-	$S_r = a_r b_r$	1
	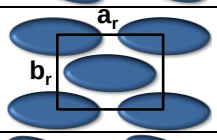		*c2mm*	*hk*: *h*+*k* = 2*n* *h*0: *h* = 2*n* 0*k*: *k* = 2*n*		2
	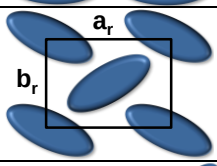		*p2gg*	*hk*: no conditions *h*0: *h* = 2*n* 0*k*: *k* = 2*n*		2
	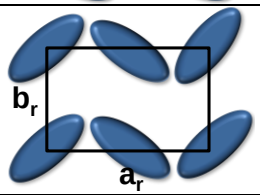		*p2mg*	*hk*: no conditions *h*0: no conditions 0*k*: *k* = 2*n*		2
	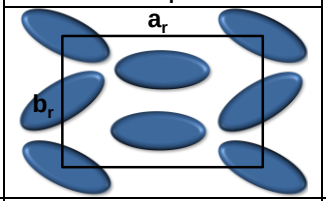		-	-		4
Columnar oblique (Col_{ob})	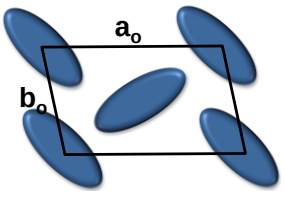	$\frac{1}{{d_{cal}}^2} = \frac{1}{Sin^2\Upsilon}\left(\frac{h^2}{{a_o}^2} + \frac{k^2}{{b_o}^2} - \frac{2hk\,cos\Upsilon}{a_o b_o}\right)$	*p*1	-	$S_o = a_o b_o \mathrm{Sin}\Upsilon$	2

To calculate the electron density, the complex structure factor F(*hk*) has to be written as the product of the phase, ϕ(*hk*) and the modulus |F(*hk*)| which is proportional to the square root of the intensity *I*(*hk*) of the observed reflection as shown below:

$$F(hk) = |F(hk)|e^{i\phi(hk)} = \sqrt{I(hk)}e^{i\phi(hk)}$$

The intensities of the different peaks in the diffraction pattern can be estimated from the areas under each peak after subtracting the background and then applying the relevant geometric and multiplicity corrections. The only information that cannot be obtained directly from experiment is the phase, ϕ(*hk*), for each diffraction peaks. However, this problem becomes easily tractable when the structure under study is centrosymmetric, i.e., if *ρ(x, y) = ρ(-x, -y)*. In that case F*(hk)* can only be real and hence ϕ(*hk*) can be either 0 or π. For non-centrosymmetric groups, the phase may take every value between 0 and 2π. As the LC phases observed are generally centrosymmetric, it is easy to reconstruct the electron density maps by taking the value of ϕ(*hk*) as 0 or π. The "correct" map is subsequently chosen on the merit of the reconstructed maps along with other physical and chemical knowledge of the system, such as chemical constituents and their sizes.

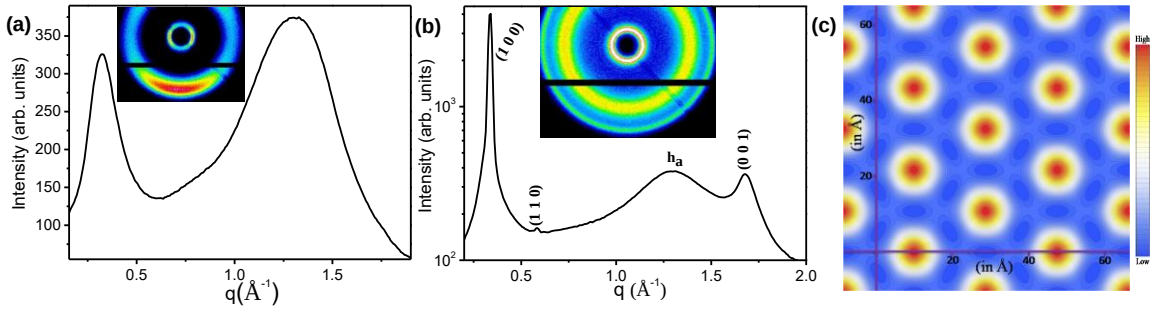

Figure 1.8 Figure showing X-ray diffraction patterns obtained for (a) a nematic mesophase where the first peak corresponds to the average length of the molecule whereas the second peak represents the lateral separation between the molecules, (b) a columnar hexagonal phase with assigned miller indices; and (c) represents the reconstructed electron density maps generated from the miller indices of columnar hexagonal phase. The insets of (a) and (b) shows the corresponding 2D diffraction patterns.

The correlation length, which can be determined from the X-ray diffractogram provides an indication of degree of order present within the mesophases. It can be calculated using the formula $\xi = [k2\pi]/[(\Delta q)]$ which is equivalent to Scherrer's equation, $\xi = [k\,\lambda]/[(\Delta 2\theta)\,\mathrm{Cos}\theta]$. Here, k is the shape factor whose typical value is 0.89, λ is the wavelength of the incident X-ray, $\Delta 2\theta$ is the broadening in 2θ at half of the maximum intensity (FWHM) in radian unit, θ is the maximum of the reflection, q is the scattering vector ($q= 4\pi\mathrm{Sin}\theta/\lambda$) and the Δq is broadening in q at half of the maximum intensity. The correlation length when divided by d-spacing values, results in a measure for the spatial order in terms of dimensions of the molecular length scale.

1.8 Applications of discotic liquid crystals

1.8.1 Discotics as organic semiconductors

The application of materials in semiconductor devices depend upon their charge carrier mobility which in turn rely on several factors such as degree of crystallinity, temperature etc. In this regard, inorganic semiconductors (e.g. Si) meet the requirements for semiconductor devices due to their high charge carrier mobilities. However, most of the inorganic semiconductors generally suffer from high cost, low efficiency and also limits fabrication in a flexible substrate. The latter option can be solved by using luminescent polymers but, they also experience trouble with low solubility, purity and stability. In this regard, small organic molecules have advantages in terms of all aspects described above.[65] In addition, columnar self-assembly formed by discotic LCs can enhance the charge carrier mobility as compared to their non-LC analogues. DLCs mainly form columnar mesophases due to strong π-π interactions between polyaromatic cores.[66-69] These columns or nano-wires act as quasi-one dimensional semi-conductors. The columns are surrounded by flexible alkyl chains and are thus insulated from each other. Therefore, the charge-migration only occurs along a column and is almost negligible between two neighbouring columns. The intercolumnar distance is usually 20-40 Å depending upon the length and number of flexible alkyl chains. The core-core distance is of the order of 3.5 Å so that there is considerable overlap of π-orbitals (Figure 1.9). These discotic LCs as compared to poly crystalline samples possess the ability of self-healing and are thus devoid of any defects and grain-boundaries.[70-74]

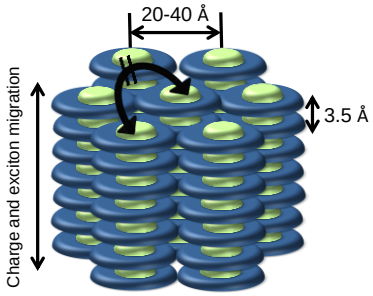

Figure 1.9 Schematic representing the charge and energy migration in discotic LCs.

The interest in DLCs as smart materials for organic semiconductor devices is due to their advantageous properties such as high intrinsic charge-carrier mobilities, ease of processability and high purity that reduce possible tapping sites for charge carriers.[75] Inherent charge-carrier mobility is important for application of discotic LCs as semiconductors in electronic devices which can be enhanced from a pronounced and defect-free long range order of columnar self-assembly. Therefore, discotic LCs provides ways to produce cheaper and flexible organic semiconductor devices. These discotic LCs have been employed as semi-conductors in various electronic devices such as organic LEDs (OLEDs), organic FETs (OFETs) and organic PVCs (OPVs).

OLEDs work on the principle of electrical excitation for generation of light. They can be single or multi-layer OLEDs. In a single-layer OLED, the organic light emitter is sandwiched between a metallic cathode and an indium tin oxide (ITO) anode.[76] However, in a multilayer device, additional hole- and electron-transporting layers are employed (Figure 1.10). The electrons and holes which are injected respectively into the LUMO and HOMO, drift due to the applied electric field. A necessity is to match the energy levels so that both electron and holes can be trapped in the emitter region. The combination of an electron and hole produces exciton, the energy released by the exciton is absorbed by the emitter which produces luminescence. For fabrication of efficient OLED devices employing discotic LCs, the columnar mesophase at room-temperature with a long-range order is required. A few derivatives of triphenylene have been explored for these applications which have shown electroluminescent properties.[77, 78]

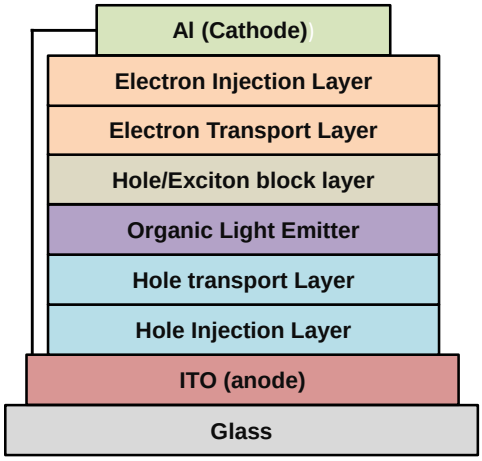

Figure 1.10 Schematic representation of a multilayer OLED device.

As the name suggests, OPVs work on the principle of generation of current by absorption of light. In OPVs, an exciton absorbs photon which leads to its dissociation into an electron and a hole and thus generation of electric current (Figure 1.11). Thus, these OPVs are completely opposite of OLEDs. For an efficient OPV device, there should be fast absorption of light by the material and high probabilities of exciton diffusion into the charge separating layers.

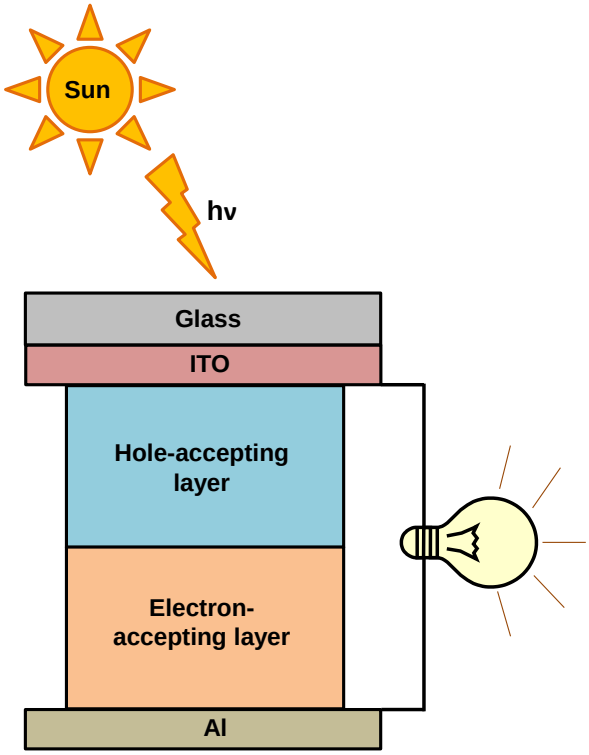

Figure 1.11 Schematic representing an OPV device.

Further, adequate charge separation at the interface as well as active charge escape from the interface and their transport to the electrodes is also required.[79] The discotic LCs have been found to exhibit exciton diffusion lengths of more than 70 nm. This is due to their self-healing tendency and better film-forming ability over large area with absence of grain boundaries. Several discotic derivatives based on triphenylene, perylene, hexabenzocoronene, porphyrin, hexabenzocoronene, phthalocyanin etc. have been explored for these OPV applications.[80-86]

OFETs consist of a semiconductor which is present on the surface of a gate electrode and function as bridge between the source and drain. The properties of columnar LCs to self-assemble together with their ability to provide anisotropic charge-carrier transport along the channel makes them viable candidates for OFETs. A typical OFET device is shown in Figure 1.12. The electron or hole conduction in an OFET can be modulated by varying the type of semiconductor (n- or p-type). The planar alignment of the columns is required for application in OFETs which can be achieved by aligning the discotic material by various techniques such as zone-casting, using a PTFE rubbed substrate etc. However, fabrication of these discotic LCs in their mesophase temperature range is difficult. This is due to the fact that thin film of discotic LCs when exposed to air becomes unstable. Further, in the LC state these films can dewet from the surface of gate due to surface tension.[87] However, the fabrication of OFETs below the mesophase range has been successfully carried out due to their easier solution processabilty, uniaxial parallel orientation and device stability.

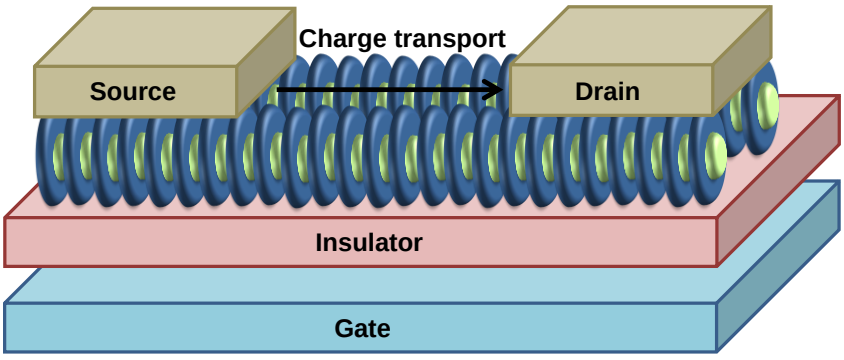

Figure 1.12 Schematic representation of an OFET device.

1.8.2 Discotic liquid crystals in display devices

The LCs being used in conventional twisted and super twisted nematic display devices are calamitic LCs. These devices which are composed of a calamitic LC layer suffer from the drawback of narrow as well as non-uniform viewing angle. This is because the conventional calamitic LCs exhibits a positive optical anisotropy due to which light leakage occurs in a LCD because of incomplete eradication of elliptically polarized light by the linear polarizer. This in turn results into a narrow viewing angle and a lower contrast ratio of the display. However, when an optical compensation film of a discotic nematic LC is employed, the optical anisotropy of similarly oriented rod-shaped and disc-shaped molecules is cancelled out (Figure 1.13). Therefore, this compensation film minimizes the light leakage and thus results in wide viewing angle and increased contrast ratio.

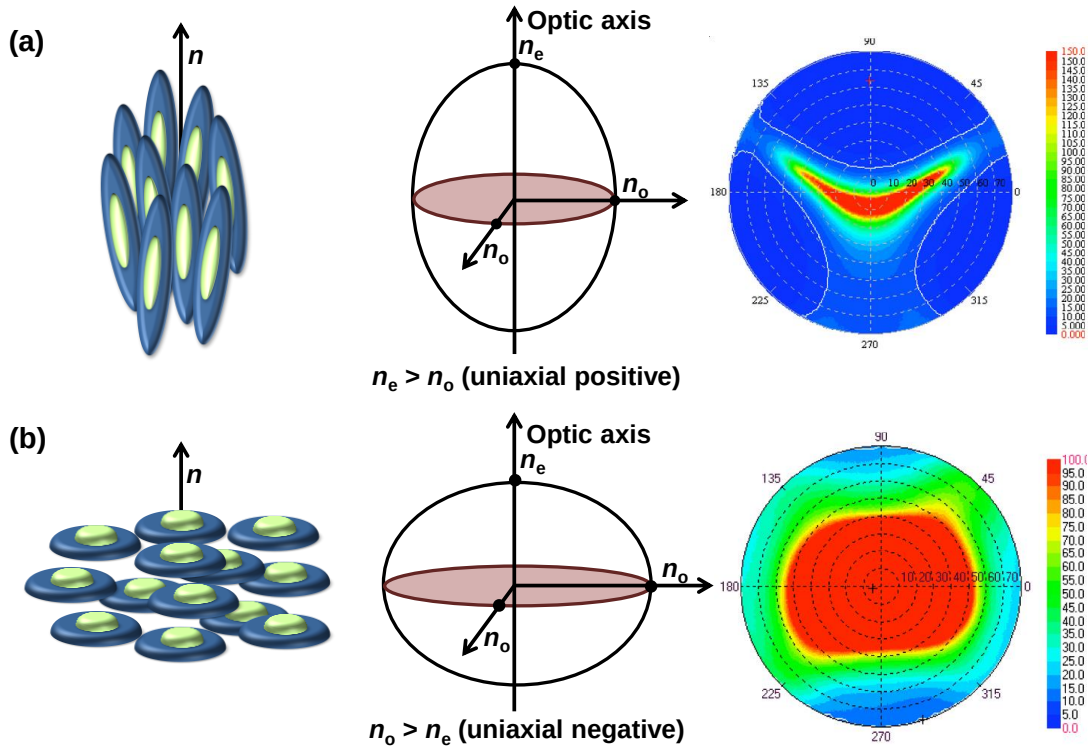

Figure 1.13 Schematic showing the index ellipsoids for (a) calamitic LCs (uniaxial positive) and (b) discotic LCs (uniaxial negative). The rightmost figure in the panels (a) and (b) shows the measured iso contrast ratio plots obtained with and without compensation film respectively.

The optical compensation film derived from triphenylene-based cross linked polymer has also been commercialized by Fuji film company which is one of the successful commercial application of discotic LCs.

However, the disc shaped molecules showing nematic phase i.e. N_D LCs are rare as the discotic units generally prefer to form columns. Further, for device applications, mesophase at room-temperature is required. Till now, very limited number of compounds exhibiting room-temperature N_D phase have been reported which limits further research in this field.[88] Most of the reported compounds are based on perturbing the pentaalkynylbenzene units which is synthetically very difficult and leads to poor yield of the final compounds. Therefore, for commercialization, the compounds which can be prepared in good yields by simple synthetic methods are required.

1.9 Outline of thesis

This thesis describes the structure and property correlation in dimeric and oligomeric LC systems. These discotic LC oligomers serve as ideal illustrative compounds for polymers due to ease of purification and characterization and remarkable similarities in their transitional behaviour. The physical properties of these discotic LC oligomers are also notably different from their constituent units. The compounds presented in this thesis mainly displayed N_D and columnar mesophases at room-temperature which makes them very interesting from the device point of view. Several other interesting properties such as reversible formation of aligned fibers (~20-40 μm) in the mesophase, switching of Col_r to Col_h assemblies induced by 2,4,7-trinitrofluorenone (TNF) and room-temperature N_D phase exhibited by gold nano-particles (GNPs) have also been explored which points the way towards new device applications of LCs. A brief overview of the subsequent chapters is given below:

Chapter 2 addresses synthesis and characterisation of two new series of oligomeric mesogens based on azobenzene core. The azobenzene tetracarboxylic acid core was attached to four cyanobiphenyl moieties (disc-rod oligomers) in the first series, whereas in the second case, it was tethered to four triphenylene moieties (disc-disc oligomers) *via* flexible alkyl spacers. Surface manometry of a compound from the first series showed the formation of a

stable monolayer at air-water interface. Interestingly, temperature dependent atomic force microscopy (AFM) revealed the reversible formation of aligned fibers (~20-40 μm) in the mesophase, which provides rational design and control over the anisotropic properties of the ordered phase for various applications. Compounds of second series were found to self-organize into room temperature columnar structures. Interestingly, we found that the Col_r self-assembly of these compounds switched to Col_h on doping the compounds with TNF. These oligomers very advantageous for new device applications due to the combination of various properties such as LC phase at room-temperature, easy alignment by mechanical shearing, increased charge hopping expected from the donor-acceptor charge transfer complexes and the transition from Col_r to Col_h phase.

Chapter 3 describes facile synthesis of a discotic mesogenic dyad (disc-disc) based on triphenylene and pentaalkynylbenzene linked via flexible alkyl spacer. The dyad self-assembled into a Col_h mesophase at room-temperature and also exhibited an excellent blue light emission property, which makes it promising for various opto-electronic applications. The second section details the synthesis of the first examples of room-temperature LC dimers (rod-disc) based on cholesterol and pentaalkynylbenzene linked via varying flexible alkyl spacers. Both the synthesized dimers displayed chiral nematic (N*) phase at room-temperature and exhibited excellent fluorescent emission properties. These compounds were synthesized in order to understand the effect of pentaalkynylbenzene units in discotic dimers.

Chapter 4 details the synthesis of multialkynylbenzene bridged discotic triads derived from triphenylene and pentaalkynylbenzene units. In the first section, a straightforward synthesis of multialkynylbenzene-bridged triphenylene based dyad system (via flexible alkyl spacers) that self-organize into room-temperature columnar structures is reported. The compound with shortest spacer displayed a columnar oblique plastic phase and showed the formation of well-nucleated spherulites of about several hundred micrometers on slow cooling from the isotropic state. All of the compounds exhibited blue luminescence in solution and in the thin-film state under long wavelength (365 nm) UV light. The second section elaborates the synthesis of lath-shaped symmetrical triads based on multialkynylbenzene linked *via* flexible alkyl spacers. The compounds with shorter spacers were found to be non-mesomorphic

whereas the derivative with longest alkyl spacer exhibited N_D phase which has been characterized by POM and detailed SAXS/WAXS studies.

Chapter 5 explains new design strategies towards the synthesis of room-temperature N_D LCs. The first section describes a new approach based-on LC dimer consisting of a triphenylene and a pentaalkynylbenzene unit linked *via* flexible alkyl spacers. The formation of the N_D phase is realized most likely through folding of the dimeric molecule that prevent stacking between the triphenylene units, as suggested by modelling in the mesophase derived from X-ray scattering results and high-level DFT calculations. The second section details the design and synthesis of three room-temperature oligomeric N_D LCs based-on azobenzene core. The presence of a short azo linking group provides more disorder in the system which reduces the packing efficiency among the pentaalkynylbenzene units and results into the formation of a room-temperature N_D phase over a wide temperature range. The third section describes the synthesis of gold nano-particles (GNPs) coated with pentaalkynylbenzene units which displayed N_D phase even at room-temperature. These discotic LC GNPs are very interesting materials as they are capable of showing enhanced dielectric response due to GNPs as well as optical compensation due to pentaalkynylbenzene units.

This thesis is concluded with **Chapter 6**, which summarizes the significant interpretations derived from all of the above chapters.

At the end of each chapter, the structural analyses (^{1}H and ^{13}C NMR, IR, UV-vis, DSC etc.) are also provided in the **Appendix**.

References

(1) Geelhaar, T.; Griesar, K.; Reckmann, B. *Angew. Chem. Int. Ed*. **2013**, *52*, 8798−8809.

(2) Bremer, M.; Kirsch, P.; Klasen-Memmer, M.; Tarumi, K. *Angew. Chem. Int. Ed*. **2013**, *52*, 8880−8896.

(3) Arakawa, K. Liquid Crystal Display Having Positive and Negative Birefringent Compensator Films; US005189538A, **1993**.

(4) Mori, H.; Ito, Y. Liquid Crystal Display with Compensators Having Minimum Retardations in the Inclined Direction; US005805253A, **1998**.

(5) Boden, N.; Clements, J.; Movaghar, B. Fluid Sensing Device Using Discotic Liquid Crystals; US006423272B1, **2002**.

(6) Pisula, W.; Müllen, K.; Goodby, J. W.; Collings, P. J.; Kato, T.; Tschierske, C.; Gleeson, H. F.; Raynes, P.; Eds.; Wiley-VCH: Weinheim, **2014**, Vol. 8, pp 627−674.

(7) Sergeyev, S.; Pisula, W.; Geerts, Y. H. *Chem. Soc. Rev*. **2007**, *36*, 1902−1929.

(8) Crispin, X.; Cornil, J.; Friedlein, R.; Okudaira, K. K.; Lemaur, V.; Crispin, A.; Kestemont, G.; Lehmann, M.; Fahlman, M.; Lazzaroni, R.; Geerts, Y.; Wendin, G.; Ueno, N.; Bredas, J. L.; Salaneck, W. R. *J. Am. Chem. Soc*. **2004**, *126*, 11889–11899.

(9) Warman, J. M.; Haas, M. P. D.; Dicker, G.; Grozema, F. C.; Piris, J.; Debije, M. G. *Chem. Mater*. **2004**, *16*, 4600–4609.

(10) An, Z.; Yu, J.; Jones, S. C.; Barlow, S.; Yoo, S.; Domercq, B.; Prins, P.; Siebbeles, L. D. A.; Kippelen, B.; Marder, S. R. *Adv. Mater*. **2005**, *17*, 2580–2583.

(11) Jones, B. A.; Ahrens, M. J.; Yoon, M. H.; Facchetti, A.; Marks, T. J.; Wasielewski, M. R. *Angew. Chem. Int. Ed*. **2004**, *43*, 6363–6366.

(12) Iino, H.; Takayashiki, Y.; Hanna, J. I.; Bushby, R. J. *Jpn. J. Appl. Phys*. **2005**, *44*, L1310–L1312.

(13) Markovitsi, D.; Marguet, S.; Bondkowski, J.; Kumar, S. *J. Phys. Chem. B* **2001**, *105*, 1299–1306.

(14) Chandrasekhar, S.; Demus, D.; Goodby, J.; Gray, G. W.; Spiess, H. W.; Vill, V.; in Handbook of Liquid Crystals Set, Wiley-VCH, **2008**, pp. 749–780.

(15) Boden, N.; Movaghar, B.; Demus, D.; Goodby, J.; Gray, G. W.; Spiess, H. W.; Vill, V.; in Handbook of Liquid Crystals Set, Wiley-VCH, **2008**, pp. 781–798.

(16) Vaughan, G. B. M.; Heiney, P. A.; McCauley, J. P.; Smith, A. B. *Phys. Rev. B*. **1992**, *46*, 2787–2791.

(17) Schouten, P. G.; Warman, J. M.; Haas, M. P. D.; Nostrum, C. F. V.; Gelinck, G. H.; Nolte, R. J. M.; Copyn, M. J.; Zwikker, J. W.; Engel, M. K. *J. Am. Chem. Soc*. **1994**, *116*, 6880–6894.

(18) Van de Craats, A. M.; Warman, J. M. *Adv. Mater*. **2001**, *13*, 130–133.

(19) Lu, M.; Yang, K. H. *Jpn. J. Appl. Phys.* **2000**, *36*, L412-L415.

(20) Mori, H.; Itoh, Y.; Nishuira, Y.; Nakamura, T.; Shinagawa, Y. *Jpn. J. Appl. Phys*. **1997**, *36*, 143-147.

(21) Braun, C. D.; Lub, L. *Liq. Cryst*. **1999**, *26*, 1501-1509.

(22) Chandrasekhar, S.; Prasad, S. K.; Nair, G. G.; Rao, D. S. S.; Kumar S.; Manickam, M.Euro Display '99, 19th international Display Research Conference, late-news, **1999**, 9–11.

(23) Nair, G. G.; Rao, D. S. S.; Prasad, S. K.; Chandrasekhar, S.; Kumar, S. *Mol. Cryst. Liq. Cryst.* **2003**, *397*, 245–252.

(24) Demus, D.; Goodby, J.; Gray, G. W.; Spiess, H. W.; Vill, V. in Handbook of Liquid Crystals, ed., Wiley-VCH, Weinheim, **1998**, Vol 1-3.

(25) Bahadur, B. in Liquid Crystals-Application and Uses, World Scientific, Singapore, **1990**, Vol 1-3.

(26) Chandrasekhar, S. in Liquid Crystals, 2nd ed., Cambridge University Press, Cambridge **1992**.

(27) Collings, P. J.; Hird, M. in Introduction to Liquid Crystals-Chemistry and Physics, Taylor & Francis Ltd., London, **1997**.

(28) Collings, P. J.; Patel, S. J. in Handbook of Liquid Crystal Research, Oxford University Press, Oxford, **1997**.

(29) Kelker, H.; Hatz, W. in Handbook of Liquid Crystals, VCH, Deerfield Beach, FL, **1980**.

(30) Collings, P. J. in Nature's delicate Phase of Matter, Princeton University Press, **1990**.

(31) De Gennes, P. G.; Prost, J. in The Physics of Liquid Crystals, 2nd ed., Oxford University Press, New York, **1993**.

(32) Reinitzer, F. *Liq. Cryst*. **1989**, *5*, 7-18.

(33) Lehmann, O. *Z. Phys. Chem*. **1889**, *4*, 462-467.

(34) Vorlander, D. *Kristallinisch-flussige Substanzen*, Enke, Stuttgart, **1905**.

(35) Vorlander, D. *Ber. Dtsch. Chem. Ges*. **1907**, *40*, 1970–1972.

(36) Friedel, G. *Ann. Phys*. **1922**, *18*, 273–274.

(37) Onsager, L. *Ann. N. Y. Acad. Sci.* **1949**, *51*, 627-659.

(38) Flory, P. J. *Proc. Roy. Soc. Ser. A. London* **1956**, *234*, 73-89.

(39) Gray, G. W.; Harrison, K. J.; Nash, J. A. *Electron. Lett*. **1973**, *9*, 130–131.

(40) Chandrasekhar, S.; Sadashiva, B. K.; Suresh, K. A. *Pramana* **1977**, *9*, 471–480.

(41) Vorlander, D. *Chemische Kristallographic der Flussigkeiten*, Akademische Verlagsgesellschaff, Leipzig,Germany, pp. 34, **1924**.

(42) Niori, T.; Sekine, T.; Watanabe, J.; Furukawa, T.; Takezoe, H. *J. Mater. Chem*. **1996**, *6*, 1231–1233.

(43) Pelzi, G.; Diele, S.; Weissflog, W. *Adv. Mater.* **1999**, *11*, 707-724.

(44) Tschierske, C.; Dantlgraber, G. *Pramana-J. Phys.* **2003**, *61*, 455-481.

(45) Ros, M. B.; Serrano, J. L.; De la Fuente, M. R.; Folcia, C. L. *J. Mater. Chem.* **2005**, *15*, 5093-5098.

(46) Reddy, R. A.; Tschierske, C. *J. Mater. Chem.* **2006**, *16*, 907-961.

(47) Takezoe, H.; Takanishi, Y. *Jpn. J. Appl. Phys.* **2006**, *45*, 597-625.

(48) Etxebarria, J.; Ros, M. B. *J. Mater. Chem.* **2008**, *18*, 2919-2926.

(49) Kumar, S. *Chem. Soc. Rev.* **2006**, *35*, 83-109.

(50) Kumar, S. in Chemistry of Discotic Liquid Crystals: From Monomers to Polymers; Percec, V., Ed., CRS Press, Taylor & Francis Group: Boca Raton, FL, **2011**.

(51) Kato, T.; Yasuda, T.; Kamikawa, Y.; Yoshio, M. *Chem. Commun.* **2009**, 729-739.

(52) Laschat, S.; Baro, A.; Steinke, N.; Giesselmann, F.; Hagele, C.; Scalia, G.; Judele, R.; Kapatsina, E.; Sauer, S.; Schreivogel, A.; Tosoni, M. *Angew. Chem. Int. Ed.* **2007**, *46*, 4832-4887.

(53) Wu, J.; Pisula, W.; Mullen, K. *Chem. Rev.* **2007**, *107*, 718-747.

(54) Boden, N.; Bushby, R. J.; Clements, J.; Movaghar, B. *J. Mater. Chem.* **1999**, *9*, 2081-2086.

(55) Bushby, R. J.; Lozman, O. R. *Curr. Opin. Solid State Mater. Sci.* **2002**, *6*, 569-578.

(56) Bushby, R. J.; Lozman, O. R. *Curr. Opin. Colloid Interface Sci.* **2002**, *7*, 343-354.

(57) Takezoe, H.; Kishikawa, K.; Gorecka, E. *J. Mater. Chem.* **2006**, *16*, 2412-2416.

(58) Ohta, K.; Hatsusaka, K.; Sugibayashi, M.; Ariyoshi, M.; Ban, K.; Maeda, F.; Naito, R.; Nishizawa, K.; van de Craats, A. M.; Warman, J. M. *Mol. Cryst. Liq. Cryst.* **2003**, *397*, 25-45.

(59) Kouwer, P. H. J.; Jager, W. F.; Misj, W. J.; Picken, S. J. *Macromolecules* **2001**, *34*, 7582-7584.

(60) Chandrasekhar, S. *Liq. Cryst.* **1993**, *14*, 3-14.

(61) Chandrasekhar, S.; Ranganath, G. S. *Rep. Prog. Phys.* **1990**, *53*, 57-84.

(62) Wöhrle, T.; Wurzbach, I.; Kirres, J.; Kostidou, A.; Kapernaum, N.; Litterscheidt, J.; Haenle, J. C.; Staffeld, P.; Baro, A.; Giesselmann, F.; Laschat, S. *Chem. Rev.* **2016**, *116*, 1139-1241.

(63) K. Kawata, *Chem. Rec*. **2002**, *2*, 59-80.

(64) F. Leenhouts, *Jpn. J. Appl. Phys*. **2000**, *39*, L741-L743.

(65) Kovac, J.; Peternai, L.; Lengyel, O. *Thin Solid Films* **2003**, *433*, 22-26.

(66) Varghese, S.; Kumar, N. S. S.; Krishna, A.; Rao, D. S. S.; Prasad, S. K.; Das, S. *Adv. Funct. Mater.* **2009**, *19*, 2064-2073.

(67) Eccher, J.; Faria, G. C.; Bock, H.; von Seggern, H.; Bechtold, I. H. *ACS Appl. Mater. Interfaces* **2013**, *5*, 11935-11943.

(68) Hassheider, T.; Benning, S. A.; Kitzerow, H. S.; Achard, M. F.; Bock, H. *Angew Chem. Int. Ed.* **2001**, *40*, 2060-2063.

(69) Seguy, I.; Jolinat, P.; Destruel, P.; Mamy, R.; Allouchi, H.; Courseille, C.; Cotrait, M.; Bock, H. *ChemPhysChem* **2001**, *2*, 448-452.

(70) Tschierske, C. *J. Mater. Chem.* **1998**, *8*, 1485-1508.

(71) Barber, J.; Rakitin, O. A.; Ros, M. B.; Torroba, T. *Angew. Chem. Int. Ed.* **1998**, *37*, 296-299.

(72) Bayer, A.; Zimmermann, S.; Wendorff, J. H. *Mol. Cryst. Liq. Cryst.* **2003**, *396*, 1-22.

(73) Kohary, K.; Cordes, H.; Baranovskii, S. D.; Thomas, P.; Wendorff, J. H. *Phys. Status Solidi B* **2004**, *241*, 76-82.

(74) Brinker, C. J.; Lu, Y.; Sellinger, A.; Fan, H. *Adv. Mater.* **1999**, *11*, 579-585.

(75) Torgova, S.; Strigazzi, A. *Mol. Cryst. Liq. Cryst.* **2002**, *375*, 61-72.

(76) Neill, M. O.; Kelly, S. M. *Adv. Mater*. **2003**, *15*, 1135-1146.

(77) Lussem, G.; Wendorff, J. H. *Polym. Adv. Technol.* **1998**, *9*, 443-460.

(78) Stapff, I. H.; Stumpflen, V.; Wendorff, J. H.; Spohn, D. B.; Mobius, D. *Liq. Cryst.* **1997**, *23*, 613-617.

(79) Mende, L. S.; Fechtenkotter, A.; Mullen, K.; Moons, E.; Friend, R. H.; Mackenzie, J. D.; *Science* **2001**, *293*, 1119-1122.

(80) Oukachmih, M.; Destruel, P.; Seguy, I.; Ablart, G.; Jolinat, P.; Archambeau, S.; Mabiala, M.; Fouet, S.; Bock, H. *Sol. Energy Mater. Sol. Cells* **2005**, *85*, 535-543.

(81) Petritsch, K.; Friend, R. H.; Lux, A.; Rozenberg, G.; Moratti S. C.; Holmes, A. B. *Synth. Met.* **1999**, *102*, 1776-1777.

(82) Li, L. F.; Kang, S. W.; Harden, J.; Sun, Q. J.; Zhou, X. L.; Dai, L. M.; Jakli, A.; Kumar S.; Li, Q. *Liq. Cryst.* **2008**, *35*, 233-239.

(83) Schmidt-Mende, L.; Fechtenkotter, A.; Mullen, K.; Moons, E.; Friend, R. H.; MacKenzie, J. D. *Science* **2001**, *293*, 1119-1122.

(84) Schmidt-Mende, L.; Fechtenkotter, A.; Mullen, K.; Moons, E.; Friend, R. H.; MacKenzie, J. D. *Physica E* **2002**, *14*, 263-267.

(85) Schmidtke, J. P.; Friend, R. H.; Kastler, M.; Mullen, K. *J. Chem. Phys.* **2006**, *124*, 174704/1-6.

(86) Hesse, H. C.; Weickert, J.; Al-Hussein, M.; Doessel, L.; Feng, X.; Mulen, K.; Schmidt-Mende, L. *Sol. Energy Mater. Sol. Cells* **2010**, *94*, 560-567.

(87) Bramble, J. P.; Tate, D. J.; Revill, D. J.; Sheikh, K. H.; Henderson, J. R.; Liu, F.; Zeng, X. B.; Ungar, G.; Bushby, R. J.; Evans, S. D. *Adv. Mater.* **2010**, *20*, 914-920.

(88) Bisoyi, H. K.; Kumar, S. *Chem. Soc. Rev.* **2010**, *39*, 264-285.

Chapter 2

Rod-disc and disc-disc oligomers based on azobenzene tetracarboxylic acid core

PART A

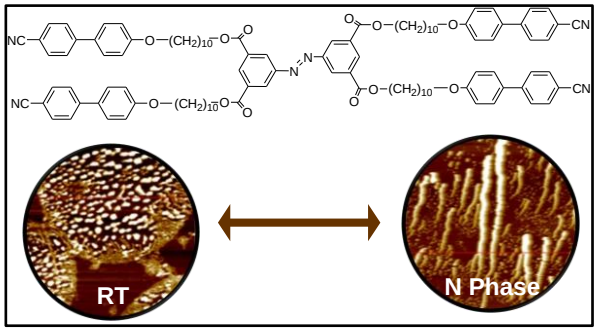

New oligomeric mesogens consisting of an azobenzene-based core attached to which are four 4-cyanobiphenyl units via *flexible alkyl spacers (n = 5-12) have been synthesized. The oligomers containing n = 8 and n = 10 were found to exhibit a monotropic nematic phase. Surface manometry of the compound with n = 10 exhibits the formation of a stable monolayer at the air-water interface. Interestingly, temperature dependent AFM topography carried out with the film deposited on a hydrophobic silicon substrate showed the reversible formation of aligned fibers (~20-40 µm) in the mesophase.*

PART B

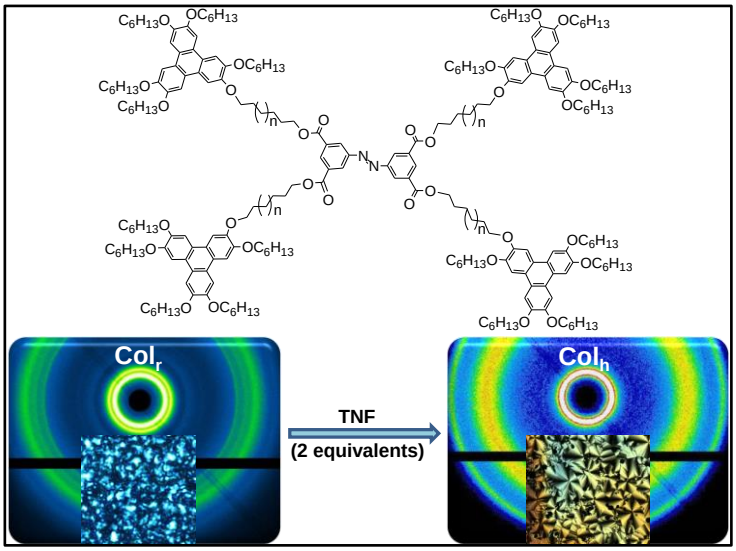

A straightforward synthesis of triphenylene-based oligomeric systems that self-organize into room temperature columnar structures was carried out. The compounds with longer spacer length (m = 10 and 12) exhibited columnar rectangular (Col$_r$) mesophase whereas the compound with m = 8 existed in glassy Col$_r$ state. Interestingly, the Col$_r$ self-assembly of these compounds switched to columnar hexagonal (Col$_h$) on doping the compounds with 2, 4, 7-trinitrofluorenone (TNF).

2.1 Part A: Synthesis and characterization of novel azobenzene-based mesogens and their organization at the air–water and air–solid interfaces

2.1.1 Introduction

Molecular order as well as structure in thin films is often different as compared to that present in the bulk.[1] Recently, thin films of organized assemblies e.g. Langmuir-Blodgett (LB) films have gained an immense interest which stems from the inherent control of their internal layer structure (even down to the molecular level) as well as the precise control of the resulting film thickness.[2,3] These monolayer films paves the way to understand the packing of molecules based on their structures and different intermolecular interactions which are otherwise difficult to study in the bulk.[4] For further studies, the stable films can be transferred onto various substrates which can easily be controlled by the hydrophilicity or hydrophobicity of the solid support. This offers pathways to tune the layer architecture which can meet the demands of the desired molecularly engineered organic thin-film devices.[5–7]

In this regard, photoactive molecules with different molecular structures have been widely used for thin film devices. Among them, azobenzene is the most extensively studied photoactive molecule. In addition, when incorporated into a liquid crystalline (LC) system, it acts as a photo-responsive trigger. The *trans*-form of azobenzene derivatives stabilizes a LC phase because of its rod-like molecular shape which is similar to that of the host LC molecule, while the *cis*-isomer shows a bent shape and destabilizes the LC phase.[8-11] Infact, the self-organization ability of LC materials and the photo-orientation ability of the azo-group mutually influence each other which leads to the amplified change in molecular alignment due to the cooperative motion.[12] The LC phase becomes light sensitive on photo-isomerization of the azobenzene moiety and thus it provides a new opportunity for switching & controlling the anisotropic properties of the ordered phase.[13] All these properties makes azobenzene chromophore ideal for many photo-devices, such as information storage devices,[14, 15] molecular switching devices,[16] and sensors.[17]

Numerous examples are also reported on the photo-responsive nature of the azobenzene moiety in thin films.[18] Photo-isomerization kinetics of the Langmuir monolayers of

mesogenic azobenzene dimers **1** at air-water interface have been thoroughly studied by Kumar *et al.*[19] Ozaki and co-workers have also reported phase transitions in the Langmuir-Blodgett (LB) films of azobenzene-containing long chain fatty acids **2** based on the spectroscopic studies of H-aggregates.[20, 21]

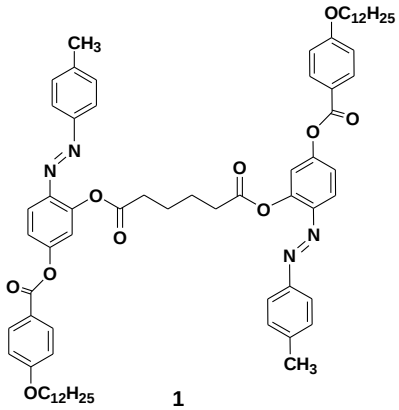

1

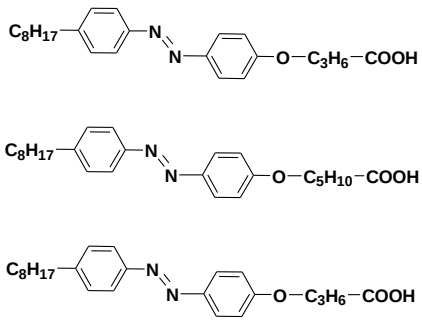

2

Thus, thin films of LC mesogens, containing the azobenzene group can form promising candidates for the fabrication of devices since LCs can offer high sensitivity and high control over the architecture using the LB technique.[19, 22]

2.1.2 Objective

We have designed mesogens **3** consisting of an azobenzene-based core attached to which are four 4-cyanobiphenyl units *via* flexible alkyl spacers of varying chain lengths. It represents a simple but also an useful advance for the design of a molecular system that enables fundamental insights into unconventional structure-mesophase morphology relationship. These molecules because of their amphiphilic character can form stable monolayers at air-water interface whose properties can be studied using the techniques of surface manometry and Brewster angle microscopy (BAM). We further aimed to study the properties of the film at air-solid interface by transferring the film onto hydrophilic (mica) and hydrophobic (silicon wafer) solid substrates through vertical LB technique whose wetting behavior can be studied using atomic force microscopy (AFM). We were also interested in investigating temperature dependent AFM topography which can provide rational design and control over the anisotropic properties of the ordered phase for various applications.

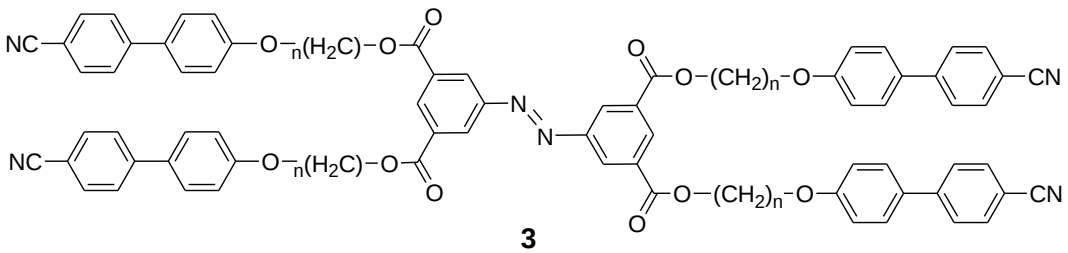

3

(*n* = 5-12)

2.1.3 Results and Discussion

2.1.3.1 Synthesis and characterization

The synthetic procedure for compounds **3** is outlined in Scheme 2.1. The starting material azobenzenetetracarboxylic acid **5** was synthesized using the procedure reported in the literature.[23] For the synthesis of the target material, compound **5** (1 equivalent) was dissolved in KOH solution so that the pH of the solution became about 8-9. To that solution, the corresponding ω-bromo terminated cyanobiphenyl precursor **6** (6 equivalents) and 100 mg of tetraoctyl ammonium bromide (TOAB) were added. The reaction mixture was refluxed under vigorous stirring for 5-6 hours. After that the reaction mixture was cooled to room temperature and extracted with chloroform. The organic layer was separated, washed with brine and dried over anhydrous sodium sulphate. The chloroform was removed by rotary evaporation and the resulting residue was purified by repeated column chromatography over silica gel using chloroform and hexane as eluent. The synthesized compounds were characterized by various spectroscopic techniques (^{1}H NMR, ^{13}C NMR, FTIR, Raman spectroscopy and UV-vis) and elemental analysis as detailed in the experimental section and representative spectra are given in appendix I (Figure A1-A5).

2.1.3.2 Thermal Behavior

The thermal behavior (phase transition temperatures and associated enthalpy values) of all the synthesized compounds was investigated by polarizing optical microscopy (POM) and differential scanning calorimetry (DSC, Table 2.1). All the compounds, except **3d** and **3f**, displayed high energy transitions from crystal to isotropic on heating followed by isotropic to crystal on cooling.

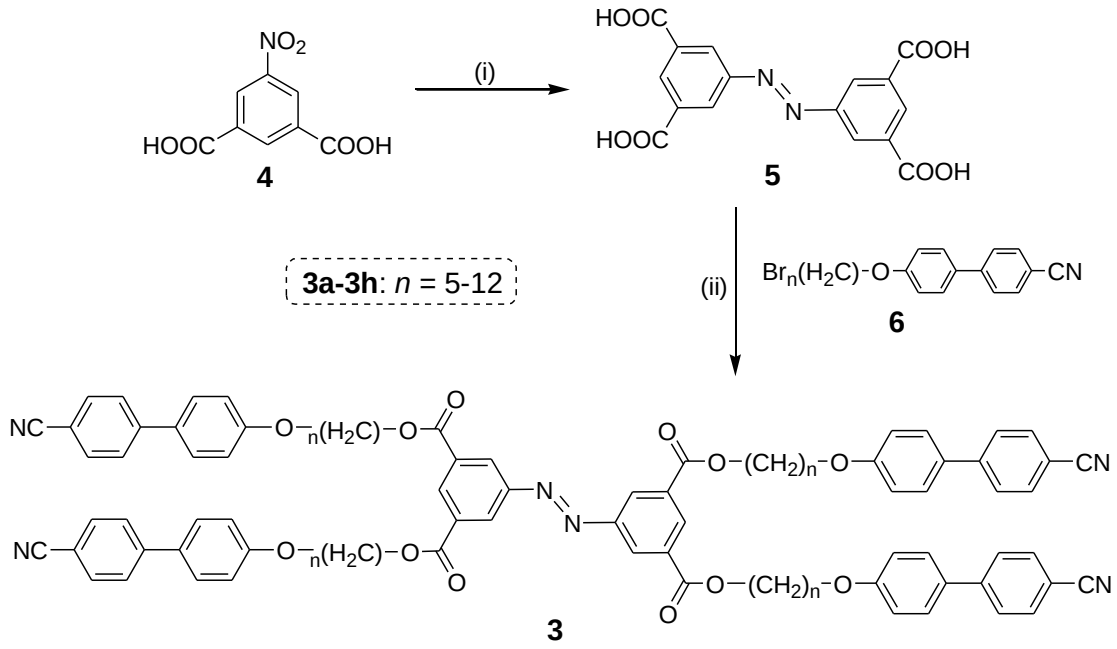

Scheme 2.1 Synthesis of compounds **3**. Reagents and conditions: (i) NaOH, Dextrose, 80 °C, HCl. Yield: 70%; (ii) KOH, H_2O, TOAB, reflux, 4h. Yield: 15-40%.

Table 2.1 Phase behavior of the target compounds [a, b]

Compound	Heating Scan	Cooling Scan
3a	Cr 212.4 (82.4) I	I 158.9 (83.4) Cr
3b	Cr 162.7 (75.3) I	I 127.8 (76.8) Cr
3c	Cr 188.5 (109.1) I	I 166.9 (119.4) Cr
3d	Cr 187.5 (159.4) I	I 120 (6.6) N 101 (60.9) Cr
3e	Cr 164.72 (135.9) I	I 148.3 (132.2) Cr
3f	Cr 125.9 (131.5) I	I 114.6 (6.5) N 102 (98.3) Cr
3g	Cr 150 (189) I	I 134.7 (137.5) Cr
3h	Cr 132.4 (142.8) I	I 108.9 (145.7) Cr

[a] Phase transition temperatures in °C and latent heat values in kJ mol^{-1} (in parentheses).

[b] Phase assignments: Cr = crystal, N = nematic phase, I = isotropic.

Compound **3a** having pentyloxy spacer showed melting transition at 212 °C (ΔH = 82 kJ mol^{-1}) to the isotropic phase which on further cooling solidified at 159 °C (ΔH = 83 kJ mol^{-1}). Similarly, compounds **3b** and **3c** on heating displayed isotropization at about 163°C and

188 °C with a transition enthalpy of 75 kJ mol^{-1} and 109 kJ mol^{-1}, respectively. On cooling, they showed the crystallization peak centered at 128 °C and 167 °C, respectively. Compounds **3d** and **3f** having octyloxy and decyloxy spacer exhibited monotropic nematic phase. On heating, they showed a melting transition at around 188 °C (ΔH = 159 kJ mol^{-1}) and 125 °C (ΔH = 131 kJ mol^{-1}), respectively. The decrease in melting temperature can be attributed to the increase in spacer length of the alkoxycyanobiphenyl derivatives connected with the azobenzene core. On cooling the compounds **3d** and **3f** from the isotropic phase, DSC thermogram showed the appearance of mesophase at about 120 °C (ΔH = 6.6 kJ mol^{-1}) and 115 °C (ΔH = 6.5 kJ mol^{-1}), respectively. The DSC traces obtained on heating and cooling runs of compound **3f** are represented in Figure 2.1a. Under a polarized optical microscope, a typical schlieren texture of the nematic phase was observed for compounds **3d** and **3f** as shown in Figure 2.1b and 2.1c. Compounds **3e**, **3g** and **3h** were prepared to examine the effect of the spacer length. Compound **3e** exhibited a melting transition at around 165 °C (ΔH = 135 kJ mol^{-1}) which then crystallizes at about 148 °C (ΔH = 132 kJ mol^{-1}) on cooling. Similarly, compounds **3g** and **3h** showed crystal to isotropic transition at around 150 °C (ΔH = 189 kJ mol^{-1}) and 132 °C (ΔH = 142 kJ mol^{-1}), respectively. Upon further cooling, the crystallization peak appeared at 134 °C (ΔH = 137 kJ mol^{-1}) and 108 °C (ΔH = 109 kJ mol^{-1}), respectively.

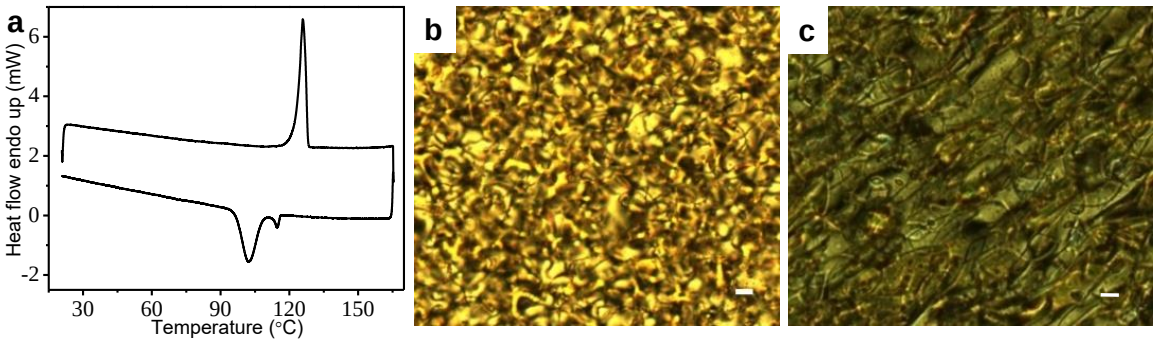

Figure 2.1 (a) The DSC trace of compound **3f** on heating and cooling (scan rate 10 °C min^{-1}). Optical photomicrograph of compounds, (b) **3d** and (c) **3f** at 119.8 °C and 110.6 °C, respectively (on cooling, crossed polarizers, scale bar 10 μm).

2.1.3.3 X-ray Diffraction Studies

The supramolecular organization of the synthesized oligomers in the mesophase was further investigated by X-ray diffraction studies (XRD). The diffractogram corresponding to mesophase of compound **3f** displayed two diffuse reflections in the wide and the small angle region (Figure 2.2a). This observation indicates the absence of any positional order in the nematic mesophase and thus excludes the existence of smectic and columnar phase structure. This is in fact also in accordance with the microscopic textures. The broad small angle reflection for **3f** showed a d-spacing of 15.50 Å in the mesophase (at 110 °C). This value corresponds to the average length of the azobenzene core (9 Å) and diameter of the rod-like cyanobiphenyl units (23 Å), indicating a molecularly mixed nematic phase. The reflection at small angle has a much smaller value of *d*-spacing than that of the total length of the oligomer which confirms the compatibility of both components (i.e. azobenzene & cyanobiphenyl) in the mesophase and absence of any nanophase segregation between them. A very diffuse peak in wide angle regime at around 4.46 Å was observed which can be attributed to the average lateral separation of the molecules in the mesophase. We have proposed a sketch of the order of nematic phase as derived from the detailed XRD analysis (Figure 2.2b).

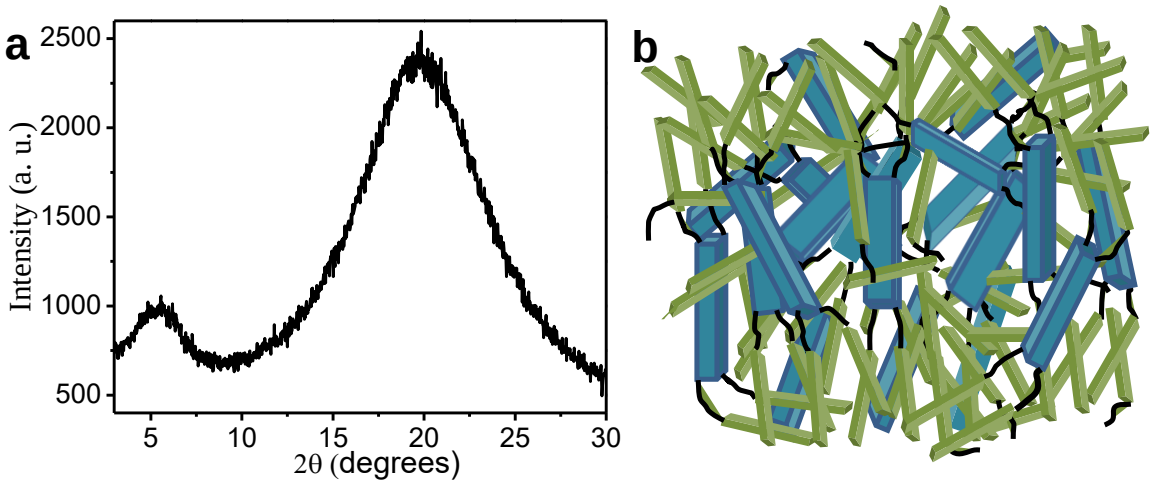

Figure 2.2 (a) An intensity versus 2θ graph derived from the X-ray diffraction pattern of compound **3f** in the mesophase. (b) Sketch of the order in the mixed nematic phase.

2.1.3.4 Thin-Film Studies

Since the synthesized molecules are amphiphilic because of the presence of highly polar cyano group as well as long alkyl chains, our next aim was to study the monolayer films of mesogenic azobenzene molecules at air-water and air-solid interfaces. We have carried out studies on compound **3f** which showed a monotropic nematic phase on cooling (114 °C) from isotropic phase (125.9 °C). Figure 2.3 shows the surface pressure (π, mN/m) vs area per molecule (A_m, nm^2) isotherm for the compound **3f**. Initially, at large area per molecule (A_m> 0.4 nm^2) the isotherm shows zero surface pressure which starts increasing upon compression.

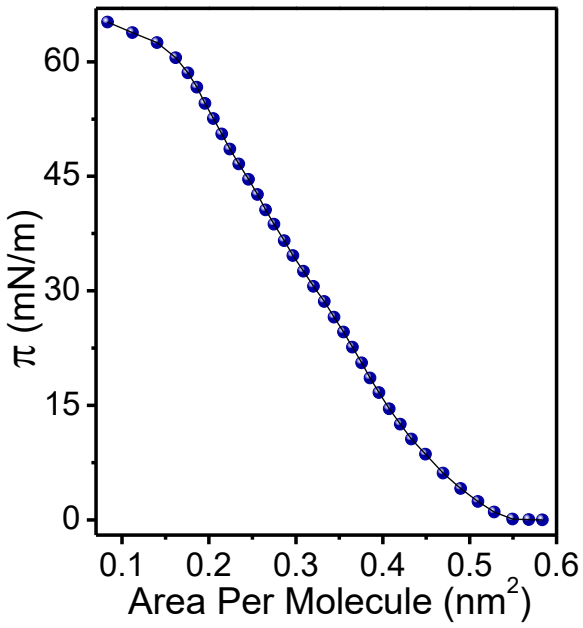

Figure 2.3 Surface pressure (π) Vs. area per molecule (A_m) isotherms of azobenzene-based mesogens synthesized in the study.

The film collapses at an A_m of 0.15 nm^2 with a collapse pressure of 60 mN/m. The high value of collapse pressure can result from the strong interactions among the 4-cyanobiphenyl units. The limiting area per molecule (A_o) value obtained by extrapolation to zero surface pressure was about 0.4 nm^2 and remains nearly same for twice the volume spread in the sub-phase. The value of limiting area corresponds to the edge to edge conformation of molecules since the area of the central azobenzene core was calculated to be around 0.36 nm^2. After collapse, there was a gradual increase in the surface pressure.

BAM images taken during expansion shows the fibre like pattern formation which is also in consistence with the isotherm corresponding to expansion which shows high hysteresis (Figure 2.4). This prominent hysteresis in the compression-expansion isotherms is most plausibly due to dipolar interactions and π-π interactions associated with the cyanobiphenyl units which lead to a rapid decrease in the surface pressure during expansion.

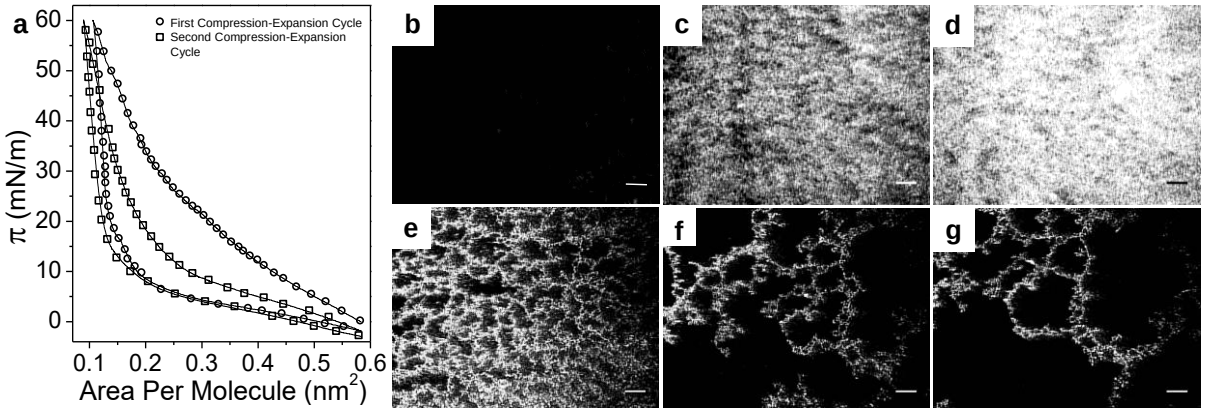

Figure 2.4 (a) The plot showing prominent hysteresis for consecutive compression-expansion π-A_m cycles of compound **3f** at air-water interface. The BAM images of compression for compound **3f** at air–water interface for the A_m values of (b) 0.6 nm^2, (c) 0.4 nm^2 and (d) 0.1 nm^2 (collapsed state). Figure (e), (f) and (g) shows the BAM images of expansion for A_m values of (e) 0.4 nm^2, (f) 0.6 nm^2 and (d) 0.8 nm^2. The scale bar in each image represents 500 μm.

The stability of the film was checked (i) by measuring the equilibrium surface pressure at a constant area and (ii) by compressing the film to a target pressure of 35 mN/m and then monitoring the change in the A_m as a function of time (see appendix I, Figure A6, A7). In both ways, the film was found to be stable for over 30 minutes with no change in the A_m as a function of time or surface pressure which suggested that film was stable to carry out deposition at air-solid interfaces.

The film was first transferred onto a hydrophilic mica substrate and was studied using AFM. Topography image of the LB film transferred onto a mica substrate at a surface pressure of 35 mN/m is shown in Figure 2.5. In less dense areas, the topography showed a uniform film with a height of about ~2.1 nm. This value corresponds to the estimated height of the

molecules when four cyano groups are in contact with the water subphase and the alkyl chains together with the azobenzene group extrude into the air. The limiting area per molecule calculated from the π - A_m isotherm also indicated similar conformation of the molecule at the interface.

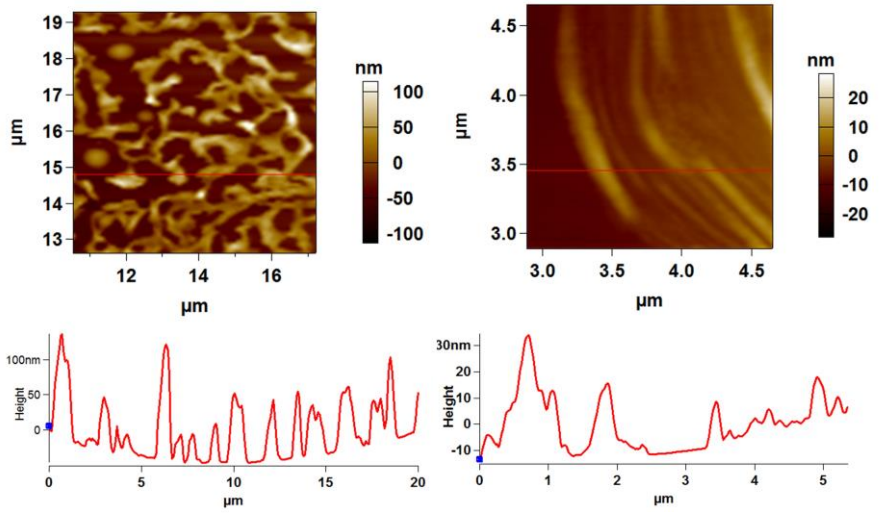

Figure 2.5 AFM topography for film of compound **3f** transferred by LB technique onto hydrophilic mica substrate at target surface pressure (π_t) of 35mN/m showing (a) dense fibres and (b) aligned fibres in less dense area. The respective height profiles corresponding to the lines drawn on the images are shown in the lower panel.

Interestingly, in high density areas the film shows network of thin fibres varying between 2 nm to 80 nm which could be associated with the dipolar interactions and π-π stacking of the cyanobiphenyl and azobenzene units (Figure 2.5a). These thin fibers bundle up to form thick ones. These results when combined with the BAM images during expansion (that shows similar fiber network pattern with a high hysteresis) demonstrated that film at the air-solid interfaces is not a monolayer. Earlier studies on monolayers of 4'-*n*-octyl-4-cyanobiphenyl (8CB) have also shown similar results.[24] The monolayer of 8CB collapses at an A_m of about 0.42 nm^2 per molecule. Below this value of A_m, the monolayer transforms into a trilayer which transforms into a coexisting phase consisting of L1, trilayer and multilayers below an A_m of 0.15 nm^2. The dipole-dipole interaction between the nitrile groups at air-water interface was considered as the main factor attributing to the formation of trilayers and

multilayers. Based on this study, we hypothesized that the strong dipole moment of about ~3.8 Debye of the cyano groups in the biphenyl rings led to substantial dipole-dipole interactions between them which is responsible for the intercalation of the molecules at air-water interface showing fiber like patterns. The exact thickness of the film at air-water interface between the A_m of 0.55 nm^2 per molecule and 0.15 nm^2 per molecule is not known. On further compression, the film forms a comparatively more condensed phase before forming a multilayer of higher thickness at about 0.15 nm^2 per molecule which is also indicated from the bright regions in the BAM images. At higher densities of film at air-water interface, the water layer is covered by a thick layer of oil and this oil-water interface is stabilized by the polar nitrile groups of the **3f** molecules. Thus, the interfacial energy decreases thereby increasing the collapse pressure to 60.55 mN m^{-1}. Such high values of collapse pressures have also been observed for monolayers of lipid molecules such as dipalmitoylphosphatidylcholine (DPPC).[25] From all these above observations, we infer that the π-π interactions between the azobenzene cores together with the dipolar interactions between nitrile groups are responsible for the observed fibre-like patterns at the air-water and air-solid interface.

In the case of hydrophobic silicon substrate, coated with HMDS, two layers of the film (bilayer) get coated in one dipping cycle (i.e. deposition takes place in both downward and upward stroke). Interestingly, the AFM topography of the films showed the formation of nanodroplets (Figure 2.6). The height of the nanodroplets varied between 20-80 nm and did not correspond to the bilayer thickness. The droplets formations with larger heights can be associated with dewetting of the film on hydrophobic silicon. Formations of such kinds of nanodroplets have been observed by other groups in past. For example, Kumar *et al*. demonstrated that the formation of nanodroplets is due to post-transfer reorganization of the film.[4] Their study revealed that the transfer of a thin liquid film to a non-wettable solid substrates leads to formation of unstable film that eventually ruptures to the droplets through spinodal dewetting.[1] Hashimoto and coworkers reported micrometer sized droplet (with controlled diameter and height) formation by dewetting.[26] We believe that a similar mechanism is associated leading to the formation of droplets of larger height with the oligomeric mesogens synthesized in our study.

We further studied the film supported on HMDS-coated silicon with respect to temperature. The study was motivated by two goals. First, we sought to characterize the film at a temperature in which compound **3f** shows the mesophase. As the most intriguing properties of LC materials are exhibited at mesophase, we thought that it would be worth to look the film topography as a function of temperature. Second, by varying temperature, we sought to provide additional insight into the physicochemical phenomena underlying the formation of nanodroplets. Figure 2.6c shows the AFM images of the LB films of **3f** (shown in 2.6a and 2.6b) at 114 °C. This was achieved by heating the film to the isotropic temperature (126 °C) followed by cooling it to the mesophase temperature.

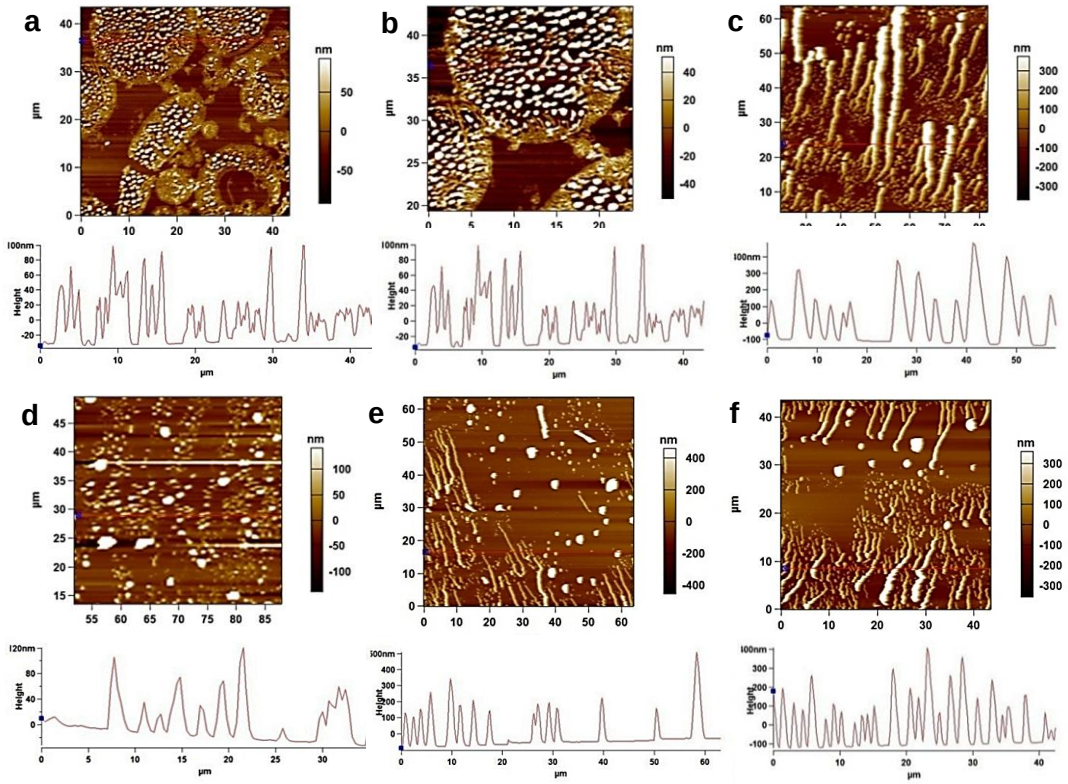

Figure 2.6 AFM topography for layer of compound **3f** transferred by LB technique onto hydrophobic HMDS coated silicon substrate at target surface pressure (π_t) of 35mN/m. (a) LC nanodroplet formation at room temperature as shown in (b). (c) shows formation of well aligned rod like structures formed when compound is in LC (nematic) phase at 115°C. (d) shows that on cooling back to room temperature, it reverts back to nanodroplets. (e) & (f) shows co-existence of rod like structures and nanodroplets at onset.

Interestingly, AFM studies revealed well-defined aligned fibers (in the same direction) of ~20-60 μm at 114 °C. The film was cooled back to room temperature that showed again the formation of small droplets as was seen earlier prior to heating the sample in the film. This result demonstrated that mesophase play an important role in the formation of aligned fibers. We hypothesized that because of inherent orientational order present in the mesophase, molecules are able to self-organize themselves through supramolecular non-covalent interactions. At room temperature, because of the crystalline nature of the molecules the thin film on hydrophobic silicon develops surface fluctuations of various wavelengths (spinodal dewetting as discussed above) and thus become unstable and ruptures in the form of droplets as also evident from the past studies.[4] Further heating to isotropic temperature and cooling back to onset temperature revealed the coexistence of both aligned fibers and the droplets. This result suggested the reversible transformation of the droplets to fibers and *vice versa* in the mesophase and at room temperature, respectively. We believe that the strong supramolecular non-covalent interactions in the nematic mesophase and in order to prevent steric hindrance from each other, these fibers align in the same direction.

2.1.4 Conclusions

In conclusion, the study reported in this chapter is three fold. Firstly, we have synthesized eight new oligomeric mesogens consisting of an azobenzene-based core attached to which are four 4-cyanobiphenyl units *via* flexible alkyl spacers. Among them, compounds having octyloxy and decyloxy spacer showed monotropic N phase. Secondly, the novel mesogenic molecules are amphiphilic and form stable monolayer at air-water interface that has been characterized through surface manometry and BAM. Thirdly, LB films transferred onto freshly cleaved hydrophilic mica substrates showed domains of height corresponding to the height of the molecule showing the formation of monomolecular film. On a hydrophobic silicon substrate, the LB transfer yield a multilayer film which could be attributed to dipolar interactions associated with the cyanobiphenyl units. The film dewets to form nanodroplets that can be attributed to spinodal dewetting. Temperature dependent AFM topography revealed the reversible formation of aligned fibers in the mesophase which provides new approaches to realization of controlling the anisotropic properties of the ordered phase.

2.2 Part B: A new class of triphenylene-based room temperature discotic oligomers exhibiting TNF induced switching of columnar rectangular to hexagonal assemblies

2.2.1 Introduction

Recently, there has been substantial interest in the field of non-conventional low molar mass LCs *i.e.* dimers and oligomers because of their fascinating mesomorphic properties due to restricted molecular motions. These LC oligomers serve as ideal illustrative compounds for polymers due to ease of purification & characterisation and remarkable similarities in their transitional behaviour.[37] The physical properties of these LC oligomers are notably different from their constituent units and they are more prone to form columnar glasses where the alignment of the columns is retained, however, the motion of alkyl chains is frozen.[38] These glasses are mechanically stiff and have potential applications in various technological fields e.g. in the vapour deposition of metal electrodes on very thin aligned films in preparation of light emitting diodes.[39] Therefore, oligomeric discogens possess the combination of desirable alignment properties of monomers with the long-lived glassy state of the polymers.[40]

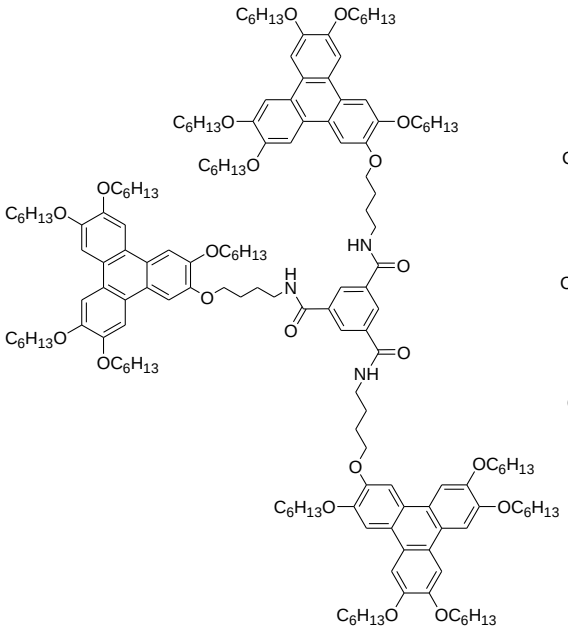

6

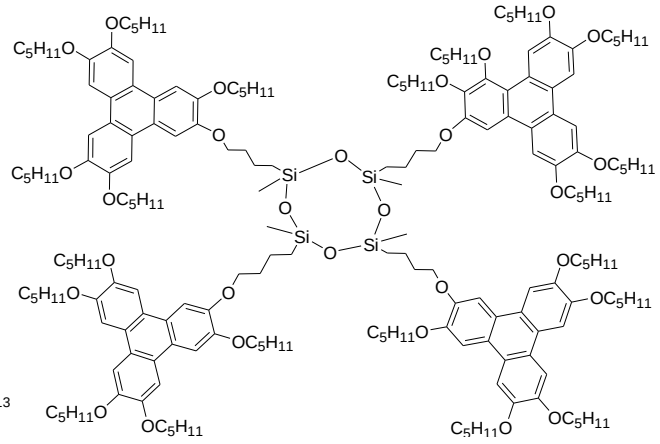

7

Till date, triphenylene (TP) is the most widely studied scaffold in the family of discotic LCs and thus its derivatives are ideal workhorses for analysing the properties of discotic LC oligomers and polymers as TP is easy to obtain in both mono as well as bifunctional forms.[41-47] Triphenylene oligomers have drawn particular attention as they show improved optical and electronic properties.[48-58] They are generally constructed by grafting triphenylenes onto various functional frameworks. Most workers have concentrated on linear & star-shaped oligomers containing three mesogenic moieties (e.g. **6**) but there has also been interest in star-shaped oligomers containing four mesogenic moieties connected to a common nucleus such as compound **7**.[59-65]

2.2.2 Objective

In this study, we have designed new oligomeric mesogens **8** in which azobenzene was chosen as rigid core attached to which are four TP units *via* flexible alkyl spacers. LCs comprising photo-responsive moieties such as azobenzene have been established as promising materials for applications in photomechanics, instant displays, reversible holographic storage and digital storage due to their high resolution and sensitivity. Therefore, azobenzene will not only act as a linker for the triphenylene cores but can also impart interesting properties to these oligomers due to its photoresponsive behaviour. We have further aimed to introduce 2, 4, 7-trinitrofluorenone (TNF) in the columnar assemblies of these oligomers. TNF which is an electron-acceptor moiety can form charge transfer (CT) interactions which can induce, stabilize as well as extend the mesomorphic range of the native compound.[30-33]

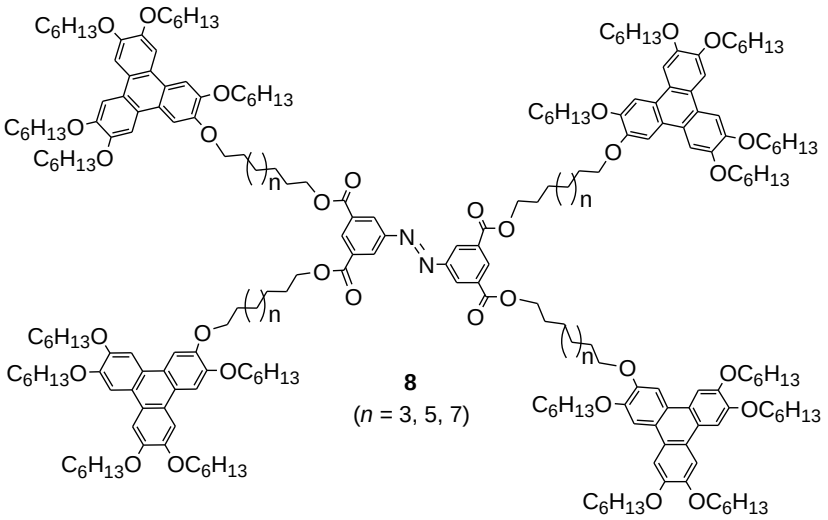

8
(*n* = 3, 5, 7)

Not only this, it can also improve the charge carrier mobilities by facilitating charge transfer and thus preventing recombination. This kind of oligomer can be aligned easily like monomers and are also prone to form glassy states on cooling which is technologically very important. Therefore, the CT complexes of these oligomeric systems containing four TP connected to an azobenzene core will be interesting from the device point of view.

2.2.3 Results and Discussion

2.2.3.1 Synthesis and characterization

The target compounds were obtained by following the synthetic route as illustrated in scheme 2.2. Synthesis of compounds **10**, **11**, **12** and **5** has been described in the earlier literature reports.[66-69] The final compounds **8** were prepared by reacting the triphenylene derivative **12** and azobenzene tetracarboxylic acid **5** in presence of potassium hydroxide and tetraoctylammonium bromide using water as solvent under reflux for around 7 hours (see experimental section for details). All the compounds were characterised by ^{1}H NMR, ^{13}C NMR, IR, UV-vis and elemental analysis (see appendix I, Figure A8-A15).

2.2.3.2 Thermal Behavior

Thermal behaviour of all the compounds was investigated with the help of Polarizing Optical Microscopy (POM) and Differential Scanning Calorimetry (DSC). Compound **8a** was a transparent glassy material and displayed a glass to isotropic transition at 77 °C on heating, whereas, on cooling it remained isotropic till room temperature. For compounds **8b** and **8c**, the presence of thermotropic LC phase at room temperature was confirmed with the highly birefringent textures and their shearability under polarizing optical microscopy (POM) observation (Figure 2.7). Compounds **8b** & **8c** exhibited isotropization at 40.3 °C & 43.5 °C respectively. However, on further cooling, the mesophase did not appear immediately till room temperature (appendix I, Figure A16). This was a general observation for all the compounds and the mesophase only reappears after keeping the isotropic melt for few hours. A possible explanation for this behaviour could be that the triphenylene molecules are connected *via* relatively short spacers to a rigid core and do not have enough freedom to self-assemble into columns on subsequent cooling from isotropic state.

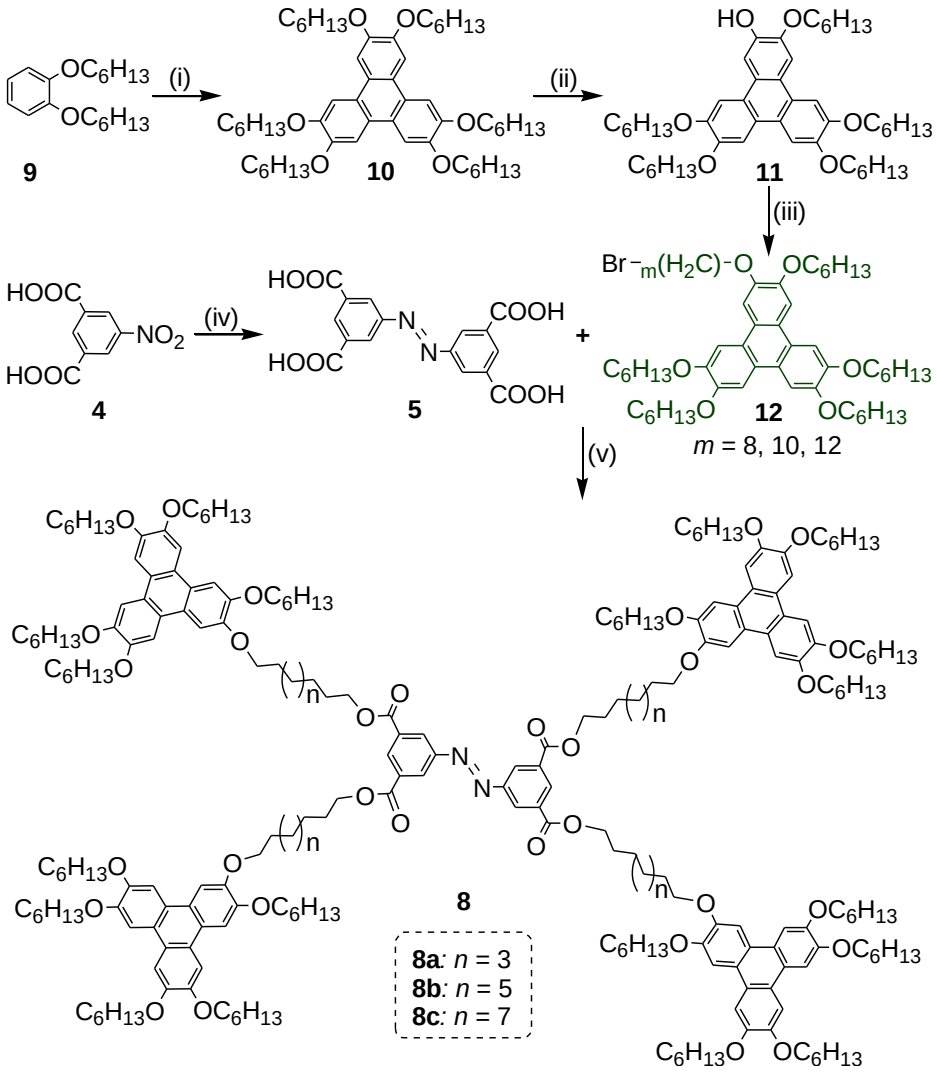

Scheme 2.2 Synthesis of the target compounds **8**. Reagents and conditions: (i) $FeCl_3$, CH_2Cl_2, H_2SO_4, RT, 1 h, 70%; (ii) Cat-B-Br, CH_2Cl_2, RT, 48 h, 40%; (iii) Cs_2CO_3, KI, butanone, 80 °C, 18 h, 85%; (iv) NaOH, dextrose, 80 °C, HCl, 70%; (v) KOH, H_2O, TOAB, reflux, 5h, 50%.

2.2.3.3 X-ray Diffraction Studies

To further explore mesophase behaviour of the synthesized compounds SAXS/WAXS experiments were carried out. POM observations revealed that compounds **8b** & **8c** were showing LC behaviour at room temperature whereas compound **8a** was glassy in nature. However, in XRD studies it was found that diffractograms of all the three compounds were similar (Figure 2.8).

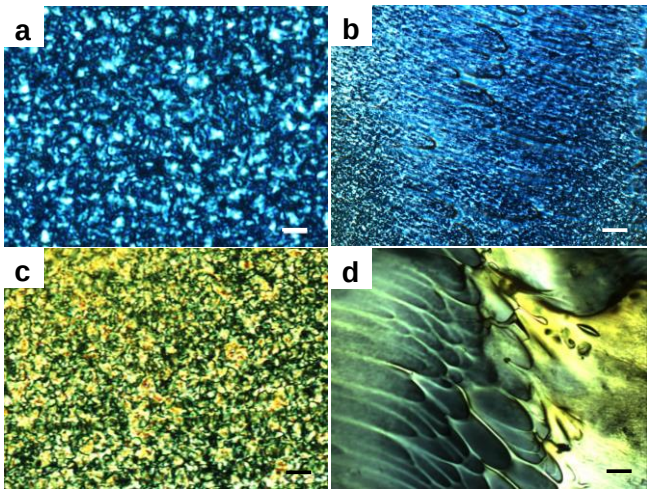

Figure 2.7 Optical photomicrograph of compound (a) **8b** and (c) **8c** obtained with a polarized optical microscope at 25 °C (crossed polarizers, magnification × 50). (b) & (d) represent the respective textures after shearing the film (scale bar = 10 μm).

This indicates that the self-assembly of molecules in **8a** is similar to that in **8b** and **8c**, however, the motion of alkyl chains is frozen in **8a**. In-order to find out the detailed structure of the assembly of compound **8**, we have carried out a thorough analysis on diffractogram of compound **8c**. This analysis could explain the structure of assembly of compound **8b** and **8a**, because the diffraction pattern for both of them are similar to **8c**.

The diffraction pattern of compound **8c** exhibits many peaks as shown in Figure 2.8. In particular, it showed h_c peak of spacing of about 3.93 Å in the wide angle region which appears due to π-π interaction and correspond to face to face separation between TP groups. Hence, it confirms the columnar nature of the structure of assembly of compound **8c** and indicates that TP cores are assembled on top of each other to form columns which are further arranged on a 2D lattice. This h_c peak gives the value of one of the lattice parameter, *i.e.*, c = 3.93 Å. However, the reported face-to-face distance between two π-conjugated molecules is in the range of 3.5-3.7 Å which suggests that the TP cores are packed with a tilting angle of 23.37 ± 3.69 degrees with respect to the columnar axis. The XRD pattern further exhibit four peaks in the small angle region. Interestingly, the *d*-spacing of the first and third peak as well as that of second and fourth peak are in the ratio of 1:1/2, indicating the lamellar nature of the structure in two different directions.

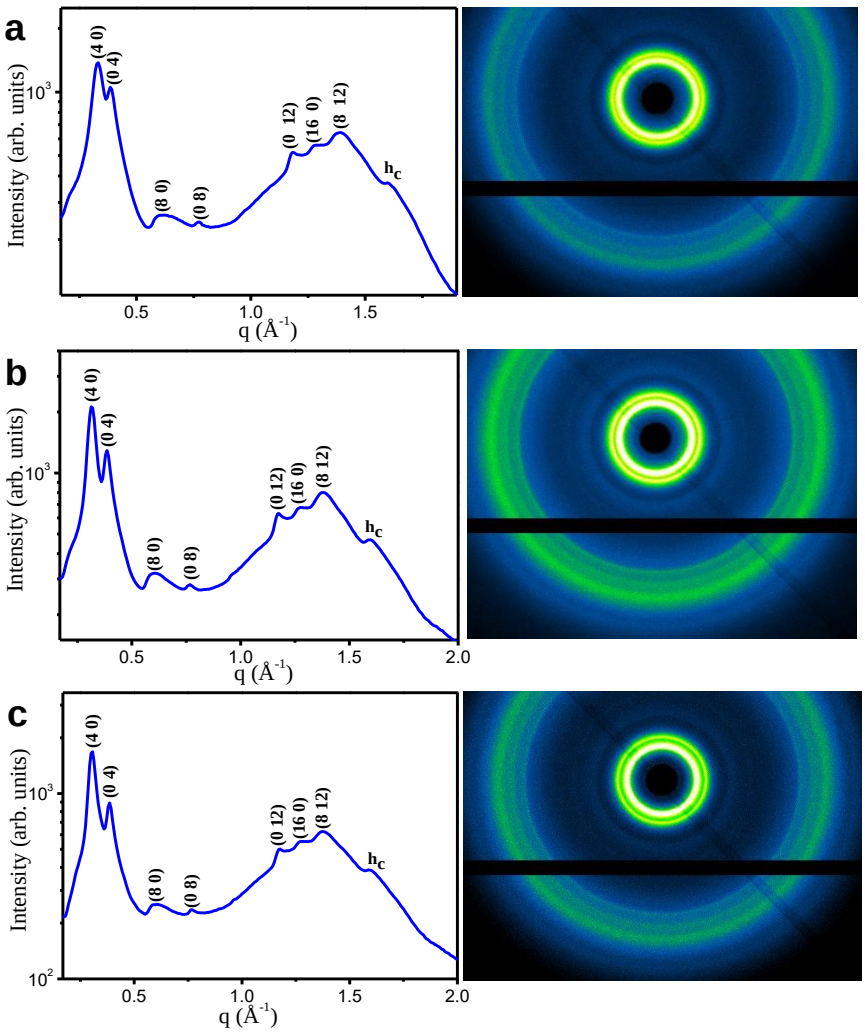

Figure 2.8 X-ray diffraction pattern corresponding to mesophases of compound (a) **8a**, (b) **8b** and (c) **8c** indexed on columnar rectangular (Col_r) phase. Right panel shows the respective 2D diffraction patterns.

In-order to understand the detailed arrangement of columns on 2D lattice and to facilitate their indexing, grazing-incidence wide-angle and small-angle X-ray scattering (GIWAXS/SAXS) experiments were also carried out on oriented thin films obtained through mechanical shearing on an ITO coated glass substrate. The GISAXS pattern of the sample showed partially aligned peaks in the small angle region (Figure 2.9a). Azimuthal plot of the first two peaks of the small angle shows that they are orthogonal to each-other (Figure 2.9b). Further, each of the first two peaks is two-fold confirming that the structure is rectangular. Therefore, combining the information from SAXS/WAXS and GISAXS, it is clear that TP

cores massed on top of each other and form columns and the arrangement of columns on 2D lattice exhibit lamellar ordering in two orthogonal directions in the columnar plane. Based on above analysis, a possible model representing the self-assembly in compounds **8** is shown in Figure 2.10.

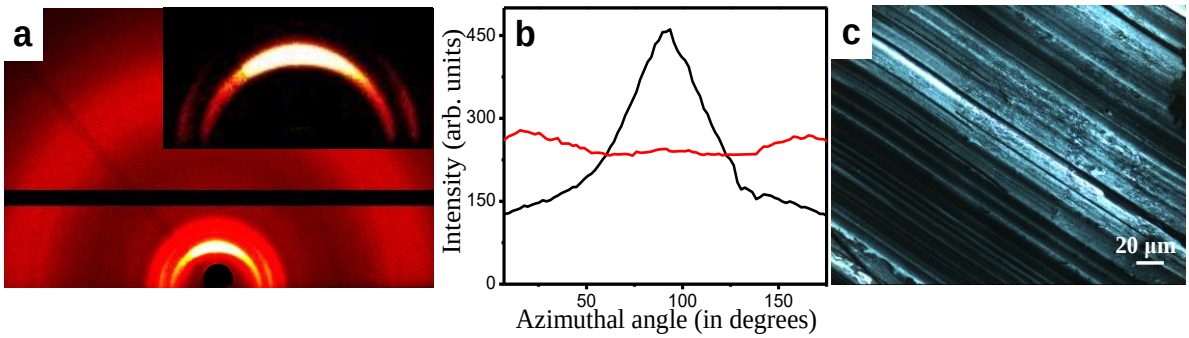

Figure 2.9 (a) GIWAXS & GISAXS (inset) pattern from a thin oriented film obtained through mechanical shearing of compound **8c** on ITO coated glass substrate. (b) Azimuthal plot of the first two peaks, (40) and (04). Both peaks are orthogonal to each other and each one is twofold in nature. (c) Optical micrograph of the oriented film of compound **8c** as viewed between crossed polarizers.

The compounds **8** are discotic mesogenic quadric based on TP linked with azobenzene group via flexible alkyl spacers. The compound could be modelled as four TP discs (blue in colour) tethered *via* flexible alkyl chains to an azobenzene group (red in color). The model shows that the centre of the azo group forms the rectangular lattice (Figure 2.10). The rectangle with black boundary shows the unit cell of the lattice. The unit cell also exhibits the lamellar of the column layers in two orthogonal directions as suggested by SAXS/WAXS and GISAXS analysis. The lamellar periodicity is $a/4$ and $b/4$ (where a and b are the lattice parameters of rectangular lattice) in two orthogonal directions of rectangle, respectively, indicating that the indexes of first two peaks would be (40) and (04) and also suggests that the allowed reflection would be h, $k = 4n$ (Figure 2.11a). Other reflection of un-oriented pattern is indexed accordingly and structure of the assembly is Col_r. The d-spacing are calculated according to equation $1/{d_{cal}}^2 = h^2/a^2 + k^2/b^2$ where h and k are the miller indices. The calculated lattice parameters are a = 81.28 Å and b = 65.20 Å. The details are summarized in

the Table 2.2. The calculated correlation lengths along the *a* and *b* axis of the rectangular lattice *i.e.* corresponding to (40) and (04) peaks are 124.27 Å and 111.84 Å respectively. The corresponding number of correlated columns are about 6 and 7, respectively. The calculated core-core correlation length corresponding to h_c peak along the column (*c*) axis is 23.23 Å which is equivalent to about 6 correlated cores (Table 2.2).

Table 2.2 The observed and calculated d-spacings and planes, correlation length of the diffraction peaks of the columnar rectangular (Col_r) phase observed in compound **8c** with the lattice parameters: *a* = 81.28 Å, *b* = 65.20 Å and *c* = 3.93 Å. d_{exp} is the observed *d*-spacing. d_{cal} is the calculated d-spacing according to formula $\frac{1}{{d_{cal}}^2} = \frac{h^2}{a^2} + \frac{k^2}{b^2}$. ξ is the correlation length.

Planes (hkl)	d_{exp} (Å)	d_{cal} (Å)	ξ	ξ/ dexp
4 0	20.32	20.32	124.2	6.11
0 4	16.30	16.30	111.8	6.86
8 0	10.25	10.16		
0 8	8.18	8.15		
12 0	6.53	6.77		
0 12	5.40	5.43		
16 0	4.95	5.08		
8 12	4.57	4.79		
h_c	3.93		23.23	5.91

As mentioned earlier, the diffraction patterns of compounds **8b** and **8a** are very similar to **8c** and explained similarly (see appendix I, Table A1-A2). Interestingly, the lattice parameter '*a*' was found to be less than **8c** in **8b** and even lesser than **8b** in compound **8a** which is obvious because spacer length in **8a** is shorter than **8b** which is further smaller than **8c**. However, the lattice parameters, *b* and *c* remain constant in compounds **8a** and **8b**. The correlation lengths corresponding to (40) and (04) peaks were found to decrease in **8b** and **8a** from its values in **8c**.

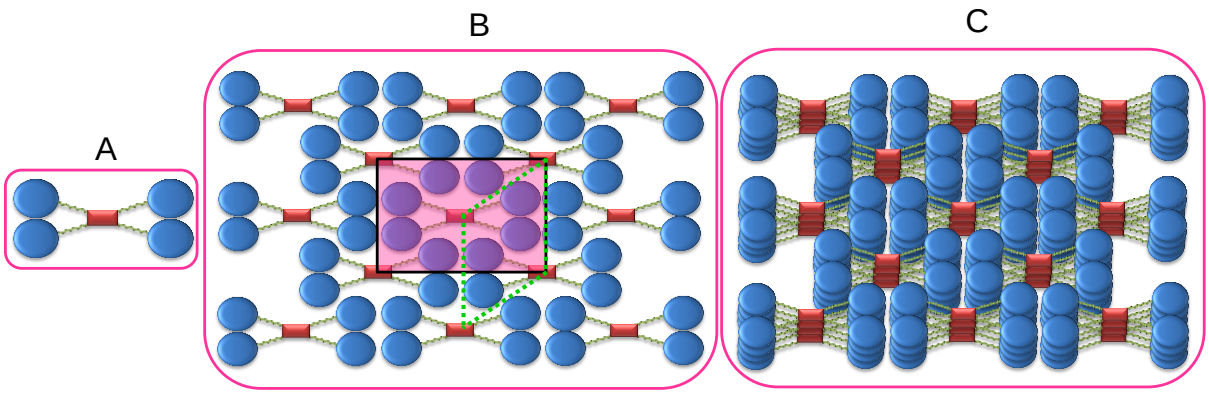

Figure 2.10 Schematic of (A) the structure of compound **8**, modelled as four triphenyl (TP) discs (in blue colour) connected with azobenzene group (in red color) *via* flexible spacers. (B) A possible arrangement of columns on 2D rectangular lattice where centre of azo group forms a rectangular lattice. Box in the black colour show the unit cell of rectangular lattice. Addition of TNF to compound **8**, transforms the rectangular lattice into hexagonal lattice. Green dotted parallelogram with modified dimensions represents the unit cell of the hexagonal lattice. (C) 3D arrangement of the structure representing the columnar rectangular (Col_r) phase.

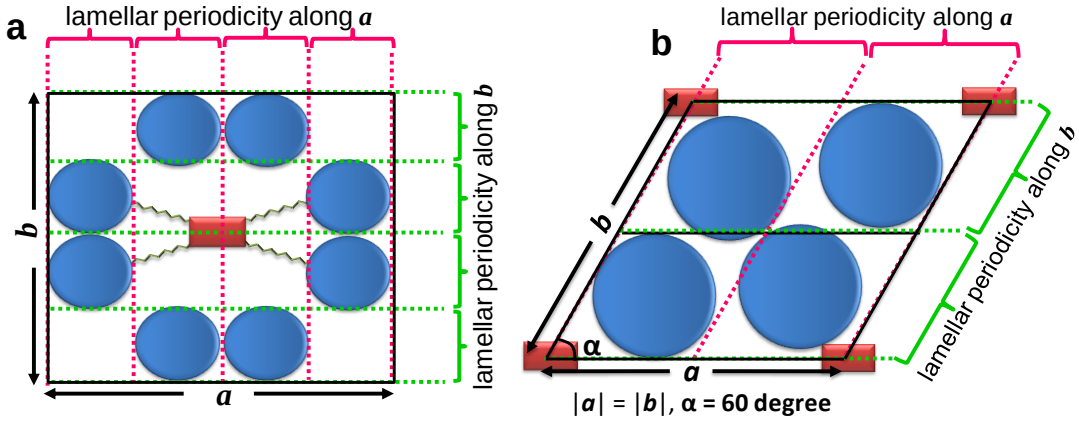

Figure 2.11 A schematic of unit cell of (a) columnar rectangular (Col_r) phase and (b) columnar hexagonal (Col_h) phase. Rectangular and hexagonal unit cell exhibit the lamellar of the column layers. The lamellar periodicities are *a*/4 and *b*/4 along the direction of *a* and *b*, respectively of the Col_r phase. The lamellar periodicity is a/2 along both the direction of Col_h phase.

The corresponding values are 101.67 Å (5 correlated columns) and 93.20 Å (about 6 correlated columns), respectively in case of compound **8b** and 78.76 Å (about 4 correlated columns) and 69.03 Å (about 4 correlated columns) for compound **8a**. Increase in correlation length along *a* and *b* direction from **8a** to **8c** attributes to the stabilization of the rectangular phase with increasing spacer length. Although, the core-core correlation length remains the same in compound **8a-c**.

2.2.3.4 Charge-transfer Complexes

Further, we aimed to improve the mesomorphic properties of these compounds by increasing molecular interactions. For this purpose, we have introduced TNF which is an electron-acceptor moiety into the columnar matrix. CT interaction of TNF with TP derivatives has been very well established. It can induce, stabilize as well as extend the mesomorphic range of the native compound.[70-73] Not only this, the introduction of dopants such as TNF moieties which act as acceptor molecules into electron rich discotic systems can improve the charge carrier mobilities by facilitating charge transfer and thus preventing recombination. This efficient charge separation is generally inhibited by strong electron-hole recombination which decreases the efficiency of electronic devices such as photovoltaic solar cells. However, when acceptor units are introduced into electron rich donor molecules, dissociation can take place at the donor-acceptor interface. In this process, intermediate excited charge-transfer (CT) states are formed where the holes are present on the donor and electron at the acceptor molecule. Thus, on applying electric field the electrical conductivity rises due to an increase in charge migration.[74-77]

CT complexes of synthesized compounds **8** were prepared with TNF in the molar proportions of 1:1, 1:2, 1:3 and 1:4 [oligomer: TNF] respectively (see experimental section for details). Interestingly, all the complexes displayed enantiotropic LC phase behaviour at room temperature which was confirmed from characteristic birefringent textures with shearability of the compound at room temperature. On cooling from the isotropic phase, these complexes displayed focal conic textures typical of a columnar mesophase (Figure 2.12, appendix I Figure A17). The precise transition temperatures and associated enthalpy changes for all the complexes are listed in Table 2.3 (appendix I, Figure A18). It was found that the doping

resulted in mesophase induction for the complexes of compound **8a** which was a glassy columnar in its pure state. Also, clearing temperatures of all the complexes increased drastically as compared to that of the undoped compounds. To confirm the mesophases and also for quantitative comparison, we have carried out XRD studies on these complexes. Surprisingly, the mesophase switched from rectangular in case of pure compounds to hexagonal phase in case of CT complexes as evident from XRD studies (*vide infra*). 1:1 complexes displayed an intermediate phase between columnar rectangular and hexagonal states and were completely transformed into columnar hexagonal (Col_h) in case of 1:2 complexes. Moreover, 1:2 CT complexes of all the compounds were found to be most stable as their clearing temperatures were highest compared to other complexes (Table 2.3).

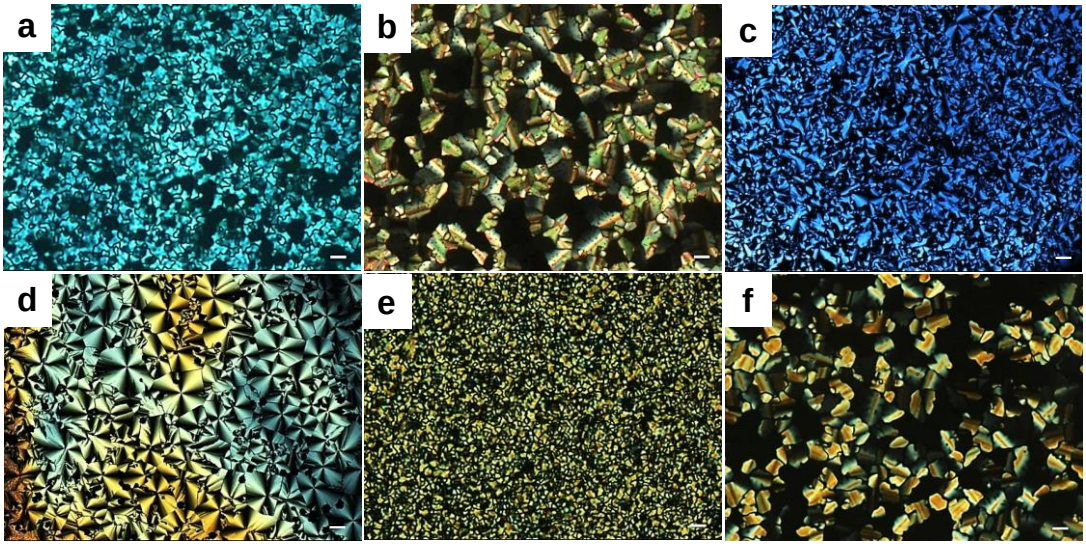

Figure 2.12 Optical photomicrographs of the doped compounds (a) **8a**: TNF [1:1] at 30.4 °C, (b) **8a**: TNF [1:2] at 121.3 °C, (c) **8b**: TNF [1:1] at 45.6 °C, (d) **8b**: TNF [1:2] at 65.2 °C, (e) **8c**: TNF [1:1] at 54 °C and (f) **8c**: TNF [1:2] at 100.2 °C as obtained on cooling from isotropic through a polarized optical microscope with crossed polarizers (scale bar = 20 μm).

We present here a detailed analysis on CT complexes of compound **8c**. The CT complexes of compounds **8a** & **8b** show similar behaviour to that of **8c**. Addition of TNF to compound **8c** leads to a stable Col_h phase. However, for the molar ratio (**8c**: TNF) 1:1 it exhibits a mixed phase which transformed into a stable Col_h phase for the molar ratio 1:2 and is retained for ratios 1:3 and 1:4 (Figure 2.13). The observation of two peaks in the small angle region with

d-spacing in ratios of $1:1/\sqrt{3}$ confirms a 2D hexagonal phase and h_c peak in the wide-angle region indicates the columnar nature of the structure.

Table 2.3 Thermal behaviour of the CT complexes of compounds **8** with TNF.[a,b,c]

Complexes	Heating Scan	Cooling Scan
8a: TNF [1:1]	Col 80 (1.28) I	I 67 Col
8a: TNF [1:2]	Col_h 135.7 (3.40) I	I 125.2 (6.16) Col_h
8a: TNF [1:3]	Col_h 134.5 (3.15) I	I 121.9 (4.98) Col_h
8a: TNF [1:4]	Col_h 118.9 (1.26) I	I 111.32 (2.20) Col_h
8b: TNF [1:1]	Col 100 I	I 83 Col
8b: TNF [1:2]	Col_h 136.9 (0.41) I	I 109 (1.28) Col_h
8b: TNF [1:3]	Col_h 132.6 (0.68) I	I 117Col_h
8b: TNF [1:4]	Col_h 130 I	I 119 Col_h
8c: TNF [1:1]	Col 100 I	I 70 Col
8c: TNF [1:2]	Col_h 121.6(2.23) I	I 103.4 (3.32) Col_h
8c: TNF [1:3]	Col_h 118.3(1.64) I	I 99.63 (2.35) Col_h
8c: TNF [1:4]	Col_h 91.98(0.51) I	I 86 (0.55) Col_h

[a]Phase transition temperatures in °C and transition enthalpies in kJ mol^{-1} (in parentheses).

[b]Phase assignments: Col = Columnar, Col_h = Columnar hexagonal, I = isotropic.

[c]For some of the complexes, transitions were not observed in DSC, however it was confirmed from POM studies.

Thus, the addition of TNF to compound **8c** leads to changes in the structure of assembly and Col_r phase is transformed into Col_h phase. In-order to get the most possible indexing of the hexagonal phase, the unit cell is derived from the model of the rectangular lattice as shown in figure 2.11b**.** The unit cell exhibits the lamellar ordering of the column layers along the two directions of hexagonal lattice with the periodicity a/2 which suggest that the allowed reflection would be *h*, *k* = 2*n*. Hence, the indexes of the first two peaks of small angle region are (20) and (22) respectively. The lattice parameter, *a* is calculated by using the relation $a = 4\, d_{20}/\sqrt{3}$. The calculated value of the lattice parameter, *a* is 43.42 Å for the complex **8c**: TNF = 1:2 and h_c peak gives the value of other lattice parameter *i.e.* c = 3.74 Å. Further, one

broad peak, h_a of spacing 4.85 Å was also found in wide angle region which is mainly originated due to alkyl chain-chain correlation (Table 2.4). The lattice parameter, *a* (column-column separation) as well as *c* (core-core separation) is found to decrease with increasing molar ratio of TNF (Table 2.5). The calculated column-column correlation length corresponding to (20) peak is ~224 Å for complex **8c**: TNF = 1:2 which is equivalent to about 12 correlated columns. The calculated core-core correlation length was found to be approximately ~43 Å, corresponding to about 11 correlated cores which is double of the value as observed in the pure compound **8c**. The number of correlated cores remains same with increasing molar ratio of TNF (Table 2.5).

Interestingly, addition of TNF to compound **8c** reduces the tilting angle of TP core with respect to the columnar axis from 23.37 ± 3.69 degrees to 9.45 ± 9.45 degrees and helps to relax the TP cores in columns leading to the transformation from Col_r to Col_h phase (Figure 2.13). Effect of introducing TNF in the compounds **8a** and **8b** is very similar to that of **8c** and can be explained similarly (appendix I, Figure A19-A21, Table A3-A4).

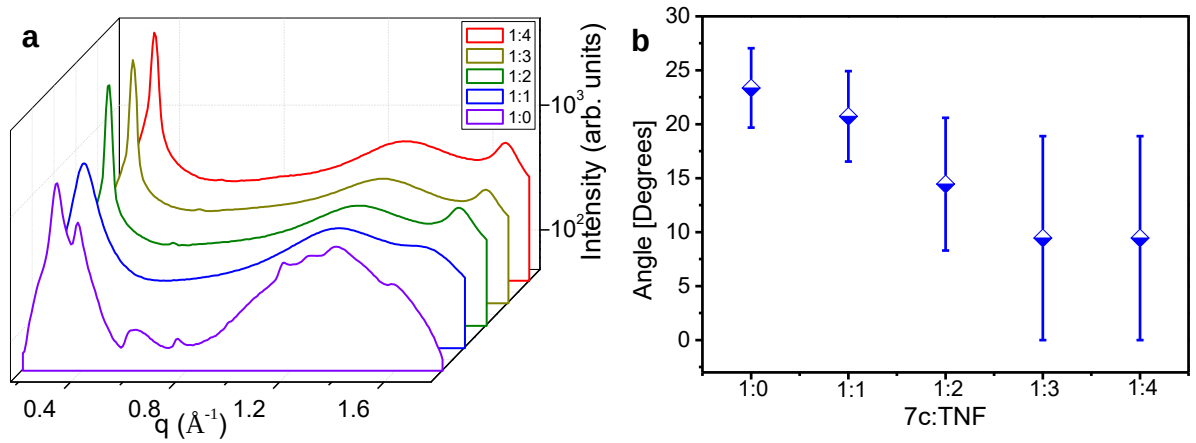

Figure 2.13 (a) X-ray diffraction pattern of compound [**8c**: TNF] = 1:0 to 1:4 which describes the changeover of columnar rectangular (Col_r) phase into columnar hexagonal (Col_h) phase on increasing the TNF concentration. (b) Variation of tilt angle (of the TP cores in column with respect column axis) with increasing concentration of TNF along with error bar.

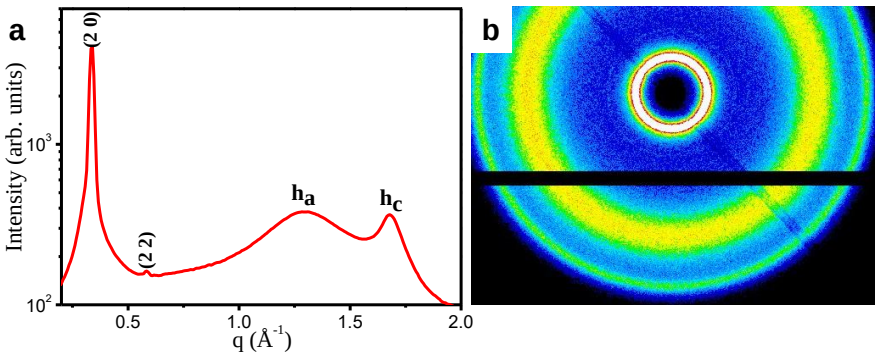

Figure 2.14 (a) X-ray diffraction pattern of compound **8c**: TNF = 1:2 with indexing on the columnar hexagonal (Col_h) phase. (b) Corresponding 2D diffraction pattern in the mesophase.

Table 2.4 The observed and calculated *d*-spacings and planes, correlation length of the diffraction peaks of the columnar hexagonal (Col_h) phase observed in compound **8c**: TNF = 1:2 with the lattice parameters: *a* = 43.42 Å and *c* = 3.74 Å. d_{exp} is the observed *d*-spacing. d_{cal} is the calculated d-spacing according to formula: $\frac{1}{{d_{cal}}^2} = \frac{4}{3}(\frac{h^2+h\,k+k^2}{a^2})$ for hexagonal phase. ξ is the correlation length.

Planes (hkl)	d_{exp} (Å)	d_{cal} (Å)	ξ	ξ/ d_{exp}
2 0	18.80	18.80	223.6	11.89
2 2	10.78	10.86		
h_a	4.85			
h_c	3.74		43.01	11.57

A thorough literature survey revealed that there are two possible ways in which TNF can be accommodated in the columnar assembly.[16, 17, 18] One of them is side by side manner and the other is in intercalated fashion. We believe that our study supports that TNF molecules are more likely to be present in an intercalated fashion rather than side by side manner which is based on the following facts: 1) Tilt angle of columns with respect to columnar axis in compound **8** exhibiting Col_r phase decreases on transformation to Col_h phase on introducing TNF. Further, tilt angle also decreases with increasing molar ratio of TNF.

Table 2.5 Variation of different observed and calculated lattice parameters and corresponding correlation lengths for compounds **8** and their mixtures with TNF.

a

Compound/ Mixtures	**8a**	**8a**:TNF [1:1]	**8a**:TNF [1:2]	**8a**:TNF [1:3]	**8a**:TNF [1:4]
Phase	Col_r	Mixed	Col_h	Col_h	Col_h
Lattice parameter: 2D (a, b) &	(77.28, 65.20)	--	40.34	40.22	39.58
Column-Column correlation length (Å)	(78.76, 69.03)	--	223.68	223.68	199.71
No. of correlated columns	(4.09, 4.23)		12.80	12.84	11.65
Core-Core correlation length (Å)	23.23	29.43	43.01	46.60	46.60
No. of correlated cores	5.23	7.68	11.50	12.60	12.53

b

Compound/ Mixtures	**8b**	**8b**:TNF [1:1]	**8b**:TNF [1:2]	**8b**:TNF [1:3]	**8b**:TNF [1:4]
Phase	Col_r	Mixed	Col_h	Col_h	Col_h
Lattice parameter: 2D (a, b) &	(80.26, 65.20)	--	41.90	41.52	40.60
Column-Column correlation length (Å)	(101.67, 93.20)	--	223.68	223.68	199.71
No. of correlated columns	(5.06, 5.72)		12.33	12.44	11.65
Core-Core correlation length (Å)	23.23	29.43	43.01	46.60	46.60
No. of correlated cores	5.91	7.68	11.57	12.53	12.53

c

Compound/ Mixtures	**8c**	**8c**:TNF [1:1]	**8c**:TNF [1:2]	**8c**:TNF [1:3]	**8c**:TNF [1:4]
Phase	Col_r	Mixed	Col_h	Col_h	Col_h
Lattice parameter: 2D (a, b) &	(81.28, 65.20)	--	43.42	41.9	42.1
Column-Column correlation length (Å)	(124.27, 111.84)	--	223.68	223.68	199.71
No. of correlated columns	(6.11, 6.86)		11.89	12.33	10.95
Core-Core correlation length (Å)	23.23	26.62	43.01	46.60	46.60
No. of correlated cores	5.91	7.68	11.57	12.53	12.53

2) The calculated intercolumnar and intracolumnar correlation lengths in the Col_h phase were found to be approximately double of the values observed for Col_r phase, confirming that the

addition of TNF into compound **8** significantly increases the ordering in the system. Moreover, the calculated volume of the unit cell of Col_r lattice is about 20,826 $Å^3$ (for compound **8c**) which contains about two oligomers (Figure 2.11a). However, the calculated volume of the unit cell of Col_h lattice is about 6,106 $Å^3$ (for compound **8c**: TNF = 1:2) which accommodates nearly one oligomeric unit (Figure 2.11b). Therefore, the available volume per molecule in the Col_h phase is significantly less in comparison to Col_r phase which indicates that the TNF molecule will most likely not arrange in the side by side fashion, due to lack of enough gap between column to accommodate TNF molecules. Further, the probability of TNF molecules being present in the fluid chain matrix can also be ignored here because that will randomise the system and hence reduce the correlation length which is in direct conflict with our experimental observations. Hence, TNF molecules are most possibly arranged in the intercalated manner. Moreover, TNF molecule can form a charge complexation with TP moiety, thus leading to an increased ordering along the column axis which was indeed observed in our studies. Charge complexation also relaxes the column and reduces the tilt angle which helps the columns to be more symmetric and arrange on 2D hexagonal lattice with significant planar ordering as seen. Therefore, all these observations support an intercalated arrangement of TNF molecules.

2.2.3.5 Photophysical & Electrochemical Studies

For estimation of electrical band gap, the electrochemical behaviour of compound 7c was studied by cyclic voltammetry of 0.001 M solution in 0.1 M of tetrabutylammonium perchlorate (TBAP) as a supporting electrolyte in dry dichloromethane (Figure 2.15). For these studies, a 0.1 M solution of tetrabutylammonium hexafluorophosphate was used as supporting electrolyte in dichloromethane. A single compartment cell fitted with $Ag/AgNO_3$ reference electrode, platinum wire counter electrode and glassy carbon working electrode was used for experiment. The reference electrode was calibrated with the ferrocene/ferrocenium (Fc/Fc^+) redox couple (absolute energy level of 4.80 eV to vacuum, see appendix). The cyclic voltammogram was recorded with a scanning rate of 0.1 V/s. For Fc/Fc^+, E_{red} and E_{oxd} were found to be -0.90 and 0.84 V respectively. The half-wave potential of the ferrocene/ferrocenium (Fc/Fc^+) redox couple was found to be 0.4335 V by the following relation:

$$(E_{1/2,\ Fc/Fc^{+}}) = (E_{\text{anodic peak potential}} + E_{\text{cathodic peak potential}})/2 = (0.525 + 0.342)/2 = 0.4335\ V$$

Compound **8c** displayed reversible oxidation and reduction curves as indicated from its anodic and cathodic peak potential responses.

The HOMO and LUMO energy levels were calculated using the formula:

$$E_{HOMO} = -\ (E_{oxd,onset} - E_{1/2,\ Fc,\ Fc^{+}} + 4.8)\ eV$$

$$E_{LUMO} = -\ (E_{red,onset} - E_{1/2,\ Fc,\ Fc^{+}} + 4.8)\ eV$$

The band gap was estimated using the relation:

$$\Delta E_g = E_{HOMO} - E_{LUMO}$$

The HOMO and LUMO energy levels were estimated to be -5.82 and -2.62 eV, respectively. The electrical band gap was calculated to be 3.20 eV. The optical band gap calculated from the red edge of the absorption spectra for compounds 7 was around 2.30 eV which is much lesser as compared to electrical band gap.

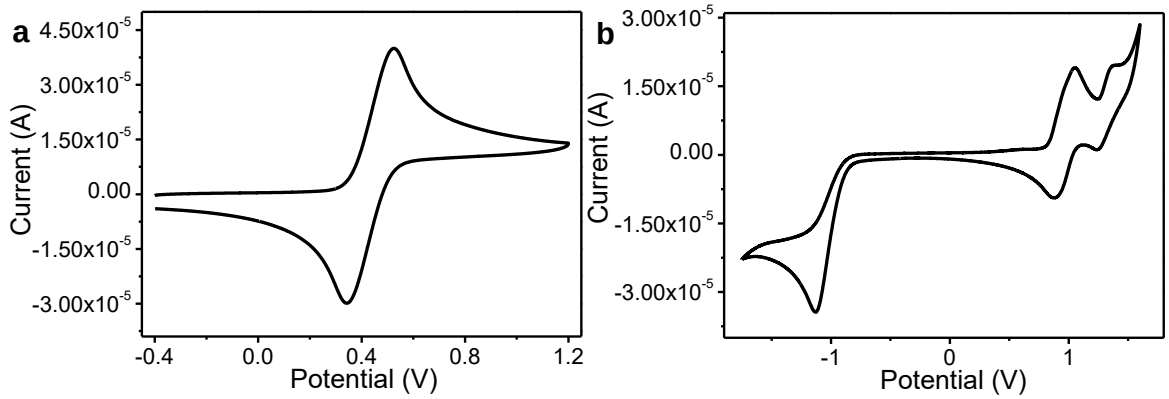

Figure 2.15 (a) Cyclic voltammogram of ferrocene in anhydrous dichloromethane solution of tetrabutylammonium hexafluorophosphate (0.1 M). (b) Cyclic voltammogram of compound **8c** in anhydrous dichloromethane solution of tetrabutylammonium hexafluorophosphate (0.1 M) at a scanning rate of 0.5 mV/s.

We did not observe any photoisomerisation effects (even in dilute solutions) in these oligomers which could be ascribed to the restricted rotation of the photoresponsive azobenzene core as it is tethered to four triphenylene units.

2.2.4 Conclusions

Triphenylene-based oligomeric LCs in which TP units were connected to an azobenzene core have been synthesized and characterized using well known characterization techniques. The compounds with spacer length *m* = 10, 12 exhibited LC properties even at room temperature as confirmed from POM and XRD studies. Compounds with spacer lengths of *m* = 8 displayed a columnar glassy state. Interestingly, the transition from Col_r to Col_h phase was observed on introducing the TNF moiety into columnar self-assemblies of these compounds. These kinds of oligomeric LCs generally possess intermediate properties between that of the monomeric LCs and those of the polymeric LCs. In addition, the observation of mesophase at room temperature and increased charge hopping arising from the donor-acceptor charge transfer complexes makes them very useful for device applications. We have also demonstrated the methodology to control self-assembly of columnar mesophase which is required for certain device applications.

2.3 Experimental Section

2.3.1 Synthesis of compound 3a The starting material azobenzenetetracarboxylic acid was synthesized using the procedure reported in the literature.[23] For the synthesis of the target material, azobenzenetetracarboxylic acid (1 equivalent) was dissolved in KOH solution so that the pH of the solution became about 8-9. To that solution, the corresponding ω-bromo terminated cyanobiphenyl precursor (6 equivalents) and 100 mg of tetraoctyl ammonium bromide (TOAB) were added. The reaction mixture was refluxed under vigorous stirring for 5-6 hours. After that the reaction mixture was cooled to room temperature and extracted with chloroform. The organic layer was separated, washed with brine and dried over anhydrous sodium sulphate. The chloroform was removed by rotary evaporation and the resulting residue was purified by repeated column chromatography over silica gel using chloroform and hexane as eluent to yield compound **3a**. ^{1}H NMR (400 MHz, $CDCl_3$, δ in ppm): 8.85-

8.80 (m, 6H), 7.70-7.68 (m, 8H), 7.64-7.62 (m, 8H), 7.53-7.51 (m, 8H), 7.01-6.99 (m, 8H), 4.48 (t, 8H, J = 4, 8 Hz), 4.07 (t, 8H, J = 8 Hz), 1.96-1.27 (m, 24H). ^{13}C NMR (400 MHz, $CDCl_3$, δ in ppm): 165.18, 159.59, 145.16, 132.58, 132.40, 132.17, 128.35, 127.96, 127.06, 119.12, 119.04, 110.06, 67.71, 65.67, 28.85, 28.46, 22.65. FT-IR (cm^{-1}): 3046.22, 2944.17, 2871.07, 2226.77, 1724.27, 1601.82, 1475.36, 1252.26. Raman Peaks (cm^{-1}): 2234, 1721, 1603, 1488, 1259. UV-vis (nm): 265.00, 325.00, 450.00. Elemental analysis (%): Calculated C 74.87 H 5.56 N 5.95. Found C 74.90 H 5.83 N 5.60.

2.3.2 Synthesis of compound 3b Compound was synthesized according to a similar procedure to **3a**. ^{1}H NMR (400 MHz, $CDCl_3$, δ in ppm): 8.84-8.83 (m, 4H), 8.79-8.78 (m, 2H), 7.71-7.68 (m, 8H), 7.65-7.62 (m, 8H), 7.54-7.50 (m, 8H), 7.00-6.97 (m, 8H), 4.46 (t, 8H, J = 4, 8 Hz), 4.04 (t, 8H, J = 8 Hz), 1.91-1.27 (m, 32H). ^{13}C NMR (400 MHz, $CDCl_3$, δ in ppm): 165.20, 161.58, 159.67, 145.18, 132.57, 131.31, 128.32, 127.92, 127.05, 119.12, 115.62, 110.05, 67.89, 65.78, 29.72, 29.11, 28.63, 25.80. FT-IR (cm^{-1}): 3045.16, 2944.87, 2869.45, 2223.63, 1715.84, 1601.25, 1473.84, 1245.14. Raman Peaks (cm^{-1}): 2229, 1725, 1603, 1446, 1250. UV-vis (nm): 265.00, 332.00, 441.00. Elemental analysis (%): Calculated C 75.28 H 5.90 N 5.72. Found C 75.59 H 6.49 N 5.20.

2.3.3 Synthesis of compound 3c Compound was synthesized according to a similar procedure to **3a**. ^{1}H NMR (400 MHz, $CDCl_3$, δ in ppm): 8.84-8.80 (m, 6H), 7.71-7.69 (m, 8H), 7.65-7.63 (m, 8H), 7.54-7.51 (m, 8H), 7.01-6.98 (m, 8H), 4.44 (t, 8H, J = 8 Hz), 4.02 (t, 8H, J = 8, 4 Hz), 1.86-1.27 (m, 40H). ^{13}C NMR (400 MHz, $CDCl_3$, δ in ppm): 165.23, 159.71, 132.58, 132.23, 131.29, 128.33, 127.06, 115.03, 110.05, 68.00, 60.17, 34.76, 29.15, 29.03, 28.62, 25.98. FT-IR (cm^{-1}): 3045.12, 2935.16, 2855.83, 2226.89, 1723.91, 1603.91, 1474.58, 1254.25. Raman Peaks (cm^{-1}): 2233, 1721, 1603, 1435, 1255. UV-vis (nm): 329.00, 448.00. Elemental analysis (%): Calculated C 75.66 H 6.21 N 5.51. Found: C 75.55 H 6.34 N 5.09.

2.3.4 Synthesis of compound 3d Compound was synthesized according to a similar procedure to **3a**. ^{1}H NMR (400 MHz, $CDCl_3$, δ in ppm): 8.84-8.83 (m, 4H), 8.80-8.79 (m, 2H), 7.71-7.69 (m, 8H), 7.65-7.63 (m, 8H), 7.54-7.50 (m, 8H), 7.01-6.96 (m, 8H), 4.43 (t, 8H, J = 8 Hz), 4.01 (t, 8H, J = 8 Hz), 1.88-1.27 (m, 48H). ^{13}C NMR (400 MHz, $CDCl_3$, δ in

ppm): 165.24, 159.73, 152.28, 145.23, 132.58, 132.23, 131.25, 128.32, 127.91, 127.06, 119.14, 115.03, 110.02, 68.06, 65.92, 31.51, 29.25, 29.19, 28.65, 25.98, 25.92. FT-IR (cm^{-1}): 3075.83, 2919.48, 2854.73, 2221.83, 1719.06, 1600.46, 1474.22, 1253.16. Raman Peaks (cm^{-1}): 2227, 1725, 1603, 1439, 1251. UV-vis (nm): 267.00, 327.00, 434.00. Elemental analysis (%): Calculated C 76.04 H 6.47 N 5.32 Found: C 76.18 H 6.26 N 4.75.

2.3.5 Synthesis of compound 3e Compound was synthesized according to a similar procedure to **3a**. ^{1}H NMR (400 MHz, $CDCl_3$, δ in ppm): 8.84-8.79 (m, 6H), 7.71-7.69 (m, 8H), 7.66-7.63 (m, 8H), 7.55-7.51 (m, 8H), 7.01-6.98 (m, 8H), 4.43 (t, 8H, J = 8 Hz), 4.01 (t, 8H, J = 4, 8 Hz), 1.88-1.27 (56H). ^{13}C NMR (400 MHz, $CDCl_3$, δ in ppm): 165.26, 159.75, 145.24, 132.58, 132.25, 131.25, 128.32, 127.90, 127.06, 115.04, 110.02, 68.10, 65.94, 29.43, 29.31, 29.20, 28.67, 26.01, 25.96. FT-IR (cm^{-1}): 3066.89, 2923.31, 2851.85, 2225.04, 1722.52, 1601.96, 1473.60, 1247.11. Raman Peaks (cm^{-1}): 2230, 1725, 1606, 1440, 1253. UV-vis (nm): 251.00, 326.00, 450.00. Elemental analysis (%): Calculated C 76.35 H 6.77 N 5.13 Found C 75.31 H 6.66 N 5.28.

2.3.6 Synthesis of compound 3f Compound was synthesized according to a similar procedure to **3a**. ^{1}H NMR (400 MHz, $CDCl_3$, δ in ppm): 8.85-8.80 (m, 6H), 7.72-7.68 (m, 8H), 7.65-7.63 (m, 8H), 7.54-7.51 (m, 8H), 7.00-6.97 (m, 8H), 4.43 (t, 8H, J = 8 Hz), 4.00 (t, 8H, J = 4, 8 Hz), 1.89-1.27 (m, 64H). ^{13}C NMR (400 MHz, $CDCl_3$, δ in ppm): 165.23, 159.78, 152.29, 145.22, 132.97, 132.56, 132.26, 131.18, 128.30, 127.90, 127.04, 119.14, 115.05, 110.00, 68.13, 65.96, 29.51, 29.46, 29.37, 29.26, 29.23, 28.69, 26.05, 25.99. FT-IR (cm^{-1}): 3074.46, 2921.56, 2852.52, 2224.91, 1719.46, 1602.70, 1471.65, 1244.72. Raman Peaks (cm^{-1}): 2227, 1720, 1604, 1439, 1250. UV-vis (nm): 265.00, 335.00, 446.00. Elemental analysis (%): Calculated C 76.65 H 7.02 N 4.96. Found: C 76.93 H 7.15 N 4.78.

2.3.7 Synthesis of compound 3g Compound was synthesized according to a similar procedure to **3a**. ^{1}H NMR (400 MHz, $CDCl_3$, δ in ppm): 8.85-8.80 (m, 6H), 7.71-7.69 (m, 8H), 7.66-7.64 (m, 8H), 7.55-7.52 (m, 8H), 7.01-6.98 (m, 8H), 4.42 (t, 8H, J = 8,4 Hz), 4.00 (t, 8H, J = 8, 4 Hz), 1.87-1.27 (72H). ^{13}C NMR (400 MHz, $CDCl_3$, δ in ppm): 165.26, 159.77, 145.26, 132.58, 132.26, 131.24, 128.32, 127.90, 127.06, 115.05, 110.02, 68.14, 65.97, 29.52, 29.40, 29.28, 29.22, 28.68, 26.04, 25.98. FT-IR (cm^{-1}): 3065.31, 2919.85,

2851.11, 2223.99, 1730.03, 1603.66, 1475.23, 1246.39. Raman Peaks (cm^{-1}): 2229, 1735, 1606, 1438, 1248. UV-vis (nm): 265.00, 333.00, 450.00. Elemental analysis (%): Calculated C 76.94 H 7.26 N 4.80. Found C 76.43 H 7.37 N 4.48.

2.3.8 Synthesis of compound 3h Compound was synthesized according to a similar procedure to **3a**. ^{1}H NMR (400 MHz, $CDCl_3$, δ in ppm): 8.84-8.80 (m, 6H), 7.71-7.69 (m, 8H), 7.66-7.64 (m, 8H), 7.55-7.53 (m, 8H), 7.01-6.99 (m, 8H), 4.42 (t, 8H, J = 8, 4 Hz), 4.01 (t, 8H, J = 4, 8 Hz), 1.89-1.28 (m, 80H). ^{13}C NMR (400 MHz, $CDCl_3$, δ in ppm): 165.26, 159.78, 152.31, 145.26, 132.58, 132.26, 131.23, 128.32, 127.90, 127.06, 119.14, 115.05, 110.02, 68.15, 65.97, 29.58, 29.54, 29.41, 29.29, 29.23, 28.69, 26.05, 25.99. FT-IR (cm^{-1}): 2957.91, 2922.32, 2851.62, 2224.68, 1718.73, 1603.49, 1468.27, 1256.86. Raman Peaks (cm^{-1}): 2236, 1725, 1607, 1447, 1249. UV-vis (nm): 265.00, 333.00, 442.00. Elemental analysis (%): Calculated C 77.21 H 7.48 N 4.65. Found C 77.28 H 7.66 N 4.64.

2.3.9 Synthesis of compounds 8a For the synthesis of the target compound **8a**, compound **6** (1 equivalent) was dissolved in aqueous KOH (1.1 equivalent) solution. To that solution, compound **4** (6 equivalents) was added followed by the addition of tetraoctylammonium bromide in catalytic amounts. The reaction mixture was refluxed under vigorous stirring for 7 hours & was then cooled to room temperature. The compound was extracted with dichloromethane. The organic layer was washed with brine & dried over anhydrous sodium sulphate. The chloroform was removed by rotary evaporation and the resulting residue was purified by column chromatography over silica gel using hexane & ethyl acetate as eluent to yield final Compound **8a**. ^{1}H NMR (400 MHz, $CDCl_3$, δ in ppm): 8.81 (t, 2H, J = 1.6 Hz), 8.77 (d, 4H, J = 1.6 Hz), 7.84 (s, 24H), 4.42 (t, 8H, J = 4, 8 Hz), 4.24 (m, 48H), 1.92 (m, 56H), 1.52 (m, 152H), 0.95 (m, 60H); ^{13}C NMR (400 MHz, $CDCl_3$, δ in ppm): 165.24, 152.27, 148.96, 148.95, 148.90, 132.17, 123.60, 123.57, 107.33, 107.25, 69.70, 69.67, 69.61, 65.91, 31.72, 29.54, 29.47, 29.45, 29.35, 28.73, 26.20, 25.97, 25.88, 22.70, 14.10; FT-IR (cm^{-1}): 3090.94, 2929.95, 2858.29, 1726.46, 1616.88, 1514.87, 1468.88, 1435.28, 1388.50, 1310.41, 1261.99, 1234.89, 1170.40, 1104.75, 1042.01, 923.59, 867.74, 837.26, 802.35, 758.78, 726.87, 684.06, 600.61; UV-vis (nm): 251, 262, 270, 280, 309, 346, 444; Elemental analysis (%): Calculated C 76.27 H 9.44 N 0.74. Found C 76.34 H 9.51 N 1.09.

2.3.10 Synthesis of compounds 8b Compound **8b** was synthesised according to a similar procedure to **8a**. ^{1}H NMR (400 MHz, $CDCl_3$, δ in ppm): 8.82 (s, 2H), 8.79 (s, 4H), 7.84 (s, 24H), 4.41 (t, 8H, J = 8 Hz), 4.24 (t, 8H, J = 8 Hz), 1.95 (m, 48H), 1.85 (m, 8H), 1.59 (m, 40H), 1.41 (m, 128H), 0.95 (m, 60 H); ^{13}C NMR (400 MHz, $CDCl_3$, δ in ppm): 165.23, 148.95, 148.92, 123.58, 107.29, 69.69, 31.71, 29.66, 29.58, 29.54, 29.45, 29.37, 28.73, 26.25, 26.00, 25.87, 22.88, 14.10, 14.08; FT-IR (cm^{-1}): 3096.6, 2929.47, 2857.75, 1726.35, 1616.93, 1514.77, 1468.61, 1435.52, 1388.47, 1310.23, 1262.48, 1235.31, 1170.73, 1042.42, 923.77, 867.46, 837.10, 802.68, 758.82, 726.10, 683.92, 600.68; UV-vis (nm): 251, 261, 270, 280, 308, 346, 443; Elemental analysis (%): Calculated C 76.54 H 9.58 N 0.72. Found C 76.16 H 9.61 N 0.99.

2.3.11 Synthesis of compounds 8c Compound **8c** was synthesised according to a similar procedure to **8a**. ^{1}H NMR (400 MHz, $CDCl_3$, δ in ppm): 8.84 (t, 2H, J = 2, 1.2 Hz), 8.80 (d, 4H, J = 1.6 Hz), 7.85 (s, 24H), 4.42 (t, 8H, J = 4, 8 Hz), 4.25 (t, 48H, J = 8 Hz), 1.96 (m, 48H), 1.85 (m, 8H), 1.60 (m, 40H), 1.40 (m, 144H), 0.96 (m, 60H); ^{13}C NMR (400 MHz, $CDCl_3$, δ in ppm): 165.27, 152.32, 148.95, 148.94, 132.24, 127.90, 123.59, 107.27, 69.68, 65.98, 31.73, 29.74, 29.71, 29.63, 29.54, 29.46, 29.38, 28.73, 26.26, 26.01, 25.89, 22.70, 14.11; FT-IR (cm^{-1}): 3100.3, 2926.32, 2855.88, 1726.58, 1615.40, 1515.54, 1469.16, 1434.76, 1389.7, 1314.5, 1264.4, 1234.79, 1170.57, 1046.2, 925.23, 869.62, 840.18, 800.93, 761.68, 722.43, 683.18, 604.68; UV-vis (nm): 251, 261, 270, 280, 309, 346, 443; Elemental analysis (%): Calculated C 76.80 H 9.72 N 0.70. Found C 76.62 H 9.76 N 0.97.

2.3.12 Preparation of CT complexes The amount of TNF and oligomer was calculated according to molar ratios. The calculated amount was dissolved in dichloromethane and both the solutions were mixed. The resulting solution which was of deep brown colour was then allowed to evaporate by leaving the solution to stand overnight. The final traces of solvent were removed under high vacuum.

References

(1) Mul, M. N. G.; Mann, J. A. *Langmuir* **1994**, *10*, 2311-2316.

(2) Roberts, G. *Langmuir-Blodgett Films;* Plenum Press: New York, **1990**.

(3) Kaganer, V.M.; Mohwald, H.; Dutta, P. *Rev. Mod. Phys.* **1999**, *71*, 779-819.

(4) Kumar, B.; Prajapati, A. K.; Varia, M. C.; Suresh, K. A. *Langmuir* **2009**, *25*, 839-844.

(5) Kuhn, H. in Modern Trends of Colloid Science in Chemistry and Biology, ed. H.-F. Eicke, Birkh¨auser Verlag, Basel, **1985**, pp. 97–125.

(6) Kuhn, H.; Möbius, D. *Angew. Chem. Int. Ed. Engl*. **1971**, *10*, 620-637.

(7) Gupta, S. K.; Setia, S.; Sidiq, S.; Gupta, M.; Kumar, S.; Pal, S. K. *RSC Adv*. **2013**, *3*, 12060-12065.

(8) Serpe, M. J.; Craig, S. L. *Langmuir* **2007**, *23*, 1626-1634.

(9) Delphia, S. R. P.; Senthil, S.; Kannan, P.; Vinitha, G.; Ramalingam, A. *J. Phys. Chem. Solids* **2007,** *68*, 1812-1820.

(10) Kumaresan, S.; Kannan, P. *J. Polym. Sci: Part A: Polym. Chem.* **2003**, *41*, 3188-3196.

(11) Kawatsuki, N.; Unisuga, S.; Neko, T.; Uchida, E.; Kondo, M. *React. Funct. Polym.* **2009**, *69*, 836-842.

(12) Fischer, T.; Läsker, L.; Rutloh, M.; Czapla, S.; Stumpe, J. *Mol. Cryst. Liq. Cryst.* **1997**, *299*, 293-299.

(13) Del Barrio, J.; Tejedor, R. M.; Chinelatto, L. S.; Sánchez, C.; Piñol, M.; Oriol, L. *J. Mater. Chem.* **2009**, *19*, 4922-4930.

(14) Matsumoto, M.; Terrettaz, S.; Tachibana, H. *Adv. Colloid Interface Sci.* **2000**, *87*, 147-164.

(15) Lui, Z. F.; Hashimoto, K.; Fujishima, A. *Nature* **1990**, *347*, 658-660.

(16) Yamamoto, T.; Umemura, Y.; Sato, O.; Einaga, Y. *Chem. Mater*. **2004**, *16*, 1195-1201.

(17) Riul, A.; Santos, D. S.; Wohnrath, K.; Tommazo, R. D.; Carvalho, A. C. P. L. F.; Fonseca, F. J.; Oliveira, O. N.; Taylor, D. M.; Mattoso, L. H. C. *Langmuir* **2002**, *18*, 239-245.

(18) Feng, C. L.; Zhang, Y. J.; Jin, J.; Song, Y. L.; Xie, L. Y.; Qu, G. R.; Jiang, L.; Zhu, D. B. *Langmuir* **2001**, *17*, 4593-4597.

(19) Kumar, B.; Suresh, K. A. *Phys. Rev. E.* **2009**, *80*, 021601(1)-021601(5).

(20) Sato, T.; Ozaki, Y.; Iriyama, K. *Langmuir* **1994**, *10*, 2363-2369.

(21) Taniike, K.; Matsumoto, T.; Sato, T.; Ozaki, Y. *J. Phys. Chem*. **1996,** *100*, 15508-15516.

(22) Velez, M.; Mukhopadhyay, S.; Muzikante, I.; Matisova, G.; Vieira, S. *Langmuir* **1997,** *13*, 870-872.

(23) Lan, A.; Padmanabhan, M.; Li, K.; Wu, H.; Emge, T. J.; Hong, M.; Li, J. *Inorg. Chim. Acta* **2011**, *366*, 68-75.

(24) Xue, J.; Jung, C. S.; Kim, M. W. *Phys. Rev. Lett*. **1992**, *69*, 474-477.

(25) Ma, G.; Allen, H. C. *Langmuir* **2006**, *22*, 5341-5349.

(26) Hashimoto, Y.; Karthaus, O. *J. Colloid Interface Sci*. **2007**, *311*, 289-295.

(27) Struijk, C. W.; Sieval, A. B.; Dakhorst, J. E. J.; Dijk, M. V.; Kimkes, P.; Koehorst, R. B. M.; Donker, H.; Schaafsma, T. J.; Picken, S. J.; Van de Craats, A. M.; Warman, J. M.; Zuilhof, H.; Sudhölter, E. J. R. *J. Am. Chem. Soc.* **2000**, *122*, 11057–11066.

(28) Wong, W. W. H.; Singh, T. B.; Vak, D.; Pisula, W.; Yan, C.; Feng, X.; Williams, E. L.; Chan, K. L.; Mao, Q.; Jones, D. J.; Ma, C.; Müllen, K.; Bäuerle, P.; Holmes, A. B. *Adv. Funct. Mater*. **2010**, *20*, 927–928.

(29) Wong, W. W. H.; Subbiah, J.; Puniredd, S. R.; Purushothaman, B.; Pisula, W.; Kirby, N.; Müllen, K.; Jones, D. J.; Holmes, A. B. *J. Mater. Chem*. **2012**, *22*, 21131–21137.

(30) Chandrasekhar, S.; Demus, D.; Goodby, J.; Gray, G. W.; Spiess, H. W.; Vill, V. in Handbook of Liquid Crystals Set, Wiley-VCH, **2008**, pp. 749–780.

(31) Boden, N.; Movaghar, B.; Demus, D.; Goodby, J.; Gray, G. W.; Spiess, H. W.; Vill, V. in Handbook of Liquid Crystals Set, Wiley-VCH, **2008**, pp. 781–798.

(32) Vaughan, G. B. M.; Heiney, P. A.; McCauley, J. P.; Smith, A. B. *Phys. Rev. B.* **1992**, *46*, 2787–2791.

(33) Schouten, P. G.; Warman, J. M.; De Haas, M. P.; Van Nostrum, C. F.; Gelinck, G. H. ; Nolte, R. J. M.; Copyn, M. J.; Zwikker, J. W.; Engel, M. K. *J. Am. Chem. Soc*. **1994**, *116*, 6880–6894.

(34) van de Craats, A. M.; Warman, J. M. *Adv. Mater*. **2001**, *13*, 130–133.

(35) Markovitsi, D.; Marguet, S.; Bondkowski, J.; Kumar, S. *J. Phys. Chem. B* **2001**, *105*, 1299–1306.

(36) Van de Craats, A. M.; Warman, J. M.; Fechtenkötter, A.; Brand, J. D.; Harbison, M. A.; Müllen, K. *Adv. Mater.* **1999**, *11*, 1469-1472.

(37) Kranig, W.; Hueser, B.; Spiess, H. W.; Kreuder, W.; Ringsdorf, H.; Zimmermann, H. *Adv. Mater*. **1990**, *2*, 36–40.

(38) Boden, N.; Bushby, R. J.; Cammidge, A. N.; Mansoury, A. E.; Martin, P. S.; Lu, Z. *J. Mater Chem*. **1999**, *9*, 1391–1402.

(39) Christ, T.; Glusen, B.; Greiner, A.; Kettner, A.; Sander, R.; Stumpflen, V.; Tsukruk, V.; Wendorff, J. H. *Adv. Mater.* **1997**, *9*, 48-52.

(40) Boden, N.; Bushby, R. J.; Lu, Z. *Liq. Cryst*. **1998**, *25*, 47-58.

(41) Kumar, S. *Liq. Cryst*. **2004**, *31*, 1037–1059.

(42) Kumar, S. *Liq. Cryst*. **2005**, *32*, 1089–1113.

(43) Pal, S. K.; Setia, S.; Avinash, B. S.; Kumar, S. *Liq. Cryst*. **2013**, *40*, 1769–1816.

(44) Adam, D.; Schuhmacher, P.; Simmerer, J.; Häussling, L.; Siemensmeyer, K.; Etzbach, K. H.; Ringsdorf, H.; Haarer, D. *Nature* **1994**, *371*, 141–143.

(45) Van de Craats, A. M.; Warman, J. M.; De Haas, M. P.; Adam, D.; Simmerer, J.; Haarer, D.; Schuhmacher, P. *Adv. Mater*. **1996**, *8*, 823–826.

(46) Kumar, S.; Naidu, J. J.; Varshney, S. K. *Mol. Cryst. Liq. Cryst*. **2004**, *411*, 355–362.

(47) Paraschiv, I.; De Lange, K.; Giesbers, M.; Van Lagen, B.; Grozema, F. C.; Abellon, R. D.; Siebbeles, L. D. A.; Ejr, S.; Zuilhof, H.; Marcelis, A. T. M. *J. Mater. Chem*. **2008**, *18*, 5475–5481.

(48) Bayer, A.; Zimmermann, S.; Wendorff, J. H. *Mol. Cryst. Liq. Cryst.* **2003**, *396*, 1-22.

(49) Kats, E.I. *Mol. Cryst. Liq. Cryst*. **2003**, *396*, 23-34.

(50) Warman, J. M.; Van de Craats, A.M. *Mol. Cryst. Liq. Cryst*. **2003**, *396*, 41-72.

(51) Marguet, S.; Markovitsi, D.; Millie, P.; Sigal, H.; Kumar, S. *J. Phys. Chem. B* **1998**, *102*, 4697-4710.

(52) Markovitsi, D.; Marguet, S.; Gallos, L.; Sigal, H.; Millie, P.; Argyrakis, P.; Kumar, S.; Ringsdorf, H. *Chem. Phys. Lett*. **1999**, *306*, 163-167.

(53) Seguy, I.; Destruel, P.; Bock, H. *Synth. Met*. **2000**, *15*, 111–112.

(54) Stapff, I. H.; Stumpflen, V.; Wendorff, J. H.; Spohn, D. B.; Mobius, D. *Liq. Cryst*. **1997**, *23*, 613-617.

(55) Christ, T.; Glusen, B.; Greiner, A.; Kettner, A.; Sander, R.; Stumpflen, V.; Tsukruk, V.; Wendorff, J. H. *Adv. Mater*. **1997**, *9*, 48-52.

(56) Heppke, G.; Kruerke, D.; Lohning, C.; Lotzsch, D.; Moro, D.; Muller, M.; Sawade, H. *J. Mater. Chem*. **2000**, *10*, 2657-2661.

(57) Perova, T.; Tsvetkov, S.; Vij, J. K.; Kumar, S. *Mol. Cryst. Liq. Cryst*. **2000**, *351*, 95-102.

(58) Ichimura, K.; Furumi, S.; Morino, S.; Kidowaki, M.; Nakagawa, M.; Ogawa, M.; Nishiura, Y. *Adv. Mater*. **2000**, *12*, 950-953.

(59) Grafe, A.; Janietz, D.; Frese, T.; Wendorff, J. H. *Chem. Mater*. **2005**, *17*, 4979–4984.

(60) Paraschiv, I.; Giesbers, M.; Lagen, B. van; Grozema, F. C.; Abellon, R. D.; Laurens, D. A.; Siebbeles, L. D. A.; Marcelis, A. T. M.; Zuilhof, H.; Sudhölter, E. J. R. *Chem. Mater*. **2006**, *18*, 968–974.

(61) Zelcer, A.; Donnio, B.; Bourgogne, C.; Cukiernik, F. D.; Guillon, D. *Chem. Mater*. **2007**, *17*, 1992–2006.

(62) Paraschiv, I.; Lange, K. de; Giesbers, M.; Lagen, B. van; Grozema, F. C.; Abellon, R. D.; Siebbeles, L. D. A.; Sudhölter, E. J. R.; Zuilhof, H.; Marcelis, A. T. M. *J. Mater. Chem*. **2008**, *18*, 5475–5481.

(63) Kumar, S.; Schuhmacher, P.; Henderson, P.; Rego, J.; Ringsdorf, H. *Mol. Cryst. Liq. Cryst*. **1996**, *288*, 211–222.

(64) Maliszewskyj, N. C.; Heiney, P. A.; Josefowicz, J. Y.; Plesnivy, T.; Ringsdorf, H.; Schuhmacher, P. *Langmuir* **1995**, *11*, 1666–1674.

(65) Plesnivy, T.; Ringsdorf, H.; Schuhmacher, P.; Nuutz, U.; Diele, S. *Liq. Cryst.* **1995**, *18*, 185–190.

(66) Gupta, M.; Agarwal, N.; Arora, A.; Kumar, S.; Kumar, B.; Sheet, G.; Pal, S. K. *RSC Adv.* **2014**, *4*, 41371-41377.

(67) Gupta, M.; Gupta, S. P.; Mohapatra, S. S.; Dhara, S.; Pal, S. K. *Chem. Eur. J.* **2017,** *23*, 10626-10631.

(68) Gupta, M.; Bala, I.; Pal, S. K. *Tetrahedron Lett*. **2014**, *55*, 5836-5840.

(69) Gupta, M.; Pal, S. K. *Langmuir* **2016**, *32*, 1120-1126.

(70) Ringsdorf, H.; Wustefeld, R.; Zerta, E.; Ebert, M.; Wendorff, J. H. *Angew. Chem.* **1989**, *28*, 914-918.

(71) Ringsdorf, H.; Wustefeld, R.; Karthaus, O.; Bengs, H.; Ebert, M.; Wendorff, J. H.; Praefcke, K.; Kohne, B. *Adv. Mater*. **1990**, *2*, 141-144.

(72) Destrade, C.; Foucher, P.; Gasparoux, H.; Nguyen, H. T.; Levelut, A. M.; Malthete, J. *Mol. Cryst. Liq. Cryst*. **1984**, *106*, 121-146.

(73) Ebert, M.; Frick, G.; Baehr, C.; Wendorff, J. H.; Wüstefeld, R.; Ringsdorf, H. *Liq. Cryst*. **1992**, *11*, 293-309.

(74) Gupta, S. K.; Raghunathan, V. A.; Lakshminarayanan, V.; Kumar, S. *J. Phys. Chem. B* **2009**, *113*, 12887-12895.

(75) Balagurusamy, V. S. K. *Pramana* **1999**, *53*, 3-11.

(76) Donovan, K. J.; Scott, K.; Somerton, M.; Preece, J.; Manickam, M. *Chem. Phys.* **2006**, *322*, 471–476.

(77) Kruglova, O.; Mendes, E.; Yildirim, Z.; Wübbenhorst, M.; Mulder, F. M.; Stride, J. A.; Picken, S. J.; Kearley, G. J. *ChemPhysChem* **2007**, *8*, 1338 – 1344.

Appendix I

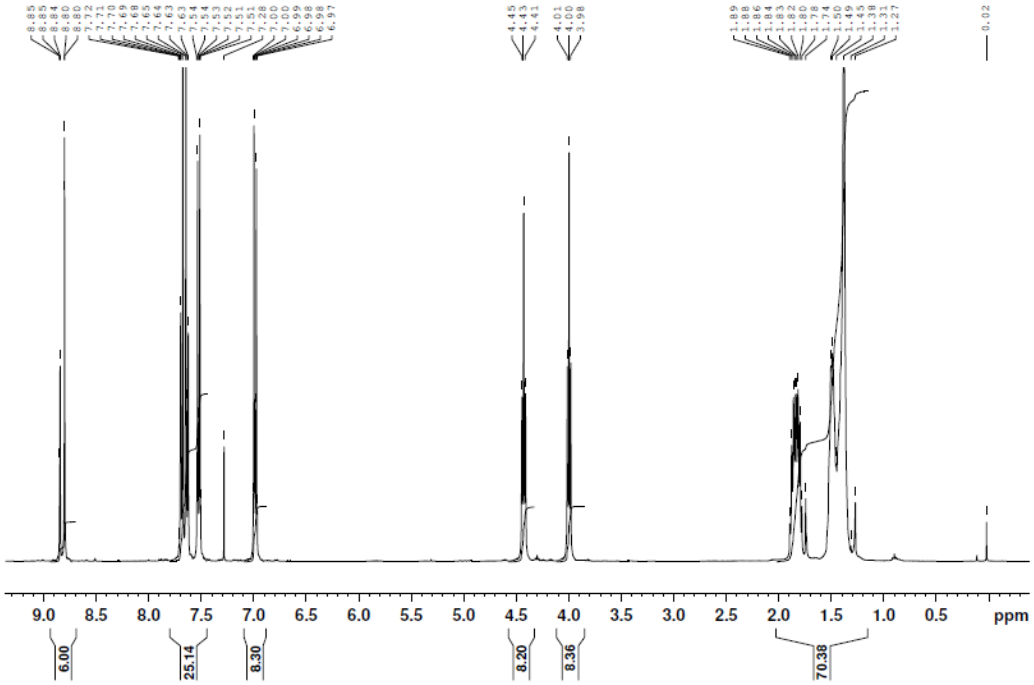

Figure A1 ^{1}H NMR spectra of compound **3f**.

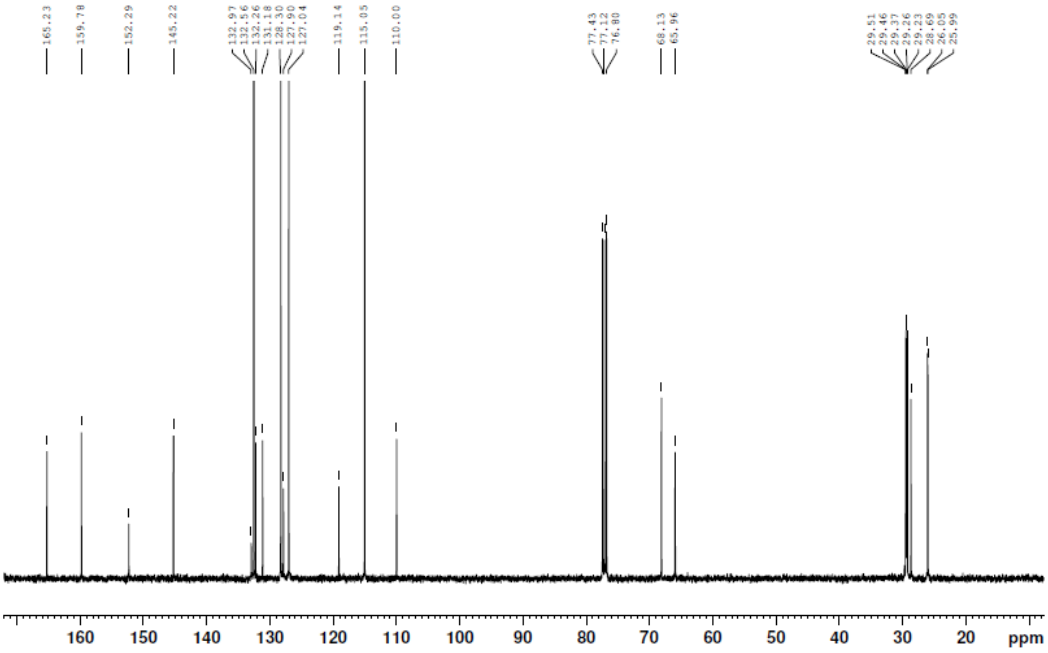

Figure A2 ^{13}C NMR spectra of compound **3f**.

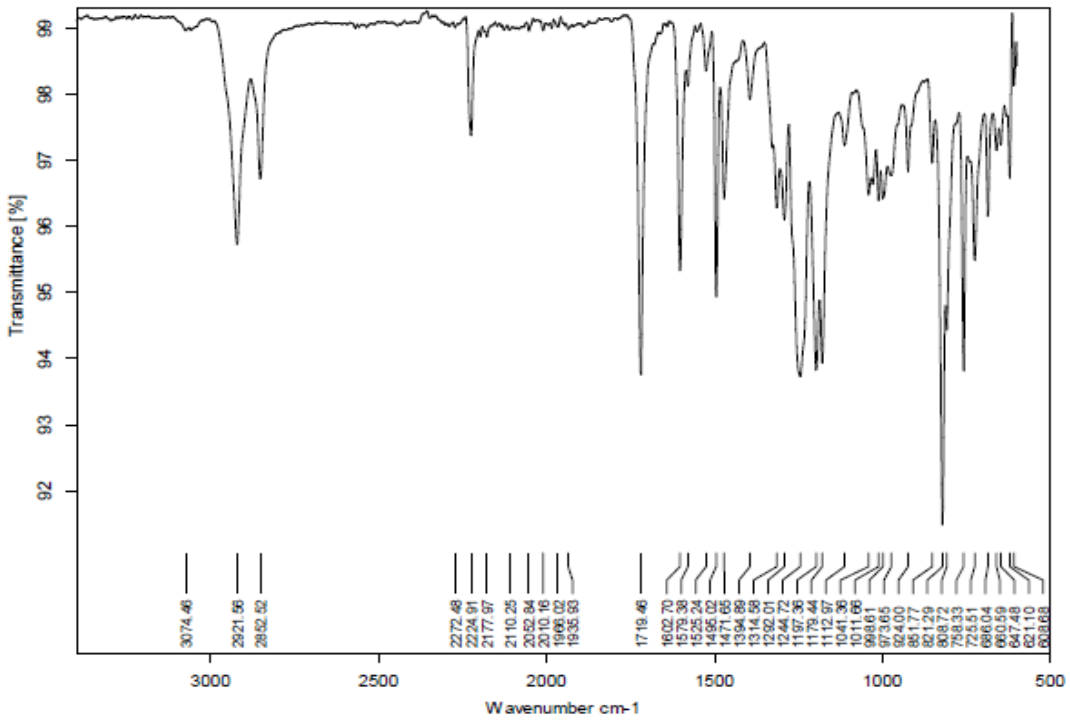

Figure A3 IR spectra of compound **3f**.

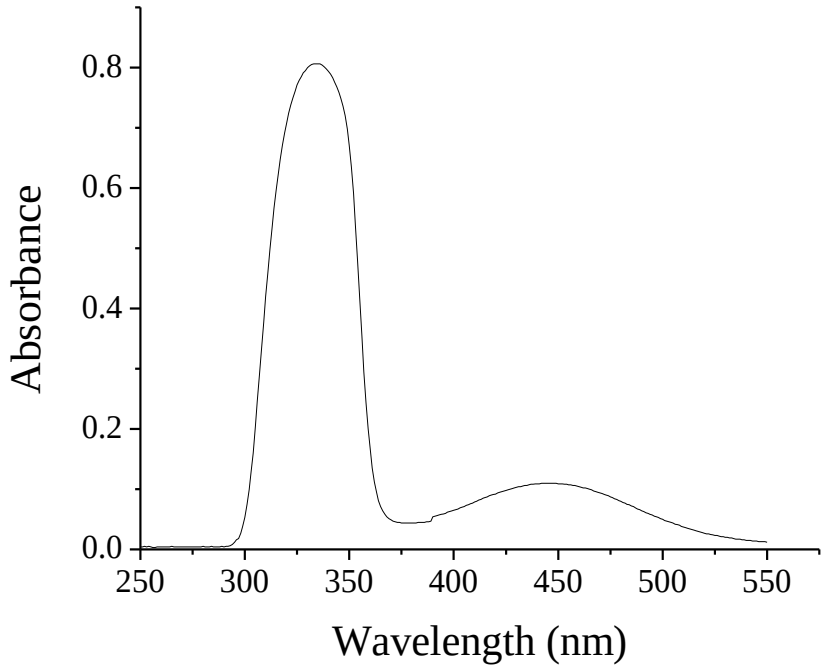

Figure A4 UV-vis spectra of compound **3f**.

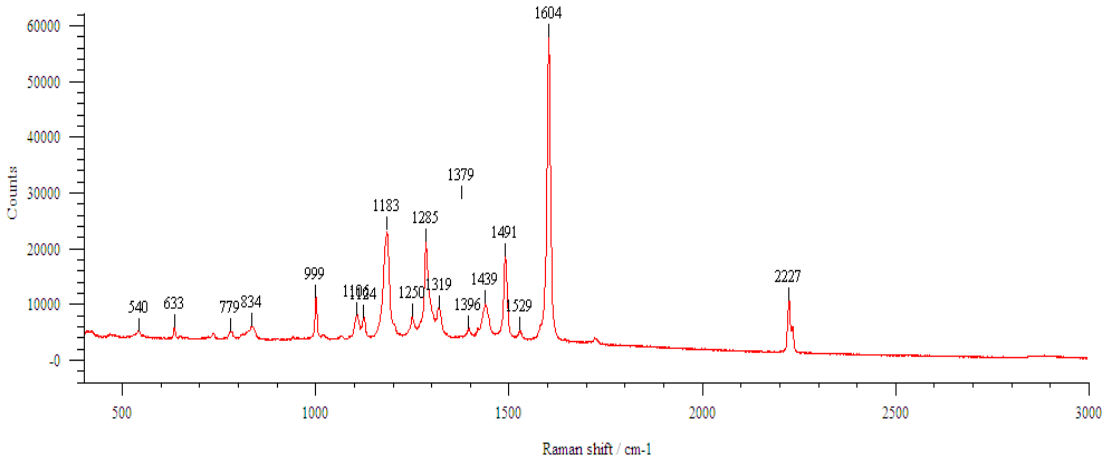

Figure A5 Raman spectra of compound **3f**.

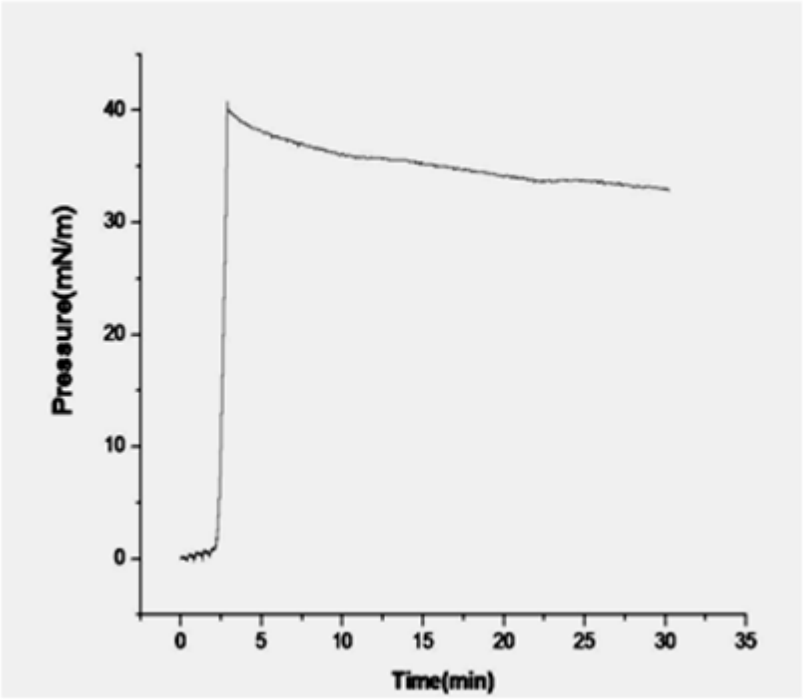

Figure A6 Equilibrium surface pressure measurement (for compound **3f** at air-water interface) by keeping the barriers constant.

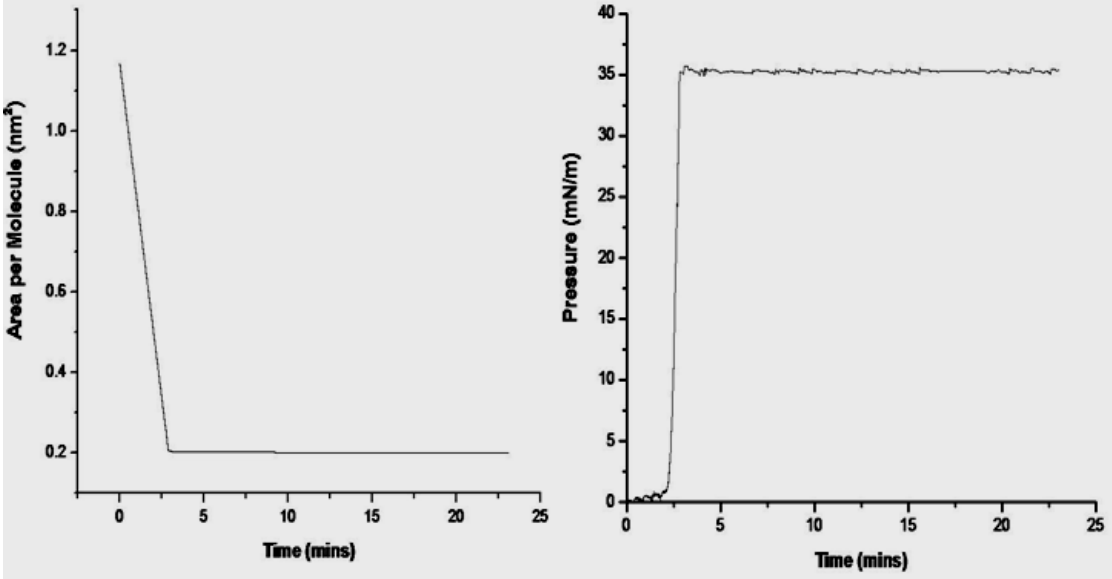

Figure A7 For stability measurement of the film of compound **3f** at air-water interface control pressure (35mN/m) was setup and the variation of area per molecule with time was observed to keep the pressure constant.

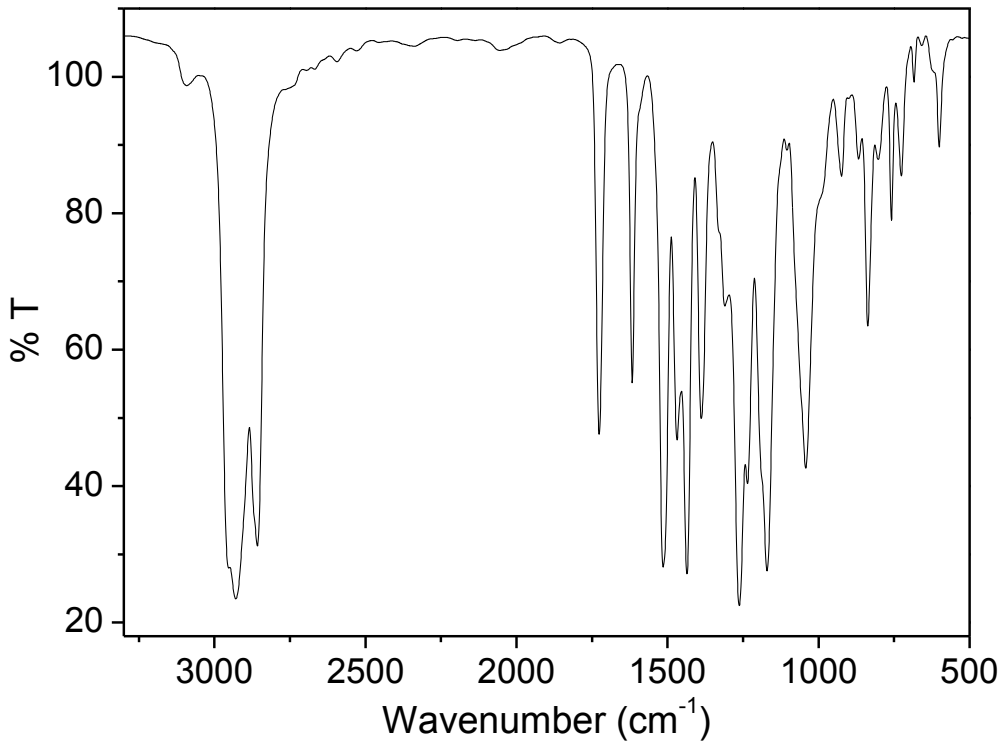

Figure A8 Representative FT-IR spectrum of compound **8b.** Other Compounds show similar spectra**.**

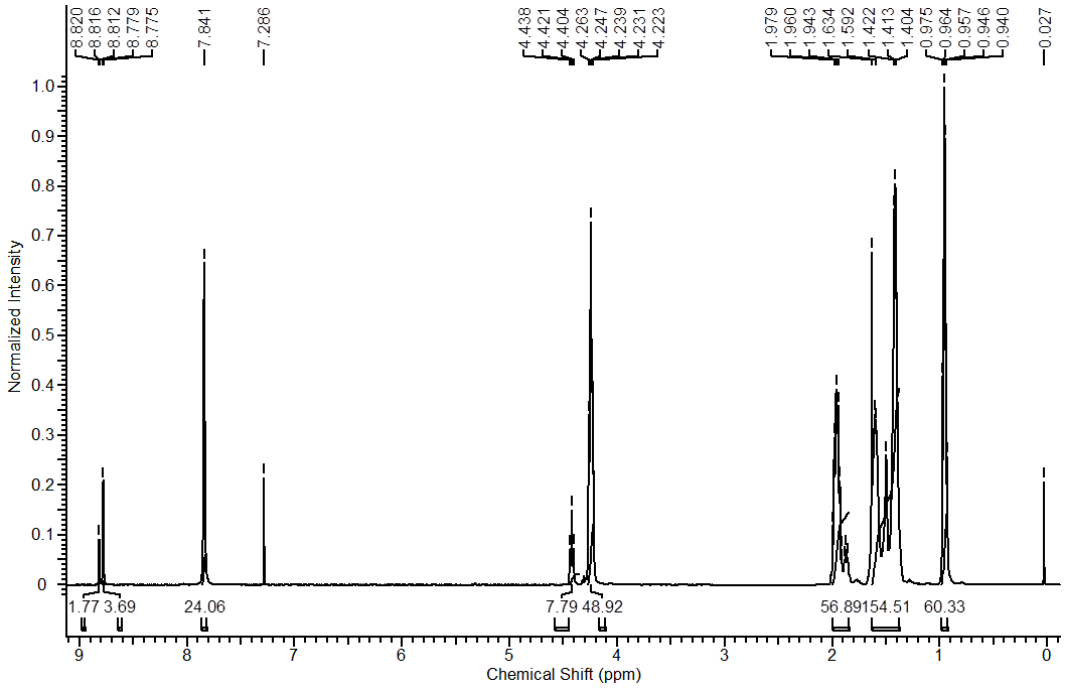

Figure A9 ^{1}H NMR spectrum of compound **8a**.

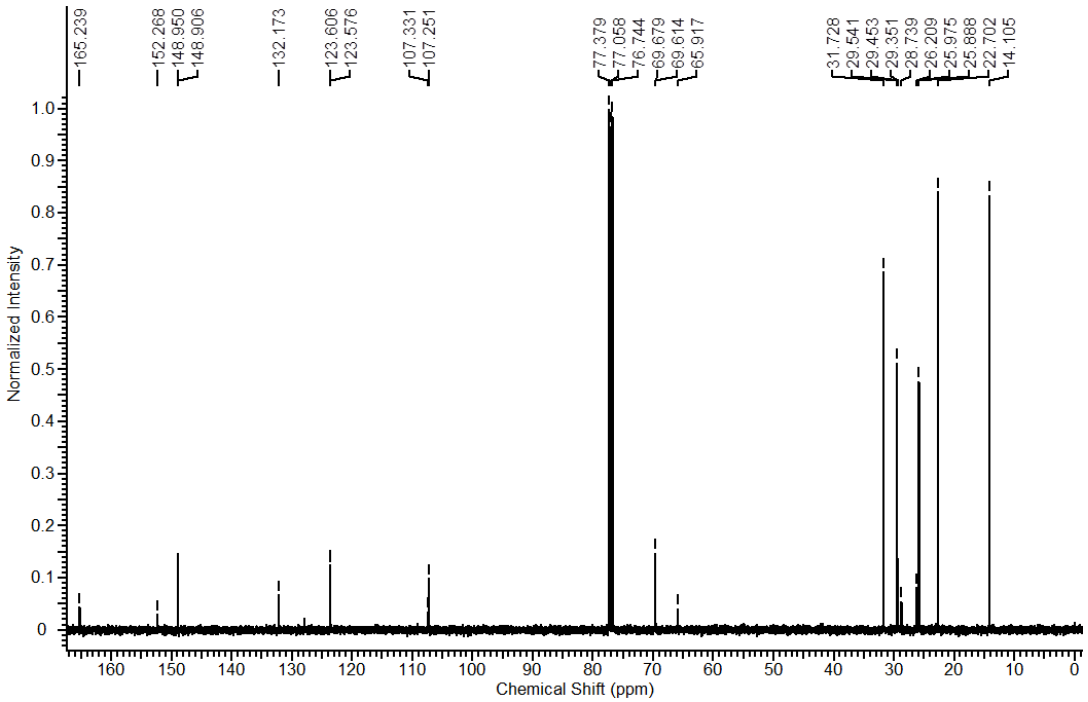

Figure A10 ^{13}C NMR spectrum of compound **8a**

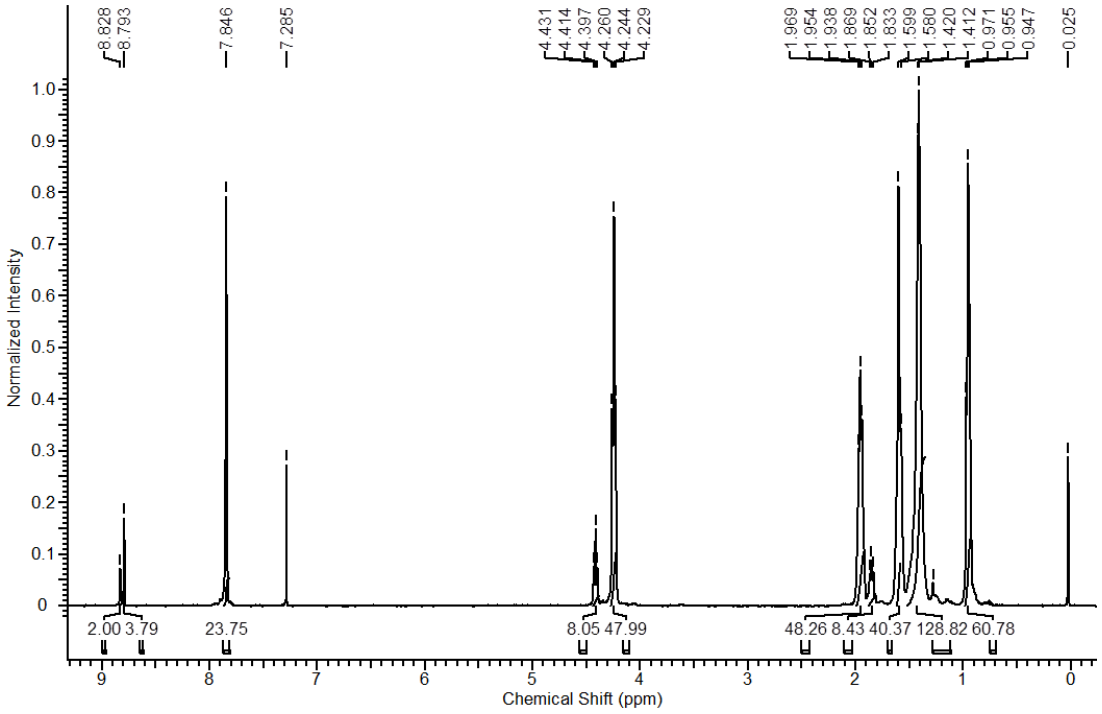

Figure A11 ^{1}H NMR spectrum of compound **8b**.

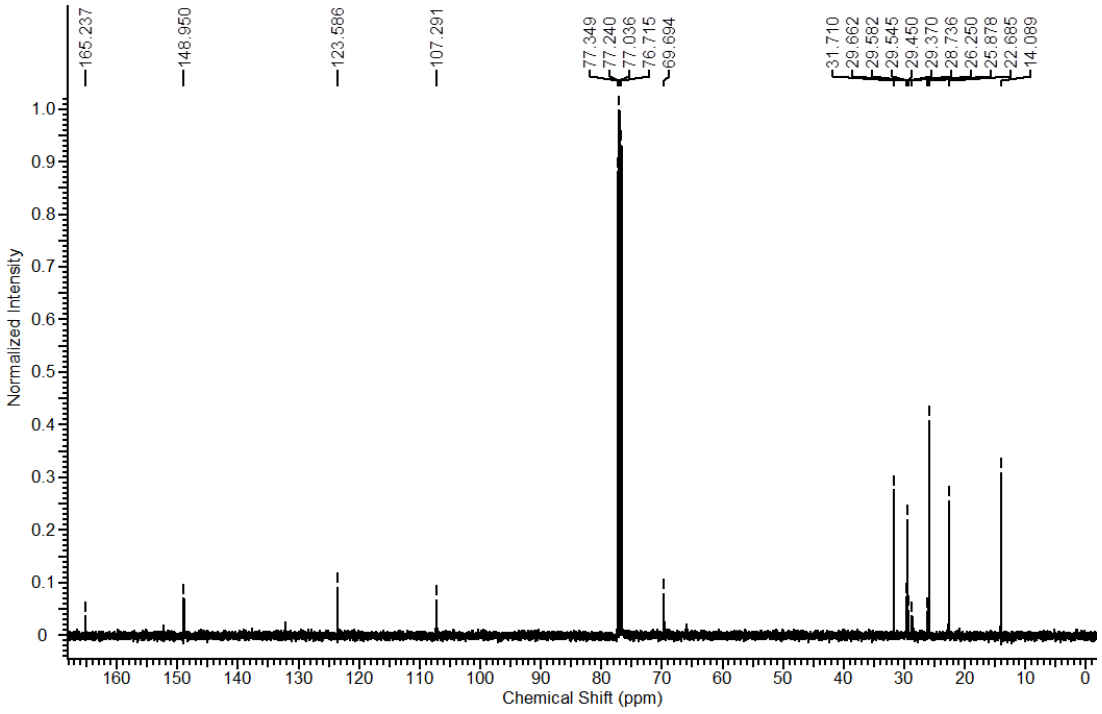

Figure A12 ^{13}C NMR spectrum of compound **8b**.

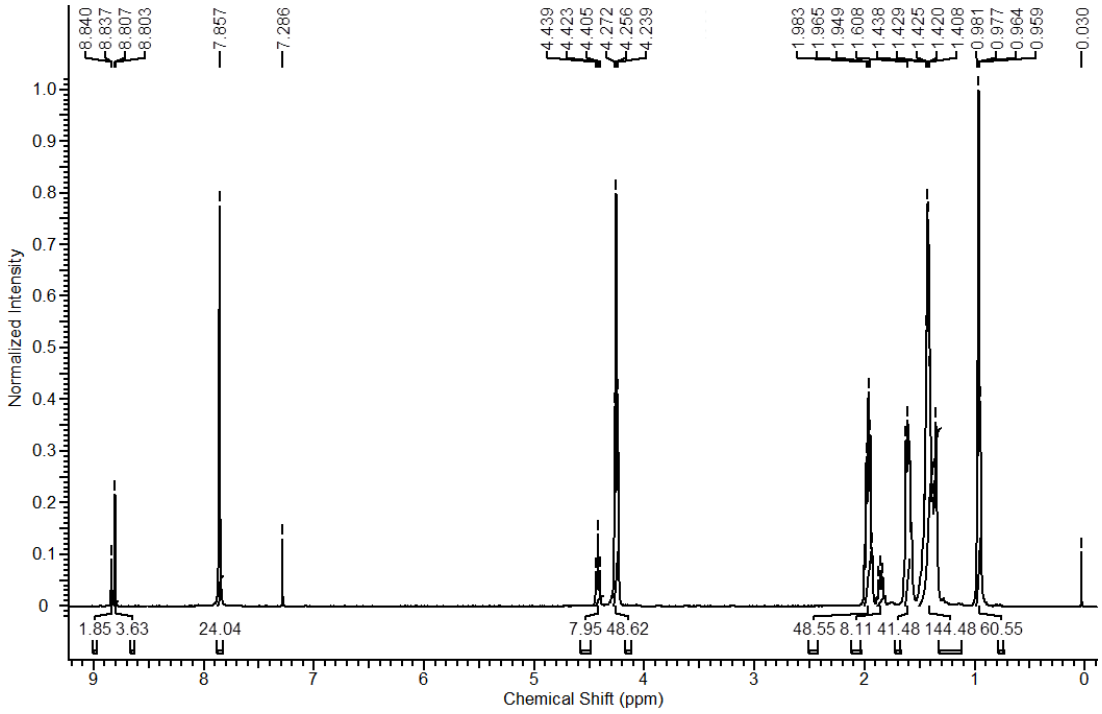

Figure A13 ^{1}H NMR spectrum of compound **8c**.

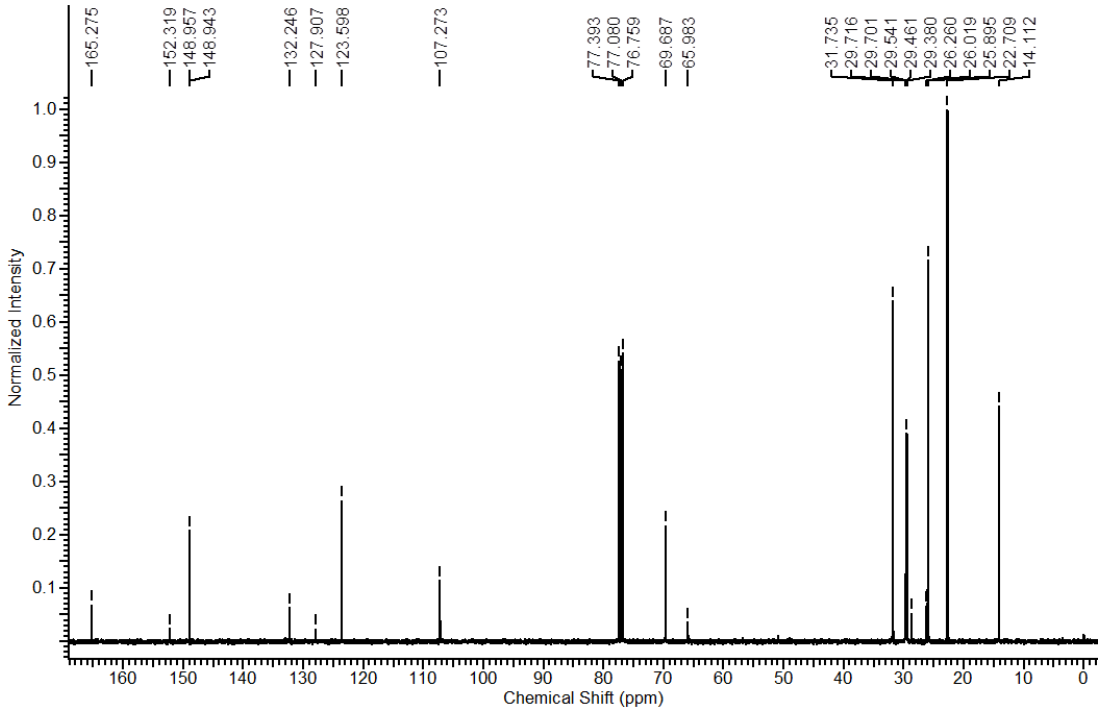

Figure A14 ^{13}C NMR spectrum of compound **8c**.

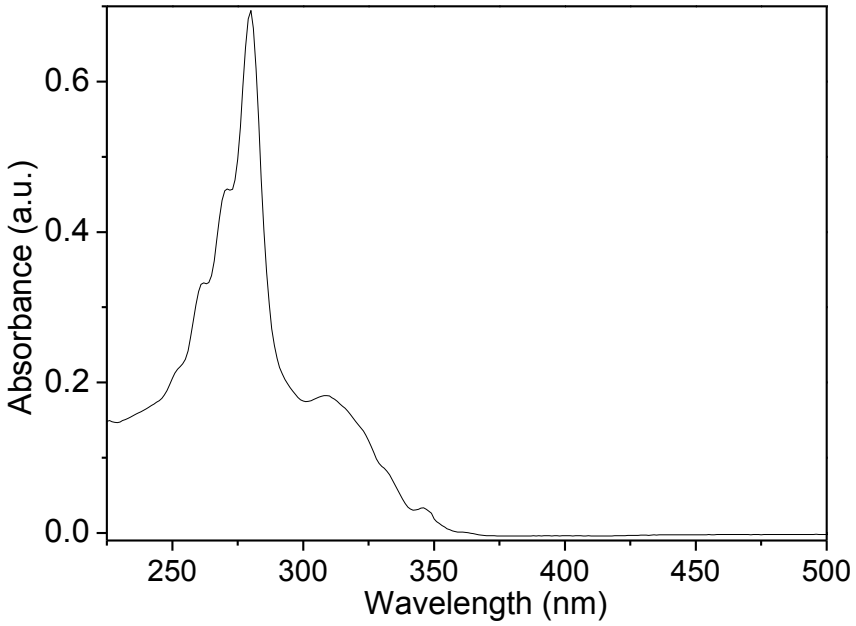

Figure A15 UV-vis absorption spectra of compound **8b** in solution (5 μM in dichloromethane).

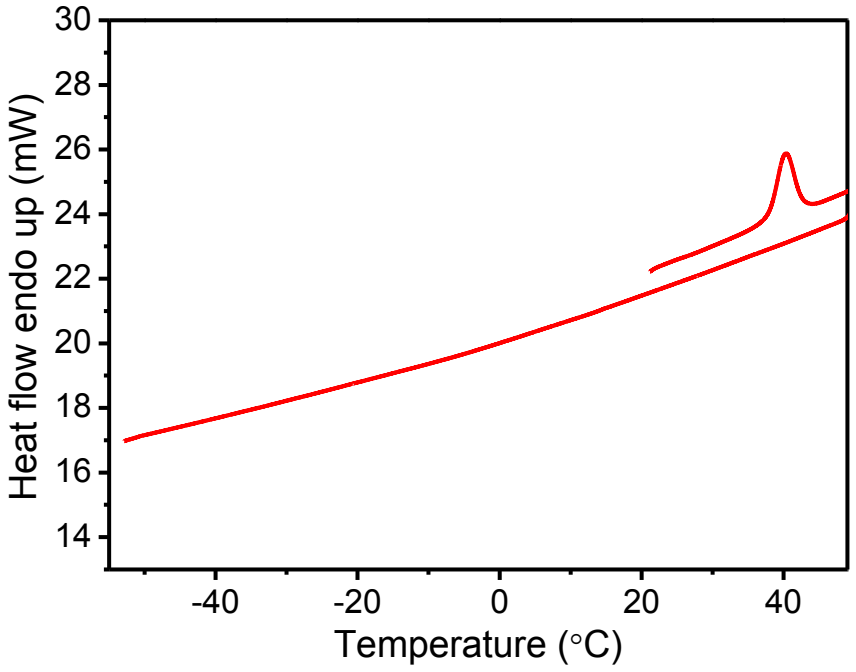

Figure A16 Representative DSC thermogram of compound **8c**.

Table A1 The observed and calculated d-spacings and planes, correlation length of the diffraction peaks of the; (a) columnar rectangular phase observed in compound **8a** with the lattice parameters a = 77.28 Å, b = 65.20 Å and c = 3.93 Å d_{exp} is the observed d-spacing. d_{cal} is the calculated d-spacing according to formula: $\frac{1}{{d_{cal}}^2} = \frac{h^2}{a^2} + \frac{k^2}{b^2}$

Planes (hk)	d_{exp} (Å)	d_{cal} (Å)	ξ	ξ/ d_{exp}
4 0	19.26	19.32	78.76	4.09
0 4	16.30	16.30	69.03	4.23
8 0	9.84	9.66		
0 8	8.11	8.15		
12 0	6.46	6.44		
0 12	5.31	5.43		
16 0	4.90	4.83		
8 12	4.51	4.73		
h_c	3.93		23.23	5.91

Table A2 The observed and calculated d-spacings and planes, correlation length of the diffraction peaks of the columnar rectangular phase observed in compound **8b** with the lattice parameters a = 80.26 Å, b = 65.20 Å and c = 3.93 Å.

Planes (hk)	d_{exp} (Å)	d_{cal} (Å)	ξ	ξ/ d_{exp}
4 0	20.07	20.07	101.67	5.07
0 4	16.30	16.30	93.20	5.72
8 0	10.08	10.03		
0 8	8.18	8.15		
12 0	6.55	6.68		
0 12	5.36	5.43		
16 0	4.95	5.01		
8 12	4.55	4.78		
h_c	3.93		23.23	5.91

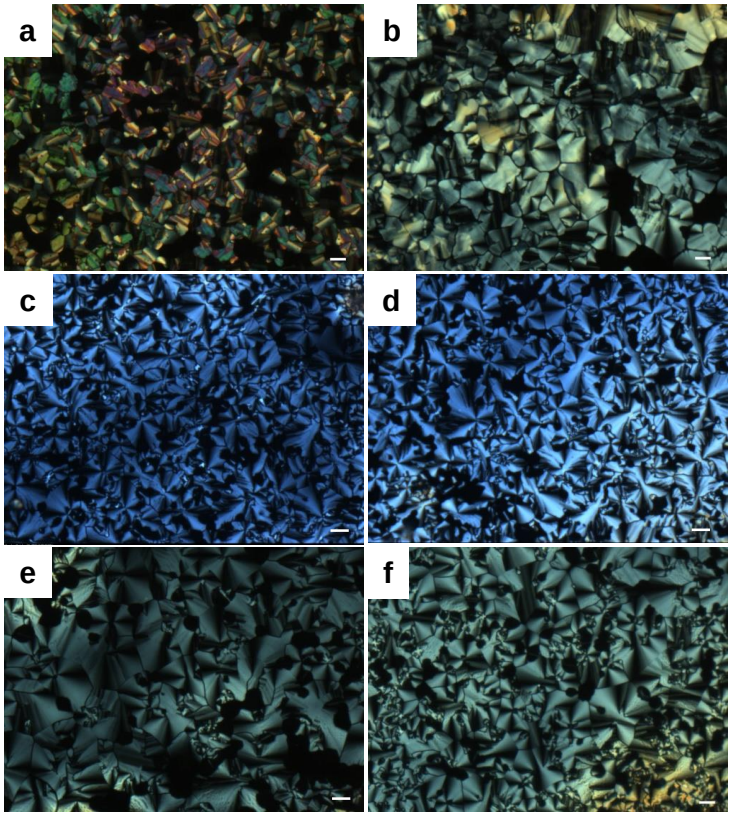

Figure A17 Polarized optical micrographs of doped compounds (a) **8a**: TNF [1:3] at 114.9 °C, (b) **8a**: TNF [1:4] at 101.5 °C, (c) **8b**: TNF [1:3] at 104.1 °C, (d) **8b**: TNF [1:4] at 103.7 °C, (e) **8c**: TNF [1:3] at 92.63 °C and (f) **8c**: TNF [1:4] at 77.3 °C as obtained on cooling from isotropic through a polarized optical microscope with crossed polarizers (scale bar = 20 μm).

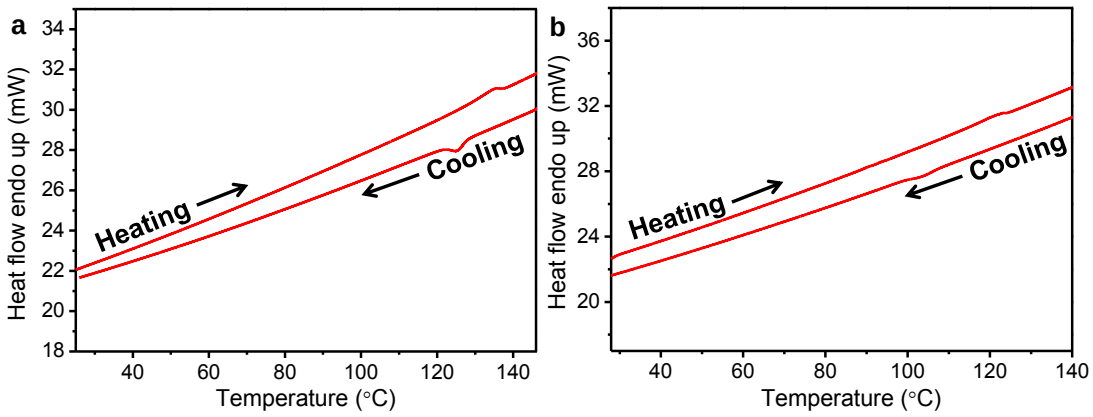

Figure A18 Representative DSC thermograms of doped compounds (i) **8a**: TNF (1:2) and (ii) **8c**: TNF (1:2).

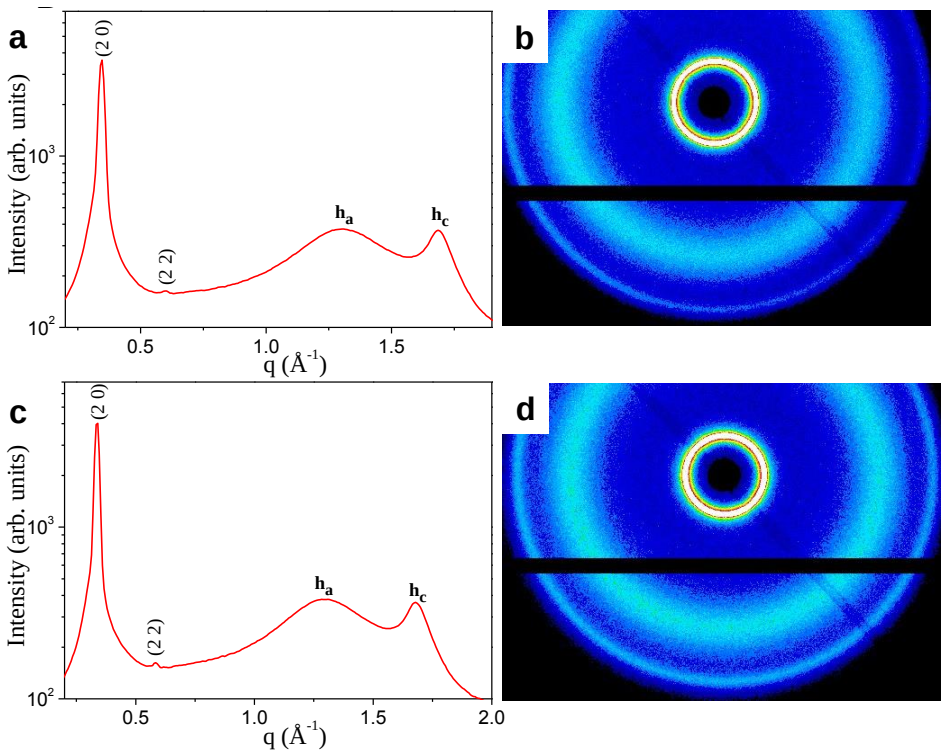

Figure A19 X-ray diffraction patterns of 1:2 complexes of (a) compound **8a** and (b) compound **8b** with TNF in their mesophase. (b) & (d) represent corresponding 2D diffraction patterns in the mesophase.

Table A3 The observed and calculated d-spacings and planes, correlation length of the diffraction peaks of the; Columnar hexagonal phase observed in compound **8a**: TNF = 1:2 with the lattice parameters, a = 40.34 Å and c = 3.74 Å . d_{exp} is the observed d-spacing. d_{cal} is the calculated d-spacing according to formula: $\frac{1}{{d_{cal}}^2} = \frac{4}{3}(\frac{h^2+h\,k+k^2}{a^2})$ for hexagonal phase. ξ is the correlation length.

Planes (hk)	d_{exp} (Å)	d_{cal} (Å)	ξ	ξ/ d_{exp}
20	17.47	17.47	223.68	12.80
22	9.99	10.09		
h_a	4.84			
h_c	3.74		43.01	11.50

Table A4 The observed and calculated *d*-spacings and planes, correlation length of the diffraction peaks of the columnar hexagonal phase observed in compound **8b**: TNF = 1:2 with the lattice parameters a = 41.90 Å and c = 3.73 Å.

Planes (hk)	d_{exp} (Å)	d_{cal} (Å)	ξ	ξ/ d_{exp}
20	18.14	18.14	223.68	12.33
22	10.41	10.48		
h_a	4.85			
h_c	3.73		43.01	11.57

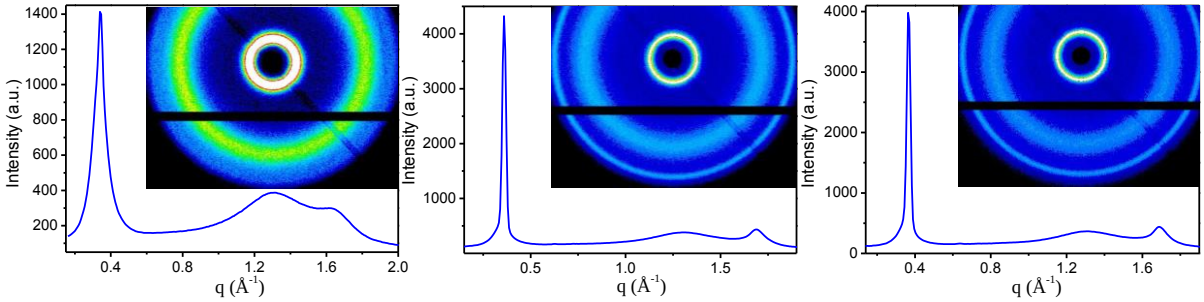

Figure A20 X-ray diffraction pattern of compound **8a**: TNF in (a) 1:1 (b) 1:3 and (c) 1:4 ratios in their mesophases. The corresponding 2D diffraction patterns are represented in the inset.

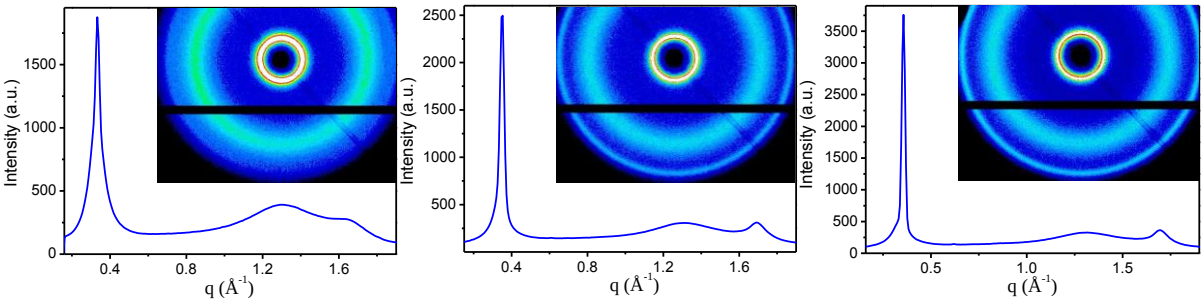

Figure A21 X-ray diffraction pattern of compound **8b**: TNF in (a) 1:1 (b) 1:3 and (c) 1:4 ratios in their mesophases. The corresponding 2D diffraction patterns are represented in the inset.

Chapter 3

Disc-disc and disc-rod dimers based on pentakis(phenylethynyl)benzene core

PART A

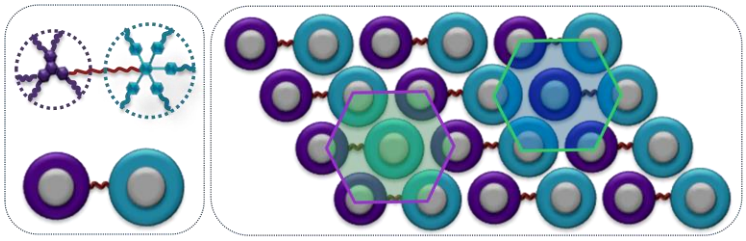

A facile synthesis of a new room temperature discotic mesogenic dyad based on triphenylene and pentaalkynylbenzene linked via flexible alkyl spacer is reported. Interestingly, the compound self-assembles into a columnar hexagonal mesophase at room-temperature and also exhibits an excellent blue light emission property which has possible potential for various opto-electronic applications. The liquid crystalline property of the dyad was further manipulated by preparing charge transfer complexes with trinitrofluorenone.

PART B

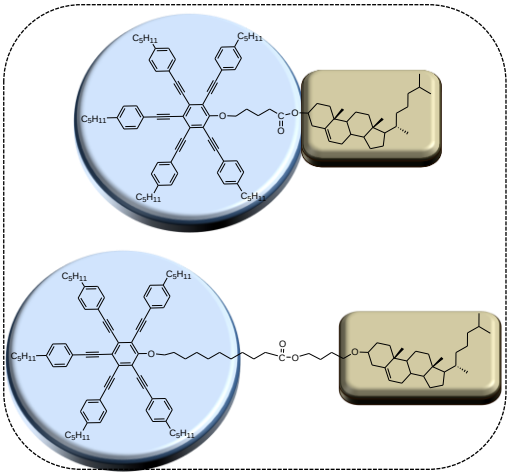

The synthesis of the first examples of room-temperature liquid crystal dimers based on cholesterol and pentaalkynylbenzene linked via varying flexible alkyl spacers is reported in this study. Both the synthesised dimers displayed chiral nematic (N) phase at room temperature and exhibited excellent fluorescent emission properties. The steady-state anisotropy and fluorescence lifetime were also measured in order to gain further insights into the supramolecular arrangement of these dimers.*

3.1 Part A: A room temperature discotic mesogenic dyad based-on triphenylene and pentaalkynylbenzene

3.1.1 Introduction

The mesogenic self-assembly of discotic molecules has been extensively studied due to their potential applications in opto-electronic devices.[1] The discoids being flat structures consist of π-electron rich aromatic rings which generally tend to form highly ordered columnar architectures that act as models for the study of one-dimensional pathways for rapid charge and energy migration in organized systems.[2] Other intermolecular interactions e.g. hydrogen bonding, metal complexation and charge transfer have also been realized in self-organization of molecules to columnar mesophases.[3-8] Various molecular electronic applications has been accomplished from these discotic columnar assemblies such as field effect transistors, organic light emitting diodes and photovoltaic cells by employing a combination of processability, self-healing and aligned directional conduction of either charge or energy.[9-13]

Further tailoring of the molecular architecture of discotic subunits can be done by linking them in defined numbers through alkyl spacers. In this respect, triphenylene (TP) derivatives have been widely investigated till date among various discotic liquid crystals (LCs).[14-17] Particularly, twinned and oligomeric TP derivatives have drawn much attention due to their enhanced processability and functionality allied with their advantageous macroscopic molecular orientation. These discotic cores linked via a long flexible alkyl chain spacer (e.g. compound **1**) generally form a columnar phase. However, when connected by a short rigid spacer such as compound **3-5**, they exhibit a weak distortion of the planarity of disk due to steric hindrance and prefer to form a nematic phase.[18-21]

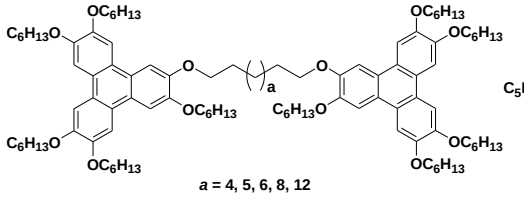

1

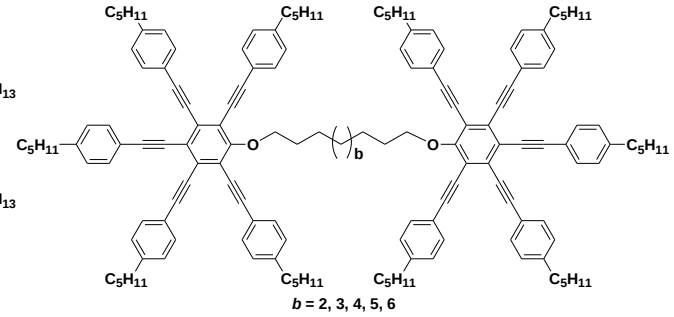

2

These discotic nematogens have been commercialized as optical compensational films for improving the viewing angle characteristics of liquid crystal displays (LCDs).[22-23] Among the various discotic nematogens reported in the literature, multialkynylbenzene have been the most investigated systems.[24] In case of multialkynylbenzene, stacking of discs for column formation is inhibited by the rotational freedom provided by ethynyl linkers which inhibit the efficient stacking of discs needed for column formation and indeed shows the discotic nematic phase (N_D). The symmetric discotic dimers based on TP and pentaalkynylbenzene (PA) linked via flexible alkyl spacers (compound **2**) have been found to display columnar hexagonal (Col_h) and N_D phase respectively.[25-31]

However, TP units when linked either through a short rigid π-conjugated diacetylene spacer or thiophene units displayed N_D mesophase having high mesophase transition temperatures and narrow mesophase temperature ranges which limits their applicability in devices.

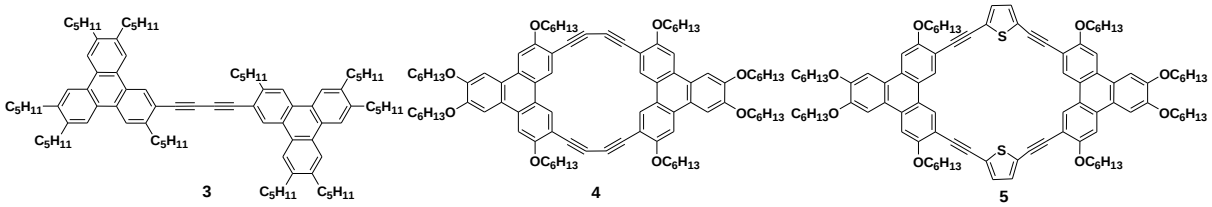

3.1.2 Objective

Till date, no effort has been made to covalently link two π-conjugated systems which can self-assemble themselves into Col_h and N_D mesophase respectively. In this regard, we endeavored to explore the self-organization of the system resulting from TP and PA units which can individually self-assemble into Col_h and N_D mesophase respectively. We thought to link these kind of units first through a long flexible alkyl spacer. It was assumed that this strategy may lead to strong enough π-π interactions between the TP units to overcome the rotational freedom provided by the side arms of PA unit. However, due to the rotational freedom of PA unit, the inter-disc interactions of TP units in the dyad may ultimately lead to mesophase even at room-temperature. In addition, PA being a blue light-emitting core can induce the same property in dimeric molecule and making it suitable for organic light

emitting devices. Therefore, it would be very interesting to investigate the self-assembly of these dyad system **6**.

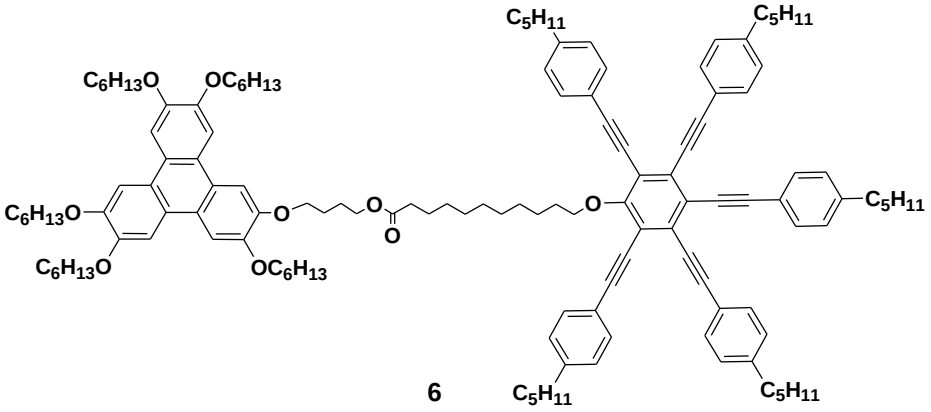

6

3.1.3 Results and Discussion

3.1.3.1 Synthesis and Characterization

The target compound **6** was prepared as depicted in Scheme 3.1. The synthesis of alkynyl substituted benzene derivative **9**, hexalkoxytriphenylene **10**, monohydroxytriphenylene **11** and ω-bromo-substituted triphenylene **12** were prepared following literature methods.[32, 33] For the synthesis of final compound **6**, the aqueous solution of pentakis(phenylethynyl)phenoxy undecanoic acid **9** in potassium hydroxide and tetraoctylammonium bromide was reacted with triphenylene bromide **12** under reflux conditions. The synthesized dyad was fully characterized by various spectroscopic techniques (^{1}H NMR, ^{13}C NMR, FTIR, UV-vis, HRMS) as detailed in the experimental section and representative spectra are given in appendix II (Figure A1-A4).

3.1.3.2 Thermal Behavior

The thermal behavior of the synthesized dimer **6** was investigated by polarizing optical microscopy (POM) and differential scanning calorimetry (DSC). Phase transitions associated with compound **6** are shown in Table 3.1. Under POM, the compound showed a highly birefringent texture in its pristine form. The presence of a LC phase at room temperature was confirmed from the shearability of the birefringent texture.

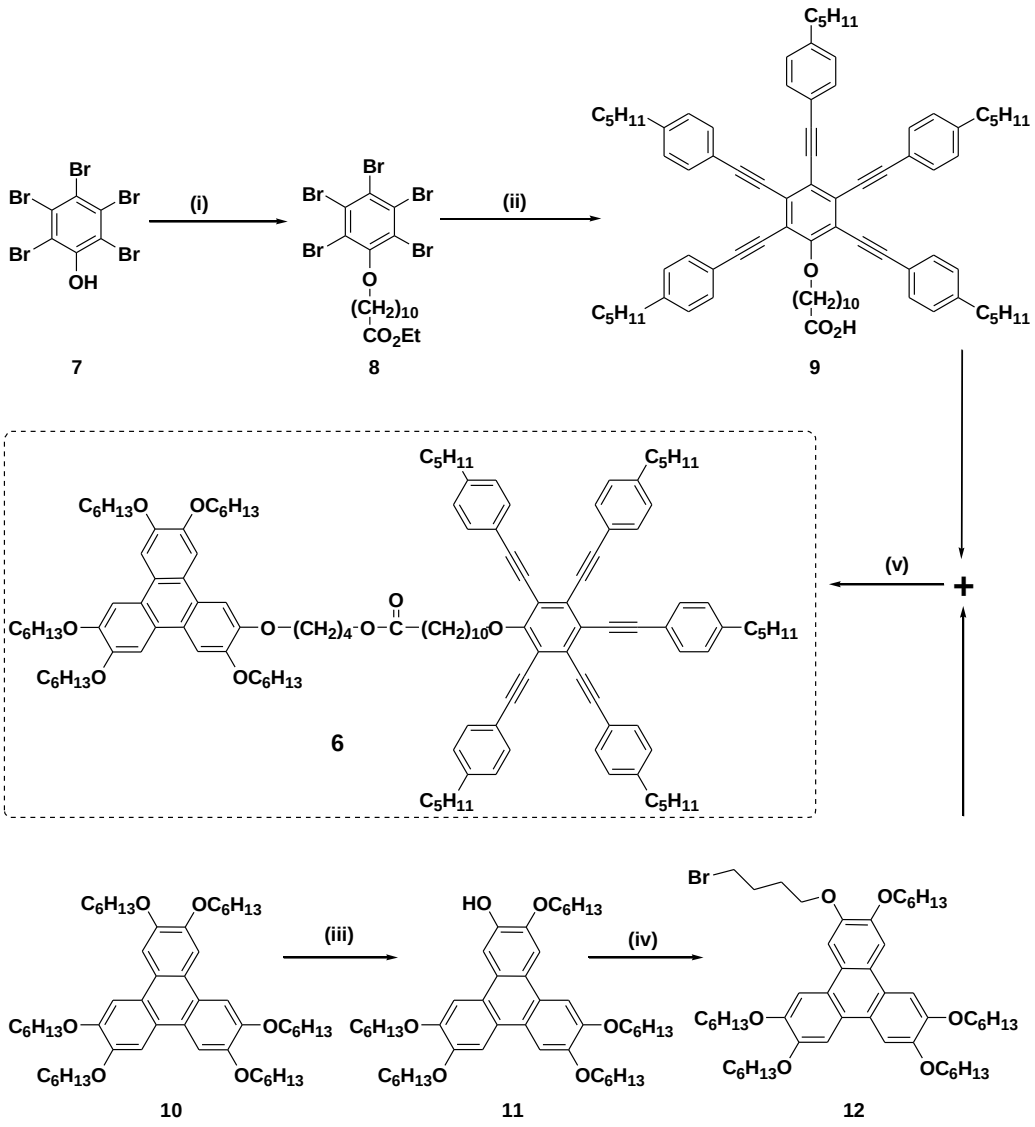

Scheme 3.1 Synthesis of Triphenylene-Pentaalkynylbenzene Dyad. Reagents and conditions: (i) $Br(CH_2)_{10}CO_2Et$, NaH, DMF, 100 °C, 10h, 83.3%; (ii) $Pd(PPh_3)_2Cl_2$, 4-pentylphenylacetylene, PPh_3, CuI, Et_3N,100 °C, 15h followed by KOH, EtOH, reflux, 80%; (iii) Cat-B-Br, CH_2Cl_2, RT, 24 h, 40%; (iv) Cs_2CO_3, KI, butanone, 80 °C, 18h, 88%; (v) KOH, TOAB, water, reflux, 3h.

On heating, the DSC thermogram of dimer **6** exhibited a peak at around 74 °C (ΔH = 1.6 kJ mol^{-1}) which corresponds to mesophase-to-isotropic transition. Before the mesophase appearance, it displayed two low energy crystal-to-crystal transitions at about -21 °C (ΔH =

3.9 kJ mol^{-1}) and 0.4 °C (ΔH = 1.9 kJ mol^{-1}) which can be associated with conformational reorganization of molecules by passing into different crystalline configurations.[34]

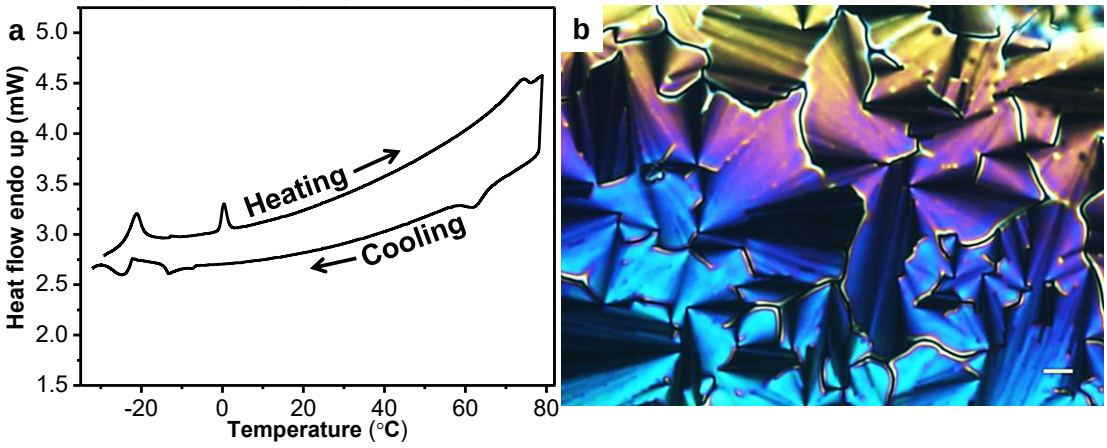

Figure 3.1 (a) DSC traces for compound **6** on heating and cooling (scan rate 5 °C/min). (b) Optical photomicrograph of **6** obtained with a polarizing microscope on cooling from the isotropic liquid at 54 °C (crossed polarizers, magnification X 200). Scale bar = 20 µm.

On further cooling, it showed the isotropic-to-mesophase transition centered at around 63 °C (ΔH = 1.9 kJ mol^{-1}) followed by two additional low energy crystal-crystal transitions. The DSC traces obtained from heating and cooling runs with **6** are shown in Figure 3.1a (appendix II, Figure A5). Under polarizing optical microscopy, on cooling from the isotropic, it showed focal conic textures typical of columnar phases shown by several other DLCs. Photomicrograph of compound **6** obtained on cooling from the isotropic liquid at about 54 °C is shown in Figure 3.1b.

Table 3.1 Thermal properties of Compound **6**.[a]

Compound	Phase transition temperature[a]
6 (*Heating*)	Cr -21 (3.9) Cr 0.4 (1.9) Col_h 74 (1.6) I
6 (*Cooling*)	I 63 (1.9) Col_h -13 (1.1) Cr -25 (3.4) Cr

[a] Transition temperatures (°C) and enthalpies of transition (kJ mol^{-1}, in parentheses) determined by DSC (scan rate 5 °C/min). Col_h: hexagonal columnar; Cr: crystalline; I: isotropic.

3.1.3.3 X-ray Diffraction Studies

For recording the X-ray diffraction pattern for the discotic dimer **6**, the compound was taken and heated to isotropic in a Lindemann's capillary of 0.7 mm diameter. The sample was cooled further at a rate of 5 °C/min to 30 °C (which depicted the columnar hexagonal arrangement of molecules within the LC phase) and diffractogram was recorded (Figure 3.2). In the small angle region, X-ray diffraction pattern showed three peaks at 21.55 Å, 12.42 Å and 10.72 Å with the ratio of $1:\frac{1}{\sqrt{3}}:\frac{1}{2}$ which were indexed as (100), (110) and (200) respectively and conclusively affirms the occurrence of a 2D Col_h phase. The column to column separation, *a* (lattice parameter), is calculated by using the relation, $a=\frac{2\,d_{100}}{\sqrt{3}}$ where d_{100} is the *d*-spacing corresponding to the peak indexed on (100) plane. The value of '*a*' was found to be 24.88 Å. In the wide angle regime, the diffraction pattern exhibited a diffuse peak at 5.02 Å (h_a) which appears due to the correlation of molten aliphatic chains. In-addition, it showed two more relatively narrow peaks at 8.06 Å and 4.04 Å which are indexed as (001) and (002). Peak at 4.04 Å corresponds to core-core separation of the discs in a column and peak at 8.06 Å can be ascribed to ABAB layering (*vide infra*) (Figure 3.2a, Table 3.2). All these features fit into the well-known model for the columnar hexagonal phase in which disc-like core of the molecules stack on the top of each other to form columns surrounded by alkyl chains & these columns in turn arrange themselves in a hexagonal lattice.

Electron density map of this dimeric system was reconstructed with the Miller indices and intensities of the reflections to determine the exact positions of the TP and PA cores in the unit cell (Figure 3.2b). Here, red represents the highest electron density and dark blue the lowest. The calculated lattice parameter *a* is approximately in accordance with the diameter for either triphenylene or pentakis(phenylethynyl)benzene units (~20 Å). No sign of the peak corresponding to the diameter of the molecule (~40 Å) was observed even on recording the diffractogram at small-angle. Therefore, the columnar layered molecular arrangements were proposed as shown in Figure 3.3. The TP units are generally prone to form the Col_h mesophase, however, PA units tend to display N_D mesophase. But PA units can easily associate with TP units to form a column where the two units are arranged in a periodic

manner. The peak at 8.06 Å corresponds to this lamella periodicity with indexing (001) whereas the one at 4.04 Å results from the second order reflection with indexing (002) and arises from core-core separation (*i.e.* separation between TP and PA units). Since the electronic distribution of TP and PA units are not identical but slightly different, 8.06 Å is not missing but is very weak.

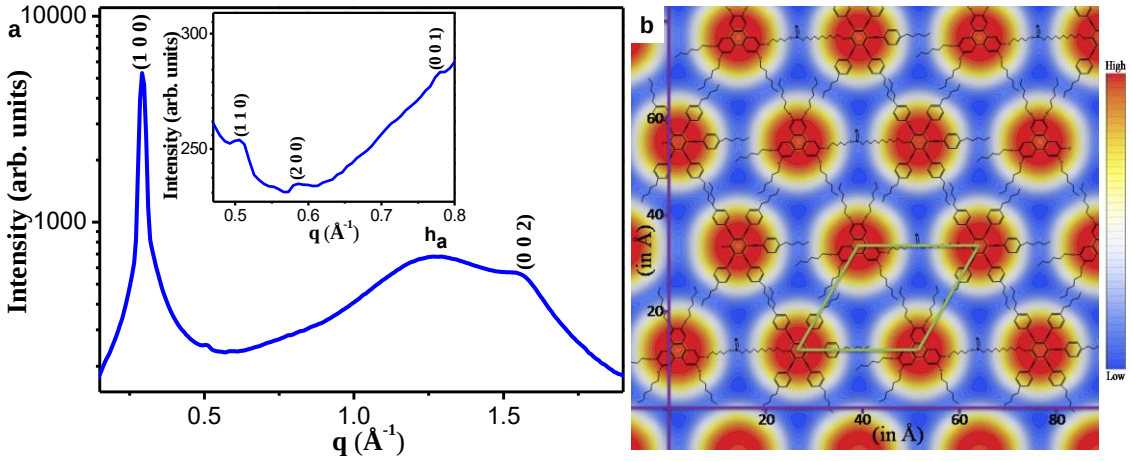

Figure 3.2 (a) X-ray diffraction pattern of compound **6** at temperature 30 °C with indexing for small angle and wide angle (inset) on the columnar hexagonal phase (Col_h). (b) Reconstructed electron density map of Col_h phase of compound **6** along with the arrangement of molecules in the lattice (red corresponds to highest electron density and deep blue is the lowest). Parallelogram on the map (in green colour) shows the unit cell of Col_h phase.

Table 3.2 The indices observed and calculated *d*-spacings, planes, intensity, multiplicity and phase of the diffraction peaks of the columnar hexagonal lattice observed at 30°C in compound **6**. The lattice parameter is a = 24.88 Å.

Planes (hkl)	dspacing d_{exp} (Å)	dspacing d_{cal} (Å)	Relative Intensity	Multiplicity	Phase (ϕ)
1 0 0	21.55	21.54	100.00	6	0
1 1 0	12.42	12.44	4.78	6	π
2 0 0	10.72	10.77	4.46	6	π
0 0 1	8.06	8.06			
h_a	5.02	Alkyl chain-chain			
0 0 2	4.04	4.03			

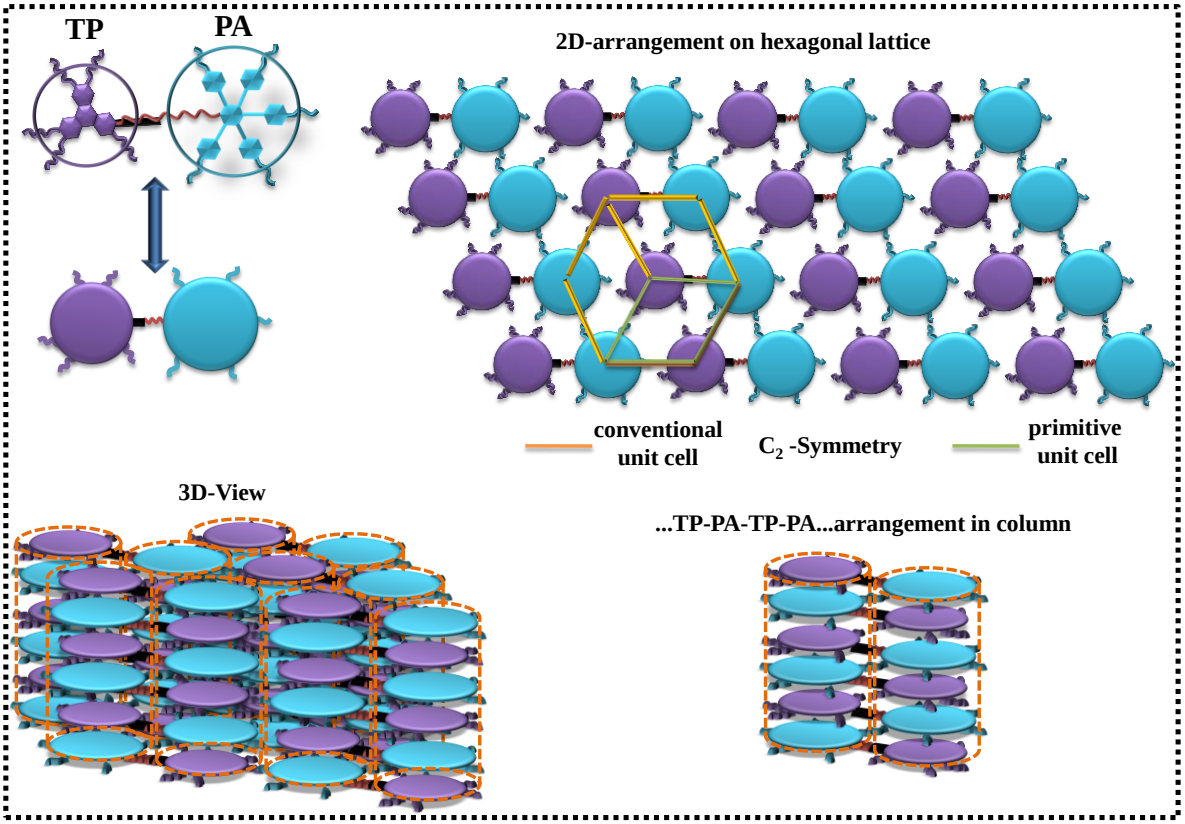

Figure 3.3 Schematic of the structure of compound **6** modelled as a two discs (TP and PA) connected with flexible chains. These discs are arranged on a 2D hexagonal lattice in the column plane. In the column TP and PA units are arranged alternatively. 3D view of the structure is also shown.

In the column plane there were four M units and two T units on the six angles of hexagonal circle and vice -versa. Hence, the symmetry is reduced from C6 to C2. As whole, the assembly can be realized as ...TP PA TP PA... layered structure where each layer is a 2D sheet on which TP and PA units are arranged on a hexagonal lattice. The second layer is identical to the first one but is translated by (*a*, 0, 0) with respect to the earlier.

3.1.3.4 Charge-transfer Complexes

Our next goal was to investigate that whether the mesomorphic properties of the compound **6** can be stabilized over a wide temperature range by inducing specific interactions of various kinds such as charge-transfer (CT) interactions. CT interactions induced by 2, 4, 7-

trinitrofluorenone (TNF) have been known to stabilize the existing mesomorphic range in a binary mixture between TP derivatives and TNF. The isotropic temperature goes up to a maximum for a particular concentration of TNF, above which there occurs phase separation. Therefore to increase molecular interactions and thus stabilization of the mesomorphic behavior, we further doped compound **6** with TNF in different molar ratio. We prepared four binary mixtures of **6**: TNF whose mesomorphic behavior was confirmed by POM. The textures were obtained by heating the binary mixtures above the isotropic temperature followed by cooling with a cooling rate of 5 °C/min (Table 3.3, Figure 3.4). As expected, all the TNF complexes displayed higher clearing temperature compared to **6**. The maximum clearing points and therefore the maximum stability is found for 1:1 molar composition (i.e., 50% TNF) of **6** and TNF.

Table 3.3 Phase transition temperatures (peak, °C) from POM studies of **6** with TNF.[a]

Compound/Mixture	First Heating Scan	First Cooling Scan
6 : TNF [2:1]	Col_h 165 I	I 161 Col_h
6 : TNF [1:1]	Col_h 166 I	I 161 Col_h
6 : TNF [1:2]	Col_h 143 I	I 140 Col_h
6 : TNF [1:3]	Col_h 120 I[a]	I 113 Col_h

[a] phase separation occurs

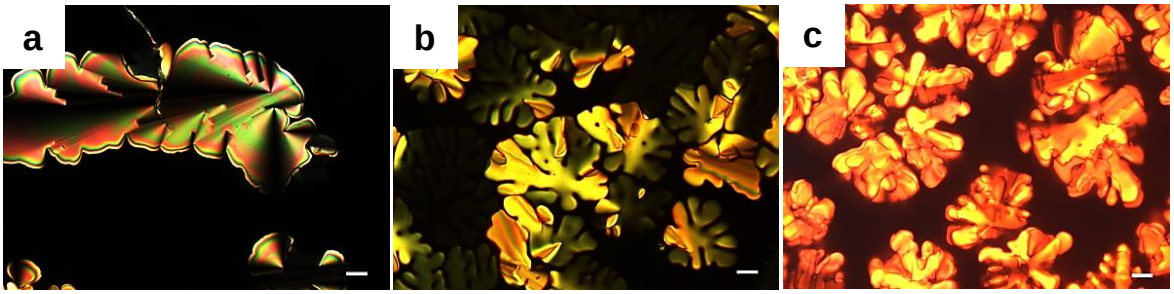

Figure 3.4 Optical texture for the mesophase of the doped dimer **6**: TNF in a (a) 1:2 ratio (b) 1:1 ratio and (c) 2:1 ratio with a cooling rate of 5 °C/min at 158 °C, 152 °C and 140 °C, respectively. Scale bar = 25 μm.

3.1.3.5 Photophysical Studies

As expected, due to incorporation of PA unit, the compound **6** showed blue fluorescence in solution even under daylight conditions. Figure 3.5 displays the absorption and fluorescence spectra of the mesogen in 5 nM $CHCl_3$ solution. The absorption bands show six peaks (including four shoulder peaks) whereas fluorescence spectrum exhibits only one peak at 447 nm. However, for the neat compound **6** the peak showed a red shift to 498 nm and was showing green emission (Figure 3.5). In order to understand the nanoenvironment of the compound **6**, fluorescence lifetime and steady state anisotropy measurements were performed in dilute solution (5 nM in $CHCl_3$). The steady state anisotropy for **6** was found to be 1.501×10^{-2} and the fluorescence lifetime was calculated to be 4.48 ns, whereas, the steady state anisotropy & fluorescence lifetime for **9** was 4.3×10^{-3} & 4.7 ns, respectively (Table 3.4, appendix II Figure A6).

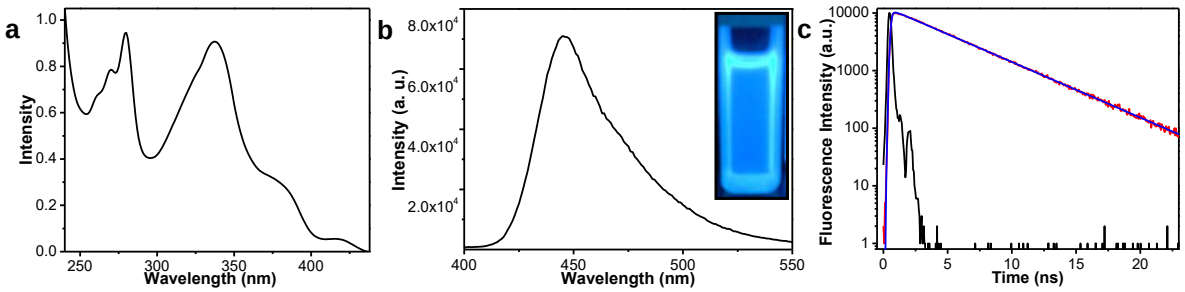

Figure 3.5 (a) UV-vis absorption spectra, (b) representative fluorescence spectra and (c) Fluorescence decay spectra of compound **6** in $CHCl_3$.

Table 3.4 Fluorescence life time (measured life time) and steady state anisotropy values of compound **9** & **6**.

Compound	r_{av} (ns)	Steady State Anisotropy
9	4.7	0.0043
6	4.48	0.015

A plausible explanation for the slight decrease in fluorescence life time of **6** could be due to a little higher non-radiative rate involved in the processes due to change in size and shape of

the hybrid molecules and thus molecular interactions.[35] The bulky triphenylene unit restricts the molecular motion of the hybrid which results into its increased fluorescence anisotropy.

3.1.4 Conclusions

In conclusion, a novel TP-PA dyad that shows Col_h phase at room temperature is reported in this study. The dyad shows excellent fluorescent emission properties which can lead to its possible potential application in opto-electronic devices. This study also points the way towards design and synthesis of new room temperature columnar LCs showing blue emission by incorporating a pentaalkynylbenzene unit.

3.2 Part B: The first examples of room temperature liquid crystal dimers based-on cholesterol and pentaalkynylbenzene

3.2.1 Introduction

LC dimers provide a wide variety of supramolecular self-arrangements due to versatility of molecular structures whose mesomorphic properties can be modulated by varying the two monomeric units as well as the central spacer.[36] Their transition properties vary dramatically due to remarkable difference in their molecular topologies. They are of immense importance to serve as precursors in the technologically important semiflexible main-chain LC polymers. The properties of these LC dimers also provide an understanding of the behaviour of these polymeric LCs.[37] In this regard, cholesterol has been incorporated into many LC dimers which can induce chirality due to the presence of the chiral centres and thus influence the formation of either chiral nematic (N*) & smectic C (SmC*) phases or in some cases the short-lived twist gain boundary (TGB) & blue phases (BP).[38]

Earlier reports show that the cholesteryl dimers with *n*-alkyl & *n*-alkoxy substituted diphenyl acetylenes exhibited similar thermal behaviour with existence of N* or SmA phase over a wide thermal range whereas the TGB or SmC* phase were found to be short-lived.[39, 40] Also the number of mesophases were reduced when the *n*-substituted moiety was chiral.[41, 42] The cholesteryl unit when linked to 2-phenyl benzoxazole through an alkylene spacer showed the formation of BP phase over a quite reasonable thermal range which have potential technological applications.[43] With 4-trans-(4-n-alkylcyclohexyl) phenoxy group, they showed SmA-N*-I transition in presence of shorter terminal alkyl chain. In contrast, longer spacer tend to exhibit only N* mesophase.[44] The cholesteric group attached to a terminal *o*-alkyl substituted phenyl benzoate unit through a thio-alkyl spacer of 5-phenyl substituted oxadiazole unit showed unusual wide thermal range for the TGBC* phase due to bent structure of molecule.[45] Majumdar *et. al.* synthesized a series of compounds by condensing ferrocenyl aldehydes with cholestryl amines. By varying the spacer length between ferrocene & aromatic ring containing aldehyde group, they observed a variety of mesophases such as N*, SmA & TGB phases.[46] The similar mesophases were also observed when cholesterol

was attached to 4-alkoxy-5-phenylthiophene unit through a schiff base linkage as well as to a biphenyl moiety through ester linkage.[47, 48]

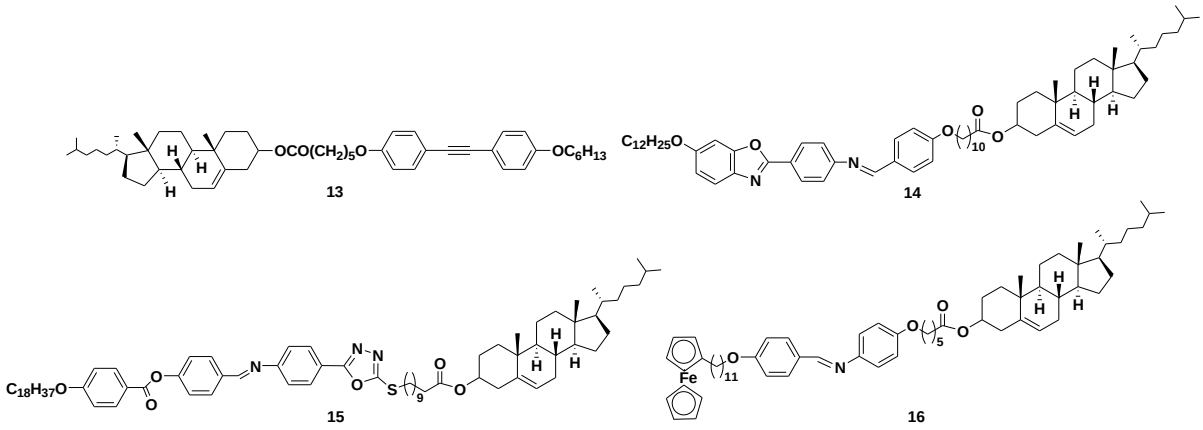

Moreover, the butyl substituted salicylidene imine core linked to a cholesterol moiety through methylene spacer exhibited N* phase whereas the compounds with the fluoro & chloro substitution exhibited BP, TGB & SmC* phase in addition to the N* phase.[49] The cholesteryl dimers with the five ring bent core molecules even showed the formation of smectic layers having the ribbon like segments in which the adjacent ribbons were having the bent direction of molecules antiparallel.[50]

Although there are many examples of various cholesteric dimers and several rod-disc dimers have also been reported[51, 52] but till now there is no report for cholesterol linked unsymmetrical rod-disc dimer LC. In a cholesteric discotic dimer, the bulky cholesteric moiety is capable of twisting the molecule whereas the discotic unit is a flat structure. Therefore, the molecular interplay of the cholesteric and discotic units in the resulting cholesteric discotic dimer can lead to interesting physical properties. There is one report for the discotic cholesterol dimer so far which is based on the cholesteryl units being attached to the TP core but the dimeric compound was found to be liquid.[53] This may be due to the bulky cholesterol unit which perturbs the molecular symmetry of the TP unit & also prevents the mesophase formation. We assumed that in case of a discotic nematic core the perturbation in molecular symmetrly will not necessarily avoid the mesophase formation and infact there is much more possibility of observing desirable BP & TGB phase as there will be much more twisting in a nematic discotic core which is a pre-requisite for the formation of these phases.

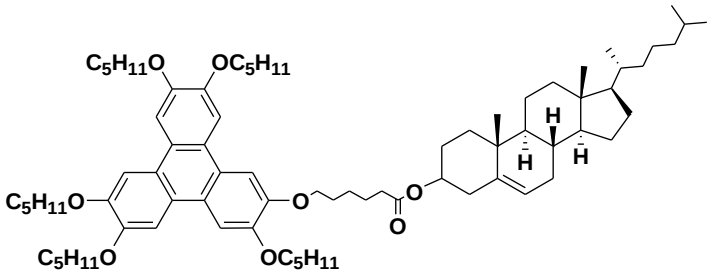

17

Hauser *et. al* have observed three distinct blue phase by doping hexakis [(4-nonylphenyl) ethynyl] benzene which shows nematic discotic phase with perlauroyl cellobioside as a chiral dopant.[54] Therefore attaching a nematic discotic unit covalently to a cholesterol group can induce blue phase. Benzene based multiynes are the most investigated system among the various discotic nematogens. The formation of discotic nematic mesophase in these compounds is favoured due to rotational freedom provided by the ethynyl linkers which prevents stacking of disks & column formation. They are of immense importance because of their application as optical compensation films for wide viewing angle in LCD devices. Hexaynes mainly exhibited the nematic discotic phase.[55] Hexaynes containing racemic side chains exhibited even room temperature N_D phase.[56] Pentaynes which can be functionalized in various ways exhibited chiral N_D phase when attached to chiral branched chains.[57] The symmetrical dimers based on the pentaynes also exhibited N_D phase.[58] The dimers of pentaynes with calamitic mesogens mainly showed the existence of nematic phase and also have been looked for much sought biaxial nematic mesophase.[51, 59-61]

3.2.2 Objective

We have explained in the earlier chapter that the PA unit linked to a TP moiety through flexible alkyl spacer exhibited room temperature Col_h mesophase.[62] Herein, we made an attempt to look into the mesomorphism of the discotic cholesteric dimers obtained by linking a PA core with the cholesterol group through flexible alkyl spacers (Scheme 3.2).

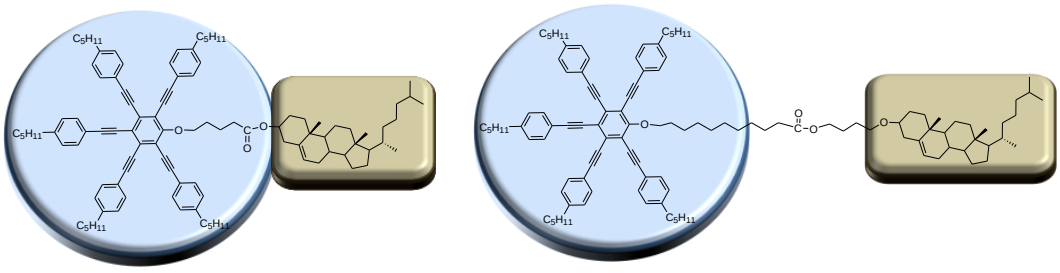

18 **19**

Scheme 3.2 Molecular design of the dimers synthesized in the study.

3.2.3 Results and Discussion

3.2.3.1 Synthesis and Characterization

The synthesis of compound **21** was done by DCC coupling reaction (Scheme 3.3).[63] For the synthesis of compound **22**, pentabromophenol (1 equivalent) was dissolved in n-butanone. To that solution, potassium carbonate (3 equivalents) was added & the mixture was stirred for 15 min followed by the addition of **21** & a catalytic amount of KI. The mixture was refluxed for 18 h. The solvent was evaporated & the crude was purified through column chromatography to obtain the compound **22**. Five-fold sonogashira coupling of compound **22** yielded one of the final dimeric compound **18**. Further, the synthesis of compounds **24** & **25** has already been described elesewhere.[62] For the synthesis of the target compound **19**, compound **25** (1 equivalent) was reacted with compound **21** in presence of a phase transfer catalyst The synthesized compounds **18** & **19** were characterized by ^{1}H NMR, ^{13}C NMR, IR, UV-vis and mass spectrometry as explained in the experimental section and appendix II (Figure A7-A12).

3.2.3.2 Thermal Behaviour

The thermal behavior of the target materials **18** & **19** was investigated by Polarizing Optical Microscopy (POM) and Differential Scanning Calorimetry (DSC). On heating, the DSC thermogram of compound **18** exhibited a peak centred at 62 °C (ΔH = 19.037 kJ mol^{-1}). This corresponds to mesophase to isotropic transition (see appendix II, Figure A13a).

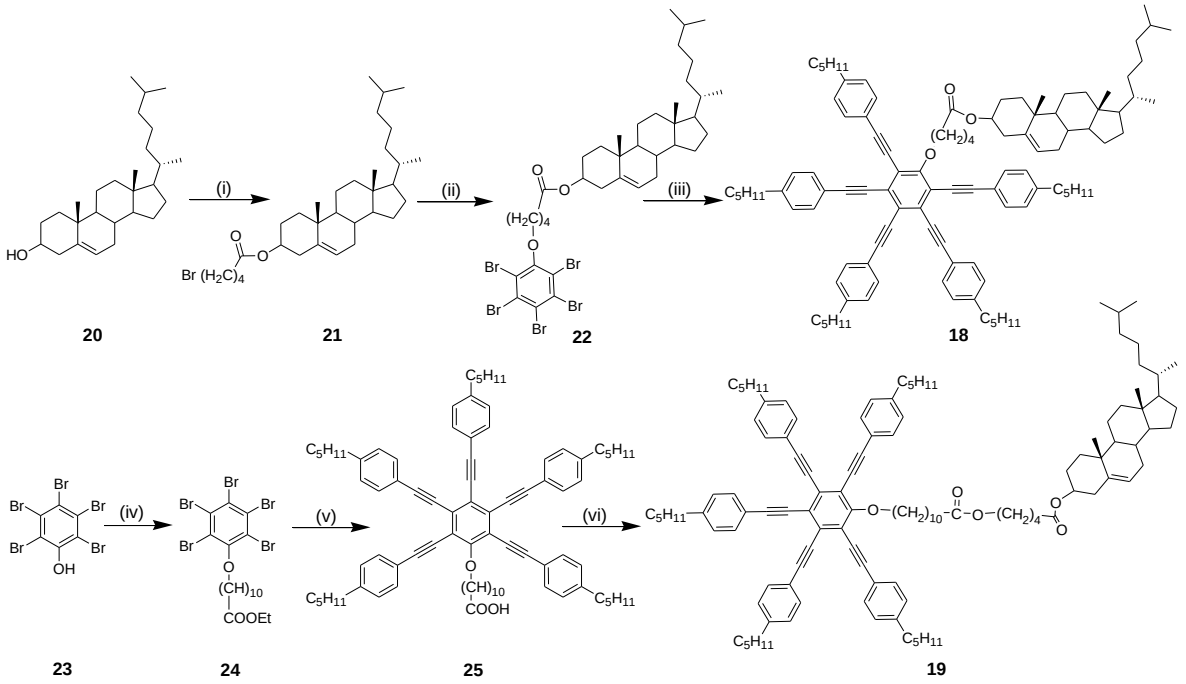

Scheme 3.3 Synthesis of the target compounds **18** & **19**. Reagents and conditions: (i) 5-bromovaleric acid, dry DCM, DCC, DMAP, 12 h, R.T., 88%; (ii) Pentabromophenol, K_2CO_3, KI, butanone, 80 °C, 18 h, 89%; (iii) $Pd(PPh_3)_2Cl_2$, 4-pentylphenylacetylene, PPh_3, CuI, Et_3N,100 °C, 15h, 82%; (iv) $Br(CH_2)_{10}CO_2Et$, NaH, DMF, 100 °C, 10h, 83.3 %; (v) $Pd(PPh_3)_2Cl_2$, 4-pentylphenylacetylene, PPh_3, CuI, Et_3N,100 °C, 15h followed by KOH, EtOH, reflux, 80 %; (vi) Compound **21**, KOH, TOAB, water, reflux, 3h, 50%.

Such a high value of transition enthalpy for isotropic to chiral nematic have also been reported for the discotic oligomer containing cholesterol group.[35] However, on cooling, no phase transition was observed till -100 °C. These results were also supported from POM studies. Under POM, the compound **18** showed a nice Grandjean texture of N* phase on heating (Figure 3.6a) followed by isotropization. On cooling the texture can be clearly seen under microscope though in DSC no peak corresponding to the isotropic-nematic transition was observed. The optical micrograph of compound **19** showed a weak birefringent texture at room temperature (Figure 3.6b). However, the birefringence increased on shearing the glass slide. The compound when filled into a homogeneous cell showed the existence of nematic droplets.

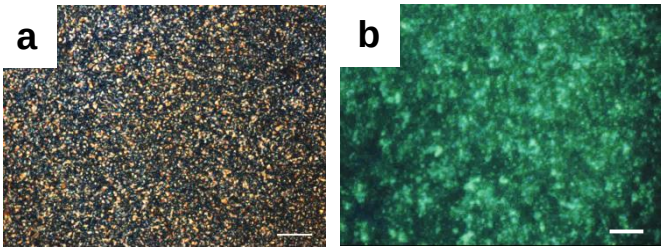

Figure 3.6 Optical photomicrograph of compounds a) **18** & b) **19** obtained with a polarizing microscope at 53 °C (on heating, magnification X 500) & 25 °C (magnification X 200) respectively. (Crossed polarizers, scale bar = 20 μm).

The texture was stable upto 175 °C after which signs of decomposition of the sample were observed. DSC thermogram of compound **19** didn't show any transition corresponding to mesophase to isotropization but rather indicated the decomposition of the compound at around 180 °C (see appendix II, Figure A13b). The low temperature DSC investigations showed the absence of crystallization till -100 °C. The reason for stabilisation of the mesophase for compound **19** could be due to increased length of the spacer which provides more freedom to the molecules to self-assemble which results into the uniformity in alignment of helices which is also evident from the weak birefringent texture of the compound which becomes more birefringent on shearing the film (see appendix II, Figure A14).

3.2.3.3 X-ray diffraction studies

The mesophase structure was further investigated by XRD studies. Both the compounds **18** and **19** showed two diffuse reflections in the wide- and the small-angle region (Figure 3.7), which indicates the absence of any positional order, thereby excluding the possibility of the existence of smectic and columnar structure of these dimers. The diffuse peak in the wide-angle region for the compounds **18** and **19** was seen at 4.44 Å and 4.56 Å, respectively, which corresponds to the average lateral separation of the molecules in the mesophase. Reflections related to planar disc–disc (001) distances and second harmonics observed for dimeric systems are not seen in the XRD pattern. This can be explained in two ways. First, energy minimized diagram of compound **18** shows that cholesterol moiety is curled to the back side of the disc-shaped mesogen. This is due to the odd spacer parity of the dimer which

gives a bent conformation to the mesogens. Thus, the observed *d*-spacing (18.4 Å) for compound **18** is almost matching with the diameter of the disc (18.1 Å), which is obtained by the space-filling-energy-minimised (all-trans) molecular model derived from molecular mechanics (MM2) method (Figure 3.8a and b).

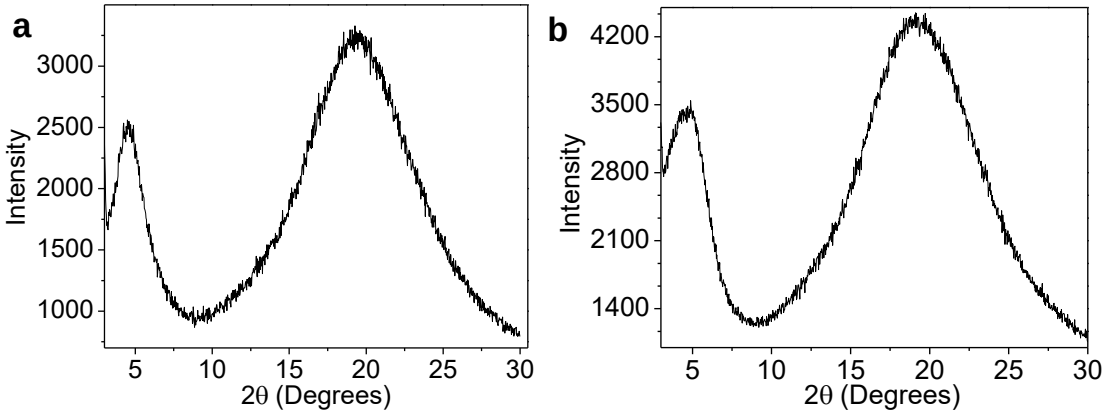

Figure 3.7 The intensity versus 2θ graph derived from the X-ray diffraction pattern of compound a) **18** and b) **19** at 57 °C & 150 °C respectively.

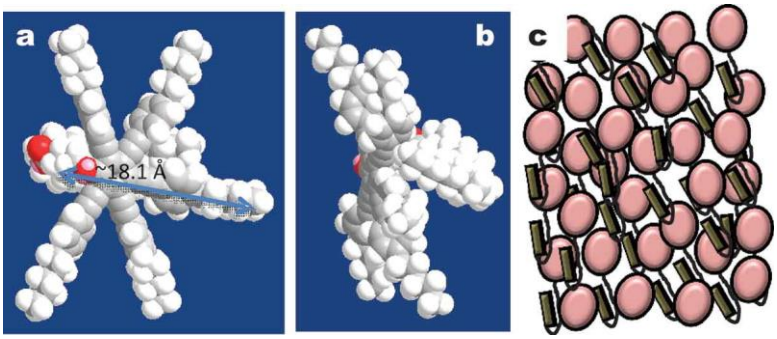

Figure 3.8 The two possible arrangements of the mesogens in the mesophase. (a) (Face on) and (b) (side view) Curling of cholesterol behind the PA disc. (c) Possible arrangement in the mixed nematic phase.

Similar organization might be possible for compound **19** that shows a *d*-spacing of 19 Å. Second, an alternative arrangement of the observed spacing of 18.4 Å and 19 Å of compounds **18** and **19**, respectively, corresponds to the average length of rod, i.e., cholesterol (~9 Å) and disc (28 Å). The diffuse peak at the low angle and absence of other reflections

(which may be occurring due to the part of the dimeric mesogen) suggest the complete compatibility and miscibility of these two anisotropic units in the N* phase (Figure 3.8c).

3.2.3.4 Photophysical Properties

Both the compounds showed blue fluorescence in solution. Figure 3.9 displays the characteristic absorption and fluorescence spectra of the mesogens in 5 nM $CHCl_3$ solution. The absorption spectrum shows four peaks whereas fluorescence spectrum exhibits only one peak at 449.2 nm characteristic of PA core. To get further insights into the ordered molecular structure of the dimers, fluorescence lifetime & steady state anisotropy measurements were performed in dilute solution (5 nM in $CHCl_3$).

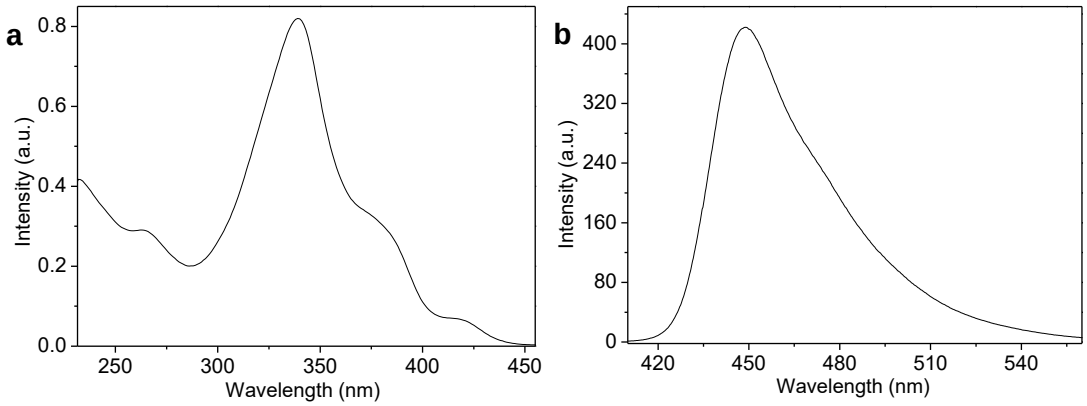

Figure 3.9 Representative (a) UV-vis absorption and (b) fluorescence spectra of compound **18** in $CHCl_3$. Compound **19** shows similar spectrum.

Table 3.5 Fluorescence life time (measured life time) and steady state anisotropy of compounds **18** & **19**.

Compound	τ_{av} (ns)	Steady State Anisotropy
18	4.8	0.005
19	4.7	0.006

The steady state anisotropy for **18** & **19** was found to be 5 X 10^{-3} & 6 X 10^{-3} respectively whereas fluorescence lifetime for **18** & **19** was 4.8 & 4.7 ns respectively (Table 3.5). Since in

the compound **19**, the spacer length is more as compared to **18**, the helices are aligned more uniformly which can lead to a lesser degree of rotational diffusion resulting in increased fluorescence anisotropy and decreased lifetime.

3.2.4 Conclusion

In conclusion, we have reported the synthesis of two novel dimeric mesogens based on cholesterol & PA units which represents the molecular interplay between the discotic & cholesterol units. The mesogens were found to exhibit chiral nematic mesophase at room temperature. For the dimer with longer spacer, the mesophase was stable up to 175 °C which can be assigned to uniform alignment of helices which was also predicted from POM studies and increased steady state anisotropy. In addition, the mesogens exhibited excellent fluorescence emission properties making them suitable for various opto-electronic properties.

3.3 Experimental Section

3.3.1 Synthesis of compound 6 For the synthesis of final compound **6**, the precursor pentakis(phenylethynyl)phenoxy undecanoic acid **9** was stirred in an aqueous potassium hydroxide solution (pH 8–9) for 20 minutes which was then followed by in situ addition of triphenylene bromide **12** and tetraoctylammonium bromide (TOAB) as a phase transfer catalyst. The resulting mixture was then refluxed vigorously for 3–4 h. The reaction mixture was then cooled to room temperature and extracted with chloroform. The organic layer was separated, washed with brine and dried over anhydrous sodium sulphate. The chloroform was removed by rotary evaporation and the resulting residue was purified by repeated column chromatography over silica gel using hexane and ethyl acetate as eluent to yield final compound **6**. FT-IR (cm^{-1}): 3027.6, 2955.45, 2929.05, 2857.10, 2206.8, 1903.7, 1737.86, 1617.27, 1514.46, 1467.57, 1435.32, 1391.14, 1348.40, 1262.22, 1170.50, 1044.31, 836.77, 755.91. UV-vis (nm): 263.00, 270.00, 280.00, 337.00, 384.00, 418.00. ^{1}H NMR (400 MHz, $CDCl_3$, δ in ppm): 7.85 (d, 6H), 7.55 (m, 10H), 7.19 (m, 10H), 4.36 (t, 2H, *J* = 8 Hz), 4.25 (tt, 14H, *J* = 4, 8, 4, 8, 4 Hz), 2.65 (t, 10H, *J* = 8 Hz), 2.32 (t, 2H, *J* = 8 Hz), 1.97 (m, 16 H), 1.63 (m, 24H), 1.37 (m, 50H), 0.91 (m, 30H). ^{13}C NMR (400 MHz, $CDCl_3$, δ in ppm): 173.96, 160.22, 148.99, 148.94, 148.65, 144.02, 143.91, 143.72, 131.78, 128.55, 128.53,

123.81, 120.54, 120.48, 120.10, 107.73, 107.02, 99.52, 99.35, 97.28, 87.08, 86.61, 84.08, 69.70, 69.51, 69.08, 64.05, 35.99, 34.40, 31.73, 31.51, 31, 29.41, 25.90, 14.08. MS (MALDI): m/z for $C_{134}H_{174}O_9$ 1928.31; found 1928.4.

3.3.2 Synthesis of compound 18 For the synthesis of compound **18**, 30 ml of dry triethylamine was taken in a round bottom flask which was degassed followed by the addition of $Pd(PPh_3)Cl_2$ (50 mg), CuI (50 mg), PPh_3 (100 mg) & compound **22** (0.63 mmol). The mixture was stirred for 15 minutes followed by the gradual addition of 1-ethynyl-4-pentyl benzene (6.3 mmol). The mixture was stirred at 100°C for 15 h under nitrogen & after cooling to room temperature it was poured into 40 ml of 5M HCl. The product was extracted with DCM & was purified through column chromatography to obtain the target compound **18**. ^{1}H NMR (400 MHz, $CDCl_3$, δ in ppm): 7.57 (m, 10H), 7.21 (m, 10H), 5.37 (m, 1H), 4.63 (m, 1H), 4.42 (t, 2H, *J* = 8, 4 Hz), 2.67 (t, 10H, *J* = 8 Hz), 2.15 (t, 2H, *J* = 8, 4 Hz), 2.31 (d, 2H, *J* = 8 Hz), 2.01 (m, 5H), 1.84 (m, 3H), 1.67 - 0.93 (m, 76H). ^{13}C NMR (400 MHz, $CDCl_3$, δ in ppm): 172.95, 159.92, 144.05, 143.97, 143.74, 131.80, 131.62, 128.62, 128.60, 124.22, 122.58, 120.70, 120.48, 120.07, 99.62, 99.52, 97.39, 87.09, 86.61, 84.04, 74.0, 73.83, 56.69, 56.14, 50.02, 42.31, 39.75, 39.54, 36.20, 36.02, 35.84, 31.85, 31.56, 31.52, 30.98, 28.28, 28.05, 24.31, 23.82, 22.87, 22.60, 21.98, 19.33, 18.74, 14.11, 11.86. FT-IR (cm^{-1}): 3082.2, 3031.7, 2932.72, 2208.78, 1903.3, 1731.74, 1606.79, 1513.63, 1465.5, 1425.80, 1378, 1346.69, 1266.8, 1177.91, 1084.86, 1019.84, 963.64, 837.96, 733.27, 551.42. UV-vis (nm): 233, 268, 339, 383, 418. MS: m/z for $C_{103}H_{128}O_3$ 1413.99; found 1413.03.

3.3.3 Synthesis of compound 19 For the synthesis of the target compound **19**, compound **25** (1 equivalent) was dissolved in aqueous KOH (1 equivalent) solution. To that solution, compound **21** (2 equivalents) was added followed by the addition of tetraoctylammonium bromide in catalytic amounts. The reaction mixture was refluxed under vigorous stirring for 3 hours & was then cooled to room temperature. The compound was extracted with chloroform. The organic layer was washed with brine & dried over anhydrous sodium sulphate. The chloroform was removed by rotary evaporation and the resulting residue was purified by column chromatography over silica gel using hexane & ethyl acetate as eluent to get the final compound **19**. ^{1}H NMR (400 MHz, $CDCl_3$, δ in ppm): 7.55 (m, 10H), 7.20 (m, 10H), 5.39 (m, 1H), 4.64 (m, 1H), 4.37 (t, 2H, *J* = 8, 4 Hz), 4.09 (t, 2H, *J* = 8, 4 Hz), 2.66 (t,

10H, *J* = 4, 8 Hz), 2.31 (m, 6H), 1.92 (m, 5H), 1.66 (m, 15H), 1.56 – 0.86 (m, 86H). ^{13}C NMR (400 MHz, $CDCl_3$, δ in ppm): 173.95, 172.73, 160.25, 144.02, 143.90, 143.70, 139.57, 131.79, 131.62, 128.76, 128.56, 128.53, 122.71, 120.73, 120.56, 120.50, 120.13, 99.55, 99.39, 97.33, 87.13, 86.65, 84.12, 74.78, 73.96, 63.61, 56.63, 56.14, 49.97, 42.29, 39.70 39.53, 38.16, 36.58, 36, 34.59, 31.85, 31.52, 31.01, 29.67, 28.05, 26.43, 23.93, 22.66, 22.59, 21.59, 21.04, 19.33, 18.71, 14.09, 11.85. FT-IR (cm^{-1}): 3027.22, 2929.23, 2856.75, 2208.51, 1732.68, 1605.80, 1513.06, 1466.50, 1424.84, 1378.26, 1347.54, 1252.04, 1175.53, 1085.02, 1019.71, 838.10, 725.79, 552.22. UV-vis (nm): 232, 267, 339, 384, 415. MS: m/z for $C_{114}H_{148}O_5$ 1598.14; found 1598.14.

References

(1) Kaafarani, B. R. *Chem. Mater*. **2010**, *23*, 378–396.

(2) Chandrasekhar, S.; Demus, D.; Goodby, J.; Gray, G. W.; Spiess, H. W.; Vill, V. Handbook of Liquid Crystals Set; Wiley-VCH, **2008**, pp 749–780.

(3) Praefcke, K.; Marquardt, P.; Kohne, B.; Stephan, W.; Levelut, A. M.; Wachtel, E. *Mol. Cryst. Liq. Cryst*. **1991**, *203*, 149–158.

(4) Beginn, U.; Lattermann, G.; Festag, R.; Wendorff, J. H. *Acta Polym*. **1996**, *47*, 214–218.

(5) Serrette, A. G.; Swager, T. M. *J. Am. Chem. Soc*. **1993**, *115*, 8879–8880.

(6) Zheng, H.; Lai, C. K.; Swager, T. M. *Chem. Mater*. **1994**, *6*, 101–103.

(7) Atencio, R.; Barbera, J.; Cativiela, C.; Lahoz, F. J.; Serrano, J. L.; Zurbano, M. M. *J. Am. Chem. Soc*. **1994**, *116*, 11558–11559.

(8) Paulus, W.; Ringsdorf, H.; Diele, S.; Pelzl, G. *Liq. Cryst*. **1991**, *9*, 807–819.

(9) Boden, N.; Movaghar, B.; Demus, D.; Goodby, J.; Gray, G. W.; Spiess, H. W.; Vill, V. Handbook of Liquid Crystals Set; Wiley-VCH, **2008**, pp 781–798.

(10) Vaughan, G. B. M.; Heiney, P. A.; McCauley, J. P.; Smith, A. B. *Phys. Rev. B* **1992**, *46*, 2787–2791.

(11) Schouten, P. G.; Warman, J. M.; de Haas, M. P.; van Nostrum, C. F.; Gelinck, G. H.; Nolte, R. J. M.; Copyn, M. J.; Zwikker, J. W.; Engel, M. K. *J. Am. Chem. Soc*. **1994**, *116*, 6880–6894.

(12) Van de Craats, A. M.; Warman, J. M. *Adv. Mater*. **2001**, *13*, 130–133.

(13) Markovitsi, D.; Marguet, S.; Bondkowski, J.; Kumar, S. *J. Phys. Chem. B* **2001**, *105*, 1299–1306.

(14) Kumar, S. *Chem. Soc. Rev*. **2006**, *35*, 83–109.

(15) Kumar, S. *Liq. Cryst*. **2004**, *31*, 1037–1059.

(16) Pal, S. K.; Setia, S.; Avinash, B. S.; Kumar, S. *Liq. Cryst*. **2013**, *40*, 1769–1816.

(17) Kumar, S. *Liq. Cryst*. **2005**, *32*, 1089–1113.

(18) Kumar, S.; Varshney, S. K. *Org. Lett.* **2002**, *4*, 157-159.

(19) Kumar, S.; Varshney, S. K. *Liq. Cryst*. **2001**, *28*, 161-163.

(20) Zhang, L.; Hughes, D. L.; Cammidge, A. N. *J. Org. Chem.* **2012**, *77*, 4288-4297.

(21) Zhang, L.; Gopee, H.; Hughes, D. L.; Cammidge, A. N. *Chem. Commun.* **2010**, *46*, 4255-4257.

(22) Mori, H.; Itoh, Y.; Nishiura, Y.; Nakamura, T.; Shinagawa, Y. *Jpn. J. Appl. Phys*. **1997**, *36*, 143–147.

(23) Kawata, K. *Chem. Rec*. **2002**, *2*, 59–80.

(24) Bisoyi, H. K.; Kumar, S. *Chem. Soc. Rev*. **2010**, *39*, 264–285.

(25) Kumar, S. Chemistry of Discotic Liquid Crystals; CRC Press, **2010**, pp 361–393.

(26) Zhao, K. Q.; Bai, Y. F.; Hu, P.; Wang, B. Q.; Shimizu, Y. *Mol. Cryst. Liq. Cryst*. **2009**, *509*, 77/[819]–88/[830].

(27) Kouwer, P.; Jager, W.; Mijs, W.; Picken, S.; Shepperson, K.; Mehl, G. *Mol. Cryst. Liq. Cryst*. **2004**, *411*, 377–385.

(28) Kouwer, P.; Mehl, G.; Picken, S. *Mol. Cryst. Liq. Cryst*. **2004**, *411*, 387–396.

(29) Kimura, M.; Moriyama, M.; Kishimoto, K.; Yoshio, M.; Kato, T. *Liq. Cryst*. **2007**, *34*, 107–112.

(30) Zelcer, A.; Donnio, B.; Bourgogne, C.; Cukiernik, F. D.; Guillon, D. *Chem. Mater*. **2007**, *19*, 1992–2006.

(31) Kumar, S.; Naidu, J. J. *Liq. Cryst*. **2002**, *29*, 899– 906.

(32) Gupta, S. K.; Raghunathan, V. K.; Lakshminarayanan, V.; Kumar, S. *J. Phys. Chem. B* **2009**, *113*, 12887–12895.

(33) Janietz, D.; Praefcke, K.; Singer, D. *Liq. Cryst*. **1993**, *13*, 247–253.

(34) Setia, S.; Sidiq, S.; Pal, S. K. *Tetrahedron Lett*. **2012**, *53*, 6446–6450.

(35) Gupta, S. K.; Setia, S.; Sidiq, S.; Gupta, M.; Kumar, S.; Pal, S. K. *RSC Adv*. **2013**, *3*, 12060–12065.

(36) Imrie, C. T.; Henderson, P. A. *Chem. Soc. Rev*. **2007**, *36*, 2096–2124.

(37) Imrie, C. T.; Henderson, P. A.; Yeap, G. Y. *Liq. Cryst*. **2009**, *36*, 755–777.

(38) Yelamaggad, C. V.; Shanker, G.; Hiremath, U. S.; Krishna Prasad, S. *J. Mater. Chem*. **2008**, *18*, 2927–2949.

(39) Cha, S. W.; Jin, J. I.; Achard, M. F.; Hardouin, F. *Liq. Cryst*. **2002**, *29*, 755–763.

(40) Yelamaggad, C. V.; Mathews, M.; Fujita, T.; Iyi, N. *Liq. Cryst*. **2003**, *30*, 1079–1087.

(41) Yelamaggad, C. V.; Nagamani, S. A.; Shankar Rao, D. S.; Prasad, S. K.; Hiremath, U. S. *Mol. Cryst. Liq. Cryst*. **2001**, *363*, 1–17.

(42) Yelamaggad, C. V.; Shashikala, I. S.; Hiremath, U. S.; Shankar Rao, D. S.; Prasad, S. K. *Liq. Cryst*. **2007**, *34*, 153–167.

(43) Majumdar, K. C.; Ghosh, T.; Rao, D. S. S.; Prasad, S. K. *Liq. Cryst*. **2011**, *38*, 1269–1277.

(44) Zhang, C.; Jin, L.; Yin, B.; Jamil, M.; Jeon, Y. J. *Liq. Cryst*. **2008**, *35*, 39–44.

(45) Majumdar, K. C.; Shyam, P. K.; Rao, D. S. S.; Prasad, S. K. *J. Mater. Chem*. **2011**, *21*, 556–561.

(46) Majumdar, K. C.; Chakravorty, S.; Pal, N.; Sinha, R. K. *Tetrahedron* **2009**, *65*, 7998–8006.

(47) Majumdar, K. C.; Ghosh, T.; Chakravorty, S.; Pal, N.; Shankar Rao, D. S. S.; Prasad, S. K. *Liq Cryst*. **2010**, *37*, 1539–1547.

(48) Yelamaggad, C. V.; Nagamani, S. A.; Hiremath, U. S.; Nair, G. G. *Liq. Cryst*. **2001**, *28*, 1009–1015.

(49) Sarkar, D. D.; Deb, R.; Chakraborty, N.; Mohiuddin, G.; Nath, R. K.; Nandiraju, V. S. R. *Liq. Cryst*. **2013**, *40*, 468–481.

(50) Reddy, R. A.; Tschierske, C. *J. Mater. Chem*. **2006**, *16*, 907–961.

(51) Hunt, J. J.; Date, R. W.; Timimi, B. A.; Luckhurst, G. R.; Bruce, D. W. *J. Am. Chem. Soc*. **2001**, *123*, 10115–10116.

(52) Attard, G. S.; Imrie, C. T.; Karasz, F. E. *Chem. Mater*. **1992**, *4*, 1246–1253.

(53) Song, Z. Q.; Zhao, K. Q.; Hu, P.; Wang, B. Q. *Acta Chim Sinica*. **2008**, *66*, 1344–1352.

(54) Hauser, A.; Thieme, M.; Saupe, A.; Heppke, G.; Krüerke, D. *J. Mater. Chem*. **1997**, *7*, 2223–2229.

(55) Chien, S. C.; Chen, H. H.; Chen, H. C.; Yang, Y. L.; Hsu, H. F.; Shih, T. L.; Lee, J. J. *Adv. Funct. Mater*. **2007**, *17*, 1896–1902.

(56) Kumar, S.; Varshney, S. K.; Chauhan, D. *Mol. Cryst. Liq. Cryst*. **2003**, *396*, 241–250.

(57) Langner, M.; Praefcke, K.; Kruerke, D.; Heppke, G. *J. Mater. Chem*. **1995**, *5*, 693–699.

(58) Praefcke, K.; Kohne, B.; Gündogan, B.; Singer, D.; Demus, D.; Diele, S.; Pelzl, G.; Bakowsky, U. *Mol. Cryst. Liq. Cryst*. **1991**, *198*, 393–405.

(59) Date, R. W.; Bruce, D. W. *J. Am. Chem. Soc*. **2003**, *125*, 9012–9013.

(60) Kouwer, P. H. J.; Mehl, G. H. *J. Am. Chem. Soc*. **2003**, *125*, 11172–11173.

(61) Fletcher, I. D.; Luckhurst, G. R. *Liq. Cryst*. **1995**, *18*, 175–183.

(62) Gupta, M.; Bala, I.; Pal, S. K. *Tetrahedron Lett*. **2014**, *55*, 5836–5840.

Appendix II

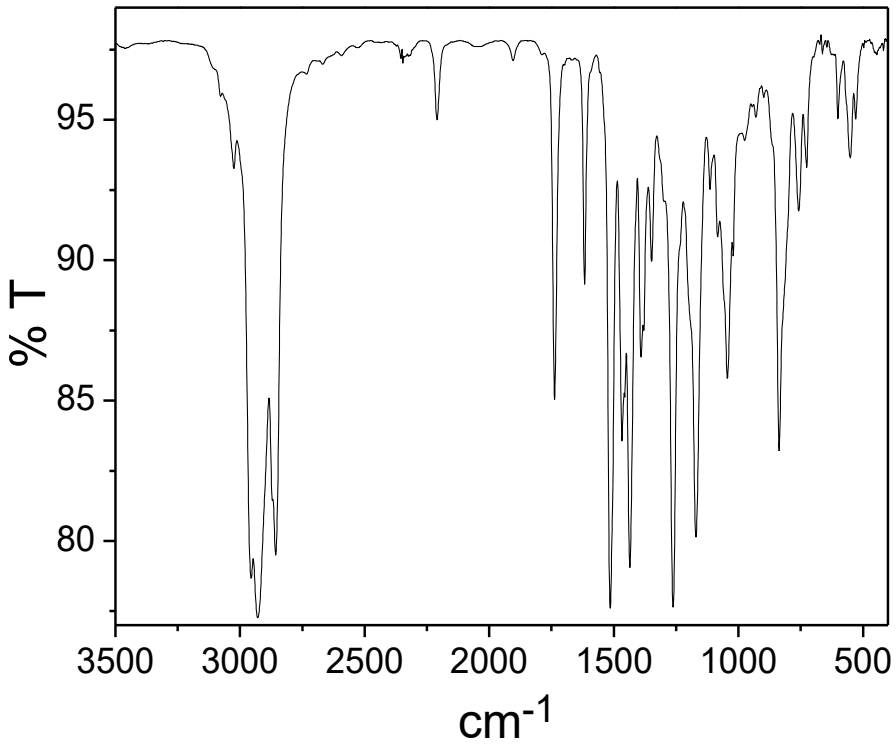

Figure A1 IR spectra of compound **6**.

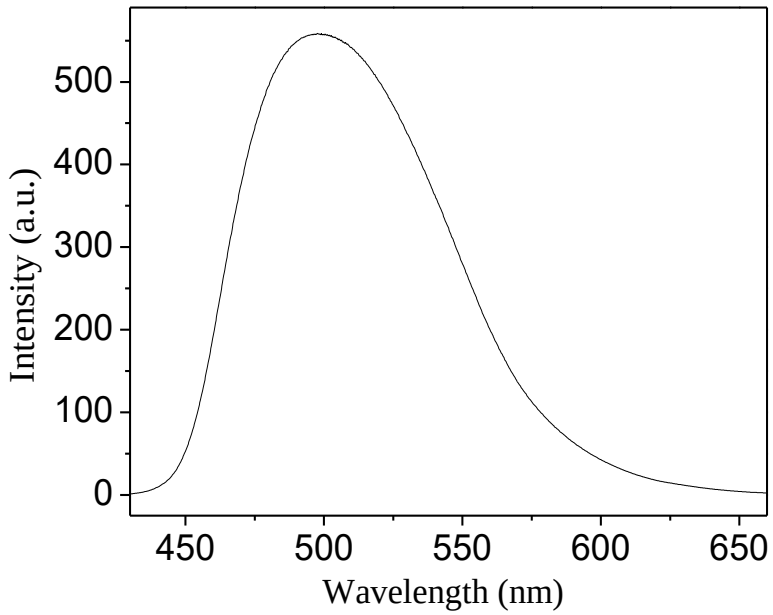

Figure A2 Fluorescence spectra of neat **6**.

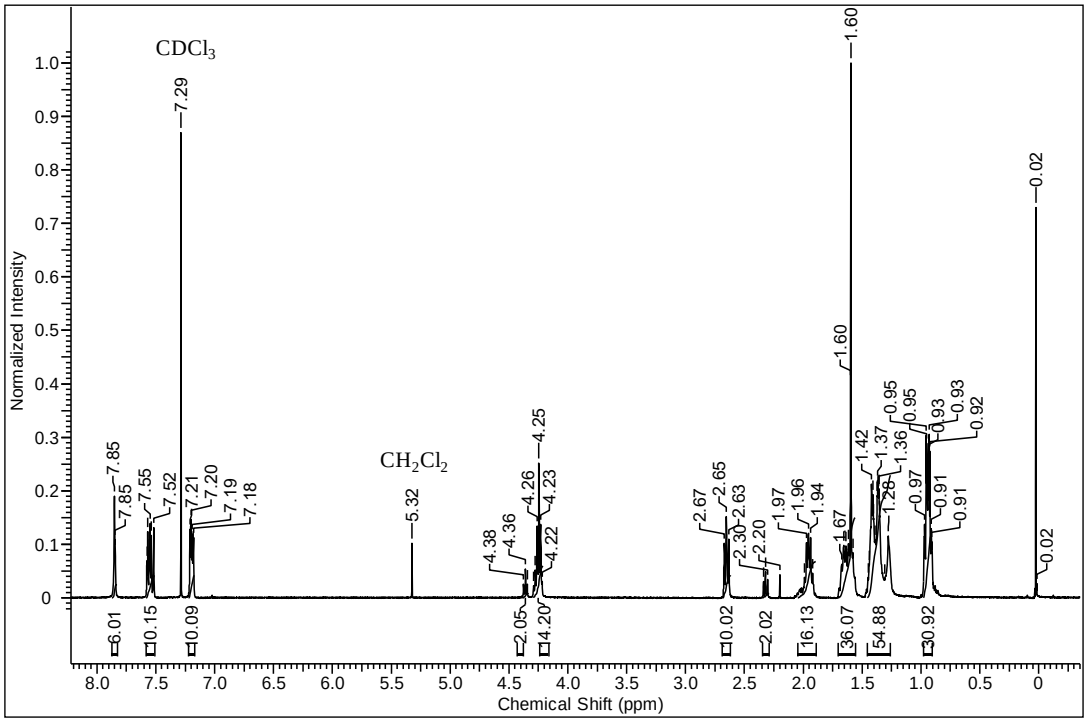

Figure A3 ^{1}H NMR of compound **6**.

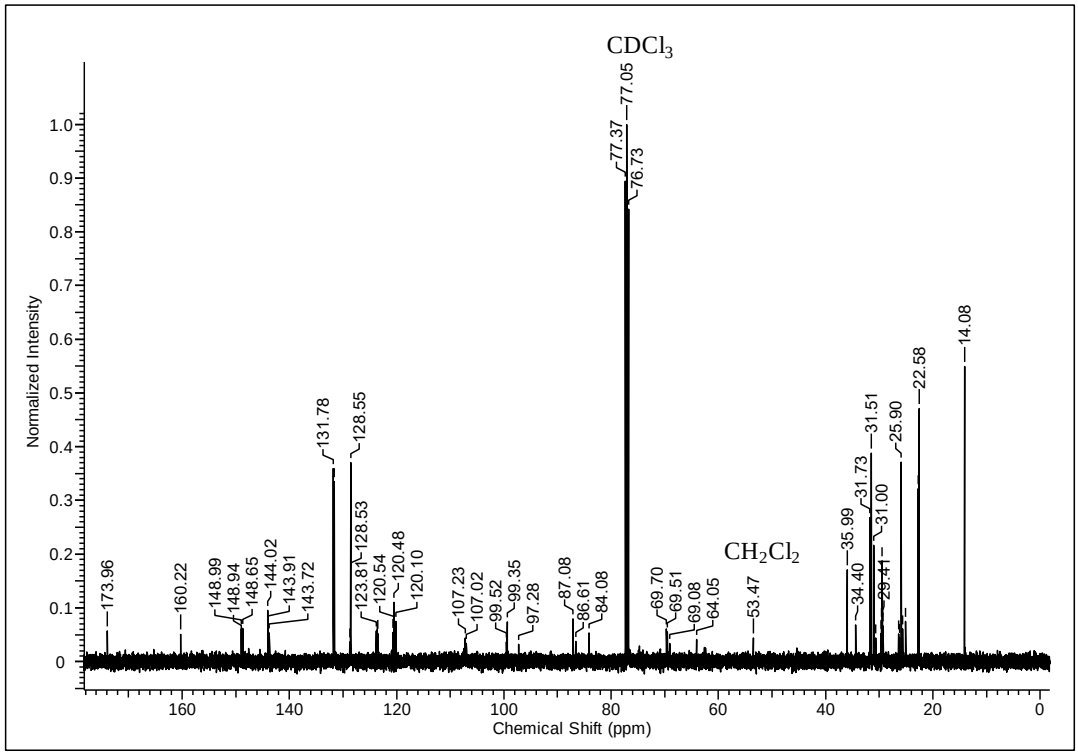

Figure A4 ^{13}C NMR of compound **6**.

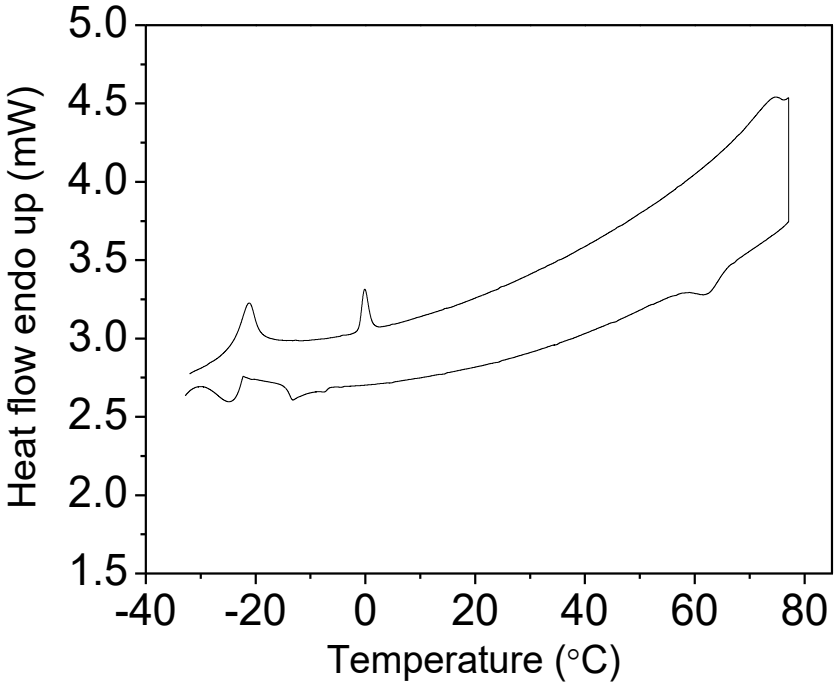

Figure A5 DSC traces for compound **6** on second heating and cooling (scan rate 5 °C/min).

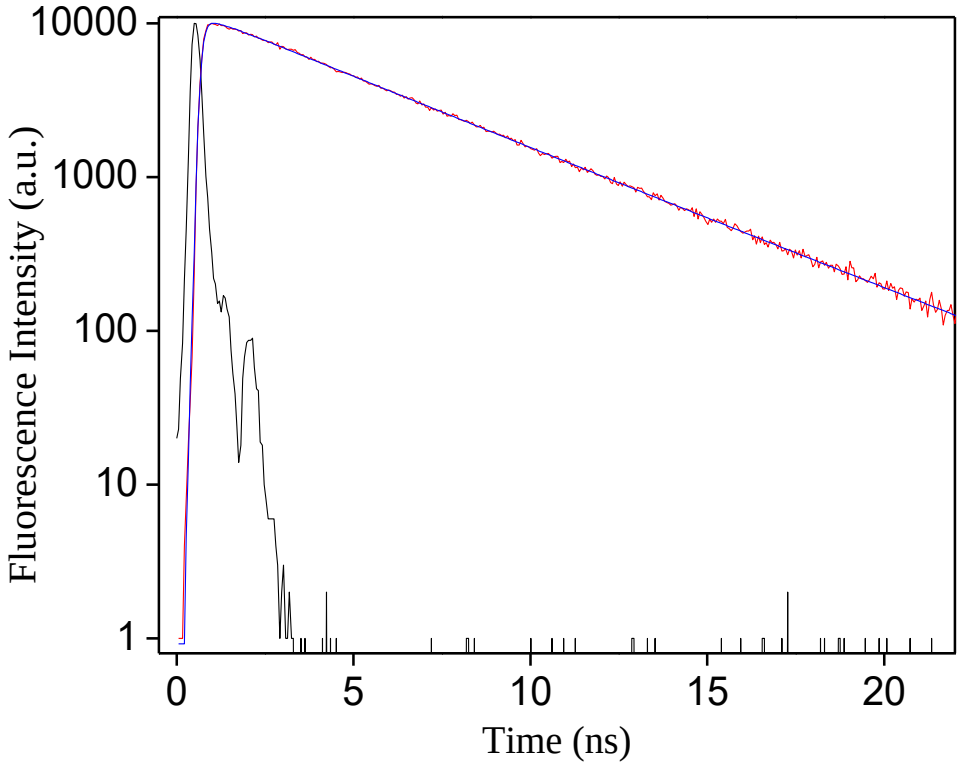

Figure A6 Fluorescence decay spectra of compound **6**.

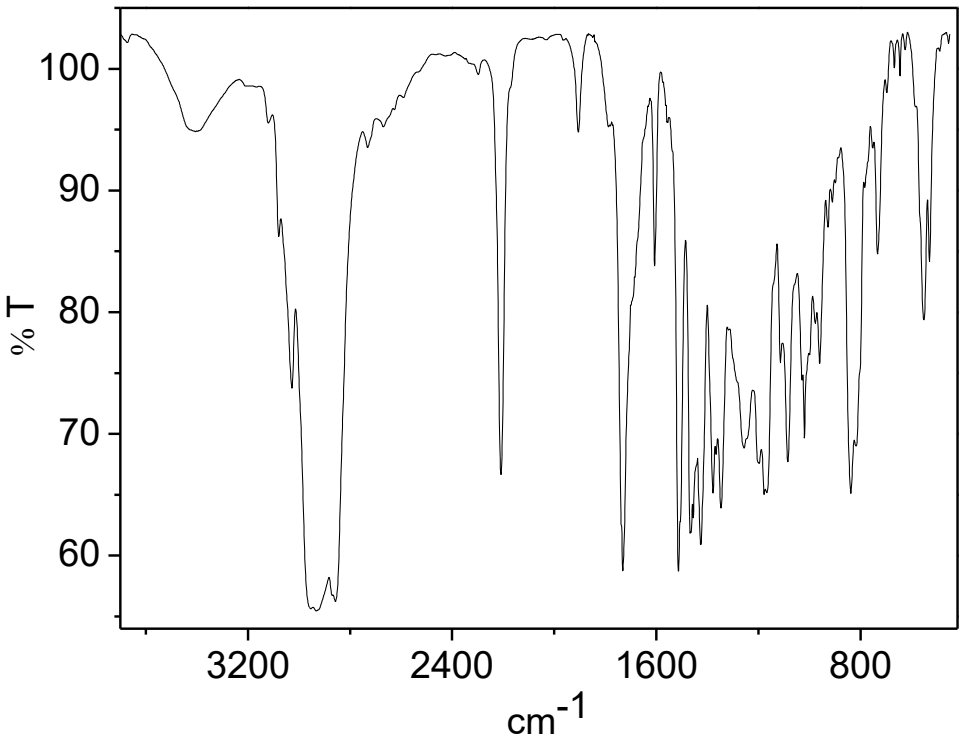

Figure A7 IR spectra of compound **18**.

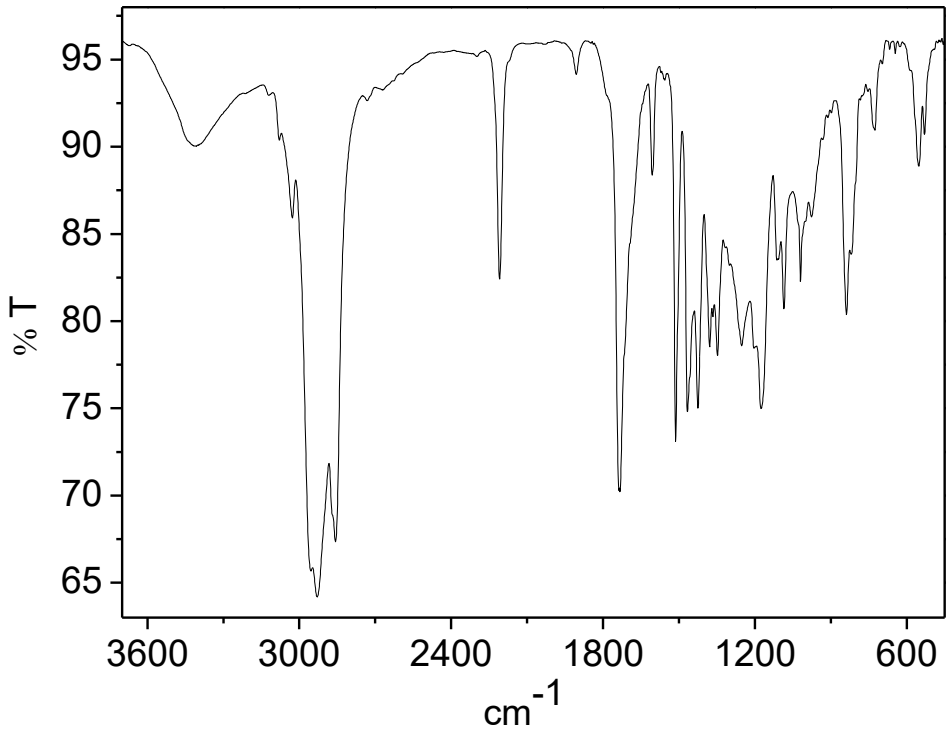

Figure A8 IR spectra of compound **19**.

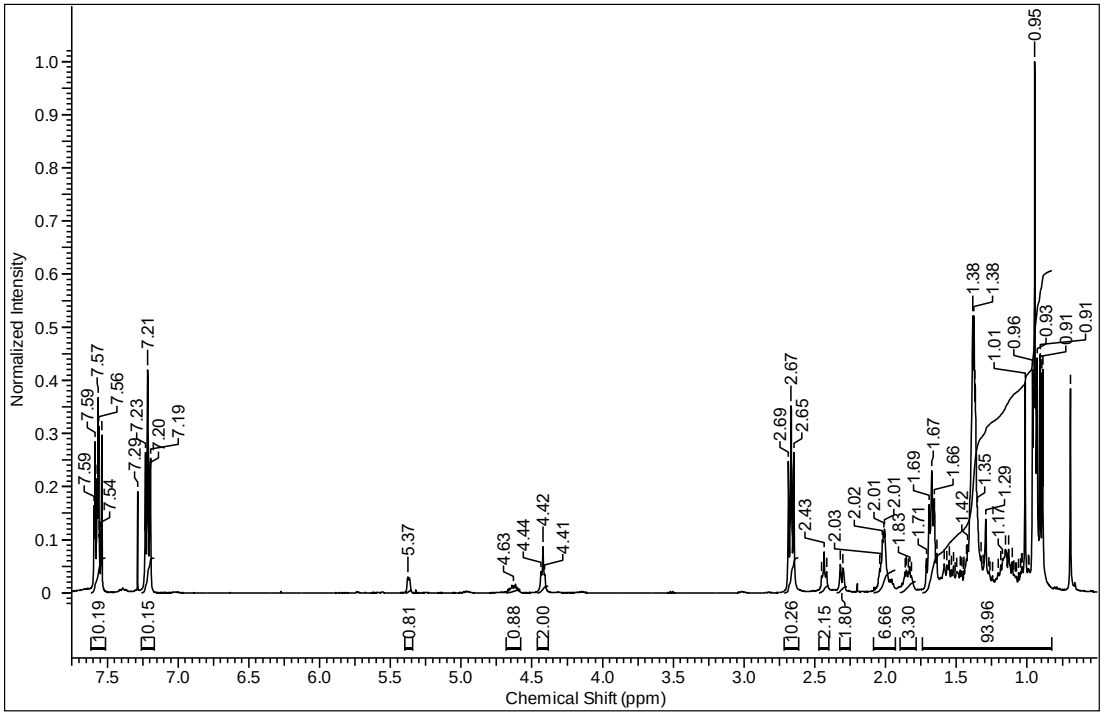

Figure A9 ^{1}H NMR of compound **18**.

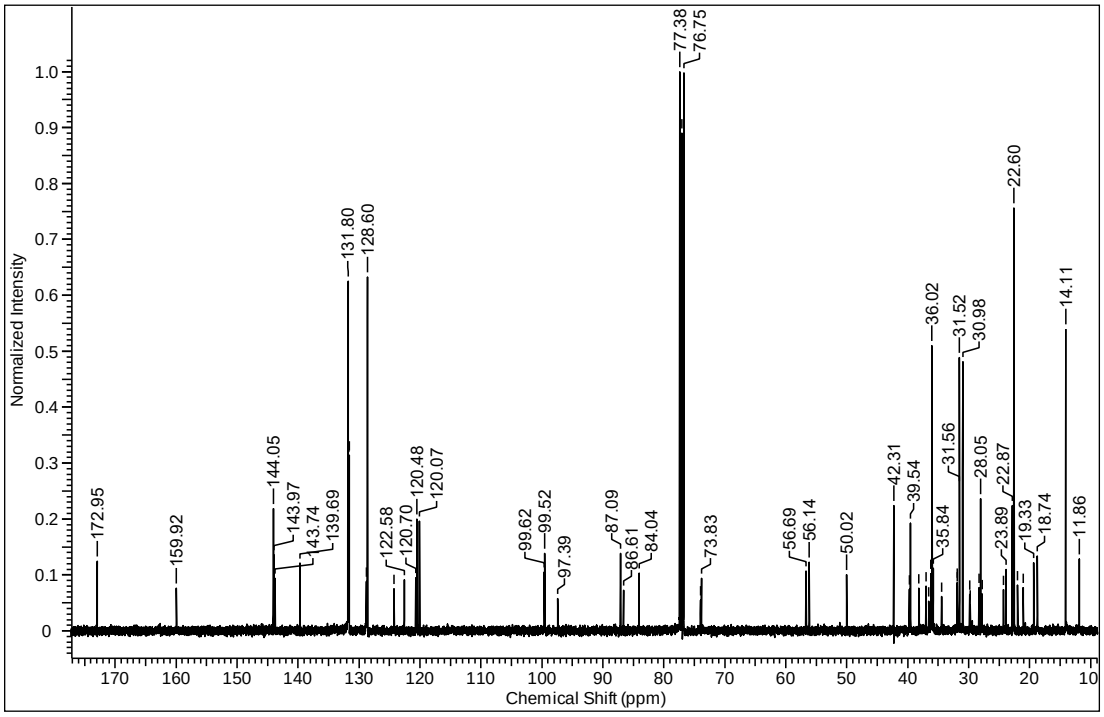

Figure A10 ^{13}C NMR of compound **18**.

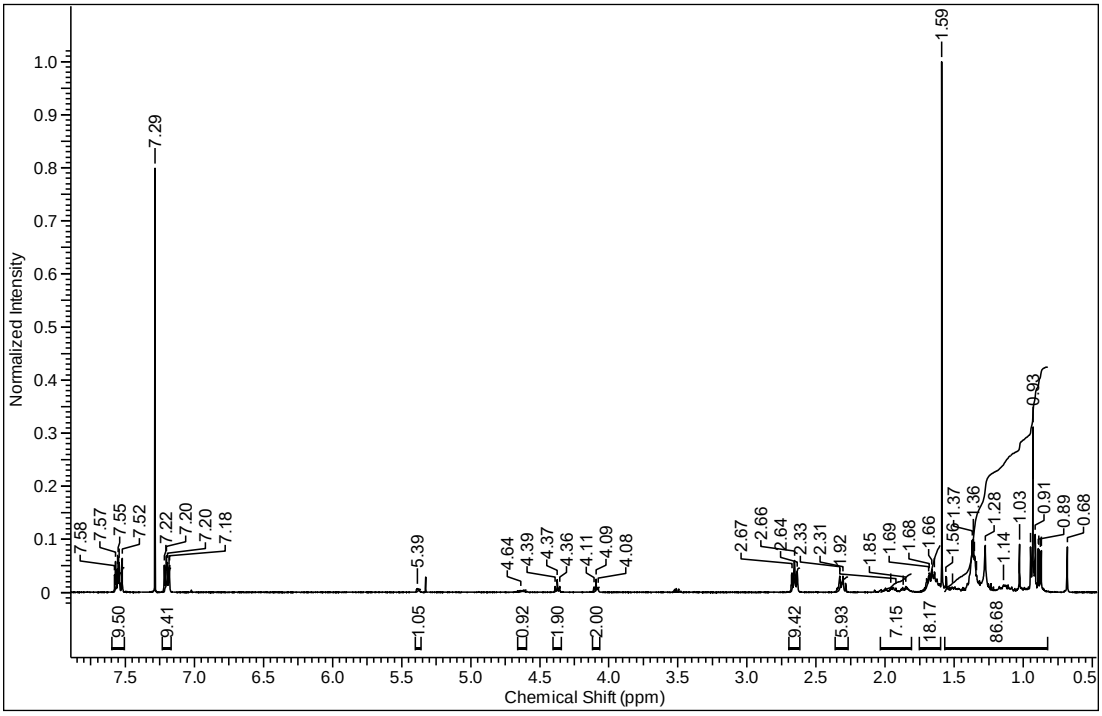

Figure A11 ^{1}H NMR of compound **19**.

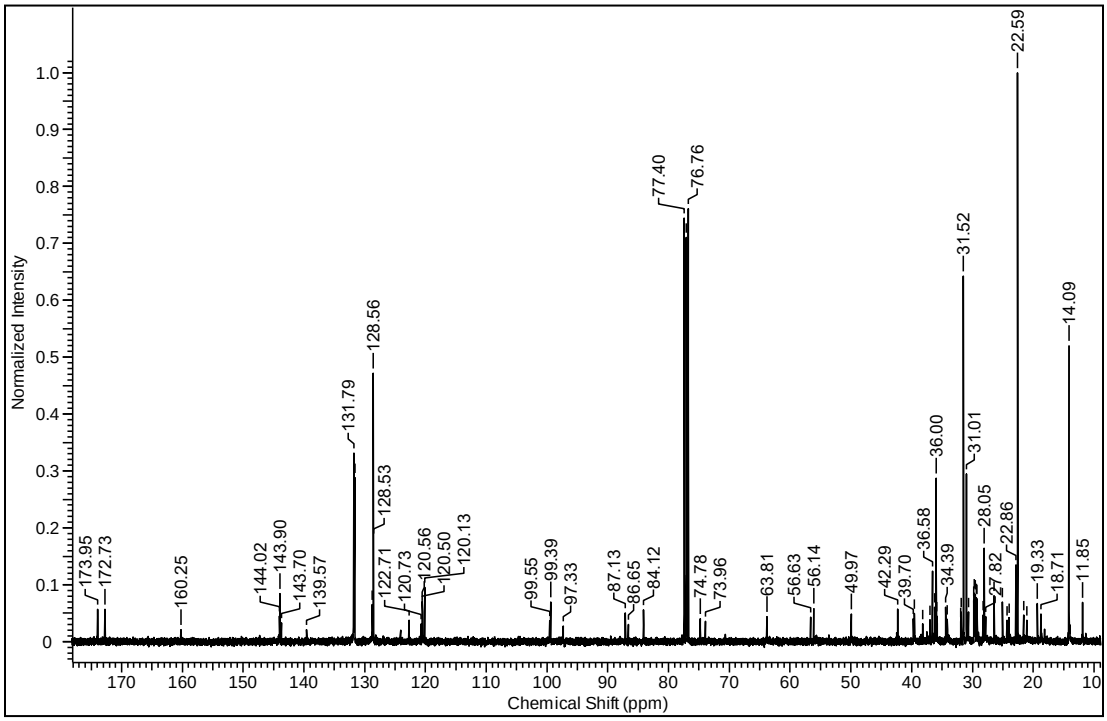

Figure A12 ^{13}C NMR of compound **19**.

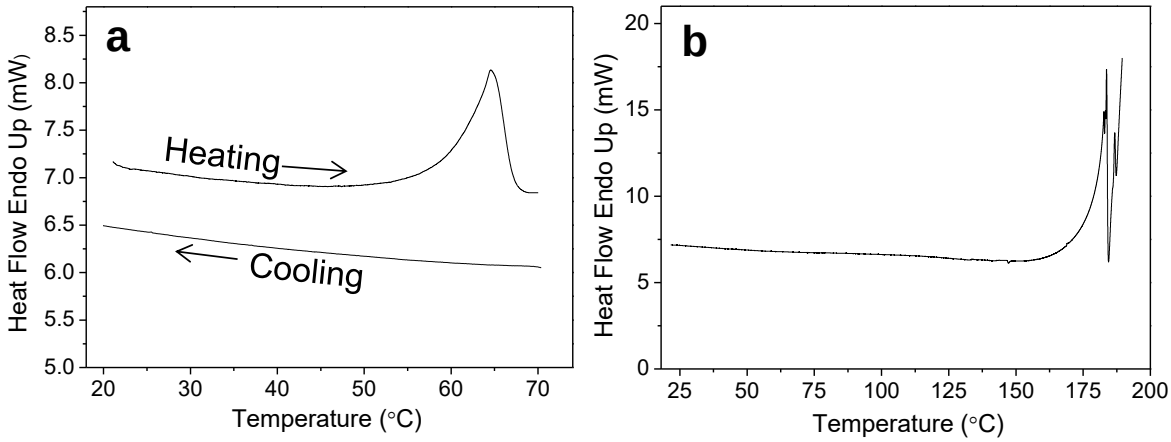

Figure A13 DSC traces of compound **18** & **19** (heating/cooling rate: 5 °C/min).

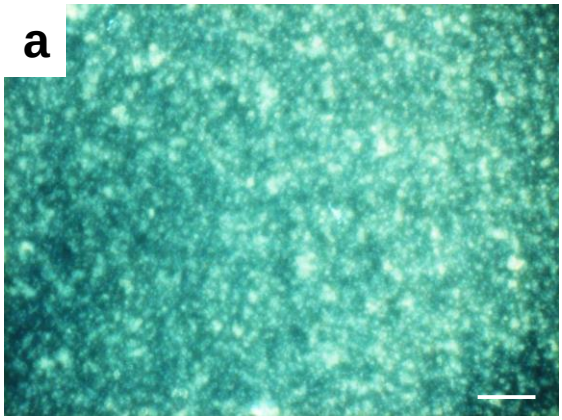

Figure A14 POM image showing increased birefringence on shearing for compound **19** at 25 °C (Crossed polarizers, scale bar = 20 μm)

Chapter 4

Multialkynylbenzene bridged discotic triads

PART A

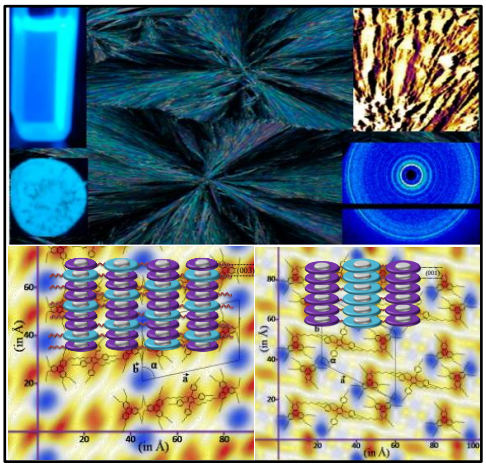

A straightforward synthesis of multialkynylbenzene-bridged triphenylene based dyad systems (via flexible alkyl spacers) that self-organize into room-temperature columnar structures over a long range is reported. The compounds with spacer lengths (n) of 8 and 10 exhibit a columnar oblique mesophase whereas the compound with n = 6 shows a columnar oblique plastic phase. Interestingly, the later compound (n = 6) shows the formation of well-nucleated spherulites of about several hundred micrometers. All of these compounds show blue luminescence in solution and in the thin-film state under long wavelength (365 nm) UV light.

PART B

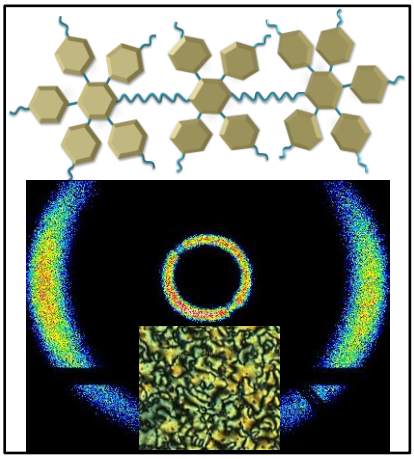

This report elaborates the synthesis of lath-shaped symmetrical triads based on multialkynylbenzene linked via flexible alkyl spacers. Four mesogens were synthesized in which multialkynylbenzene units were connected to each other in a side-by-side fashion with varying flexible alkyl spacers. The compound with longest alkyl spacer i.e. n = 12 exhibited N_D phase which has been characterized by polarized optical microscopy (POM) and detailed X-ray scattering studies (SAXS/WAXS).

4.1 Part A: Triphenylene-based room-temperature discotic liquid crystals: A new class of blue-light emitting materials with long-range columnar self-assembly

4.1.1 Introduction

Among various emissive materials, organic semiconductors have gained a particular interest in the last few years for the development of various electronic devices e.g. white light emitting diodes (WOLEDs). These WOLEDs have been applied for the next-generation solid-state light sources, field effect transistors and display devices.[1-6] However, for the generation of white light, the triads of red-, green- and blue-emissive materials are required.[7-9] Although, red and green emissive materials are widely reported in the literature, blue-light emitting materials are scarce and have remained a challenge for three decades. The invention of the efficient blue LED based on inorganic semiconductors has contributed for creating white light in an entirely new way to us.[10] Unfortunately, most of the inorganic semiconductors suffer from high cost, low efficiency and limits fabrication in a flexible substrate. The latter problem can be solved by using luminescent polymers but, they also experience trouble with low solubility, high purity and stability. In this regard, luminescent small organic molecules have advantages in terms of all the aspects described above.[11] Moreover, the combination of luminescence with columnar self-assembly which is formed by discotic liquid crystals (DLCs) can enhance the applicability of these emissive molecules in OLED applications.[12-15]

The interest in DLCs as smart materials for OLED devices is due to their advantageous properties such as high intrinsic charge-carrier mobilities, ease of processability and high purity that reduces possible tapping sites for charge carriers.[16-18] In an OLED, the opposite charges from the two electrodes undergo recombination in the emissive layer to generate the light. Therefore, inherent charge carrier mobility of the emissive material plays a key role which can be favoured from pronounced and defect-free long range order of Columnar (col) self-assembly. In literature, there are only a few reports that described long range self-assembly in molecules such as terphenyls, crowded arenes, hexa-*peri*-hexabenzocoronene, graphite oxide LCs, etc (**1**-**3**).[19-22] Also, some examples of blue light emitting molecules

based on discotics are reported recently but, most of them exhibited blue photoluminescence in solution which is shifted to higher wavelengths in case of neat samples and thus were not suitable for device fabrication.[23-26] Longo et al. reported a new core for blue luminescent DLCs based on tristriazolotriazines.[27]

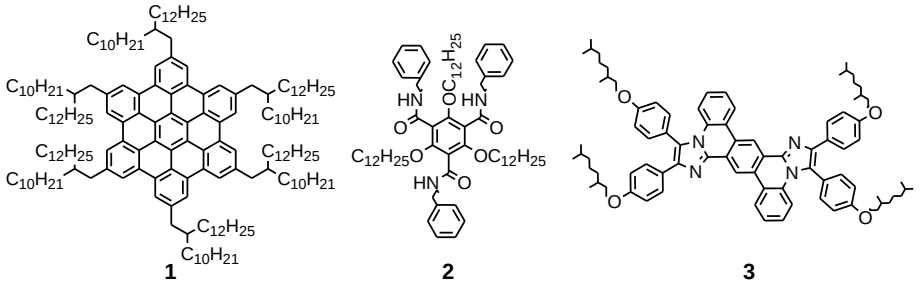

1 **2** **3**

Although few reports on blue luminescent materials based-on tristriazolotriazine, 1, 3, 4-oxadiazole and thiadiazole are there that exhibit blue luminescence in solid state, but, in most of these cases, materials exhibit columnar phase at very high temperature with absence of any long range columnar self-assembly (**4**-**7**).[28-33] In some of the system, although they show glassy characteristics with retention of columnar order (on cooling from isotropic liquid), they are not suitable to use as pristine because of their crystalline nature at room temperature. They also exhibit very high isotropization temperatures and thus low processability which limits their widespread use in various opto-electronic devices.

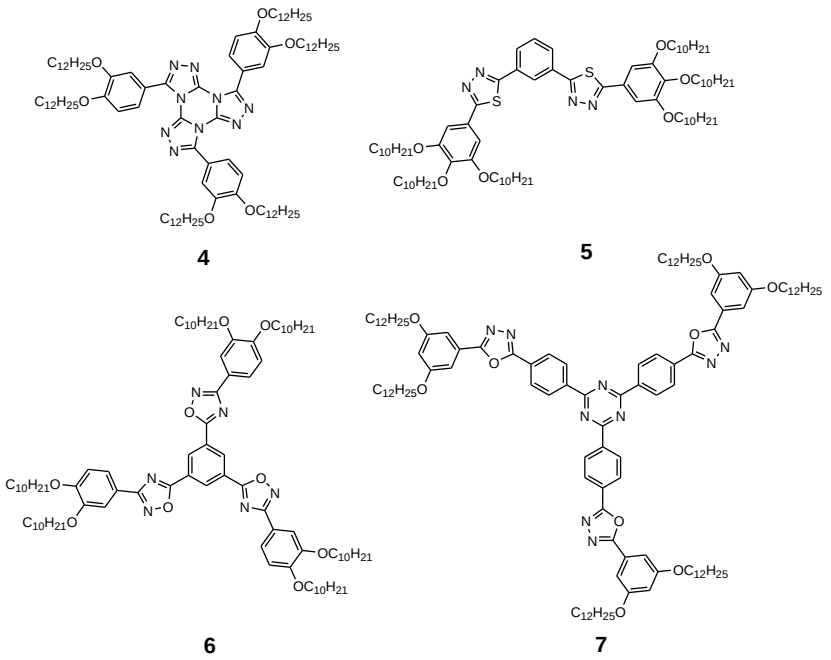

4 **5**

6 **7**

Therefore, design of new materials possessing a combination of long-range col self-assembly around room temperature and strong photo-luminescent behaviour in the neat state is essential for reliable and cost-efficient WOLED manufacturing.

4.1.2 Objective

In the earlier chapter, we have shown that a triphenylene-pentaalkynylbenzene based dimer exhibited Col_h mesophase at room-temperature with blue light emission in solution, whereas, in neat state, a green emission was observed. Also, the dyad didn't display any long-range columnar self-assembly. Therefore, we thought of modifying the above design. We have designed the molecule **8** in which two triphenylene (TP) units were linked via a multialkynylbenzene (MB). Firstly, increasing the number of TP can lead to increased columnar order. Secondly, the restriction imposed by additional TP unit can lead to a drastic change in the photoluminescence behaviour of the molecule as compared to the earlier synthesized dyad.

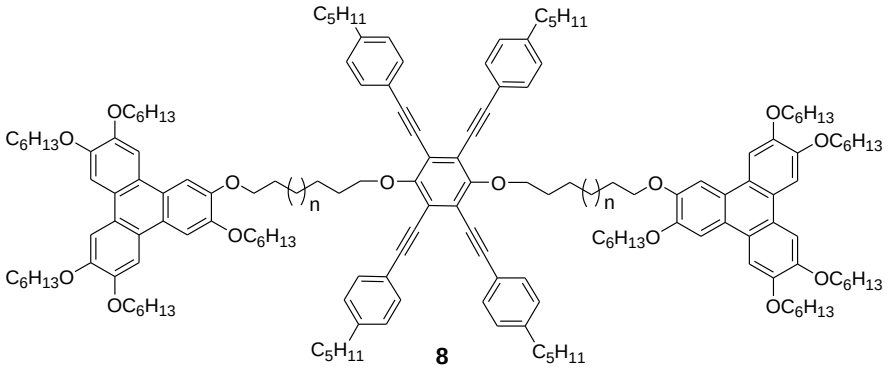

8
(*n* = 1, 3, 5)

4.1.3 Results and Discussion

4.1.3.1 Synthesis and Characterization

Scheme 4.1 shows the straightforward synthetic route for tetra-alkynylbenzene-bridged triphenylene (TP) derivatives. Synthesis of monohydroxytriphenylene **9** and ω-bromo-substituted triphenylene **10** (Scheme 4.1) have been reported earlier.[34] The synthesis of compound **12** was not feasible using the conventional alkylation methods due to the rapid formation of quinone, therefore, it was carried out using solvent-free conditions.

Tetrabromohydroquinone **11** (1 equivalent) was finely grounded with potassium hydroxide (2.5 equivalents) and a small amount of tetraoctylammonium bromide (0.09 equivalents) followed by the addition of compound **10** (2.5 equivalents). The mixture was transferred to a 10 ml round bottom flask and was heated to 80 °C for 12 hours with continuous stirring. On completion of the reaction, as monitored by TLC, the mixture was diluted with water and the product was extracted with dichloromethane which was further purified by column chromatography over silica gel to yield compound **12**.

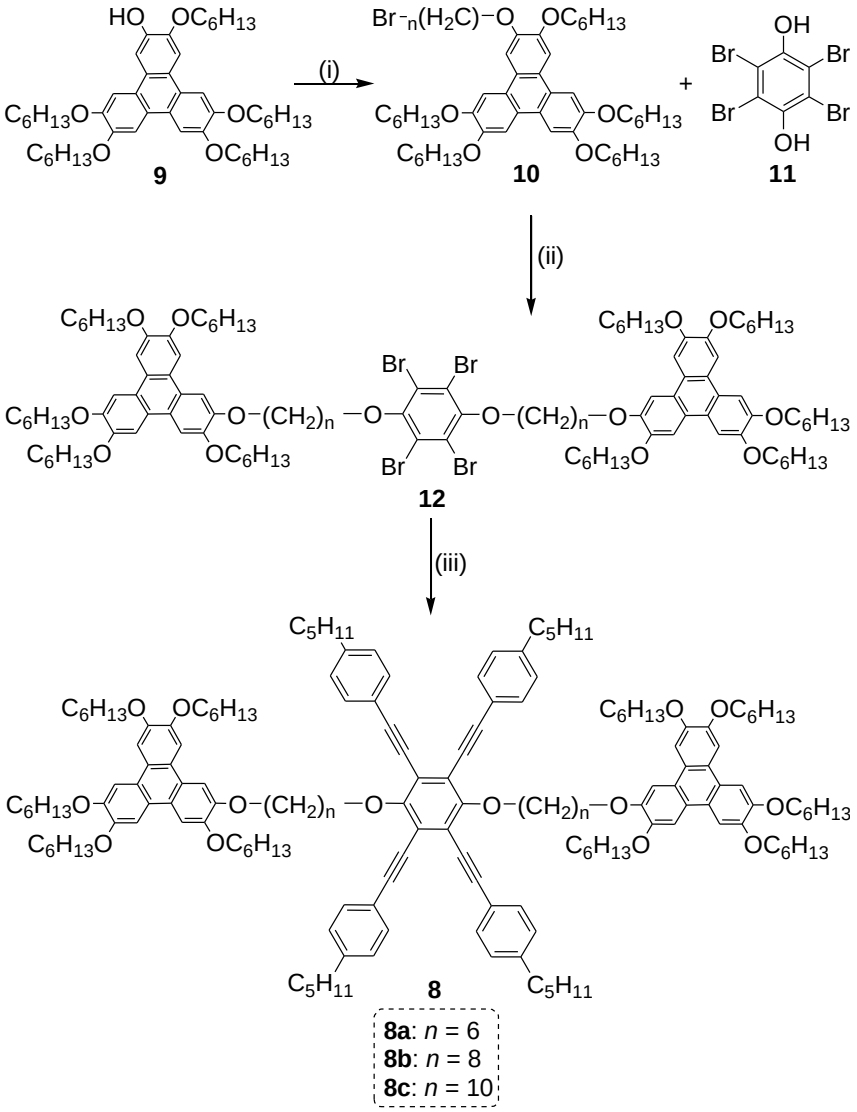

Scheme 4.1 Synthesis of the target compounds **8**. Reagents and conditions: (i) Cs_2CO_3, KI, Br-$(CH_2)_n$-Br, butanone, 80 °C, 18h, 88%; (ii) KOH, THAB, 80 °C, 12h, 60%; (iii) $Pd(PPh_3)_2Cl_2$, 4-pentylphenylacetylene, PPh_3, CuI, Et_3N,100 °C, 24h, 80%.

The compound **12** was subsequently coupled in a four-fold sonogashira reaction to get the final target material **8** on multigram scale (see experimental section for detailed synthetic procedures). The synthesized compounds were characterized by ^{1}H NMR, ^{13}C NMR, FT-IR, UV-vis and mass spectrometry as described in the experimental section and appendix III (Figure A1-A7).

4.1.3.2 Thermal Behavior

The thermal behavior of all the compounds **8** as investigated by polarizing optical microscopy (POM) and differential scanning calorimetry revealed a phase transition from LC phase to the isotropic melt (appendix III, Figure A8). We found that this new class of TP derivative, in comparison with most of other TP-based dyads forms an enantiotropic LC at room temperature with a wide LC temperature range and lower isotropization temperatures.[35-39] As shown in Figure 4.1a, POM of **8a** on cooling from isotropic melt (75 °C), under crossed polarizing conditions displayed a texture characteristic of a columnar mesophase. Surprisingly, at a slow cooling rate (1 °C/min) well-ordered randomly nucleated spherulite like domains over the whole sample area were observed indicating high anisotropy and long-range self-assembly (Figure 4.1b & c). This behaviour is unusual for discotics and has been found for some low molar mass LCs and only a few reports for high molar mass LCs have been reported so far.[20-22] These spherulites can be demonstrated as Maltese cross where the isogyres followed the extinction of the polarizer/analyzer indicating an edge-on arrangement of the molecules.[40] This observation was further confirmed by AFM imaging depicting the topography of the spherulites with growth originating from the nucleation centre that expanded radially up to several hundred micrometres (Figure 4.1d).

The morphology of spherulitic texture was further examined by scanning electron microscopic (SEM) studies. The radius of a typical grown spherulite of compound **8a** was found to be approximately 230 μm as shown in figure 4.2a. SEM micrograph also indicates plate-like fibres diverging from a common centre having a smooth outer surface as shown in Figure 4.2b. To study the extent of ordering present in the mesophase, the correlation length in the plastic phase of compound **8a** was calculated from the Scherrer equation: $\xi = 0.89\lambda / \beta\text{Cos}\theta$, where 0.89 is the correction factor, β represents FWHM of the peak obtained for

core-core spacing, λ and θ represents the wavelength of x-rays and Bragg's angle respectively.

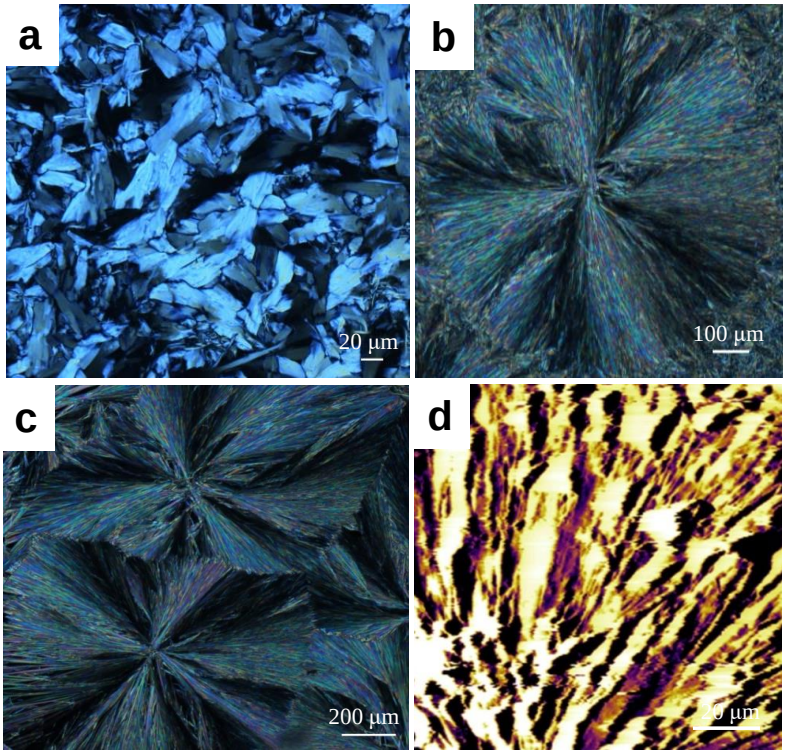

Figure 4.1 Polarized optical micrographs of the compound **8a** at (a) 50 °C on cooling at a rate of 5 °C/min (crossed polarizers, magnification × 200). (b) & (c) shows spherulitic domains at 55 °C on cooling at a rate of 1 °C/min. from the isotropic (crossed polarizers, magnification × 50). (d) AFM image revealing the radial growth of the spherulitic domains.

The correlation length was calculated to be around 256 Å which denotes approximately 66-67 nearest discotic neighbours and is higher as compared to other columnar phases.[41] In general, the correlation lengths were the result of about 14 to 18 stacked discotic units, depending on the mesophase composition. In our case, the correlation length is found to be much higher in the mesophase with the formation of well-ordered spherulites that nucleated randomly over the whole sample during the cooling scan. These sherulites revealed high anisotropy and thus cogent long-range columnar self-assembly as convincingly supported by the POM and SEM observations. Consequently, the columns are arranged in the spherulite growth direction in an edge-on arrangement of the molecules up to several hundred

micrometers as also observed in earlier studies.[20, 22] All of these factors denote a long-range columnar self-assembly of compound **8a**.

Compound **8b** and **8c** with longer alkyl spacers showed lower isotropization temperatures at 66 °C and 64 °C, respectively. They showed typical focal conic texture of columnar mesophase on cooling, although no spherulitic growth was observed in the POM (Figure 4.3). A possible reason for the formation of long-range order for compound **8a** could be due to its smallest alkyl spacer which allows the molecule to be much more sterically hindered as compared to the other longer spacer derivatives. The more steric hindrance can lead to weaker intermolecular interaction, resulting in lower growth rate and therefore the formation of long-range self-assembled domains.

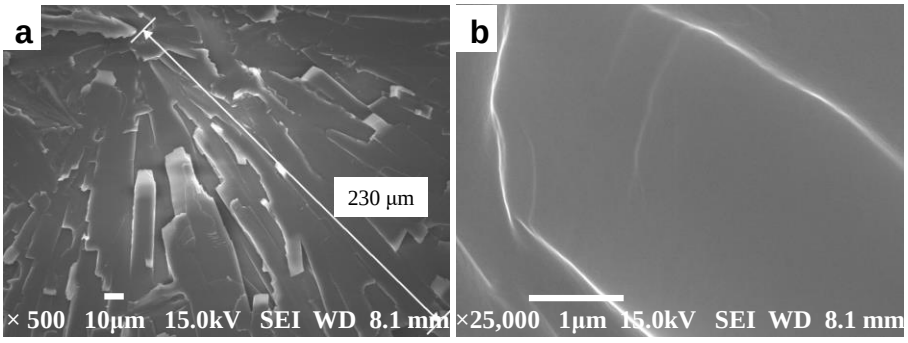

Figure 4.2 SEM Micrograph of (a) a grown spherulite of compound **8a** shows the radius of the spherulite to be round 230 µm and (b) the plate like fibril showing smooth outer surface.

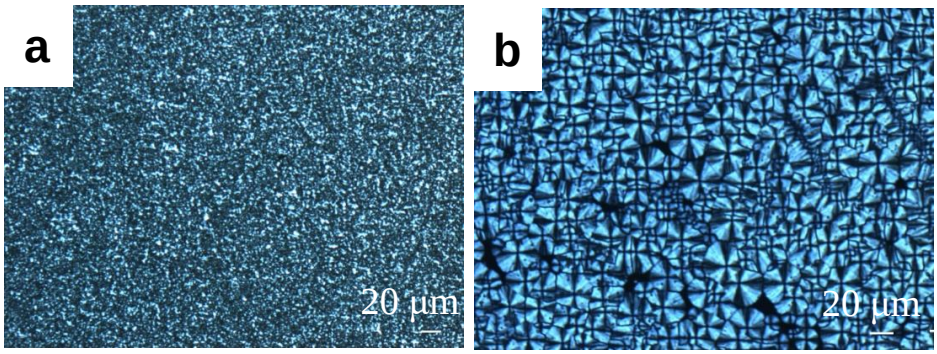

Figure 4.3 Polarized optical micrographs of the compounds (a) **8b** at 52 °C and (b) **8c** at 31 °C on cooling at a rate of 5 °C/min. from the isotropic (Crossed polarizers, magnification × 200).

4.1.3.3 X-ray Diffraction Studies

The supramolecular organization of these dyads in the columnar mesophase was studied by X-ray diffraction experiments. The results of indexing of one-dimensional (1D) intensity vs. 2θ profile obtained from the powder 2D pattern (appendix III, Figure A9) of the columnar phases on cooling from isotropic melt are summarized in Table 4.1. The X-ray diffraction pattern of compound **8a** showed many reflections in the small angle as well as in wide angle region which were indexed on the oblique lattice (Figure 4.4, Table 4.1a). The first three peaks of the small angle region were assigned to be (100), (010) and (110) respectively. The lattice parameters of the 2D oblique lattice were calculated to be; a = 42.41 Å, b = 24.71 Å and α = 78.12 degrees.

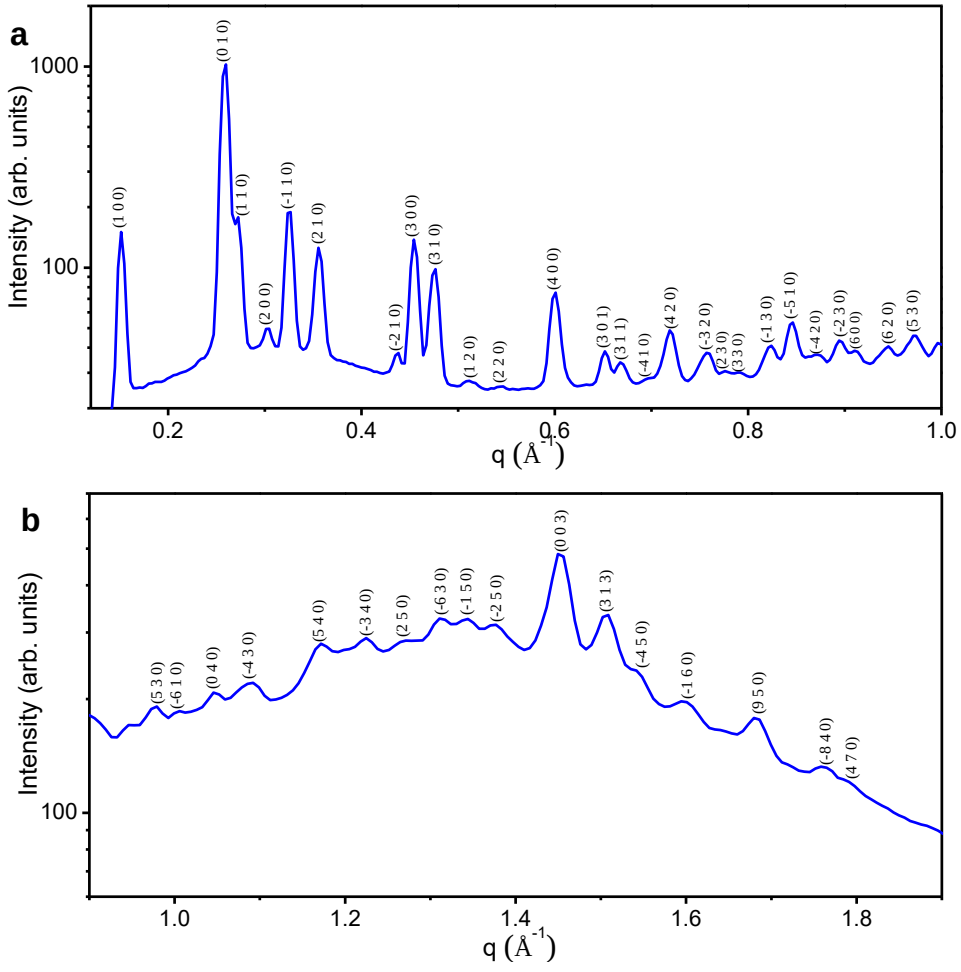

Figure 4.4 X-ray diffraction pattern of compound **8a** with indexing for (a) small angle and (b) wide angle peaks on the columnar oblique plastic phase (Col_{obp}).

All the peaks of small/wide angle were indexed on the same lattice with (hk) indexing except four peaks; two in the small angle and other two in the wide angle region which required mixed indexing. These two peaks in small angle are the bifurcation of a single peak and were indexed on mixed indexing (301) and (311) which indicate the plastic nature of this mesophase. Two more peaks of the wide angle are indexed on (003) and (313). Peak indexed on (003) gives the value of one of the lattice parameter, *c* =13.08 Å. The observed structure can thus be concluded as columnar oblique plastic (Col_{obp}). Reconstructed electron density map shows that the molecules are packed side by side on the oblique lattice (Figure 4.5).

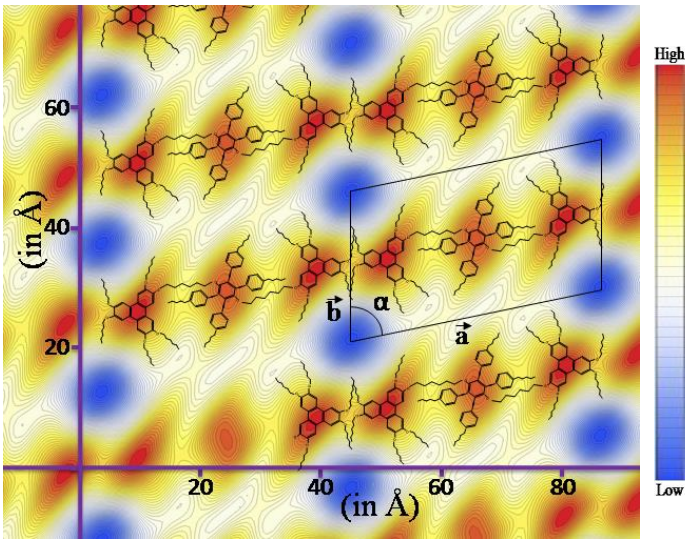

Figure 4.5 Reconstructed electron density map of Col_{obp} phase of compound **8a** showing side by side packing of molecules on the lattice. Red corresponds to highest electron density and deep blue is the lowest. Parallelogram on the map (in black colour) shows the 2D unit cell of Col_{obp} phases. $\vec{a}$, $\vec{b}$ and α are the lattice parameter of the unit cell.

This oblique lattice can be realized in various ways, one of them is as the lattice of voids. Further the peak indexed as (003) confirms the layered structure of compound **8a** as of ...ABCABC...kind. Here, A, B and C are identical but B and C layers are translated by (*a*/3, 0, 0) and (2*a*/3, 0, 0) with respect to A layer in the direction of *a*, respectively. Based on the X-ray diffraction results and electron density map, we proposed a model as shown in Figure 4.10. The three dimensional structure of this assembly can be realized in terms of the arrangement of columns as follows. Column (2) arranged after column (1) followed by

column (3) in a side by side in the direction that makes an angle of 11.88 degrees (calculated from electron density map) with respect to positive horizontal axis, together act as motif. The constituent columns of motif are linked to each-other *via* flexible alkyl spacers. These motifs are amassed on the oblique lattice (a = 42.41Å, b = 24.71Å and α = 78.12 degrees) and exhibit the present three dimensional structure. Moreover, in the column two TP discs are followed by one MB disc as shown in Figure 4.11. The calculated effective number of molecules of compound **8a** per unit cell is 3.

The diffraction pattern of the compound **8b** shows diffuse peaks in the small angle and relatively weak peaks in the wide angle region (Figure 4.6). The observed peaks were indexed on a 2D columnar oblique lattice with lattice parameters, a = 38.26 Å, b = 31.38 Å and α = 95.2 degrees. The lattice parameter c calculated from the wide angle peak indexed on (001) is found to be 3.75 Å (Table 4.1b).

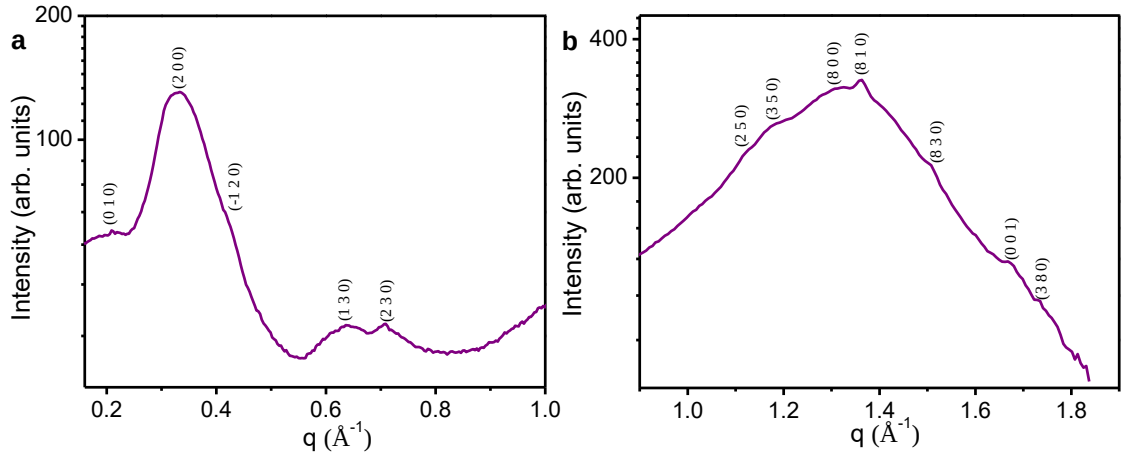

Figure 4.6 X-ray diffraction pattern of compound **8b** for (a) small and (b) wide angle with peaks indexed on the columnar oblique phase (Col_{ob}).

Reconstructed electron density map derived from the assigned miller indices is shown in the Figure 4.7. The details of intensity, phase and multiplicity is given in the Table 4.1b. The packing of the molecules in compound **8b** is different as compared to that in **8a**. Here, molecules are arranged on a 2D oblique lattice in such a way that the TP units are interdigitated.

Based on the X-ray diffraction results and electron density map, we proposed a model as shown in Figure 4.10. Compound **8b** is arranged on a 2D oblique lattice in such a way that TP units of one compound unit are sandwiched between the TP units of others compound units, representing a layer. These layers aggregate exactly on top of each other that result into the present assembly. This kind of layering leads to two different kind of pure columns (1) composed of TP units and (2) composed of MB units (as shown in Figure 4.11). These columns are arranged one after another and make an angle of about 159 degree (as calculated from electron density map) with respect to positive horizontal axis. The effective number of molecules of compound **8b** in a unit cell is 1.

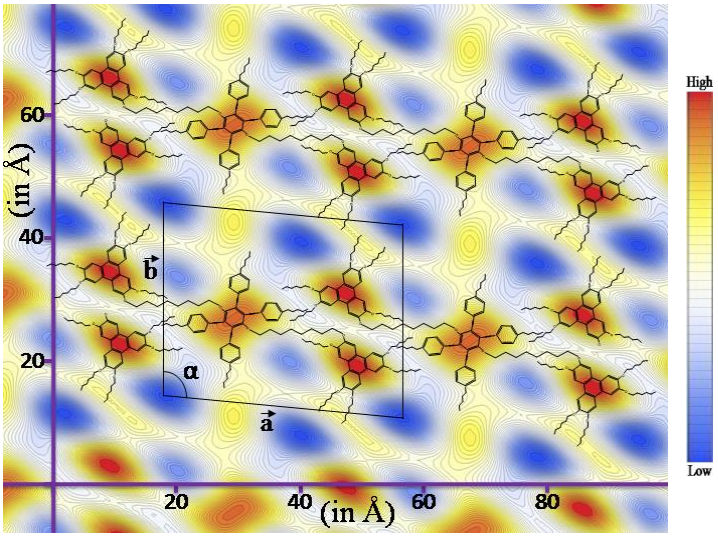

Figure 4.7 Reconstructed electron density map of Col_{ob} phase of compound **8b** showing interdigitation of TP units. Red corresponds to high electron density and deep blue is the lowest. Parallelograms on the map (in black colour) shows the 2D unit cell of Col_{ob} phase. $\vec{a}$, $\vec{b}$ and α are the lattice parameter of the unit cell.

The diffraction pattern of the compound **8c** exhibits many peaks in the small as well as wide angle region which were also indexed on 2D columnar oblique lattice (Figure 4.8). The lattice parameter are calculated to be, a = 42.51 Å, b = 33.95 Å, α = 115.8 degrees and lattice parameter c calculated from the wide angle peak indexed as (001) is 3.71 Å (Table 4.1c). Reconstructed electron density map for **8c** as shown in the Figure 4.9 is very similar to that of compound **8b**. But here the columns of the motif are arranged side by side in the

horizontal direction (as calculated from electron density map) and these motifs further assembled on the oblique lattice to form the three dimensional structure (Figure 4.10 & 4.11).

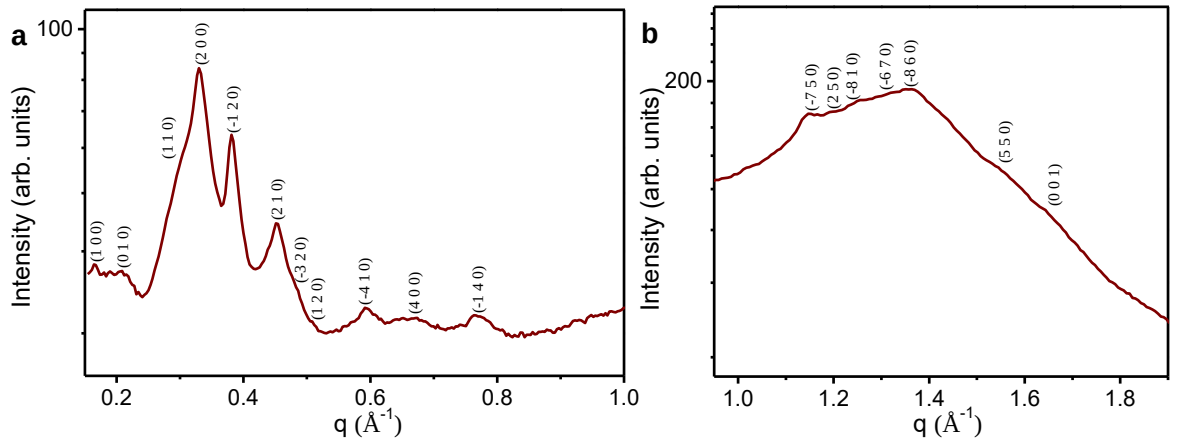

Figure 4.8 X-ray diffraction pattern of compound **8c** for (a) small and (b) wide angle with peaks indexed on the columnar oblique phase (Col_{ob}).

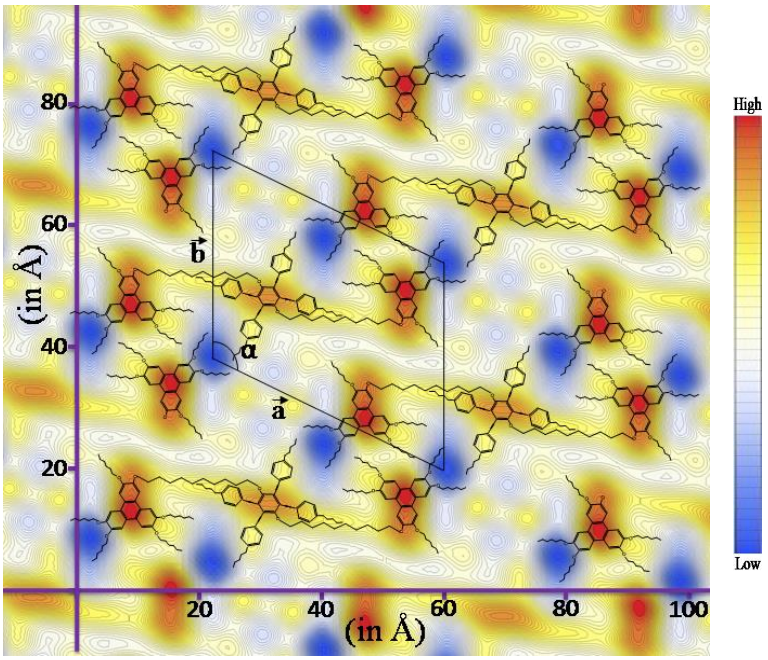

Figure 4.9 Reconstructed electron density map of Col_{ob} phase of compound **8c** showing interdigitation of TP units. Red corresponds to high electron density and deep blue is the lowest. Parallelograms on the map (in black colour) show the 2D unit cell of Col_{ob} phase. $\vec{a}$, $\vec{b}$ and α are the lattice parameter of the unit cell.

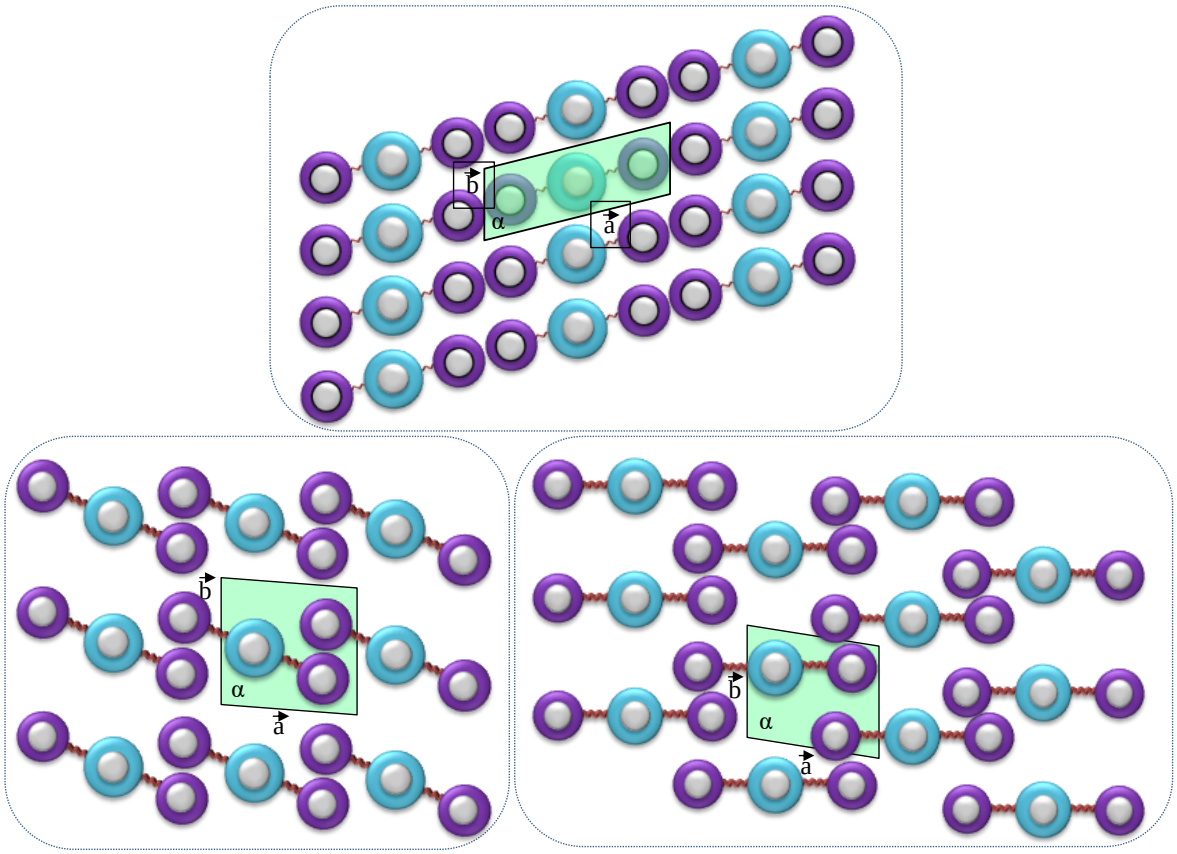

Figure 4.10 The proposed schematic representation of the arrangement of the TP and MB units of the triad compounds: **8a** (on the top), **8b** (bottom left) and **8c** (bottom right) on the 2D oblique lattice. Parallelograms in green colour on the 2D lattices represent the unit cell. $\vec{a}$, $\vec{b}$ and α are the unit cell parameters.

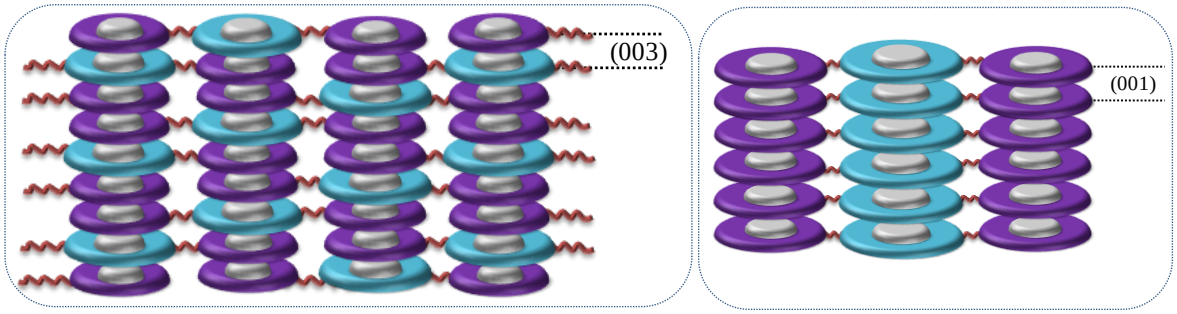

Figure 4.11 The proposed schematic representation of the arrangement of TP and MB units of the triad compound **8a** (left) and compounds **8b** & **8c** (right) in a column.

Table 4.1 The Indices observed and calculated d-spacings and planes, intensity, multiplicity and phase of the diffraction peaks of the; (a) Columnar oblique plastic phase observed in compound **8a** with the lattice parameters: a = 42.41 Å, b = 24.71 Å, c = 13.08 Å and α = 78.12°. (b) Columnar oblique phase observed in compound **8b** with the lattice parameters: a = 38.26 Å, b = 31.38 Å, c = 3.75 Å and α = 95.27° and (c) Columnar oblique phase observed in compound **8c** with the lattice parameters: a = 42.51 Å, b = 33.95 Å, c = 3.71 Å and α = 115.83°. d_{exp} and d_{cal} are the experimental and calculated d-spacings respectively; d_{cal} is calculated by using the relation: $\frac{1}{d_{cal}^2} = \frac{1}{Sin^2\alpha}\left[\frac{h^2}{a^2} + \frac{k^2}{b^2} - \frac{2\,h\,k\,Cos\alpha}{a\,b}\right] + \frac{l^2}{c^2}$; h, k and l are the indices of the reflections corresponding to the columnar oblique phase; a, b & c are the unit cell parameters, α is the angle between $\vec{a}$ and $\vec{b}$ where $|\vec{a}|$ = a and $|\vec{b}|$ = b.

a

Planes (hkl)	d-spacing d_{exp} (Å)	d-spacing d_{cal} (Å)	Relative Intensity	Multiplicity	Phase (ϕ)
1 0 0	41.50	41.50	14.66	2	0
0 1 0	24.18	24.18	100.00	2	π
1 1 0	23.06	23.06	16.03	2	0
2 0 0	20.79	20.75	4.79	2	π
-1 1 0	19.38	19.24	18.18	2	0
2 1 0	17.68	17.64	12.22	2	π
-2 1 0	14.33	14.35	3.62	2	π
3 0 0	13.83	13.83	13.39	2	0
3 1 0	13.18	13.24	9.58	2	π
1 2 0	12.28	12.31			
2 2 0	11.56	11.53			
4 0 0	10.46	10.38	7.33	2	0
3 0 1	9.58	9.50			
3 1 1	9.38	9.30			
-4 1 0	9.02	8.89			
4 2 0	8.74	8.82	4.69	2	π
-3 2 0	8.28	8.30			
2 3 0	8.09	8.10			
3 3 0	7.90	7.69			
-1 3 0	7.62	7.62			
-5 1 0	7.42	7.40			
-4 2 0	7.21	7.18			
-2 3 0	7.03	7.04			
6 0 0	6.90	6.92			

6 2 0	6.65	6.62
5 3 0	6.46	6.49
-6 1 0	6.31	6.31
0 4 0	6.04	6.04
-4 3 0	5.80	5.81
5 4 0	5.40	5.45
-3 4 0	5.15	5.16
2 5 0	4.94	4.94
-6 3 0	4.79	4.78
-1 5 0	4.66	4.69
-2 5 0	4.56	4.51
0 0 3	4.33	4.36
3 1 3	4.18	4.14
-4 5 0	4.08	4.07
-1 6 0	3.93	3.93
9 5 0	3.74	3.74
-8 4 0	3.57	3.59
4 7 0	3.51	3.50

b

Planes (hkl)	*d*-spacing d_{exp} (Å)	*d*-spacing d_{cal} (Å)	Relative Intensity	Multiplicity	Phase (ϕ)
0 1 0	31.04	31.35	44.62	2	0
2 0 0	19.04	19.05	100.00	2	0
-1 2 0	14.99	14.99	55.48	2	π
1 3 0	9.83	9.85	27.20	2	π
2 3 0	8.86	8.83	27.44	2	π
2 5 0	5.60	5.80			
3 5 0	5.36	5.43			
8 0 0	4.79	4.76			
8 1 0	4.61	4.64			
8 3 0	4.17	4.19			
2 8 0	3.75	3.77			
3 8 0	3.62	3.65			

c

Planes (hkl)	*d*-spacing d_{exp} (Å)	*d*-spacing d_{cal} (Å)	Relative Intensity	Multiplicity	Phase (ϕ)
1 0 0	38.26	38.26	37.80	2	0
0 1 0	30.56	30.56	40.24	2	0
1 1 0	20.00	20.00	65.85	2	π
2 0 0	19.04	19.13	100.00	2	0
-1 2 0	16.50	16.96	72.20	2	π
2 1 0	13.87	13.74	40.49	2	π
-3 2 0	13.02	12.95			

1 2 0	12.36	12.44			
-4 1 0	10.57	10.53	36.59	2	0
4 0 0	9.50	9.57	26.83	2	π
-1 4 0	8.23	8.21	28.05	2	π
-7 5 0	5.42	5.41			
2 5 0	5.21	5.20			
-8 1 0	5.05	5.07			
-6 7 0	4.70	4.67			
-8 6 0	4.61	4.64			
5 5 0	3.99	4.00			
7 4 0	3.71	3.74			

4.1.3.4 Photophysical Studies

All the compounds were showing light yellow tinge in solution. Figure 4.12a displays the representative UV-vis absorption spectra of compound **8c** in 5 μM dichloromethane solution which shows absorption maxima centred at 280, 318 and 373 nm with two shoulder peaks at 262 & 272 nm.

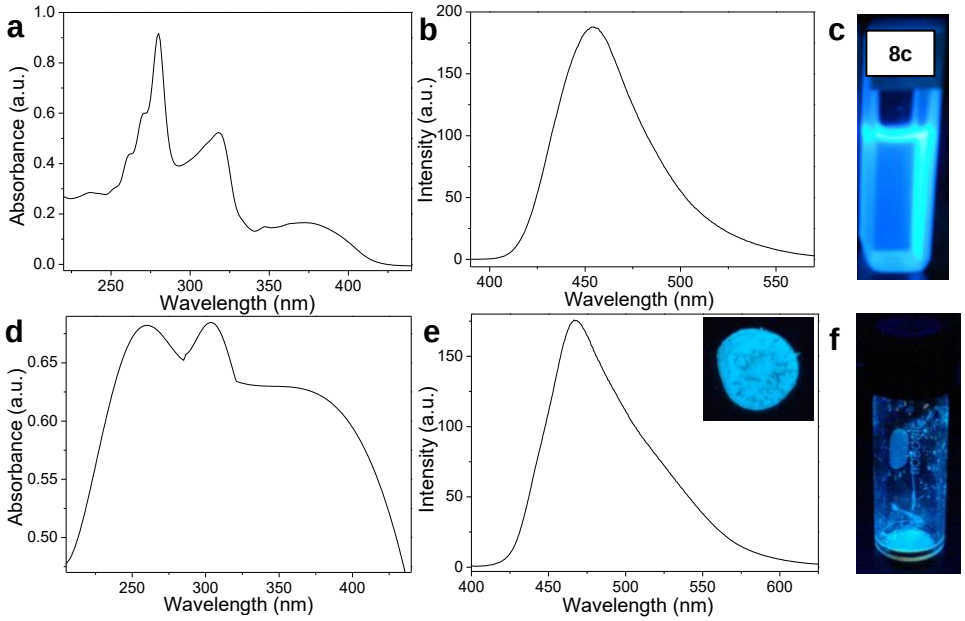

Figure 4.12 Representative (a), (d) UV-vis absorption & (b), (e) emission spectra of compound **8c** in solution (5 μM in dichloromethane) &.of thin film respectively. (c) Picture of compound **8c** in solution (5 μM in dichloromethane) & (f) in neat condition under UV illumination of wavelength 365 nm showing blue light emission. The inset picture in (e) shows blue light emission from the thin film of compound **8c**.

Emission spectra of all the compounds were recorded by exciting the solutions of these compounds at their absorption maxima which shows blue light emission with maxima centred at 454 nm (Figure 4.12b-c) for all the fluorophores (appendix III, Figure A10-A12). A stoke's shift of 76-81 nm was observed for all the compounds. For recording the spectra in neat conditions, a thin film of compound **8c** was prepared by drop casting method on a glass slide. The absorption spectrum of the film showed absorption maxima at 255, 303 & 407 nm (Figure 4.12d) whereas the emission spectrum showed a maximum at 467 nm. A blue shift in the λ_{max} of absorption in the solid state indicates a possibility of the formation of H-aggregates. A red shift of 13 nm was observed for the emission of neat sample as compared to that in the solution state. Moreover, a stoke's shift of 60 nm was observed from the absorption & emission spectra of thin film. As evident from the emission spectrum, the thin film showed blue luminescence when irradiated with UV light of 365 nm wavelength (inset in Figure 4.12e). Figure 4.12f shows blue luminescence from the neat compound **8c** under 365 nm UV light. Thin film of compound **8b** also showed similar characteristics (appendix III, Figure A13). However, for compound **8a**, the emission spectra in thin film became broader (indicating increased intermolecular interactions) with a peak at 465 nm and a shoulder peak at 498 nm. The film displayed cyan coloured photoluminescence under 365 nm UV light. The quantum yields relative to quinine sulfate in 0.1 N H_2SO_4 (appendix III, Figure A14), for compounds **8a-c** in micromolar solutions in dichloromethane were found to be in the range of 0.20 to 0.24 (Table 4.2) which is comparable to some of the 1, 3, 4-oxadiazole and thiadiazole based LC blue light emitters. [31-33] The optical band gap for compounds **8a-c** calculated from the red edge of absorption spectra was found to be in the range of 2.87-2.9 eV (Table 4.2). In order to get insights into the nano-environment of the fluorophores, fluorescence lifetime and steady-state anisotropy were also measured in dilute solutions (5 μM in dichloromethane). All the compounds showed single exponential decay in the fluorescence decay spectra (appendix III, Figure A15). The average fluorescence lifetime for compounds **8a**, **8b** and **8c** was about 1.39, 1.60 and 2.42 ns respectively (Table 4.2). The compound **8a** due to restricted molecular motion exhibits a larger degree of association between the molecules leading to lesser rotational diffusion and a faster relaxation of S1 state and thus decreased lifetime. Similarly, the increased steady-state anisotropy for **8a** can be attributed to the lesser displacement of emission dipole of the fluorophores.

Table 4.2 Optical data of the compounds synthesized in the study[a, b, c, d]

Compound	Absorption (nm)	Emission (nm)	ΔE_g [b] (eV)	Φ_{FL} [c]	τ_{av} [d] (ns)	Steady State Anisotropy
8a	280, 318, 377	453	2.87	0.20	1.39	13.04×10^{-3}
8b	280, 318, 373	454	2.90	0.24	1.60	7.17×10^{-3}
8c	280, 318, 373	454	2.90	0.24	2.42	5.26×10^{-3}

[a] in μm solutions in CH_2Cl_2; [b] optical bandgap calculated from the λ_{onset}; [c] relative to quinine sulfate in 0.1 N H_2SO_4 ($\Phi_{FL} = 0.54$); [d] fluorescence lifetime.

The estimation of frontier orbitals i.e. HOMO and LUMO levels and electrical band gap for compound **8c** was done from cyclic Voltammetry studies in micromolar dichloromethane solution of compound **8c** (Figure 4.13). For these studies a 0.1 M solution of tetrabutylammonium hexafluorophosphate was used as supporting electrolyte in dichloromethane. A single compartment cell fitted with $Ag/AgNO_3$ reference electrode, platinum wire counter electrode and glassy carbon working electrode was used for experiment. For ferrocene/ferrocenium (Fc/Fc^+) redox couple, E_{red} and E_{oxd} were found to be -0.90 and 0.84 V respectively. Consequently, the half-wave potential was calculated to be 0.433 V by the following relation:

$(E_{1/2,\ Fc/Fc^+}) = (E_{\text{anodic peak potential}} + E_{\text{cathodic peak potential}})/2 = (0.525 + 0.342)/2 = 0.4335$ V

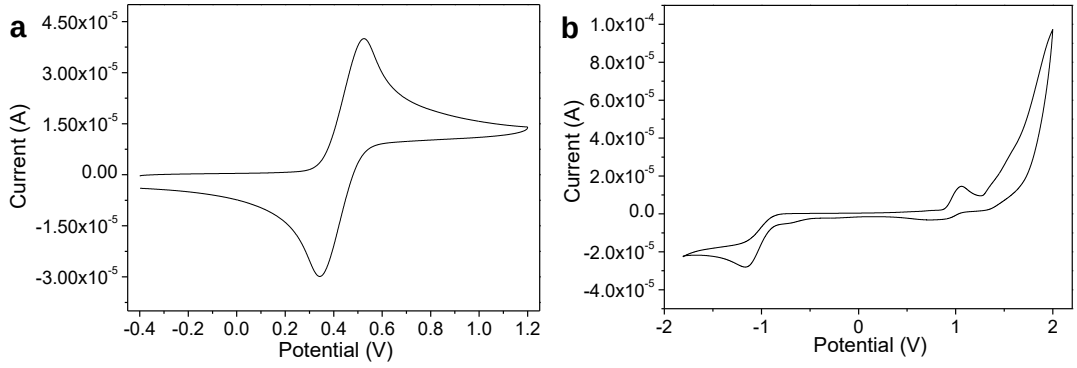

Figure 4.13 (a) Cyclic voltammogram of ferrocene in anhydrous dichloromethane solution of tetrabutylammonium hexafluorophosphate (0.1 M). (b) Cyclic voltammogram of compound **8c** in anhydrous dichloromethane solution of tetrabutylammonium hexafluorophosphate (0.1 M) at a scanning rate of 0.5 mV/s.

The band gap was calculated using the following relation:

$E_{HOMO} = - (E_{oxd,onset} - E_{1/2, Fc, Fc}^{+} + 4.8)$ eV

$E_{LUMO} = - (E_{red,onset} - E_{1/2, Fc, Fc}^{+} + 4.8)$ eV

$\Delta Eg = E_{HOMO} - E_{LUMO}$

For compound **8c**, the HOMO and LUMO energy levels were estimated to be -5.20 and -3.46 eV, respectively (appendix III, Figure A16). The electrical band gap was calculated to be 1.74 eV which is lesser as compared to the optical bandgap.

4.1.4 Conclusion

Multialkynyl bridged triphenylene based dimers having different length of spacer have been synthesized and characterized. All these compounds exhibited LC properties even at room temperature as confirmed by POM and XRD. The compounds with spacer length, *n* = 8, 10 exhibited columnar oblique mesophase whereas the compound with the shortest spacer length *i.e*. *n* = 6 exhibited columnar oblique plastic phase. In addition to this, the compound exhibited a long-range self-assembly showing the formation of well-nucleated spherulites of about several hundred micrometres. All the compounds exhibited blue light emission on irradiation at their absorption maxima in solution as well as in neat conditions. The property of room temperature columnar self-assembly over long range, together with blue light emission in neat state make these compounds very promising for possible potential applications in semiconductor devices.

4.2 Part B: Structure property relationships in lath-shaped triads based on multialkynylbenzene

4.2.1 Introduction

Disc shaped molecules are more prone to form columnar phases due to π-π interactions among the poly-aromatic cores and thus discs which are only orientationally ordered (*i.e.* exhibiting nematic discotic, N_D phase) are rarely seen.[42-44] However, the importance of discogens exhibiting nematic mesophase in optical compensation films for magnifying the viewing angle has led to an intense research in this field.[45, 46] The discotic cores such as triphenylene, truxene, thiotruxene, naphthalene, 1,3,5-trisalkynylbenzene etc. have been derivatized in various ways to show N_D phase.[47-59] Other molecular interactions e.g. hydrogen bonding has also been explored to generate N_D phase. For example, hydrogen bonded phenol and pyridine moieties as well as phloroglucinol and alkoxystillbazole moieties have also been reported to show N_D mesophase.[60, 61] Till date, hexa- and pentaalkynylbenzene derivatives have been the most investigated systems among various discotic nematogens.[62] However, in most of the cases, N_D phase appears at higher temperature that limits their widespread use in applications. The first example of room-temperature N_D mesogen was reported by Kumar and co-workers, using a pentaalkynylbenzene (PA) derivative with branched alkyl spacers.[63] Till date, only a very few approaches have been reported to obtain room-temperature N_D mesophase.[64-68] Recently, we have reported a new design for the realization of room-temperature discotic N_D dyads derived from TP & PA units linked via flexible alkyl spacers.[69] The improper packing resulting from incompatibility of the two discs in the folded mesogenic dyad was considered as the most possible reason for the observation of room-temperature N_D phase. We have further shown another new strategy to obtain a room-temperature N_D phase over a wide temperature range by connecting four PA units to an azobenzene core via flexible alkyl spacers.[70] The presence of short rigid azo group in these oligomers led to a system in which PA units were disordered enough to prevent efficient packing of the molecules and thus forms room temperature N_D phase which persists over a wide temperature range.

4.2.2 Objective

In this report, we have further aimed to synthesise multialkynylbenzene based linear symmetric triads in which three multialkynylbenzene units are linked together *via* flexible alkyl spacers. The earlier reported examples of symmetric dimers based on PA displayed N_D phase at higher temperature.[71, 72] Therefore, we were further interested to investigate the mesomorphism resulting from these symmetrical triads. In this study, we have synthesized four compounds in which the length of the alkyl spacers was varied. We have found that the triads with the shorter spacers were found to be non-mesomorphic. However, the compound with the longest flexible alkyl spacer displayed enantiotropic N_D phase as confirmed from POM and XRD studies.

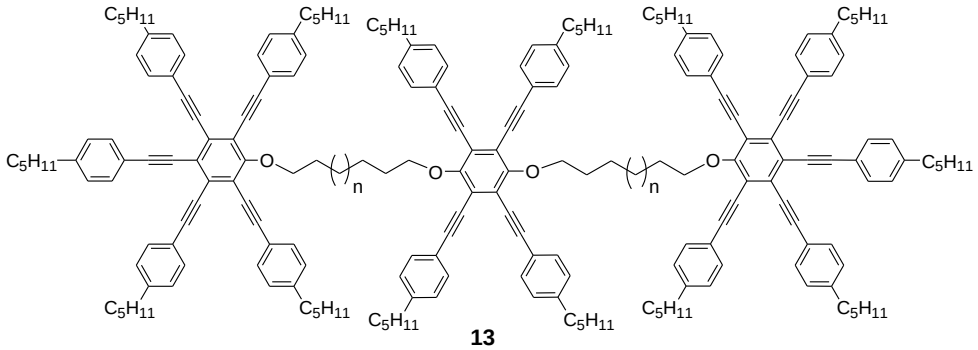

13
(*n* = 1, 3, 5, 7)

4.2.3 Results and Discussion

4.2.3.1 Synthesis and Characterization

The target compounds (**13a–d**) were synthesized by the route depicted in 4.2. The synthesis of intermediate compounds **15** was carried out in neat conditions by heating with KOH and TOAB at 80 °C for 12 hours (see experimental section for details).[73] The synthesis of compounds **16** and **13** was carried out using earlier reported procedures.[74-56] All compounds were characterised by ^{1}H & ^{13}C NMR, IR, UV-vis and mass (MALDI) spectrometry (appendix III, Figure A17 – A26). The thermal behaviour of the synthesized triads was investigated by differential scanning calorimetry (DSC) and the mesophase behaviour was analysed by polarized optical microscopy (POM) as well as small- and wide-angle X-ray scattering studies (SAXS/WAXS).

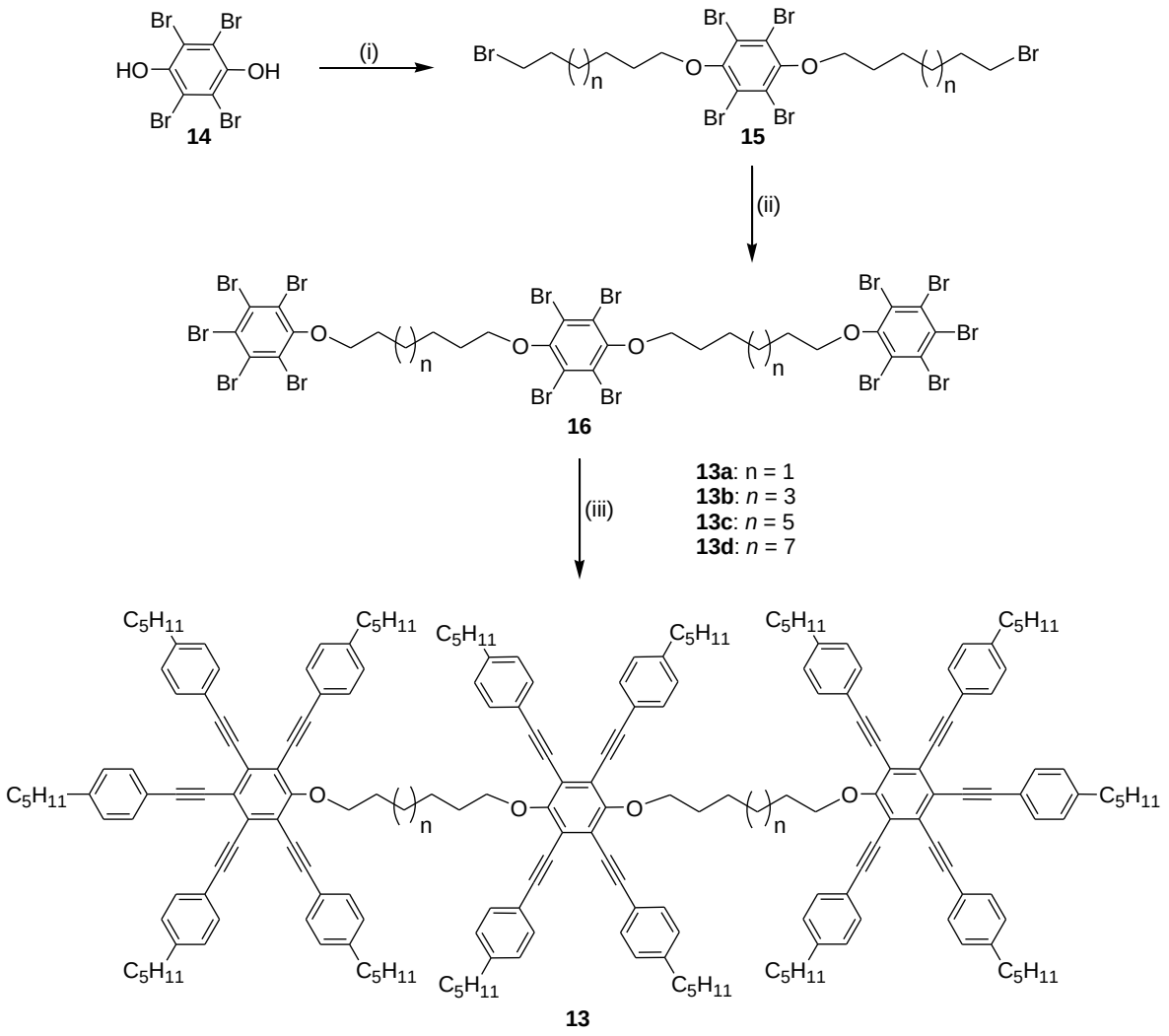

Scheme 4.2 (i) KOH, TOAB, Br-$(CH_2)_n$-Br, 12 h, 80 °C, 60%; (ii) Pentabromophenol, K_2CO_3, KI, butanone, 18 h, 80 °C, 80% and (iii) $Pd(PPh_3)_2Cl_2$, CuI, PPh_3, 1-ethynyl-4-pentylbenzene, Et_3N, 24h, 100 °C, 78%.

4.2.3.2 Thermal Behavior

Compounds **13a- 13c** were found to be non-LC as confirmed from their DSC and POM studies. In DSC scan, they displayed a peak corresponding to transition from crystal to isotropic phase (Table 4.3). While, on subsequent cooling, a phase transition from isotropic to crystal was observed for these triads. Compound **13d** was solid at room temperature and displayed a melting transition peak at 114.44 °C (ΔH = 18.42 kJ mol^{-1}, Figure 4.14a, 4.14b) to the mesophase which cleared at 121.5 °C (ΔH = 0.20 kJ mol^{-1}). On further cooling, it

showed the emergence of a well-defined schlieren texture typical of a nematic phase at 119.2 °C (ΔH = 0.11 kJ mol^{-1}, Figure 4.14c) which persisted till 82.23 °C (ΔH = 25.63 kJ mol^{-1}) and transformed to crystalline state thereafter. It can be thus inferred that the mesophase in case of **13d** is enantiotropic only over a short temperature range (~ 7 °C) and a lower temperature monotropic.

Table 4.3 Thermal behavior of the synthesized compounds **13**[a, b]

Compound	Heating Scan	Cooling Scan
13a	Cr 125.68 (12.76) I	I 109.84 (21.12) Cr
13b	Cr 124.23 (13.58) I	I 109.55 (20.86) Cr
13c	Cr 124.11 (15.34) I	I 110.11 (22.33) Cr
13d	Cr 114.44 (18.42) N_D 121.5 (0.20) I	I 119.5 (0.11) N_D 82.23 (25.63) Cr

[a]Phase transition temperatures (peak) in °C and transition enthalpies in kJmol^{-1} (in parentheses). [b]Phase assignments: Cr = Crystalline, N_D = discotic nematic, I = isotropic.

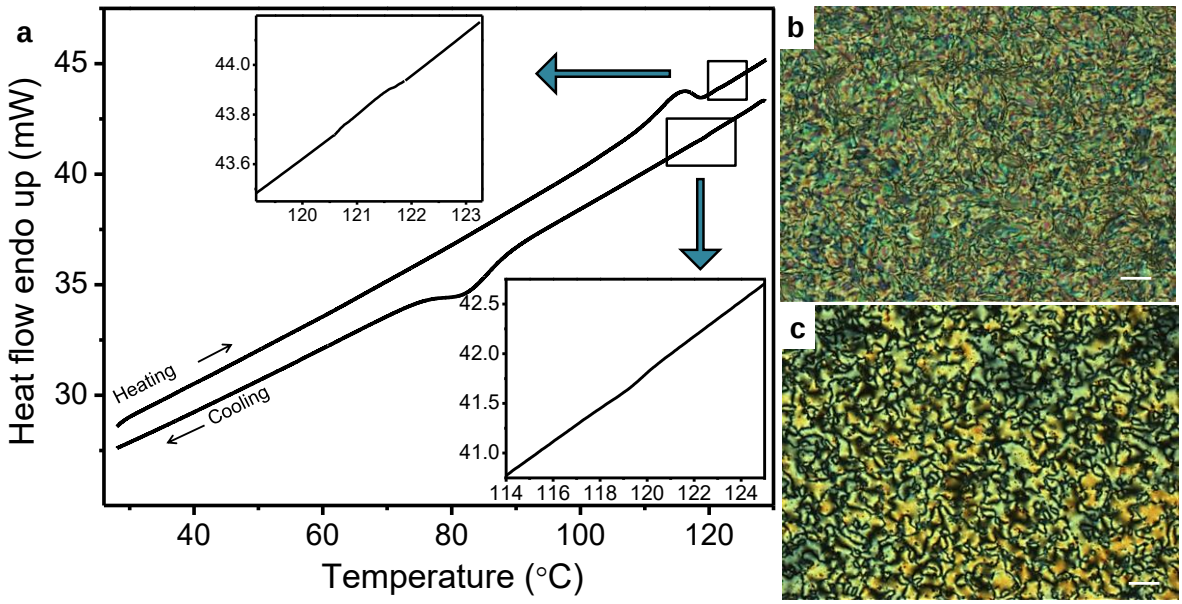

Figure 4.14 (a) DSC thermogram of compound **13d** obtained on heating and cooling cycle with a scan rate of 2 °C/min. Optical photomicrograph of compound **13d** obtained with a polarized optical microscope at (b) 118 °C on heating and (c) 110 °C on cooling from the isotropic melt (crossed polarizers, magnification × 200, scale bar = 20 μm).

4.2.3.3 X-ray Diffraction Studies

To investigate the detailed structure of the N_D phase of compound **13d**, X-ray diffraction experiments were performed. Diffractogram corresponding to mesophase of compound **13d** (Figure 4.15a) displayed a comparatively sharp peak at small angle and a broad peak at wide angle regime. This XRD pattern confirms the presence of a N_D phase. The 2D diffraction pattern for compound **13d** shows a partially aligned peak at small-angle which is however less oriented in comparison to wide-angle halo (Figure 4.15b). A possible reason for this behaviour could be due to random orientation of multialkynylbenzene units in the mesophase.

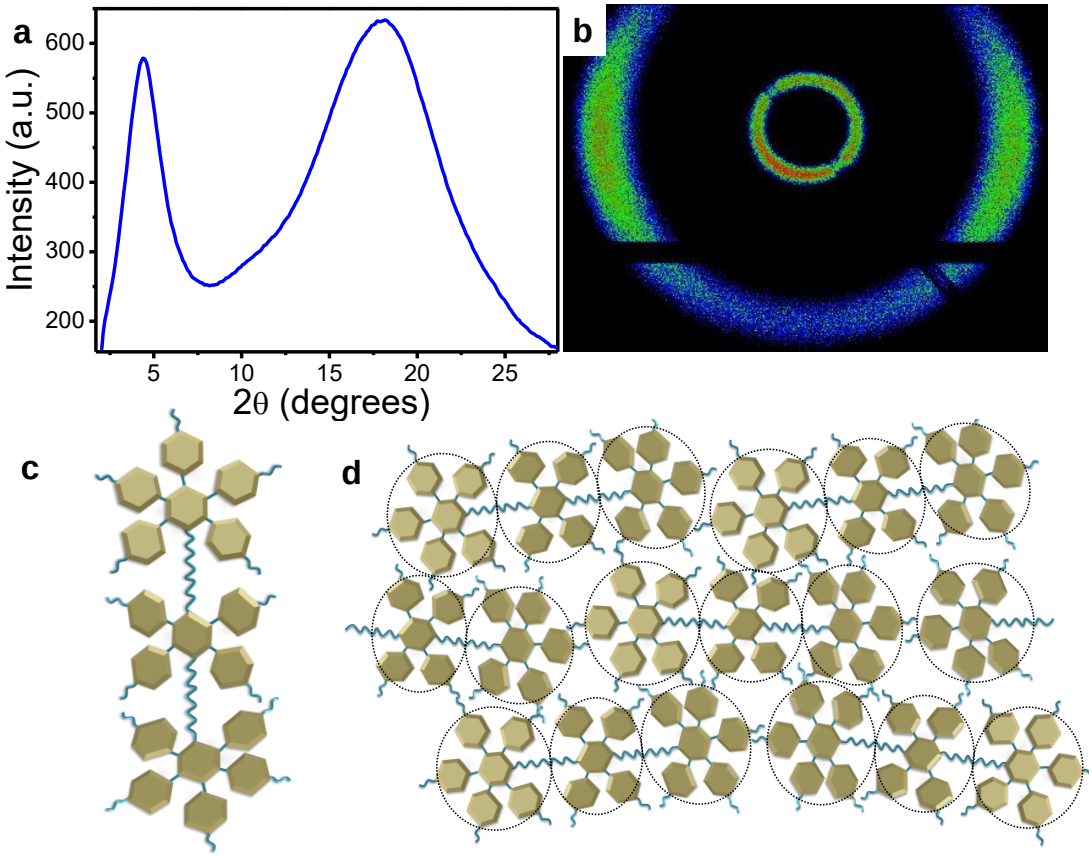

Figure 4.15 (a) X-ray diffraction pattern of compound **13d** in its mesophase at 110 °C on cooling from the isotropic and its corresponding 2D diffraction pattern (b). (c) Schematic of the structure of compound **13**, modelled as three multialkynylbenzene discs linked via flexible alkyl spacers. (d) Local arrangement of the model unit in the nematic discotic phase.

Further, the intensity maximum at small-angle as observed from azimuthal intensity variations was found to be oriented with an angle of ~57 °C with respect to the maximum of the halo present at wide-angle. It reflects that the growth of the side by side correlation of the composite disc and chain–chain correlation are at an angle of about 57 °C. The *d*-spacing for the signal in the small angle was calculated to be 19.39 Å which corresponds to the average inter-disc distance i.e. side by side separation of the discs along the disc plane and is approximately equal to the diameter of a single disc unit of the triad, ~19 Å.

The compound **13d** can be modelled as discotic mesogenic triad based on multialkynylbenzene units linked via flexible alkyl spacers in a side-by-side fashion (Figure 4.15c). The phenyl rings of multialkynylbenzene unit are generally not in plane because of rotational freedom provided by ethynyl linkers which prevents columnar stacking. The peak observed at small-angle *i.e.* at 19.39 Å cannot be attributed to the length of molecule as that is calculated to be around 53 Å which is much higher as compared to the observed value. However, it can be most likely due to inter- and intra-molecular correlation of multialkynylbenzene discs in the mesophase and thus is approximately equal to diameter of a single disc unit of the triad. The correlation length, the degree of order within the mesophases, was calculated from the Scherrer's equation, $\xi = 0.89\lambda/\beta\cos\theta$, where 0.89 is the correction factor, β represents the full width at half-maximum (FWHM) of the peak obtained for core-core spacing, and λ and θ represent the wavelength of incident X-rays and Bragg's angle, respectively. The correlation length (ξ) for the reflections at 19.39 Å and 5.02 Å were calculated to be 27.90 and 7.90 Å respectively (Table 4.4). The correlation length was further divided by the *d*-spacing values (ξ/d), which results in a measure for the length scale of spatial order in terms of the dimensions of the molecular length scale.

Table 4.4 X-ray reflections and the corresponding correlation lengths obtained in the nematic phase of compound **13d**.

Compound	Properties	Small angle peak	Wide angle peak
13d	*d*-spacing (Å)	19.39 ± 0.37	5.02 ± 0.006
	Correlation Length (ξ) (Å)	27.90 ± 0.53	7.90 ± 0.12
	ξ/d	1.43 ± 0.03	1.57 ± 0.02

This value was found to be around 1.43 for the peak at small angle which corresponds to nearly one multialkynylbenzene disc. This indicates that there is no correlation among the triads which is also expected from their orientationally ordered arrangement in nematic phase.

A possible reason for the absence of mesophase in case of compounds **13a-13c** could be due to incommensurate volume fractions of aliphatic chains and aromatics which make them unable to self-organize and thus these materials crystallize. Further, the observation of N_D phase at high temperature for compound **13d** could be due to the fact that the multialkynylbenzene units are connected in a side-by-side manner *via* relatively short alkyl spacers and thus do not have enough freedom to create disorder in the system to result into a room-temperature mesophase. Earlier reported examples of symmetric dyads based on pentaalkynylbenzene also shows N_D phase at high temperature. However, in comparison, the phase transition temperatures are reduced in case of triads. This could be due to introduction of one more multialkynylbenzene unit which induces more disorder in the system.

4.2.4 Conclusion

In conclusion, we have synthesized four triads in which three multialkynylbenzene units were linked to each other with varying flexible alkyl spacers (*n* = 6, 8, 10, 12). The first three derivatives were found to be non-LC. However, the derivative with longest alkyl spacer i.e. *n* = 12 exhibited an enantiotropic N_D phase which was confirmed from POM and XRD studies. Overall, this study provides new insights into the structure-property relationships of multialkynylbenzene systems.

4.3 Experimental Section

4.3.1 Synthesis of compound 8a For the synthesis of compound **8a**, 30 ml of dry triethylamine was taken in a round bottom flask and was degassed followed by the addition of $Pd(PPh_3)Cl_2$ (50 mg), CuI (50 mg) PPh_3 (100 mg) & compound **4** (0.63 mmol). The mixture was stirred for 15 minutes followed by the gradual addition of 1-ethynyl-4-pentyl benzene (6.3 mmol). The reaction mixture was stirred at 100°C for 24 h under nitrogen. After the completion of reaction as monitored by TLC, it was cooled to room temperature and

poured into 30 ml of 5M HCl. The product was extracted with DCM & was purified by column chromatography over silica gel to obtain the target compounds **8a**. ^{1}H NMR (400 MHz, $CDCl_3$, δ in ppm): 7.85 (d, 12H, *J* = 12 Hz), 7.51 (d, 8H, *J* = 8 Hz), 7.13 (d, 8H, *J* = 8 Hz), 4.36 (t, 4H, *J* = 4, 8 Hz), 4.24 (m, 24H), 2.53 (t, 8H, *J* = 8 Hz), 1.97 (m, 28H), 1.76 (m, 8H), 1.59 (m, 28H), 1.35 (m, 60H), 0.92 (m, 42 H). ^{13}C NMR (400 MHz, $CDCl_3$, δ in ppm): 157.28, 157.12, 149.0, 148.94, 143.94, 131.63, 128.53, 123.63, 121.09, 120.45, 107.29, 99.38, 84.12, 69.70, 35.88, 31.71, 31.46, 30.87, 29.45, 26.29,25.88, 22.69, 22.50, 14.09. FT-IR (cm^{-1}): 3035.0, 2954.59, 2929.83, 2857.83, 2209.8, 1616.87, 1516.30, 1467.64, 1434.78, 1388.36, 1330.31, 1262.88, 1173.22, 1043.52, 838.30, 726.50, 601.28. UV-vis (nm): 262, 272, 280, 318, 377. MS (MALDI): *m/z* for $C_{166}H_{266}O_{14}$ 2444.7006; found 2444.7664.

4.3.2 Synthesis of compound 8b Compound was synthesized according to a similar procedure as explained for **8a**. ^{1}H NMR (400 MHz, $CDCl_3$, δ in ppm): 7.86 (s, 12H), 7.51 (d, 8H, *J* = 8 Hz), 7.17 (d, 8H, *J* = 8 Hz), 4.32 (t, 4H, *J* = 4, 8 Hz), 4.25 (m, 24H), 2.59 (t, 8H, *J* = 8 Hz), 1.96 (m, 28H), 1.6 (m, 28H), 1.36 (m, 92H), 0.93 (m, 42 H). ^{13}C NMR (400 MHz, $CDCl_3$, δ in ppm): 157.15, 148.93, 143.91, 131.93, 131.58, 128.54, 123.59, 121.07, 120.52, 107.25, 99.34, 98.02, 97.50, 84.16, 74.71, 69.69, 69.07, 64.64, 35.94, 31.72, 31.48, 30.96, 29.44, 25.88, 22.70, 22.54, 14.11, 14.06. FT-IR (cm^{-1}): 2960.8, 2929.12, 2857.44, 2214.8, 1616.27, 1512.91, 1467.79, 1434.76, 1386.01, 1262.61, 1171.09, 1039.87, 838.88, 726.28, 600.67. UV-vis (nm): 262, 272, 280, 318, 373. MS (MALDI): *m/z* for $C_{170}H_{234}O_{14}$ 2500.7632; found 2500.7691.

4.3.3 Synthesis of compound 8c Compound was synthesized according to a similar procedure as explained for **8a**. ^{1}H NMR (400 MHz, $CDCl_3$, δ in ppm): 7.85 (s, 12H), 7.51 (d, 8H, *J* = 12 Hz), 7.18 (d, 8H, *J* = 8 Hz), 4.30 (t, 4H, *J* = 8, 4 Hz), 4.25 (m, 24H), 2.63 (t, 8H, *J* = 8 Hz), 1.96 (m, 28H), 1.6 (m, 28H), 1.36 (m, 84H), 0.93 (m, 42 H). ^{13}C NMR (400 MHz, $CDCl_3$, δ in ppm): 157.16, 148.95, 143.86, 131.98, 131.59, 128.52, 123.61, 121.05, 120.55, 107.32, 99.33, 84.18, 74.75, 69.70, 35.96, 31.72, 31.48, 30.96, 29.73, 29.45, 26.49, 26.28, 25.88, 22.69, 22.55, 14.11, 14.09, 14.05. FT-IR (cm^{-1}): 3026.21, 2954.02, 2928.65, 2856.77, 2210.06, 1616.65, 1514.01, 1467.59, 1434.93, 1387.78, 1330.08, 1262.57, 1170.96, 1041.82, 928.52, 838.08, 725.79, 600.93, 550.16, 528.02. UV-vis (nm): 237, 262, 271, 280, 318, 373. MS (MALDI): *m/z* for $C_{174}H_{242}O_{14}$ 2556.8258; found 2556.8027.

4.3.4 Synthesis of compound 13a The di-alkylation of tetrabromohydroquinone was not possible using conventional methods due to rapid formation of quinone. Therefore, the reaction was carried out under solvent free conditions. Compound **14** (1 equiv.) was finely ground with KOH (2.5 equiv.) and tetraoctylammonium bromide (0.09 equiv.) followed by the addition of dibromoalkane (10 equiv.). The mixture thus obtained was heated at 80 °C for 12 h with continuous stirring. After completion of the reaction, the mixture was poured into water and the compound was extracted with dichloromethane which was further purified by column chromatography. For synthesis of compound **16**, pentabromophenol (5 equiv.) was dissolved in n-butanone. To the above solution, K_2CO_3 (5 equiv.) was added and the mixture was stirred for 15 min. followed by the addition of compound **15** (1 equiv.). The mixture was refluxed for 24 h. The reaction mixture was filtered and the filtrate was concentrated and purified through column chromatography. The 14-fold sonogashira coupling of compound **16** was carried out similarly as reported in the earlier reports to get the final compounds **13**. ^{1}H NMR (400 MHz, $CDCl_3$, δ in ppm): 7.52 (m, 28H), 7.16 (m, 28H), 4.30 (t, 4H, J = 4, 8 Hz), 4.22 (t, 4H, J = 8, 4 Hz), 2.60 (m, 28H), 1.93 (m, 8H), 1.69 (m, 28H), 1.32 (m, 64H), 0.91 (m, 42H). ^{13}C NMR (400 MHz, $CDCl_3$, δ in ppm): 160.16, 157.18, 143.97, 140.91, 139.80, 131.77, 131.65, 131.54, 128.53, 121.03, 120.50, 120.41, 120.15, 101.96, 99.46, 99.39, 84.02, 60.20, 53.44, 45.32, 35.99, 35.93, 31.52, 31.49, 30.95, 30.93, 26.42, 22.53, 14.05. FT-IR (cm^{-1}): 3026.94, 2956.10, 2929.02, 2857.47, 2207.50, 1513.07, 1463.86, 1427.50, 1379.01, 1346.73, 1330.03, 1263.06, 1198.73, 1179.4, 1114.14, 1082.04, 1072.8, 1041.67, 1019.72, 995.54, 836.61, 812.47, 737.99, 549.17, 528.08. UV-vis (nm): 237, 268, 338, 381, 418. MS (MALDI): *m/z* for $C_{212}H_{234}O_4$ 2845.8174; Found 2845.6030.

4.3.5 Synthesis of compound 13b Compound was synthesized according to a similar procedure as explained for **13a**. ^{1}H NMR (400 MHz, $CDCl_3$, δ in ppm): 7.53 (m, 28H), 7.17 (m, 28H), 4.36 (t, 4H, J = 8, 4 Hz), 4.29 (t, 4H, J = 4, 8 Hz), 2.63 (m, 28H), 1.92 (m, 8H), 1.63 (m, 28H), 1.30 (m, 72H), 0.90 (m, 42H). ^{13}C NMR (400 MHz, $CDCl_3$, δ in ppm): 160.25, 157.16, 143.99, 143.94, 143.87, 131.77, 131.65, 131.56, 128.74, 128.54, 128.51, 120.72, 120.52, 120.49, 120.14, 111.45, 99.40, 99.33, 84.18, 84.06, 35.95, 31.49, 30.98, 30.95, 30.68, 29.73, 26.43, 22.54, 14.04. FT-IR (cm^{-1}): 3030.6, 2954.4, 2927.45, 2854.58, 2206.96, 1512.04, 1465.1, 1424.01, 1381.3, 1350.8, 1328.17, 1278.5, 1261.15, 1198.5,

1179.4, 1110.9, 1080.4, 1020.26, 836.61, 813.96, 750.53, 543.32. UV-vis (nm): 237, 267, 338, 380, 417. MS (MALDI): *m/z* for $C_{216}H_{242}O_4$ 2901.88; found 2901.68.

4.3.6 Synthesis of compound 13c Compound was synthesized according to a similar procedure as explained for **13a**. ^{1}H NMR (400 MHz, $CDCl_3$, δ in ppm): 7.53 (m, 28H), 7.17 (m, 28H), 4.29 (m, 8H), 2.61 (m, 28H), 1.90 (m, 8H), 1.64 (m, 28H), 1.31 (m, 80H), 0.90 (m, 42H). ^{13}C NMR (400 MHz, $CDCl_3$, δ in ppm): 160.84, 157.81, 144.42, 144.00, 143.24, 140.61, 135.61, 131.78, 131.67, 131.58, 128.55, 123.98, 121.57, 110.54, 92.54, 89.30, 82.88, 63.05, 56.86, 54.29, 48.57, 36.00, 35.92, 31.50, 30.97, 28.44, 22.56, 14.06. FT-IR (cm^{-1}): 3026.8, 2954.4, 2928.25, 2855.35, 2207.40, 1512.28, 1465.1, 1425.16, 1377.5, 1347.01, 1328.92, 1259.4, 1194.7, 1183.2, 1118.5, 1088.00, 1019.42, 992.78, 969.93, 840.42, 813.70, 729.96, 547.13. UV-vis (nm): 239, 265, 338, 380, 414. MS (MALDI): *m/z* for $C_{220}H_{250}O_4$ 2958.3366; found 2958.3164.

4.3.7 Synthesis of compound 13d Compound was synthesized according to a similar procedure as explained for **13a**. ^{1}H NMR (400 MHz, $CDCl_3$, δ in ppm): 7.53 (m, 28H), 7.18 (m, 28H), 4.37 (t, 4H, J = 4, 8 Hz), 4.29 (t, 4H, J = 4, 8 Hz), 2.63 (m, 28H), 1.93 (m, 8H), 1.63 (m, 28H), 1.28 (m, 88H), 0.91 (m, 42H). ^{13}C NMR (400 MHz, $CDCl_3$, δ in ppm): 161.06, 157.15, 141.36, 136.03, 131.77, 131.65, 131.57, 128.53, 128.51, 110.12, 99.51, 64.34, 53.45, 49.14, 35.98, 31.48, 30.96, 29.80, 22.56, 14.06. FT-IR (cm^{-1}): 3026.8, 2958.2, 2927.97, 2855.53, 2204.39, 1511.82, 1461.3, 1424.37, 1385.10, 1346.63, 1263.2, 1202.3, 1179.4, 1118.59, 1084.2, 1023.3, 1000.4, 947.08, 889.94, 840.42, 812.20, 722.34, 531.9. UV-vis (nm): 238, 268, 336, 380, 417. MS (MALDI): *m/z* for $C_{224}H_{258}O_4$ 3011.9985; found 3011.8007.

References

(1) Muccini, M. *Nat Mater* **2006**, *5*, 605-613.

(2) Meerholz, K.; Müller, C.-D.; Nuyken, O. In *Organic Light Emitting Devices*, Wiley-VCH Verlag GmbH & Co. KGaA: **2006**, 293-318.

(3) Forrest, S. R.; Thompson, M. E. *Chem. Rev.* **2007**, *107*, 923-925.

(4) Jian, W.; Gang, Y. In *Organic Light-Emitting Materials and Devices*, CRC Press: **2006**.

(5) Norman, H.; Hong, M. In *Organic Light-Emitting Materials and Devices*, CRC Press: **2006**.

(6) Köhler, A.; Wilson, J. S.; Friend, R. H. *Adv. Mater.* **2002**, *14*, 701-707.

(7) Yook, K. S.; Lee, J. Y. *Adv. Mater.* **2012**, *24*, 3169-3190.

(8) D'Andrade, B. W.; Brooks, J.; Adamovich, V.; Thompson, M. E.; Forrest, S. R. *Adv. Mater.* **2002**, *14*, 1032-1036.

(9) Xiao, L.; Chen, Z.; Qu, B.; Luo, J.; Kong, S.; Gong, Q.; Kido, J. *Adv. Mater.* **2011**, *23*, 926-952.

(10) Schubert, E. F.; Kim, J. K. *Science* **2005**, *308*, 1274-1278.

(11) Kovac, J.; Peternai, L.; Lengyel, O. *Thin Solid Films* **2003**, *433*, 22-26.

(12) Varghese, S.; Kumar, N. S. S.; Krishna, A.; Rao, D. S. S.; Prasad, S. K.; Das, S. *Adv. Funct. Mater.* **2009**, *19*, 2064-2073.

(13) Eccher, J.; Faria, G. C.; Bock, H.; von Seggern, H.; Bechtold, I. H. *ACS Appl. Mater. Interfaces* **2013**, *5*, 11935-11943.

(14) Hassheider, T.; Benning, S. A.; Kitzerow, H.-S.; Achard, M.-F.; Bock, H. *Angew Chem. Int. Ed.* **2001**, *40*, 2060-2063.

(15) Seguy, I.; Jolinat, P.; Destruel, P.; Mamy, R.; Allouchi, H.; Courseille, C.; Cotrait, M.; Bock, H. *ChemPhysChem* **2001**, *2*, 448-452.

(16) Torgova, S.; Strigazzi, A. *Mol. Cryst. Liq. Cryst.* **2002**, *375*, 61-72.

(17) Boden, N.; Movaghar, B.; Demus, D.; Goodby, J.; Gray, G. W.; Spiess, H. W.; Vill, V. In *Handbook of Liquid Crystals Set*, Wiley-VCH Verlag GmbH: **2008**, 781-798.

(18) Markovitsi, D.; Marguet, S.; Bondkowski, J.; Kumar, S. *J. Phys. Chem. B* **2001**, *105*,1299-1306.

(19) Bushey, M. L.; Hwang, A.; Stephens, P. W.; Nuckolls, C. *J. Am. Chem. Soc.* **2001**, *123*, 8157-8158.

(20) Pisula, W.; Kastler, M.; Wasserfallen, D.; Pakula, T.; Müllen, K. *J. Am. Chem. Soc.* **2004**, *126*, 8074-8075.

(21) Tong, L.; Qi, W.; Wang, M.; Huang, R.; Su, R.; He, Z. *Chem. Commun.* **2014**, *50*, 7776-7779.

(22) Pisula, W.; Dierschke, F.; Mullen, K. *J. Mater. Chem.* **2006**, *16*, 4058-4064.

(23) Cristiano, R.; Santos, D. M. P. d. O.; Gallardo, H. *Liq. Cryst.* **2005**, *32*, 7-14.

(24) Wen, C.-R.; Wang, Y.-J.; Wang, H.-C.; Sheu, H.-S.; Lee, G.-H.; Lai, C. K. *Chem. Mater.* **2005**, *17*, 1646-1654.

(25) Vinayakumara, D. R.; Kumar, M.; Sreekanth, P.; Philip, R.; Kumar, S. *RSC Adv.* **2015**, *5*, 26596-26603.

(26) Gupta, R. K.; Pradhan, B.; Pathak, S. K.; Gupta, M.; Pal, S. K.; Ammathnadu Sudhakar, A. *Langmuir* **2015**, *31*, 8092-8100.

(27) Cristiano, R.; Gallardo, H.; Bortoluzzi, A. J.; Bechtold, I. H.; Campos, C. E. M.; Longo, R. L. *Chem. Commun.* **2008**, 5134-5136.

(28) Vieira, A. A.; Gallardo, H.; Barbera, J.; Romero, P.; Serrano, J. L.; Sierra, T. *J. Mater. Chem.* **2011**, *21*, 5916-5922.

(29) Srivastava, R. M.; Neves Filho, R. A. W.; Schneider, R.; Vieira, A. A.; Gallardo, H. *Liq. Cryst.* **2008**, *35*, 737-742.

(30) Cristiano, R.; Eccher, J.; Bechtold, I. H.; Tironi, C. N.; Vieira, A. A.; Molin, F.; Gallardo, H. *Langmuir* **2012**, *28*, 11590-11598.

(31) Westphal, E.; Prehm, M.; Bechtold, I. H.; Tschierske, C.; Gallardo, H. *J. Mater. Chem. C* **2013**, *1*, 8011-8022.

(32) Pathak, S. K.; Gupta, R. K.; Nath, S.; Rao, D. S. S.; Prasad, S. K.; Achalkumar, A. S. *J. Mater. Chem. C* **2015**, *3*, 2940-2952.

(33) Pathak, S. K.; Nath, S.; Gupta, R. K.; Rao, D. S. S.; Prasad, S. K.; Achalkumar, A. S. *J. Mater. Chem. C* **2015**, *3*, 8166-8182.

(34) Gupta, M.; Bala, I.; Pal, S. K. *Tetrahedron Lett.* **2014**, *55*, 5836-5840.

(35) Kimura, M.; Moriyama, M.; Kishimoto, K.; Yoshio, M.; Kato, T. *Liq. Cryst.* **2007**, *34*, 107-112.

(36) Zhao, K. Q.; Bai, Y. F.; Hu, P.; Wang, B. Q.; Shimizu, Y. *Mol. Cryst. Liq. Cryst.* **2009**, *509*, 77/[819]-88/[830].

(37) Pal, S. K.; Kumar, S. *Tetrahedron Lett.* **2006**, *47*, 8993-8997.

(38) Kumar, S.; Gupta, S. K. *Tetrahedron Lett.* **2010**, *51*, 5459-5462.

(39) Gupta, S. K.; Kumar, S. *Liq. Cryst.* **2012**, *39*, 1443-1449.

(40) Hutter, J. L.; Bechhoefer, J. *J. Cryst. Growth* **2000**, *217*, 332-343.

(41) Prasad, S. K.; Rao, D. S. S.; Chandrasekhar, S.; Kumar, S. *Mol. Cryst. Liq. Cryst.* **2003,** *396*, 121-139.

(42) Kumar, S. *Chem. Soc. Rev*. **2006**, *35*, 83-109.

(43) Wöhrle, T.; Wurzbach, I.; Kirres, J.; Kostidou, A.; Kapernaum, N.; Litterscheidt, J.; Haenle, J. C.; Staffeld, P.; Baro, A.; Giesselmann, F.; Laschat, S. *Chem. Rev*. **2016**, *116*, 1139-1241.

(44) Kumar, S. in Chemistry Of Discotic Liquid Crystals: From Monomers to Polymers, CRS Press, Taylor & Francis Group: Boca Raton, **2011**.

(45) Lu, M.; Yang, K. H. *Jpn. J. Appl. Phys*. **2000**, *36*, L412-L415.

(46) Mori, H.; Itoh, Y.; Nishuira, Y.; Nakamura, T.; Shinagawa, Y. *Jpn. J. Appl. Phys*. **1997**, *36*, 143-147.

(47) Phillips, T. J.; Jones, J. C.; McDonnell, D. G. *Liq. Cryst*. **1993**, *15*, 203-215.

(48) Hindmarsh, P.; Watson, M. J.; Hird, M.; Goodby, J. W. *J. Mater. Chem*. **1995**, *5*, 2111-2123.

(49) Praefcke, K.; Kohne, B.; Singer, D. *Angew. Chem. Int. Ed. Engl*. **1990**, *29*, 177-179.

(50) Destrade, C.; Gasparoux, H.; Babeau, A.; Tinh, N. H. *Mol. Cryst. Liq. Cryst*. **1981**, *67*, 37-47.

(51) Lee, W. K.; Wintner, B. A.; Fontes, E.; Heiney, P. A.; Ohba, M.; Haseltine, J. N.; Smith, A. B. *Liq. Cryst*. **1989**, *4*, 87-102.

(52) Mamlock, L.; Malthete, J.; Tinh, N. H.; Destrade, C.; Levelut, A. M. *J. Phys. Lett*. **1982**, *43*, 641-647.

(53) Praefcke, K.; Kohne, B.; Gutbier, K.; Johnen, N.; Singer, D. *Liq. Cryst*. **1989**, *5*, 233-249.

(54) Imrie, C. T.; Lu, Z.; Picken, S. J.; Yildirim, Z. *Chem. Commun*. **2007**, 1245-1247.

(55) Kim, B. G.; Kim, S.; Park, S. Y. *Tetrahedron Lett*. **2001**, *42*, 2697-2699.

(56) Kumar, S.; Varshney, S. K. *Org. Lett*. **2002**, *4*, 157-159.

(57) Kumar, S.; Varshney, S. K. *Liq. Cryst*. **2001**, *28*, 161-163.

(58) Zhang, L.; Hughes, D. L.; Cammidge, A. N. *J. Org. Chem*. **2012**, *77*, 4288-4297.

(59) Zhang, L.; Gopee, H.; Hughes, D. L.; Cammidge, A. N. *Chem. Commun*. **2010**, *46*, 4255-4257.

(60) Lee, J. H.; Jang, I.; Hwang, S. H.; Lee, S. J.; Yoo, S. H.; Jho, J. Y. *Liq. Cryst.* **2012**, *39*, 973–981.

(61) Lee, J. H.; Han, M.-J.; Hwang, S. H.; Jang, I.; Lee, S. J.; Yoo, S. H.; Jho, J. Y.; Park, S.-Y. *Tetrahedron Lett.* **2005**, *46*, 7143–7146.

(62) Bisoyi, H. K.; Kumar, S. *Chem. Soc. Rev*. **2010**, *39*, 264–285.

(63) Kumar, S.; Varshney, S. K. *Angew. Chem. Int. Ed*. **2000**, *112*, 3270–3272.

(64) Kumar, S.; Varshney, S. K.; Chauhan, D. *Mol. Cryst. Liq. Cryst*. **2003**, *396*, 241–250.

(65) Varshney, S. K.; Prasad, V.; Takezoe, H. *Liq. Cryst*. **2011**, *38*, 53–60.

(66) Kohmoto, S.; Mori, E.; Kishikawa, K. *J. Am. Chem. Soc*. **2007**, *129*, 13364–13365.

(67) Chien, S. C.; Chen, H. H.; Chen, H. C.; Yang, Y. L.; Hsu, H. F.; Shih, T. L.; Lee, J. J. *Adv. Funct. Mater*. **2007**, *17*, 1896–1902.

(68) Chen, H.-H.; Lin, H.-A.; Chien, S.-C.; Wang, T.-H.; Hsu, H.-F.; Shih, T.-L.; Wu, C.; *J. Mater. Chem.* **2012**, *22*, 12718–12722.

(69) Gupta, M.; Gupta, S. P.; Rasna, M. V.; Adhikari, D.; Dhara, S.; Pal, S. K. *Chem. commun.* **2017**, *53*, 3014-3017.

(70) Gupta, M.; Gupta, S. P.; Mohapatra, S. S.; Dhara, S.; Pal, S. K. *Chem. Eur. J.* **2017**, *23*, 10626-10631.

(71) Praefcke, K.; Kohne, B.; Singer, D.; Demus, D.; Pelzl, G.; Diele, S. *Liq. Cryst*. **1990**, *7*, 589–594.

(72) Praefcke, K.; Kohne, B.; Gundogan, B.; Singer, D.; Demus, D.; Diele, S.; Pelzl, G.; Bakowsky, U. *Mol. Cryst. Liq. Cryst*. **1991**, *198*, 393–405.

(73) Gupta, M.; Pal, S. K. *Langmuir* **2016**, *32*, 1120–1126.

(74) Gupta, M.; Agarwal, N.; Arora, A.; Kumar, S.; Kumar, B.; Sheet, G.; Pal, S. K. *RSC Adv*. **2014**, *4*, 41371-41377.

(75) Gupta, M.; Bala, I.; Pal, S. K. *Tetrahedron Lett*. **2014**, *55*, 5836–5840.

(76) Gupta, M.; Pal, S. K. *Liq. Cryst*. **2015**, *42*, 1250–1256.

Appendix III

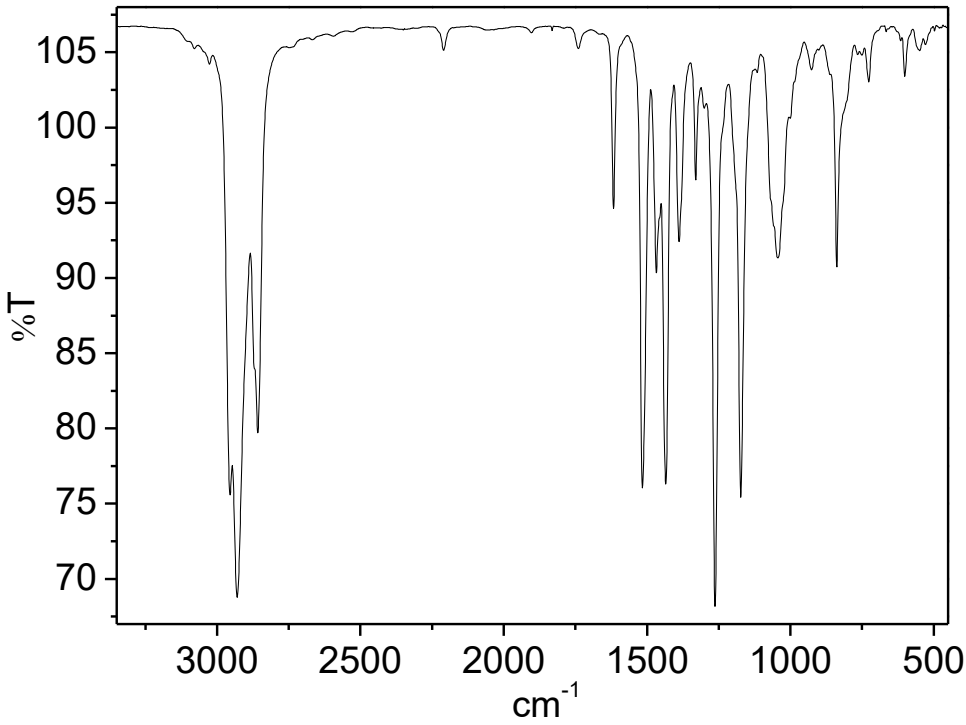

Figure A1 FT-IR spectrum of compound **8a.** Compound **8b** and **8c** shows similar spectra**.**

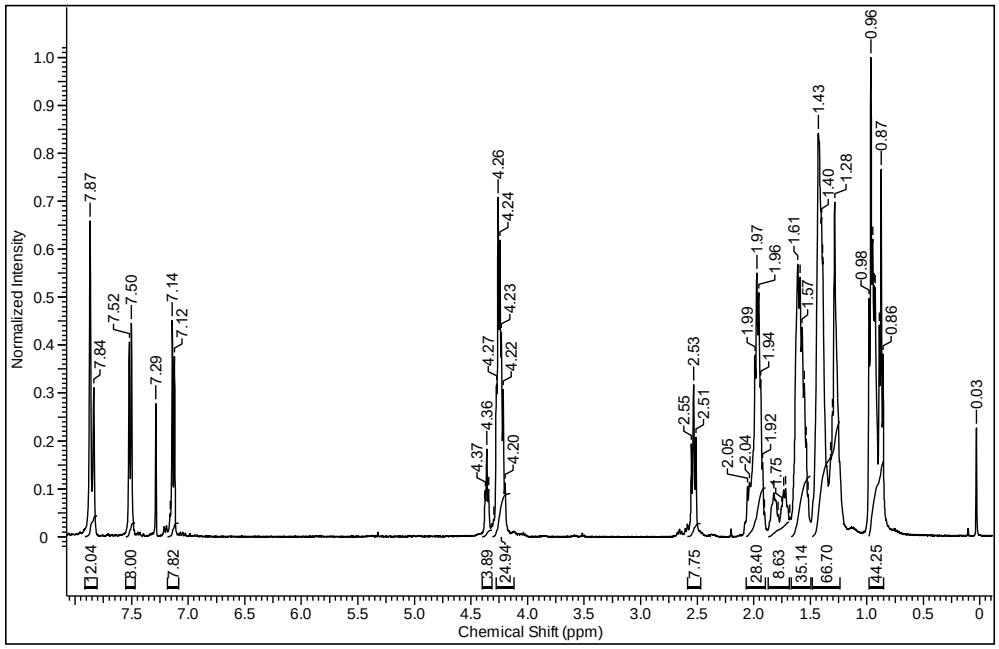

Figure A2 ^{1}H NMR spectrum of compound **8a.**

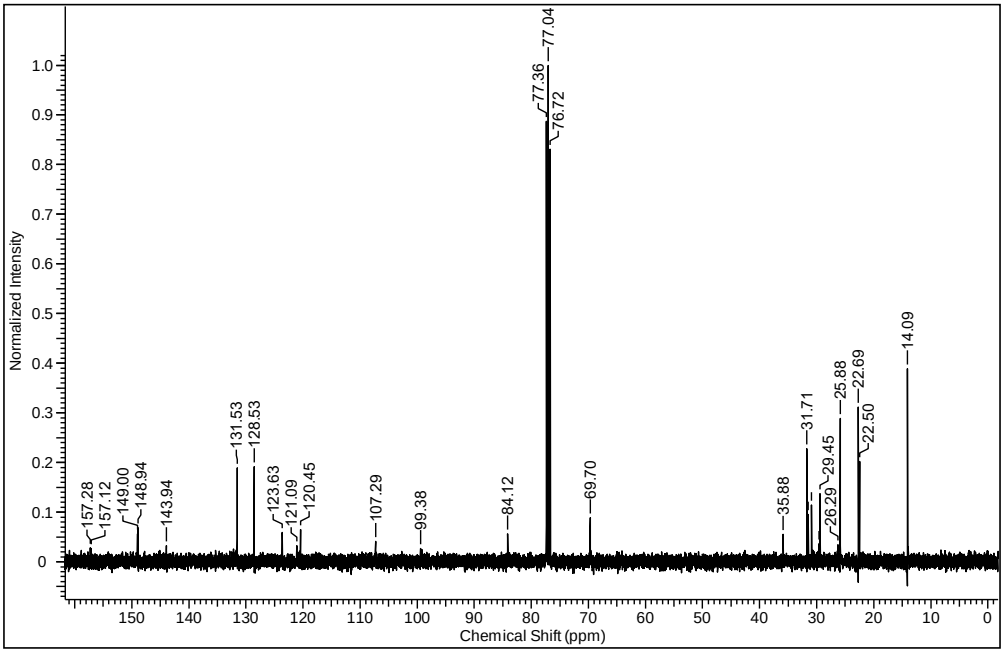

Figure A3 ^{13}C NMR spectrum of compound **8a.**

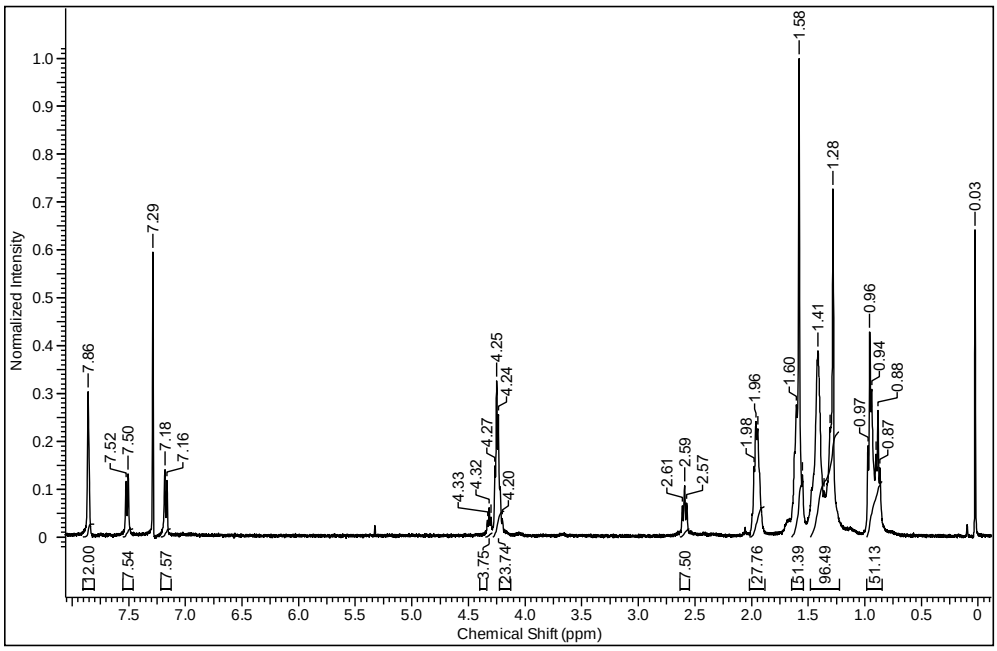

Figure A4 ^{1}H NMR spectrum of compound **8b.**

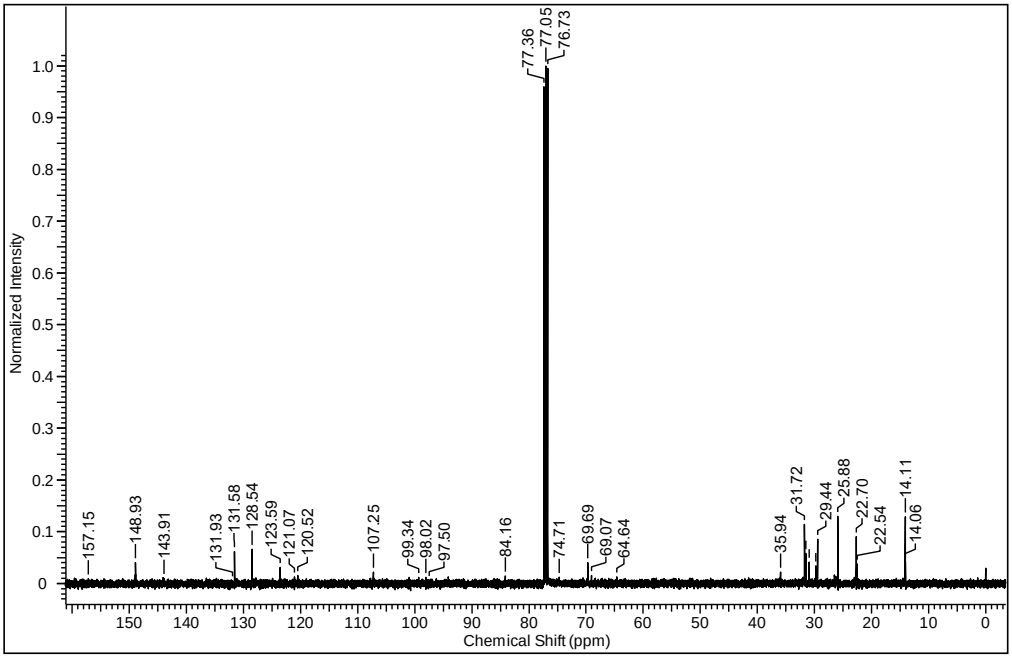

Figure A5 ^{13}C NMR spectrum of compound **8b.**

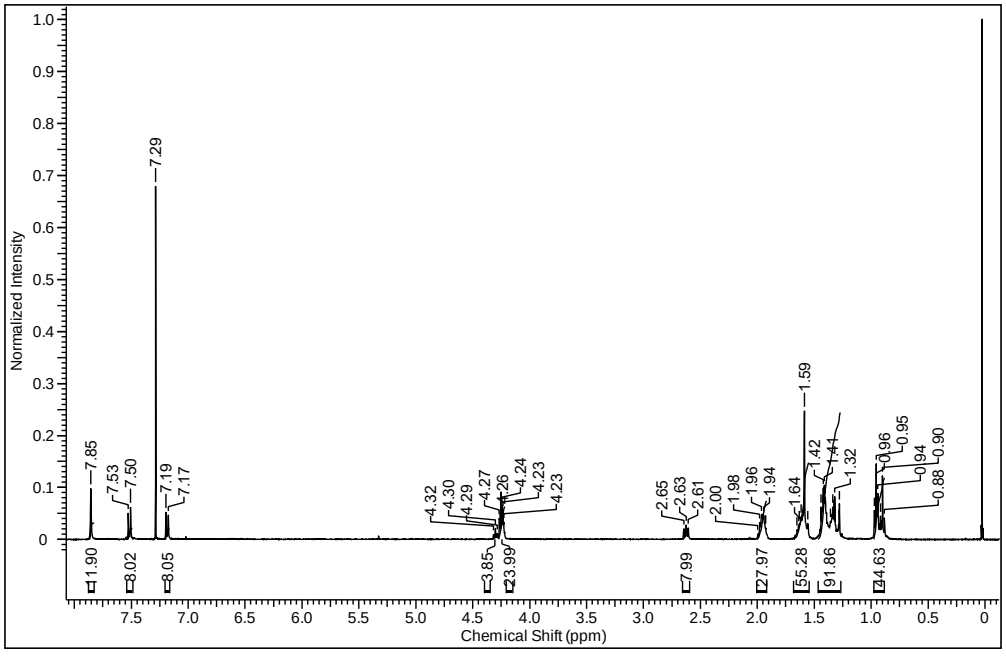

Figure A6 ^{1}H NMR spectrum of compound **8c.**

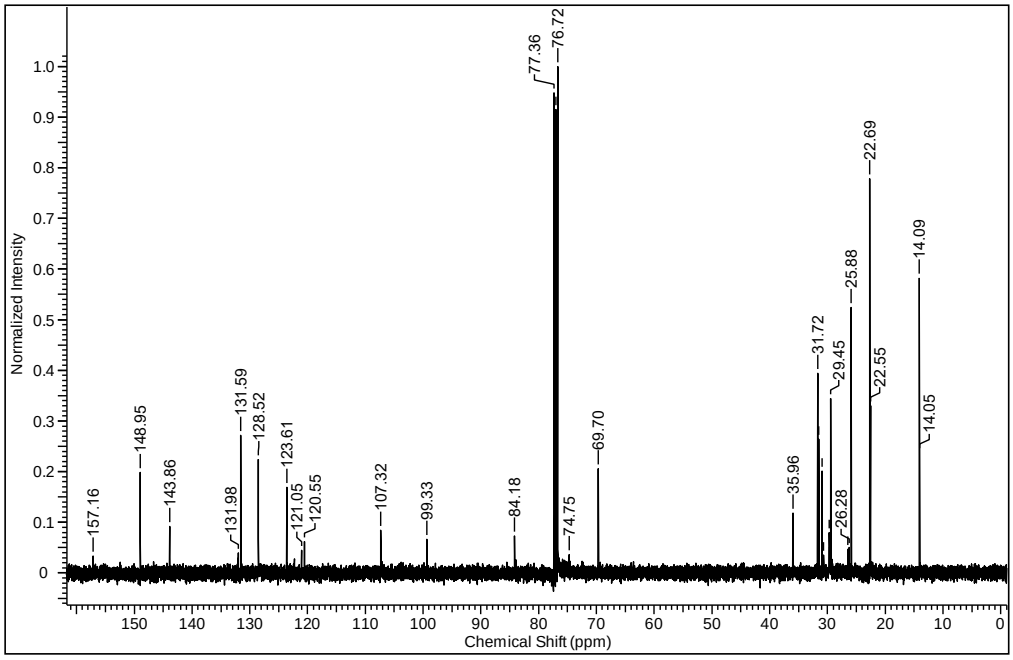

Figure A7 ^{13}C NMR spectrum of compound **8c.**

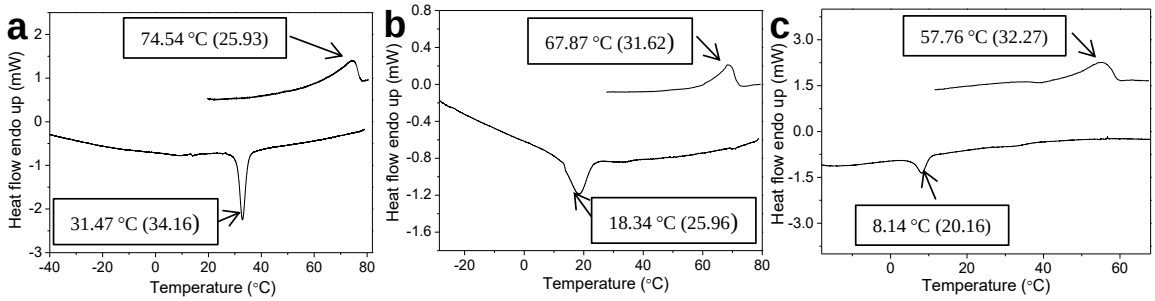

Figure A8 DSC thermograms of compound (a) **8a**, (b) **8b** & (c) **8c** on heating and cooling cycles with a scan rate of 5 °C/min. Inset above the peaks shows the peak transition temperature with latent heat values in kJ/mol (in parentheses).

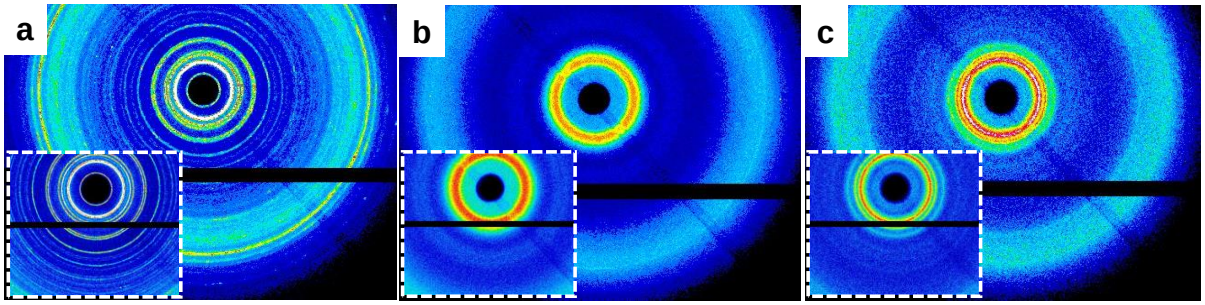

Figure A9 2D diffraction patterns obtained for (a) **8a** at 50 °C, (b) **8b** at 42 ° and (c) **8c** at 30 °C on cooling from the isotropic (insets show the respective 2D diffraction pattern in small-angle region).

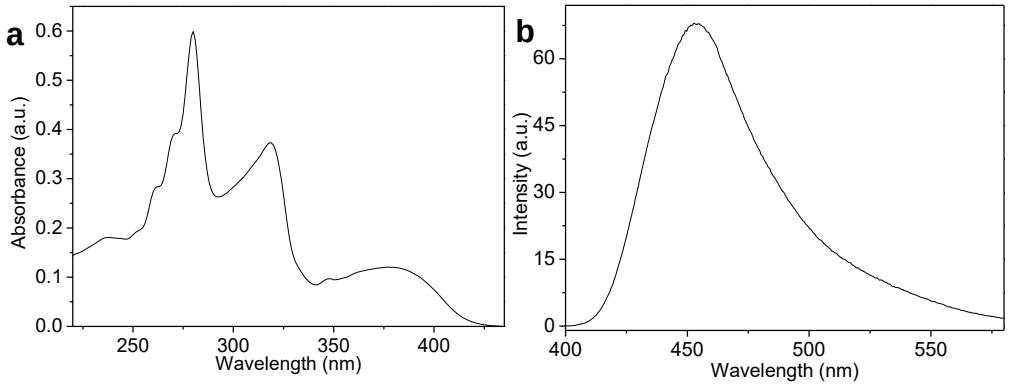

Figure A10 (a) UV-vis absorption & (b) emission spectra of compound **8a** in solution (5 μM in dichloromethane)

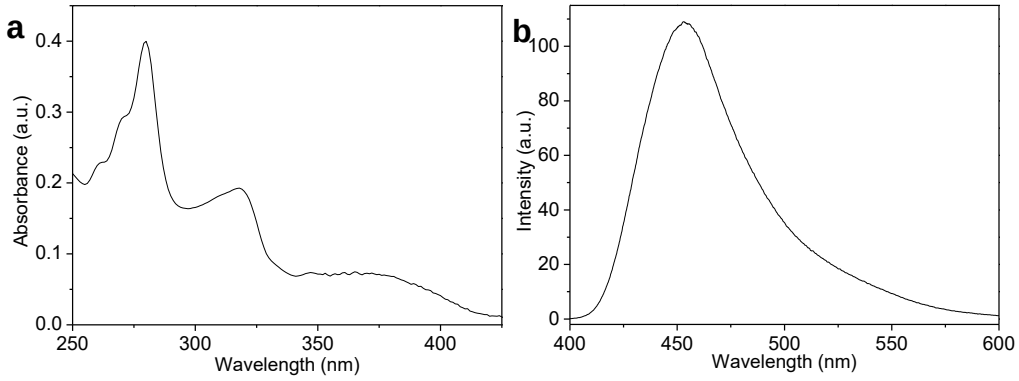

Figure A11 (a) UV-vis absorption & (b) emission spectra of compound **8b** in solution (5 μM in dichloromethane)

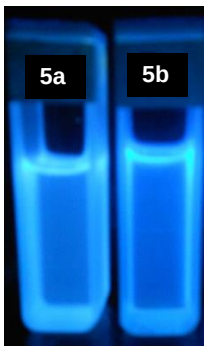

Figure A12 Picture of compound **8a** & **8b** in solution (5 μM in dichloromethane) under UV illumination of wavelength 365 nm showing blue light emission.

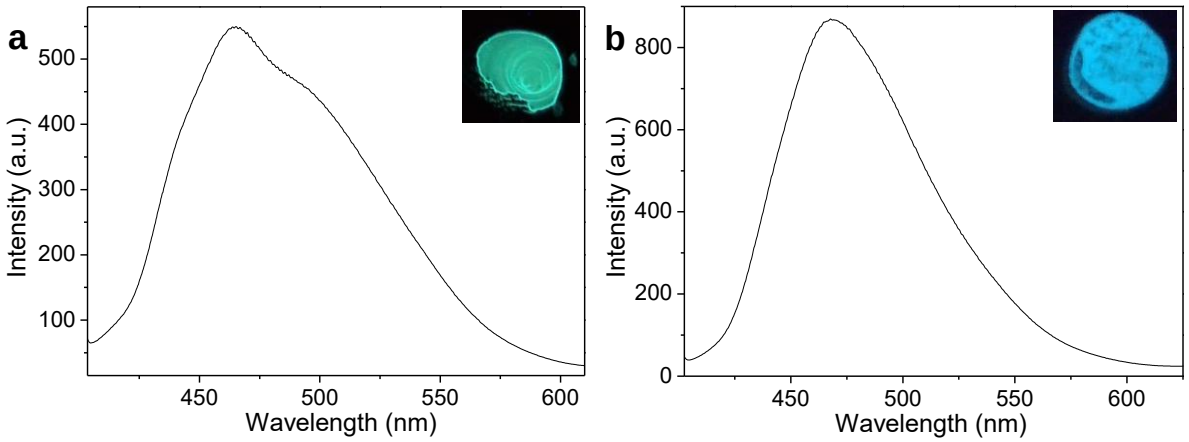

Figure A13 Emission spectra of thin films of compound (a) **8a** and (b) **8b** respectively. The inset picture in both cases shows photoluminescence from the thin films under UV illumination of wavelength 365 nm.

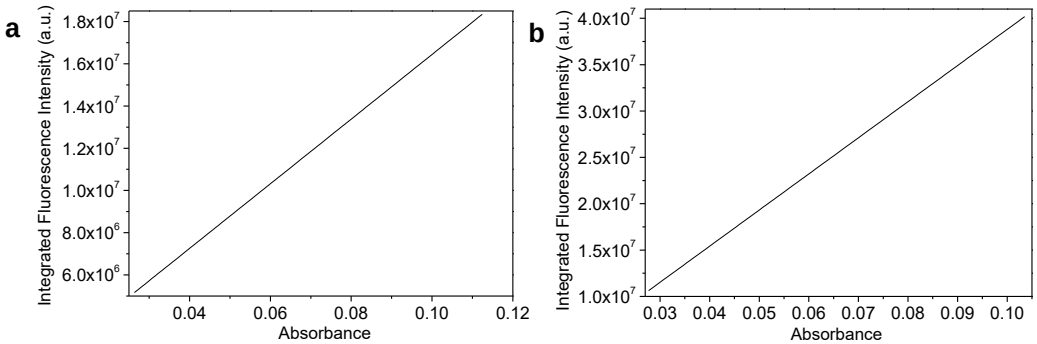

Figure A14 Plots of integrated fluorescence intensity vs absorbance of (a) compound **8c** and (b) quinine sulphate in 0.1 N H_2SO_4.

The quantum yield was calculated from the relation:
$Q_S = Q_R \times (m_S/m_R) \times (n_S/n_R)^2$
Here, Q_R(quantum yield) = 0.54; m_S (slope) = 1.53×10^8 ; $m_R = 3.89 \times 10^8$; n_S (refractive index) = 1.42 and n_R = 1.33.
Therefoe, after substituting above values, Q_S = 0.24.

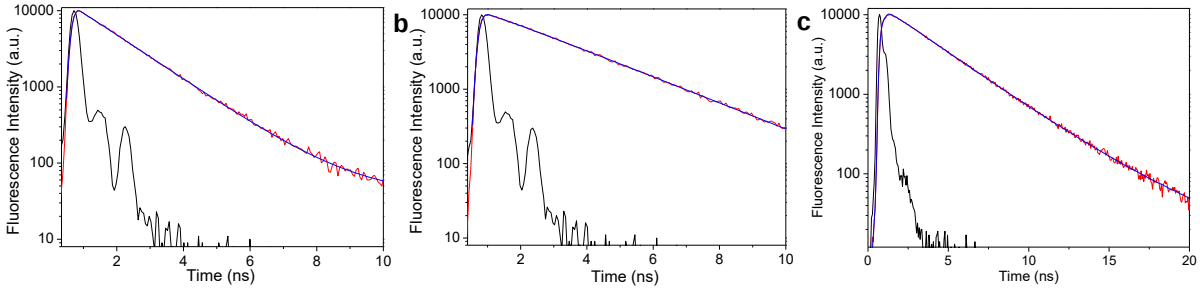

Figure A15 Fluorescence decay spectra of compounds a) **8a**, b) **8b** and c) **8c** respectively.

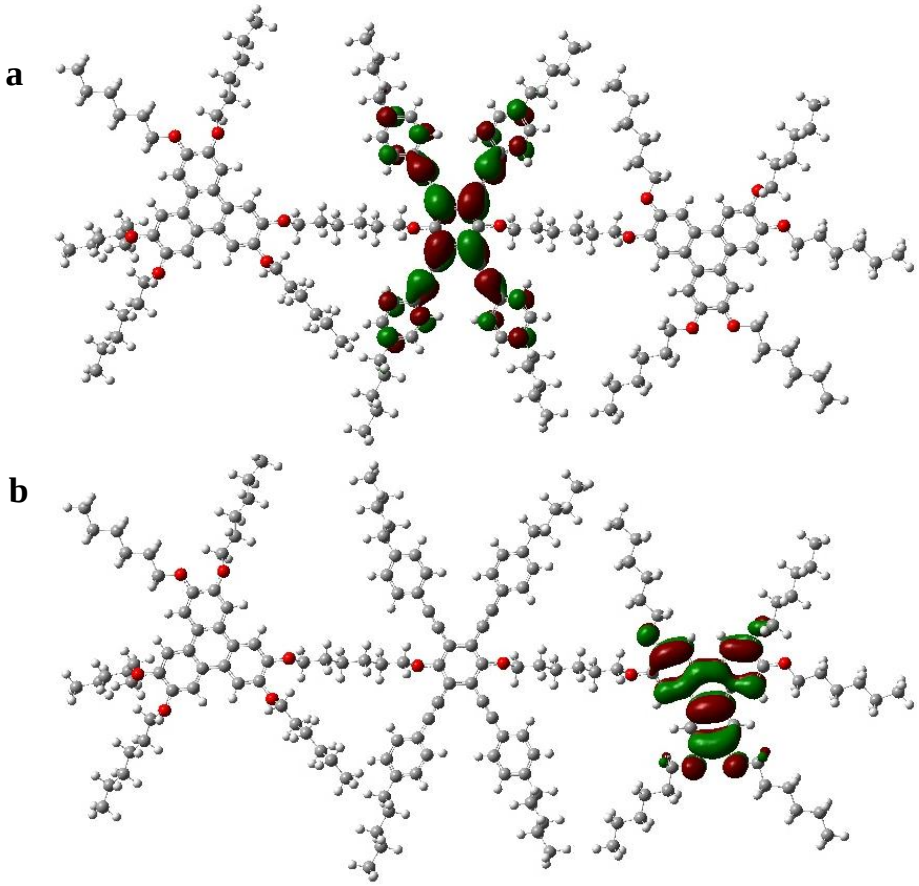

Figure A16 Figure showing LUMO (a) and HOMO (b) in the backbone of compound **8a** synthesized in the study, as determined from the DFT method.

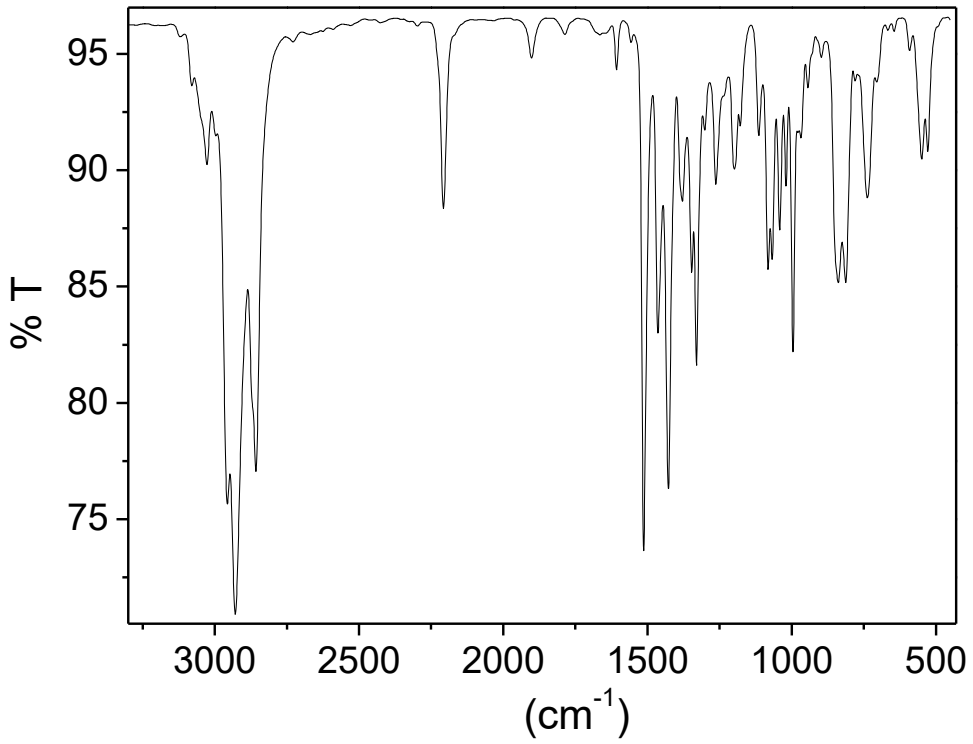

Figure A17 FT-IR spectrum of compound **13a.** Compound **13b** and **13c** shows similar spectra**.**

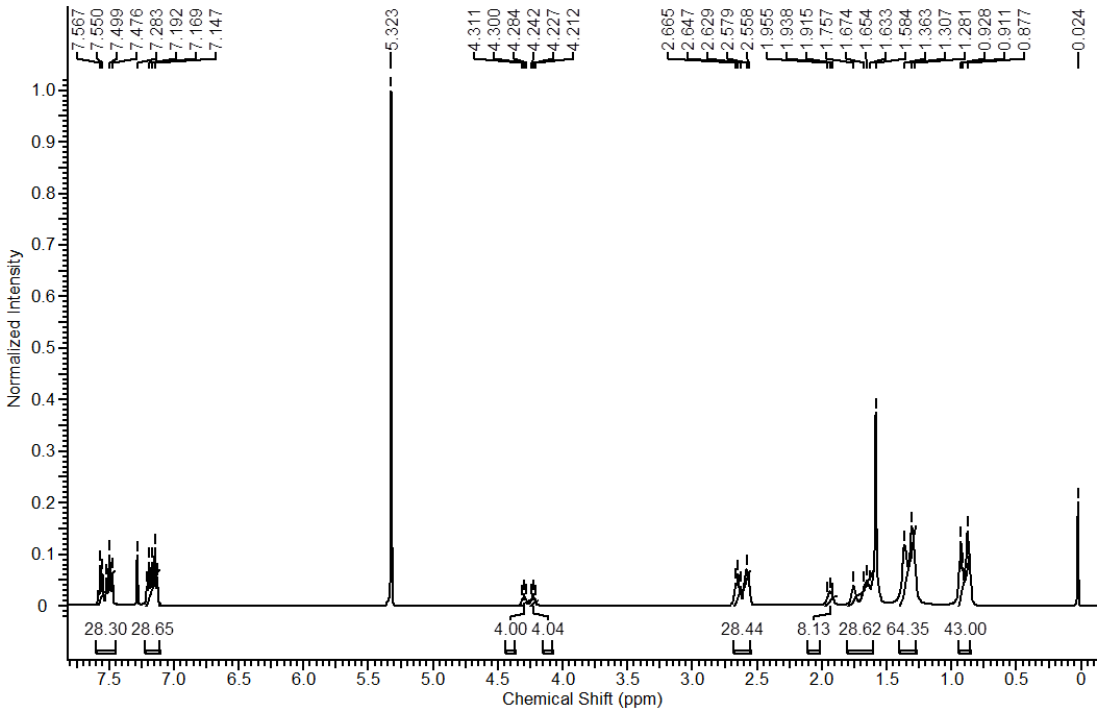

Figure A18 ^{1}H NMR spectrum of compound **13a.**

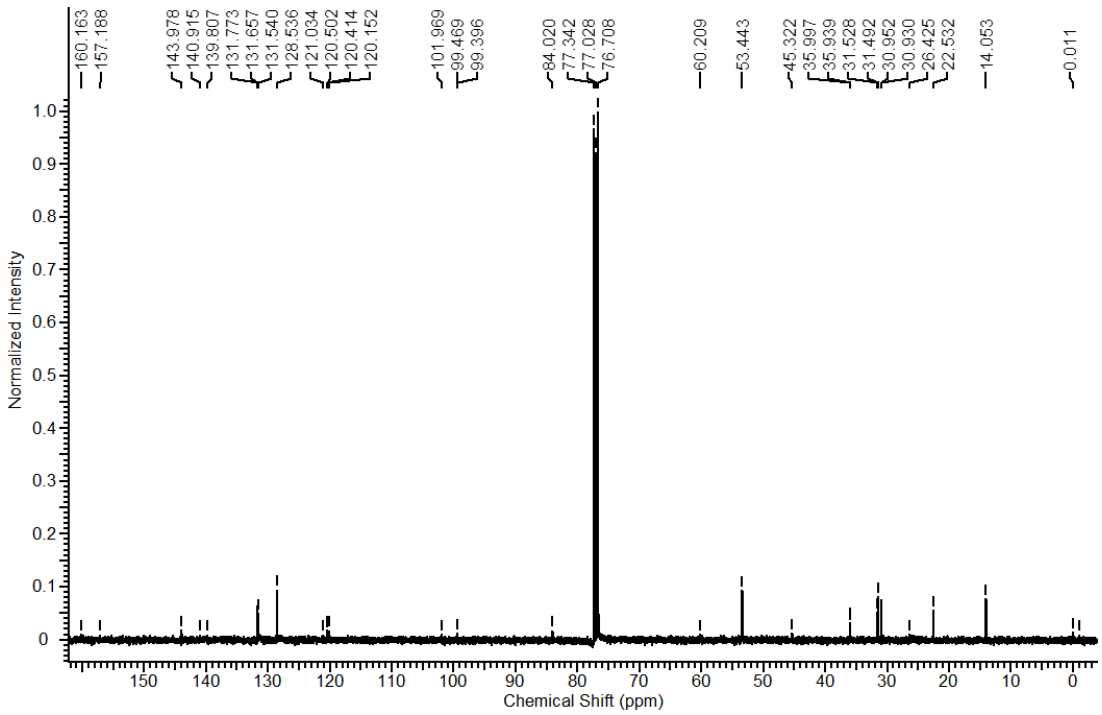

Figure A19 ^{13}C NMR spectrum of compound **13a.**

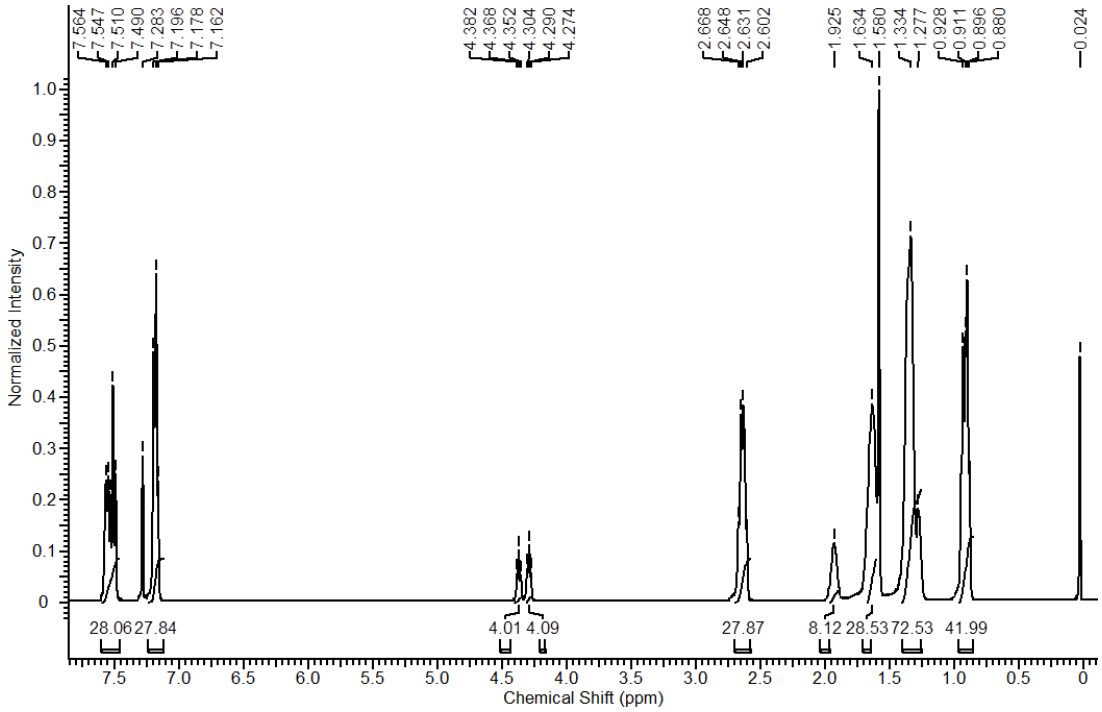

Figure A20 ^{1}H NMR spectrum of compound **13b.**

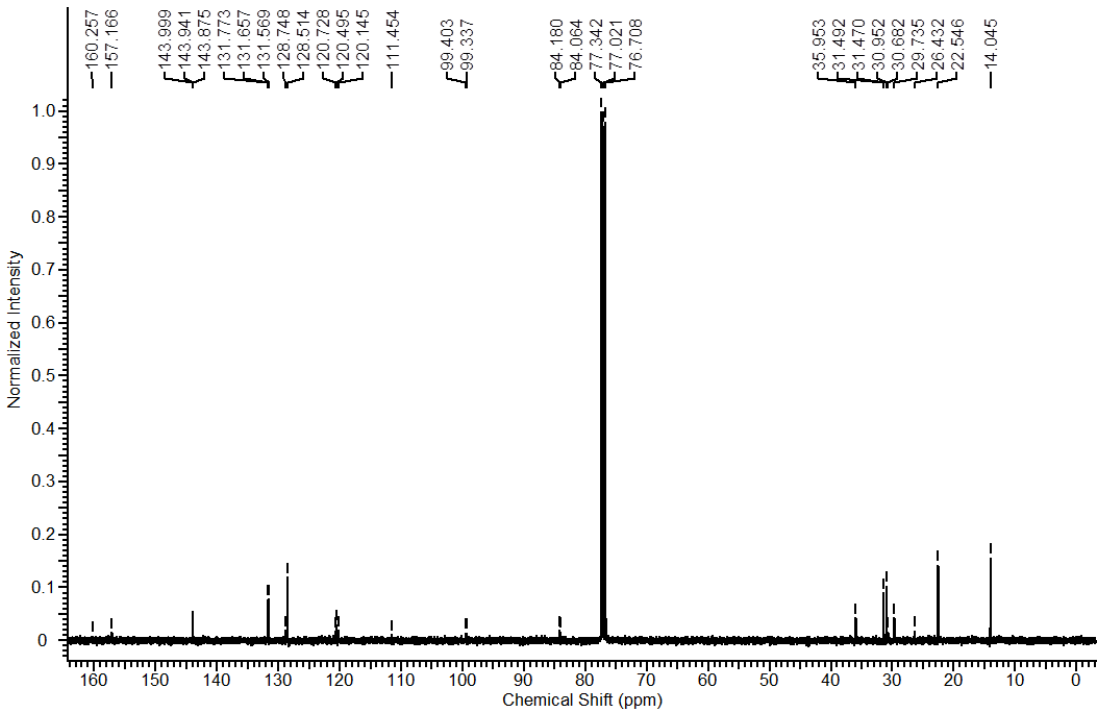

Figure A21 ^{13}C NMR spectrum of compound **13b.**

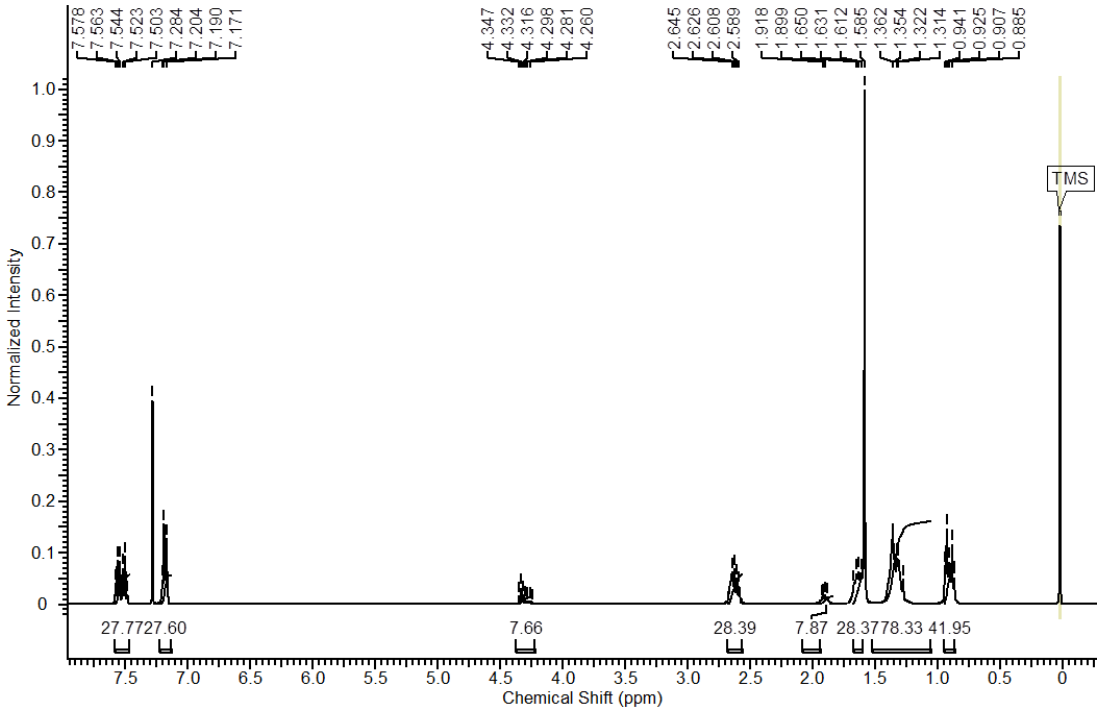

Figure A22 ^{1}H NMR spectrum of compound **13c.**

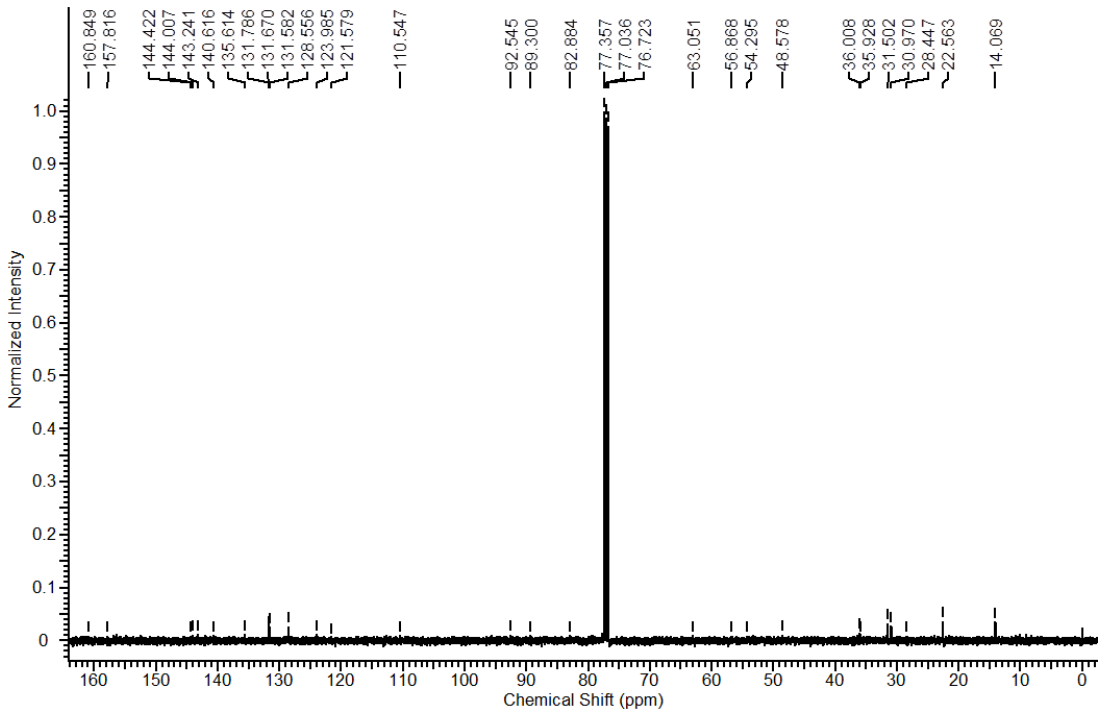

Figure A23 ^{13}C NMR spectrum of compound **13c.**

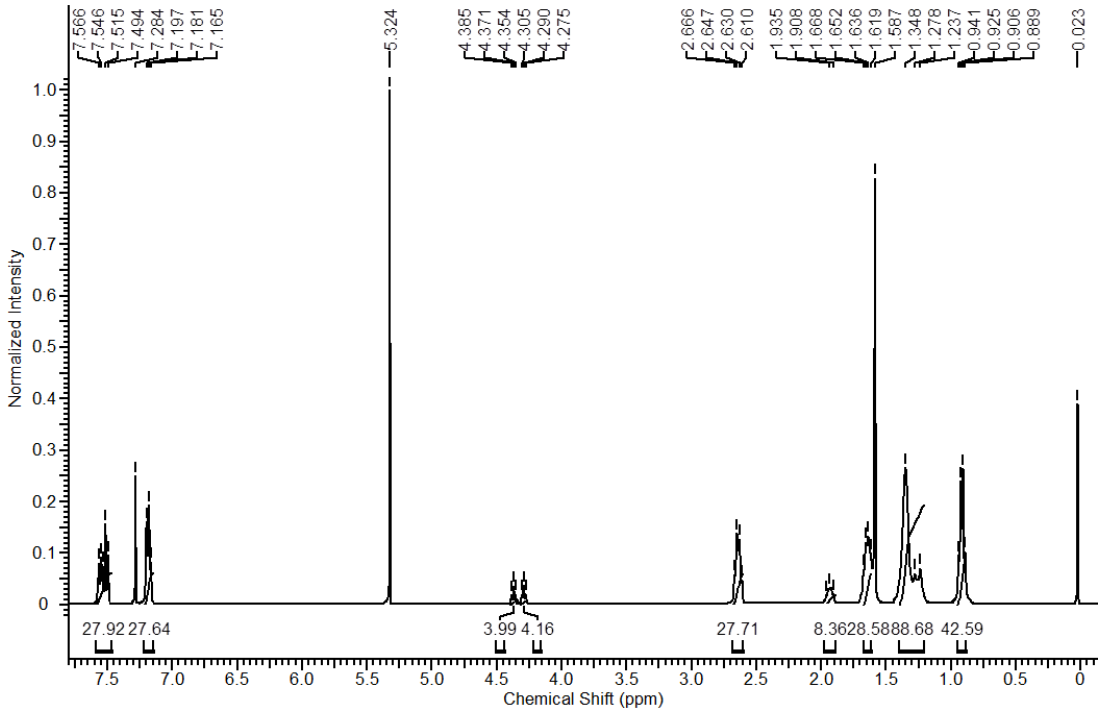

Figure A24 ^{1}H NMR spectrum of compound **13d.**

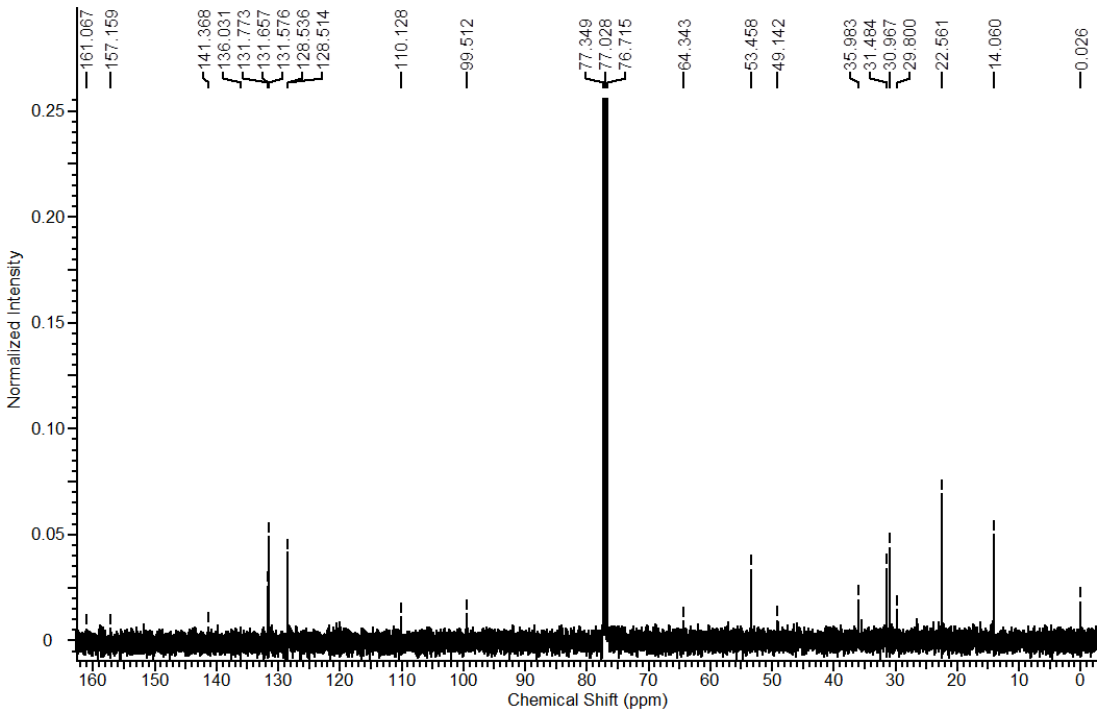

Figure A25 ^{13}C NMR spectrum of compound **13d.**

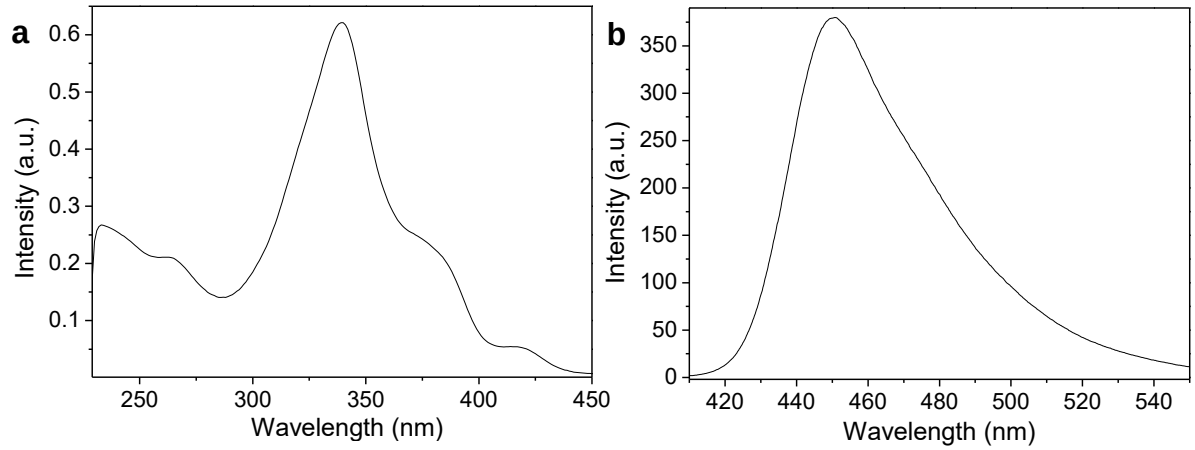

Figure A26 (a) UV-vis absorption & (b) emission spectra of compound **13d** in solution (5 μM in dichloromethane).

Chapter 5

New design strategies towards the synthesis of room-temperature discotic nematic liquid crystals

PART A

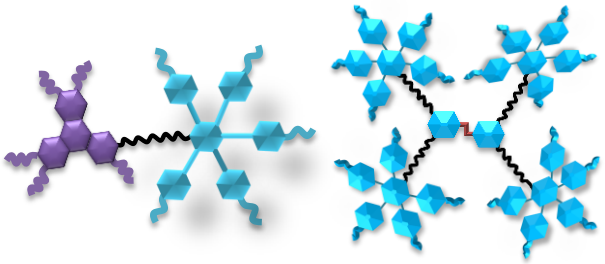

Design -I **Design -II**

In this section, we have described various approaches to obtain room-temperature discotic nematic (N_D) phase. The first approach is based-on the design of a room-temperature N_D LC dimer consisting of a triphenylene and a pentaalkynylbenzene unit linked via flexible alkyl spacers. The formation of the N_D phase is realized most likely through folding of the dimeric molecule that prevent stacking between the triphenylene units. The second approach is based-on the design and synthesis of three room-temperature oligomeric N_D LCs consisting of an azobenzene core attached to which are four pentaalkynylbenzene units through flexible alkyl spacers. The presence of a short azo linking group provides more disorder in the system, thereby reducing the packing efficiency among the pentaalkynylbenzene units and resulting into the formation of a room-temperature N_D phase over a wide temperature range.

PART B

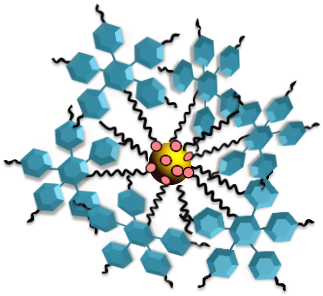

This section describes the synthesis of gold nano-particles (GNPs) coated with pentaalkynylbenzene units which displayed N_D phase even at room-temperature. These LC GNPs are very interesting materials as inherent property of LCs to form mesophases due to their shape and polarizability anisotropy also influences the self-assembly of GNPs whereas the GNPs affects the electro-optic and alignment properties of LCs in devices which leads to collective advantages for both the components. Thus, they are promising materials which exhibit the property of optical compensation (due to nematic discotic pentaalkynylbenzene units) with enhanced dielectric response (because of GNPs).

5.1 Part A: Design, synthesis and characterization of room-temperature discotic nematic liquid crystals by employing pentaalkynylbenzene units

5.1.1 Introduction

Discotic liquid crystals (LCs) formed mainly by disc-shaped molecules generally give rise to columnar mesophase because of strong π-π interaction among the aromatic cores.[1-3] In contrast, disc shaped molecules showing nematic (N_D) phase where the discs have only long-range orientational order are rare, but are of particular importance in many display devices. However, they have sustained a specific interest since the commercialization of optical compensation film based on polymerized nematic discogens for enlarged viewing angle in LC displays because of their negative optical anisotropy.[4-5] Unfortunately, among the limited number of discotic nematogens, most are often accompanied by high clearing temperatures and narrow mesophase ranges.[6] However, for implementation in devices, N_D phase at room-temperature and over a wide temperature range is vital.

A detailed literature survey reveals that hexa- and pentaalkynylbenzene (PA) derivatives have been the most investigated system among various N_D LCs.[6] In these cases, the stacking of discs in columns is inhibited by the rotational freedom provided by the ethynyl linkers. Subsequently, few other derivatives (**1-3**) based on triphenylene (TP), truxene, thiotruxene, naphthalene *etc*. have also been reported to show N_D phase.[7-14]

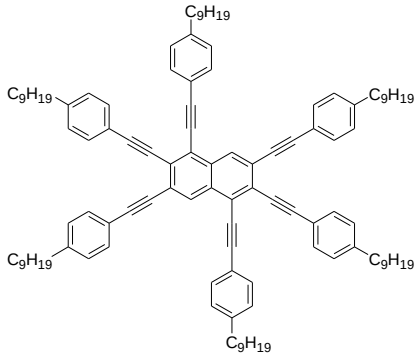

1

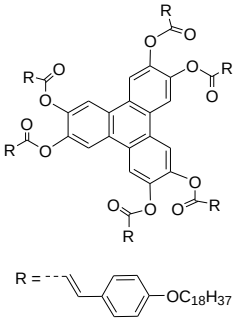

2

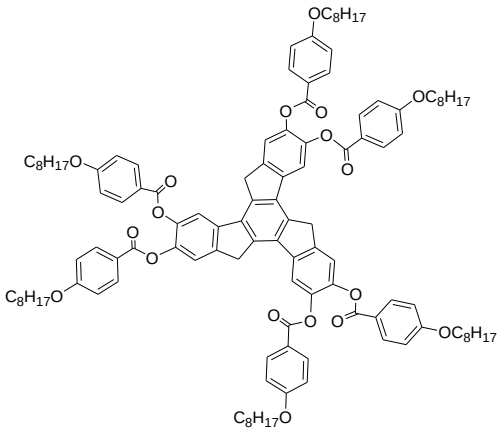

3

Star-shaped 1, 3, 5-trisalkynylbenzene **4** and discotic twins (e.g. **5**) containing two TP units linked through diacetylene spacer or thiophene units were also found to display N_D mesophase.[15-19]

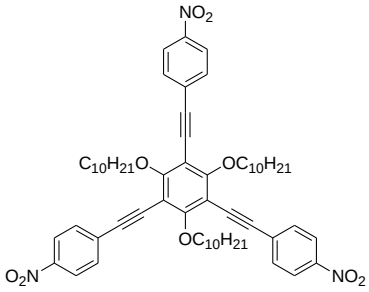

4

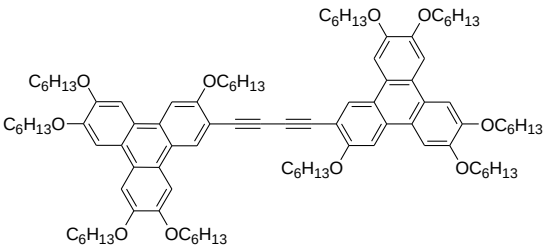

5

N_D phase has also been obtained through hydrogen bonding between phenol and pyridine moieties as well as between phloroglucinol and alkoxystillbazole moieties. Recently, hydrogen bonding has also been employed for the preparation of N_D LCs. For example, Lee *et al*. have reported discotic nematogens through H-bonding between phenol and pyridine moieties as well as between phloroglucinol and alkoxystillbazole moieties.[20, 21] However, in all of the above cases, N_D phase appears at higher temperature that limits their widespread use in applications.

Till date, only fewer approaches have been reported in the literature for the formation of room-temperature N_D phase. Kumar *et al*. reported first example of room temperature N_D mesogen by using pentaalkynyl benzene derivative **6** with branched alkyl spacers.[22-24] In addition to that, the discotic triphenylene core **8** possessing poly(ethylene oxide) side chains also possess a room-temperature N_D phase.[25]

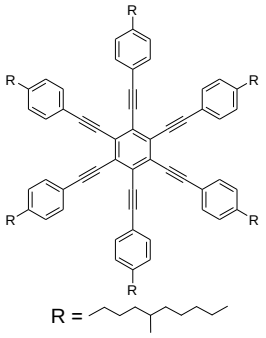

6

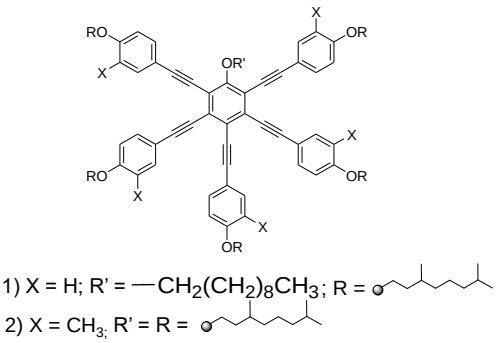

7

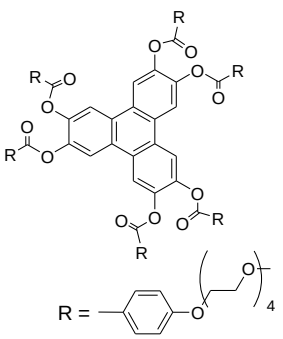

8

Room-temperature nematic discogens were also obtained by Lee and co-workers by replacing one side-arm of the discotic multialkynylbenzene **9** with a trisalkoxy sidearm.[26] They further showed that introduction of an attraction-enhancing unit in the lateral side arm of hexa(phenylethynyl)benzene **10** also leads to N_D phase at room temperature.[27]

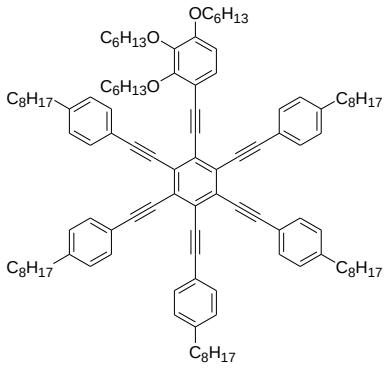

9

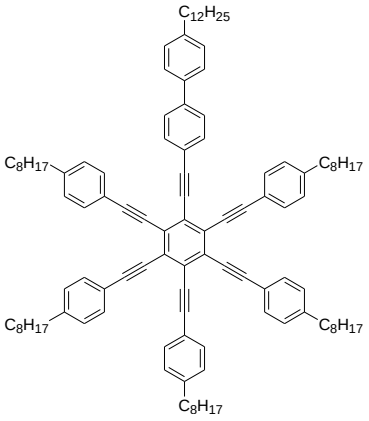

10

5.1.2 Objective

Considering the importance of N_D phases for display applications, new design strategies are required for the room-temperature discotic nematogens. In this study, we have designed two new compounds employing PA units which can show room-temperature N_D phases. The first design for the realization of room-temperature N_D phase is based-on folding of two disc-like cores consisting of a TP & PA unit linked via flexible alkyl spacers (compound **11**).

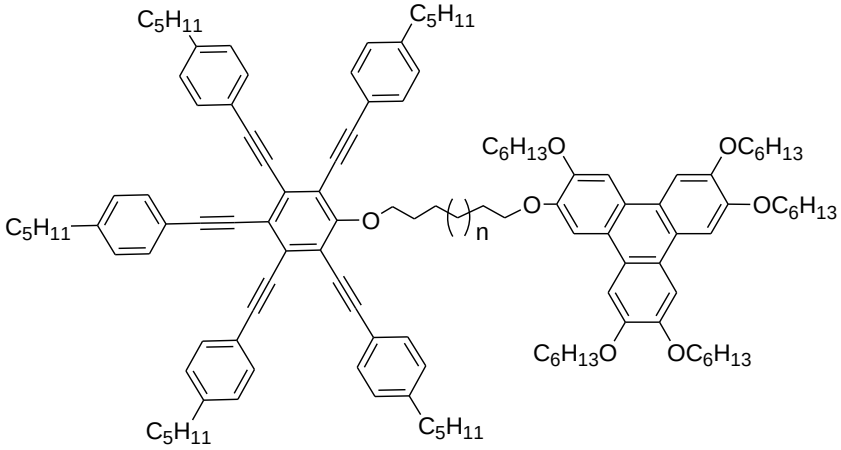

11

(*n* = 1, 3, 5, 7)

The earlier examples of symmetric dimers based on PA displayed N_D phase at higher temperature.[28] Here, the incompatibility of the two discs in the folded mesogen can lead to improper packing resulting into the formation of a room-temperature N_D phase. We have demonstrated earlier that linking a PA unit with a TP core through flexible alkyl spacer containing a short rigid ester group in centre leads to columnar mesophase at ambient temperature.[29] In contrast, further increasing the flexibility of spacer, i.e., by introducing only alkyl chains can lead to the desired mesophase.

The second design **12** is based-on four PA units connected to an azobenzene core *via* flexible alkyl spacers. We hypothesized that the presence of short rigid azo group in these oligomers can lead to a system in which PA units will be randomly oriented with respect to each other. Consequently, these oligomeric units could be disordered enough which will prevent efficient packing of the molecules and thus, may lead to the realization of a room temperature N_D phase.

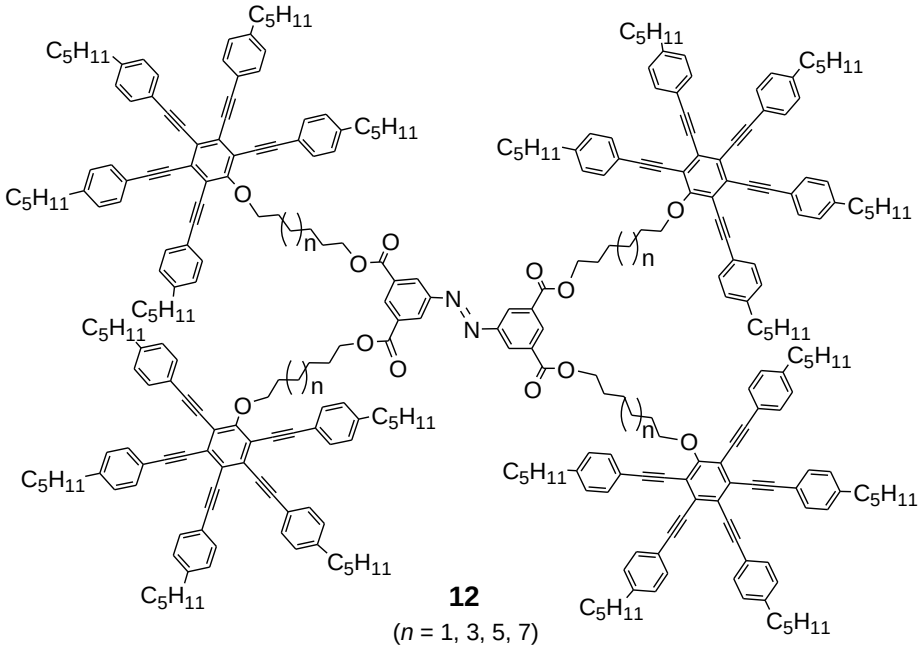

12
(*n* = 1, 3, 5, 7)

This section is further divided into two sections. The first section deals with the synthesis and characterization of the dimeric mesogens based on first design *i.e*. **11**. The second section deals with the next design strategy *i.e*. oligomeric mesogens **12**.

5.1.3 Design-I

5.1.3.1 Synthesis and characterization

The target compounds (**11a-d**) were synthesized by the route as depicted in scheme 5.1. The synthesis of intermediate compounds **14**, **15**, **17** and **18** has been discussed elsewhere.[29-31] Compounds **11a-d** were prepared by reacting the pentayne **15** and monohydroxy triphenylene **18** in presence of cesium carbonate and potassium iodide using butanone as solvent under reflux condition (see experimental section for details).

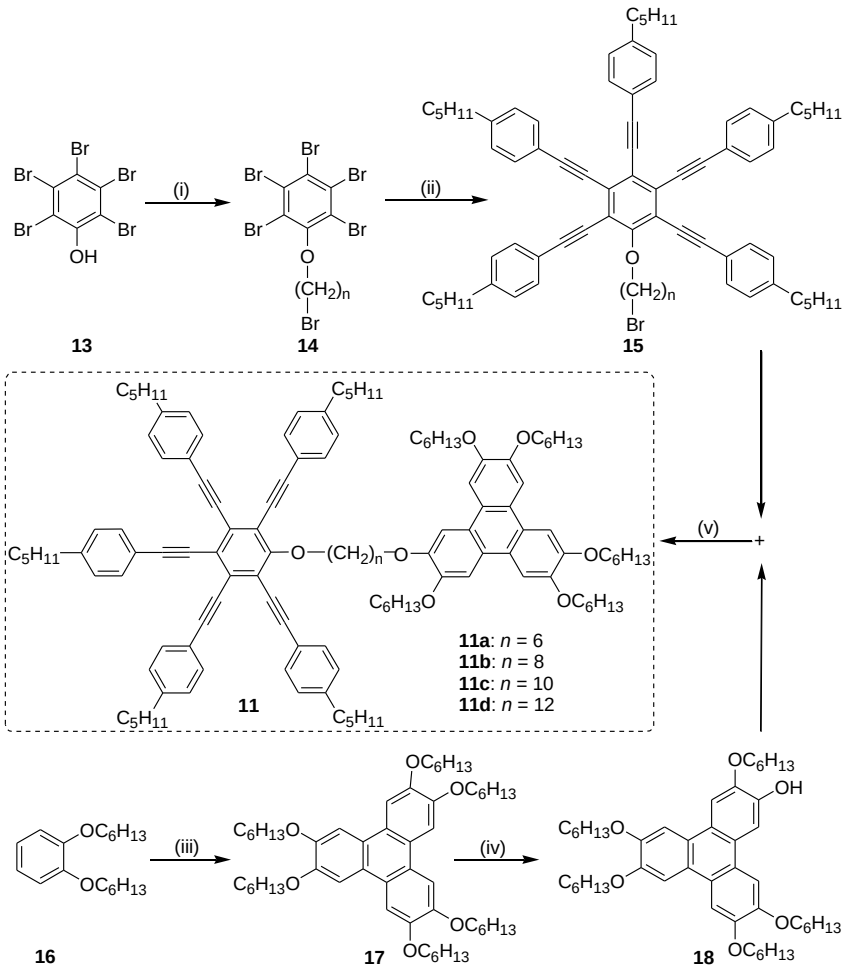

Scheme 5.1 Synthesis of the target compounds **11**. Reagents and Conditions: (i) Dibromoalkane, K_2CO_3, KI, butanone, 80 °C, 18 h, 89%; (ii) $Pd(PPh_3)_2Cl_2$, 4-pentylphenylacetylene, PPh_3, CuI, Et_3N,100 °C, 15h, 82%; (iii)$FeCl_3$, CH_2Cl_2, H_2SO_4, RT, 1 h, 70%; (iv) Cat-B-Br, CH_2Cl_2, RT, 48 h, 40%; (v) Cs_2CO_3, KI, butanone, 80 °C, 18 h, 85%.

All the compounds were characterised by ^{1}H & ^{13}C NMR, IR, UV-vis and mass spectrometry (appendix IV, Figure A1-A9). The thermal behaviour of synthesized compounds was investigated by differential scanning calorimetry (DSC) and the changes in their physical properties were analysed by polarized optical microscopy (POM) and X-ray scattering studies. All compounds exhibited light blue fluorescence in solution. The representative absorption spectrum obtained for **11b** showed the maxima centred at 264, 280, 338 and 416 nm with two shoulder peaks at 237 & 380 nm (appendix IV, Figure A10). Emission spectra of all compounds were recorded by exciting the solutions of these compounds at their absorption maxima. The spectra showed blue light emission with the maxima centred at 452 nm for all fluorophores. The representative emission spectrum for compound **11b** is also shown in Figure A10, appendix IV.

5.1.3.2 Thermal Behavior

Compounds **11a** and **11d** were found to be non-LC. Compound **11b** was solid at room temperature and displayed a melting transition (centred at 39.93 °C) to the mesophase with a heat of transition (ΔH) of 1.57 kJ mol^{-1}. On further heating, mesophase was cleared at 57.48 °C (ΔH = 0.48 kJ mol^{-1}). On the other hand, cooling scan showed the appearance of a well-defined schlieren texture (Figure 5.1c) at 55 °C that remained stable down to room temperature (even upto -19.4 °C). Compound **11c** was LC at room temperature and exhibited isotropization at 50 °C (ΔH = 0.30 kJ mol^{-1}).

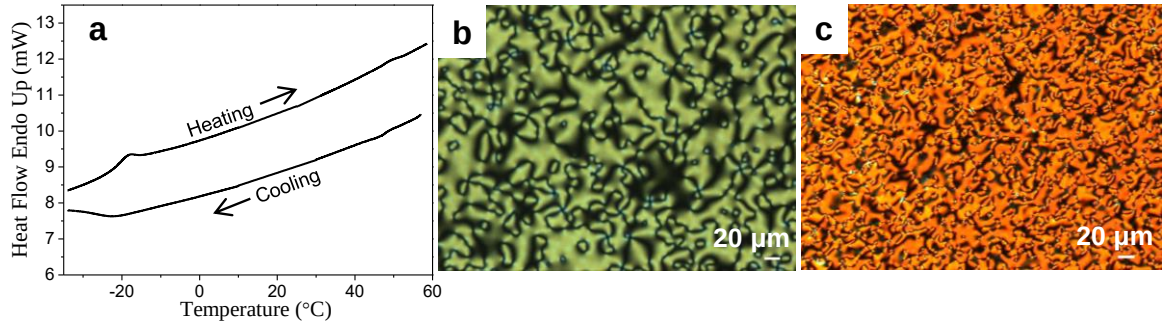

Figure 5.1 (a) DSC trace of compound **11c** on heating and cooling (scan rate 5 °C min^{-1}). (b) Polarizing optical photomicrograph of compounds (b) **11c** at 40 °C and (c) **11b** at 35 °C (on cooling, crossed polarizers).

On further cooling, mesophase emerged at 46.83 °C (ΔH = 0.29 kJ mol^{-1}) which was stable upto -22.36 °C. The DSC traces obtained from heating and cooling runs with **11c** are shown in Figure 5.1a. Gratifyingly, the photomicrograph of compound **11c** at 40 °C (Figure 5.1b) obtained during cooling from the isotropic liquid clearly displays a signature of N_D phase.

5.1.3.3 X-ray Diffraction Studies

To quantify the detailed structure of the N_D phase, X-ray diffraction experiments were performed. Diffractograms of mesophases of both **11b** and **11c** (Figure 5.2 & Figure A11, appendix IV) displayed a sharp small angle peak corresponding to the presence of local columnar-like orientational alterations within the nematic phase, and a broad peak at wide angle which is ascribed to liquid like order of alkyl chains. This pattern conclusively affirms the presence of a N_D phase. In addition to that one broad peak in the mid-angle range was also observed which was further confirmed by full q range fitting of diffraction pattern with Lorentzian profiles.

The calculated d- spacing of 19.81 Å for the signal in the small angle for **11b** (Figure 5.2a) represents the average inter-disc distance (side by side separation) along the disc plane and approximates the diameter of the composite disc unit, ~19 Å. The spacing from the wide angle peak is calculated to be 4.68 Å which mainly originates from the liquid-like correlation of the molten chains. The reflection in the mid-angle region corresponds to a distance of 8.78 Å which is attributable to the weak correlation of dyad along normal to the disc plane and corresponds to the thickness of the dimer. This disc thickness, ~8 Å is a result of folding of dyad which was further validated by DFT calculations (*vide infra*). The diffraction pattern for the nematic phases of compound **11c** is very similar to **11b** and provides very similar conclusions (Figure 5.2b).

The correlation length, the degree of order within the mesophases, was calculated using the formula $\xi = [k2\pi]/[(\Delta q)]$ which is equivalent to Scherrer's equation, $\xi = [k\,\lambda]/[(\Delta 2\theta)\,\mathrm{Cos}\theta]$. In the above formula, k is the shape factor whose typical value is 0.89, λ is the wavelength of the incident X-ray, $\Delta 2\theta$ is the broadening in 2θ at half of the maximum intensity (FWHM) in radian unit, θ is the maximum of the reflection, q is the scattering vector ($q= 4\pi\mathrm{Sin}\theta/\lambda$) and

the Δq is broadening in q at half of the maximum intensity. The Δq is obtained by Lorentzian fitting of the diffraction pattern.

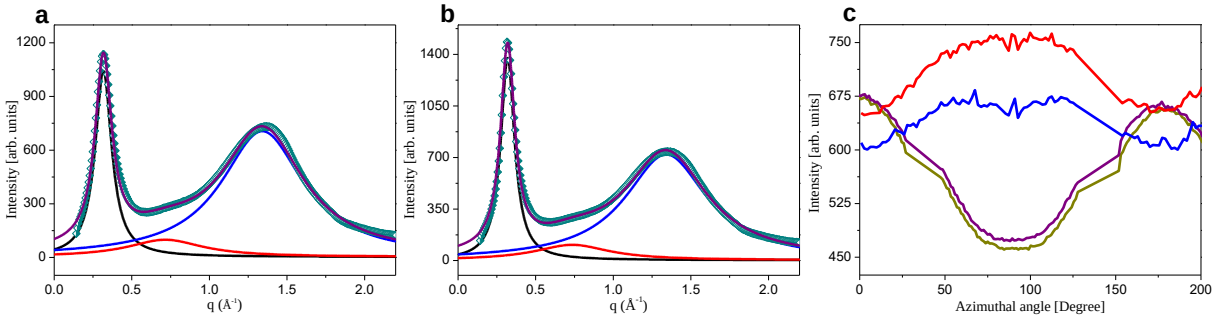

Figure 5.2 X-ray diffraction patterns of compound (a) **11b** and (b) **11c** (half-filled diamond in dark cyan colour) along with the Lorentzian fittings). Black, red and blue colour is the Lorentzian profiles corresponding to small, mid and wide angle peak, respectively. Purple colour is the sum of all these Lorentzian profiles and fits to the full q range profile of the data. (c) Azimuthal plot for small and wide angle peak of the compound **11b** (blue & dark yellow) and **11c** (red & purple) respectively.

For compound **11b**, the correlation lengths for the reflections at 19.81, 8.78 and 4.68 Å are calculated to be 43.05, 9.48 and 8.66 Å respectively (Table 5.1). For compound **11c** the respective correlation lengths have been increased and this is more prominent for the reflection in the small angle region. For direct comparison, the correlation length was divided by *d*-spacing, which results in a measure for the spatial order in terms of dimensions of the molecular length scale. Figure 5.2c displays the azimuthal plot for small and wide angle peaks of compounds **11b** and **11c**. Azimuthal intensity variations in small and and wide angles are in opposite phase which reflects that the growth of the side by side correlation of the composite disc and chain-chain correlation are in orthogonal plane. Since the intensity variation is broad, it can be assumed that the structure is locally planar.

To substantiate our assertion regarding the folding behavior of two discs in **11b**, we carried out a high-level DFT analysis. The computational analysis reveals that the folded form of the molecule is electronically stable by 22.6 kcal mol^{-1} (B3LYP-d3/6-311G**) over its unfolded linear congener.[32, 33]

Table 5.1 X-ray reflections and corresponding correlation lengths obtained after fitting the full q range profile with Lorentzian profiles in the nematic phases of compound **11b** & **11c**.

Sample Name	Properties	Small angle peak	Mid angle peak	Wide angle peak
11b	*d*-spacing d(Å)	19.808 ± 0.012	8.779 ± 0.021	4.685 ± 0.012
	FWHM ($Å^{-1}$)	0.1299	0.5901	0.6456
	Correlation Length (ξ) (Å)	43.049 ± 0.031	9.476 ± 0.122	8.662 ± 0.021
	ξ/d	2.173 ± 0.002	1.079 ± 0.015	1.849 ± 0.005
11c	*d*-spacing d(Å)	19.666 ± 0.012	8.539 ± 0.021	4.685 ± 0.012
	FWHM ($Å^{-1}$)	0.1092	0.5811	0.6436
	Correlation Length (ξ) (Å)	51.209 ± 0.031	9.623 ± 0.122	8.689 ± 0.021
	ξ/d	2.604 ± 0.002	1.127 ± 0.015	1.854 ± 0.005

Considering the entropic penalty associated with the folding event, free energy difference (ΔG) was calculated to be 14.7 kcal mol^{-1} in favor of the folded state. As can be observed from Figure 5.3, one of the phenyl group of the phenyl acetylenes is nicely engaged in π-π interaction, keeping the interacting C…C distances within 3.5-3.7 Å. To ensure further that the stabilization for folded state is not much biased by the choice of the level of theory, we recalculated the electronic energy difference in M06-d3/6-311G**.[34] The difference came out to be 29.4 kcal mol^{-1} in favor of folded State, unambiguously confirming that the folded form is significantly stable over the unfolded one and should remain as exclusive. Most notably, this folded behavior of **11b** is also fully consistent with our previous X-ray analysis.

5.1.3.4 Dielectric and Birefringence Studies

To investigate the physical properties of the room temperature N_D LCs, dielectric constant and birefringence were measured as a function of voltage and temperature (details of the cell preparation for these measurements are given in the experimental section). The dielectric constant of samples was measured as a function of voltage at a fixed frequency of 1 KHz (Figure 5.4a). The dielectric constant increases beyond the Freedericksz' threshold voltage and tend to saturate at higher voltages. In particular, for sample **11b** and **11c** the threshold voltages are 9.5 V and 11.8 V, respectively.

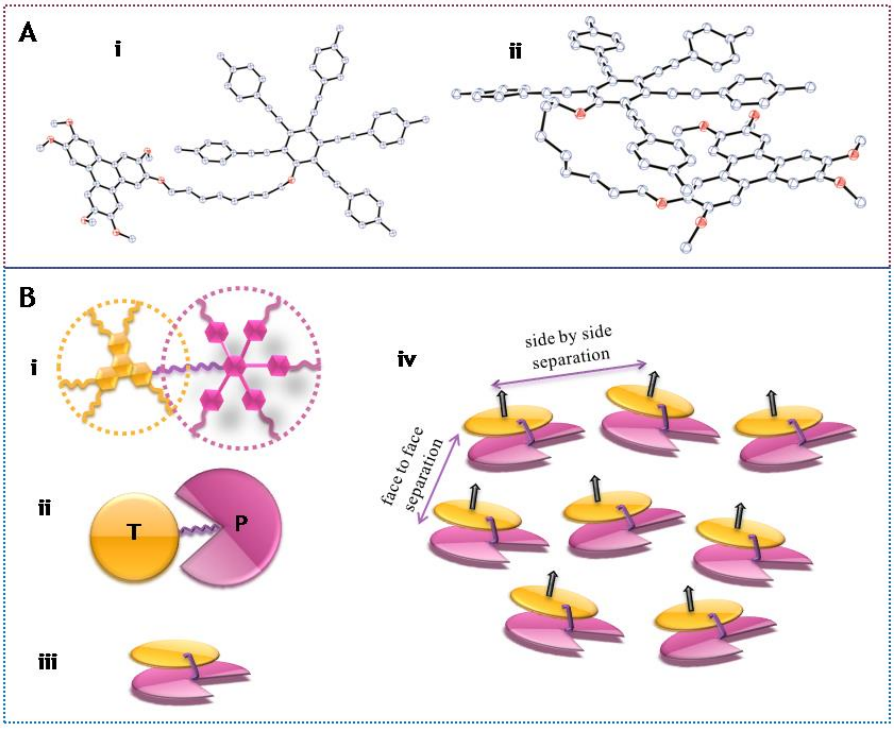

Figure 5.3 Panel A: Computionally optimized structures of (i) linear and (ii) folded dimer. The folded form is electronically stable by 22.6 kcal mol^{-1} (B3LYP-D3/6-311G**) over unfolded form. Panel B: Schematic of (i) the structure of compounds **11**. (ii) Modeled as two discs connected with a flexible chain (T- triphenylene, P- pentaalkynylbenzene) in which disc P is truncated. (iii) A composite disc which turnout after folding of these two discs. (iv) Nematic phase of the composite discs. Alkyl chains are omitted for better clarity. Arrow in black color show the direction of the composite disc normal.

The director is homeotropic below the Freedericksz threshold voltage and becomes planar at much higher voltage. This voltage-scan enables us to measure the effective dielectric anisotropy at a particular temperature. The dielectric anisotropy of the samples was found to be negative and very small (≈ -0.01). Although the value of the dielectric constant is comparable to other room-temperature N_D LCs, the anisotropy is much smaller than most of the other N_D compounds known in the literature.[35]

To measure the change in birefringence ($\Delta n = n_e - n_o$) of samples, its voltage dependence was tested in the N_D phase at a fixed temperature which is shown in Figure 5.4b. Above the

Freedericksz threshold voltage, Δn increases gradually and saturates at ≈20 V. The saturation of Δn indicates the planar state of the director as discussed earlier. Furthermore, a voltage of 23 V was applied to measure the temperature dependent birefringence. As shown in Figure 5.4c, the birefringence increases gradually with voltage along the isotropic to N_D transition instead of a discontinuous jump, often seen for first order phase transitions. This is due to the large isotropic-N_D coexisting region (≈ 5 to 9 °C), which was observed indeed under POM. The maximum birefringence obtained at room temperature for the compounds **11b** and **11c** are ≈ 0.082 and ≈ 0.071, respectively. The very small anisotropy in dielectric and the optical birefringence indicates that the orientational order in such systems is relatively lower than many other discotic compounds at room temperature. Most possibly, this stems from the folding of the two disc units and the presence of a flexible linking chain. Such linking is responsible for poor stacking of the two disc-like units that prevent short-range columnar order in the nematic phase. Notably, the present study did not show any evidence of phase biaxiality in these systems, which may originate from improper stacking of the two neighbouring disc-like units.

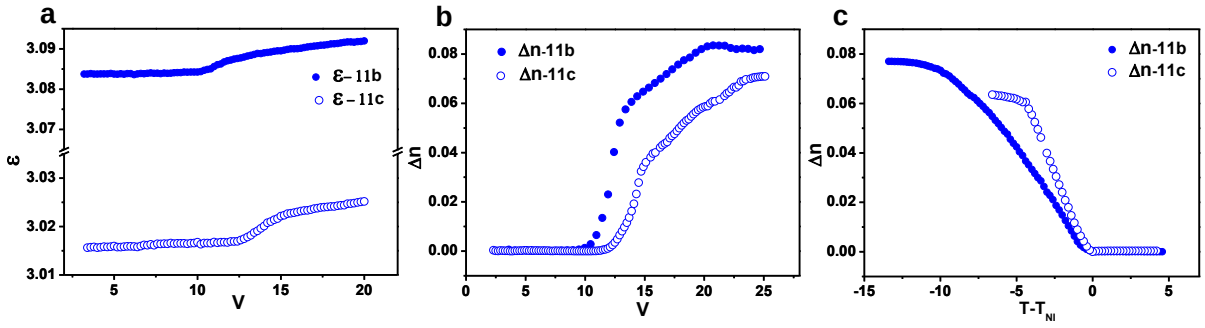

Figure 5.4 (a) The voltage dependent dielectric constant for **11b** and **11c**. (b) voltage dependent birefringence of compounds **11b** (37 °C) and **7c** (43 °C) and (c) the temperature dependent birefringence of compounds **11b** and **11c**.

Earlier reports disclosed that the mesophase behaviour of a discotic dimer generally relies on the position of equilibrium existing between the folded and unfolded conformers which in turn depends on the subtle interactions between the two discs, linking as well as the peripheral alkyl chains.[36-38] In our studies, we noticed that due to π-π interactions between the TP unit and phenyl rings of PA, the molecule tends to fold itself and forms a composite disc.

In fact the folded geometry is very much favoured over the unfolded conformer. We are confident for the folded state of **11c** from three different experiments; i) the spacing of the mid angle peak in X-ray diffraction corresponding to double of the thickness of the mesogenic dyad, ii) DFT calculations disclosing that the folded state is significantly more stable than the unfolded state iii) smaller values of dielectric anisotropy and optical birefringence. On the basis of these results we proposed a schematic of N_D phase shown in Figure 5.3, where, mesogenic dyad (**11b** or **11c**) could be modelled as two discs linked via flexible chains, in which one of the disc is truncated. These discs of the dyad fold to form a composite disc which are orientationally linked among themselves and thus form a N_D phase (Figure 5.3). The slight non-planarity of these composite discs avoids the formation of columnar phase as it prevents the π-π stacking between the triphenylene units. Also, the incompatibility of the two discs present in the composite disc leads to improper packing resulting into mesophase at room temperature.

5.1.4 Design-II

5.1.4.1 Synthesis and Characterization

Target compounds (**12a-d**) were synthesized by the route as outlined in Scheme 1. Compounds **12** were prepared by reacting the pentayne **15** and azobenzene tetracarboxylic acid **20** in presence of potassium hydroxide and tetrabutylammonium bromide under reflux conditions (see experimental section for details).[39] All the compounds were characterised by ^{1}H NMR, ^{13}C NMR, IR, UV-vis and elemental analysis (appendix IV, Figure A12-A21).

5.1.4.2 Thermal Behavior

The thermal behaviour of the compounds **12a-d** (precise transition temperatures in °C and respective enthalpy changes in kJ mol^{-1}) was examined by differential scanning calorimetry (DSC, Table 5.2) whereas the mesophase behaviour was investigated by polarizing optical microscopy (POM) and X-ray scattering studies. Among the synthesized compounds, **12a-c** displayed bright birefringent textures at room temperature (with shearability) and were transformed to isotropic liquids at various temperatures on heating (*vide infra*).

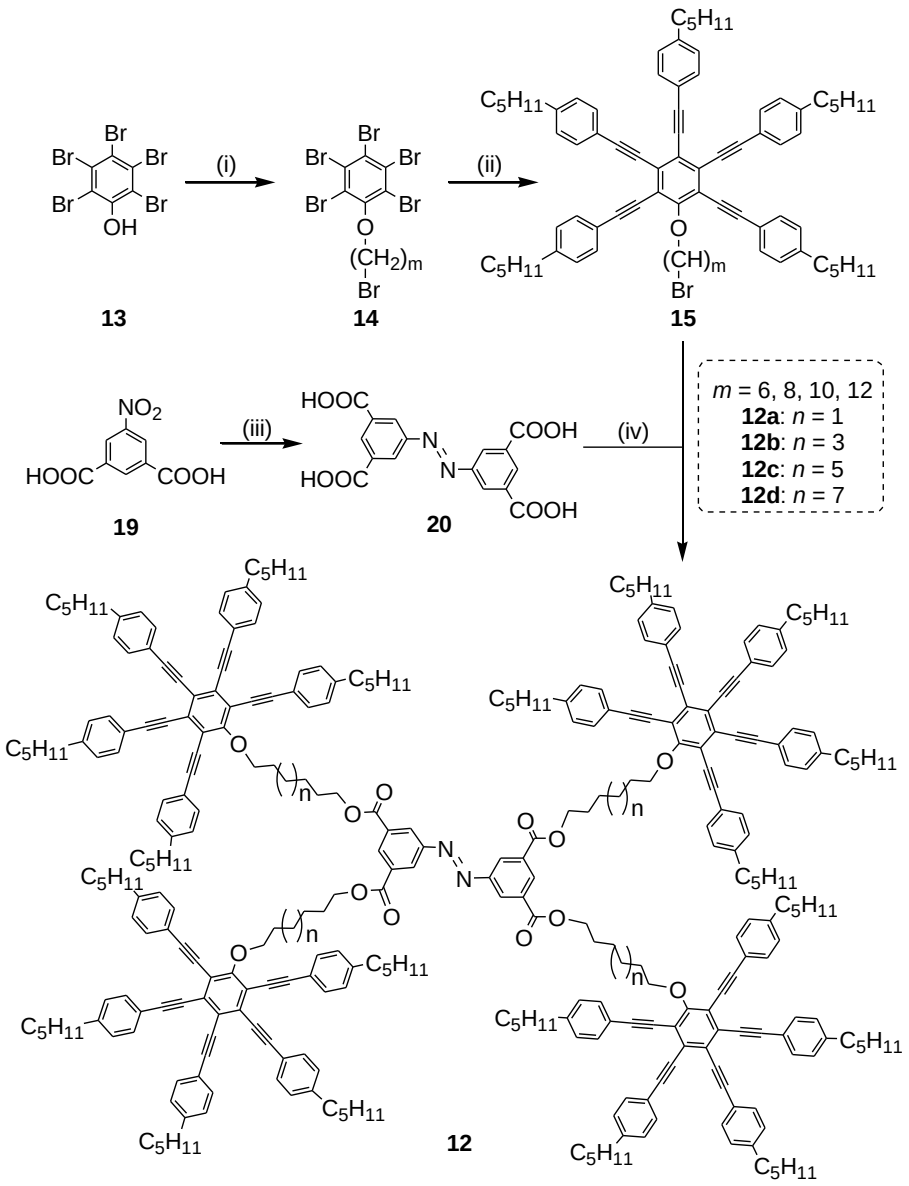

Scheme 5.2 Synthesis of the target compounds **12**. Reagents and conditions: (i) K_2CO_3, KI, Br-$(CH_2)_n$-Br, butanone, 80 °C, 18h, 88%; (ii) $Pd(PPh_3)_2Cl_2$, 4-pentylphenylacetylene, PPh_3, CuI, Et_3N, 100 °C, 15h, 85%; (iii) NaOH, dextrose, 80 °C, HCl, 70%; (iv) KOH, H_2O, TOAB, reflux, 5h, 50%.

On cooling from isotropic phase, a nice schlieren texture (typical of a nematic phase) was obtained for all of these oligomers (Figure 5.5a, appendix IV Figure A22). Interestingly, compound **12d** was in isotropic state at room-temperature as it displayed dark appearance in POM observation (appendix IV, Figure A22). On cooling below room-temperature,

compound **12d** displayed a transition from isotropic to glassy state at -51.57 °C (ΔH = 3.55 kJ mol^{-1}) which on heating reverts to its native state at 4.57 °C (ΔH = 3.92 kJ mol^{-1}). The presence of glassy state was confirmed from the POM observations at low temperatures where the compound does not show any birefringence but was also not shearable as in isotropic state. This indicates that the isotropic compound **12d** freezes to glassy form at lower temperatures. This observation is further supported by the fact that the X-ray diffractogram of compound **12d** does not display any additional peak on cooling the sample upto -60°C (appendix IV, Figure A23).

Table 5.2 Thermal behavior of the synthesized compounds **12**[a, b]

Compound	Heating Scan	Cooling Scan
12a	N_D 45.44 (0.42) I	I 42.08 (0.32) N_D
12b	N_D 57.50 (0.52) I	I 51.16 (0.37) N_D
12c	N_D 60.44 (1.02) I	I 55.68 (0.78) N_D
12d	G 4.57 (3.92) I	I -51.57 (3.55) G

[a]Phase transition temperatures (peak) in °C and transition enthalpies in $kJmol^{-1}$ (in parentheses). [b]Phase assignments: N_D = discotic nematic, I = isotropic, G = Glass.

The DSC thermogram of compound **12a** exhibited a peak at 45.44 °C (Δ*H* = 0.42 kJ mol^{-1}) corresponding to mesophase to isotropic transition (appendix IV, Figure A24). On cooling, it displayed a transition from isotropic to mesophase at 42.08 °C (Δ*H* = 0.32 kJ mol^{-1}). Similarly, the isotropization temperatures for compounds **12b** and **12c** were found to be 57.50 °C (Δ*H* = 0.52 kJ mol^{-1}) and 60.44 °C (Δ*H* = 1.02 kJ mol^{-1}), respectively. Upon further cooling, mesophase appeared at 51.16 °C for **12b** (Δ*H* = 0.37 kJ mol^{-1}) and 55.68 °C (Δ*H* = 0.78 kJ mol^{-1}) for **12c**. No sign of crystallization was observed till -50 °C for all the compounds.

5.1.4.3 X-ray Diffraction Studies

The quantitative study of the nematic phases of these compounds was detailed by SAXS/WAXS investigations (Figure 5.5b, appendix IV Figure A25). Diffraction patterns of

compounds **12a-12c** (recorded at 25 °C) are very similar to the monomeric PA derivatives.[3] However, in comparison to most of the PA derivatives, N_D mesophase is observed even at room temperature for compounds **12a-12c**.

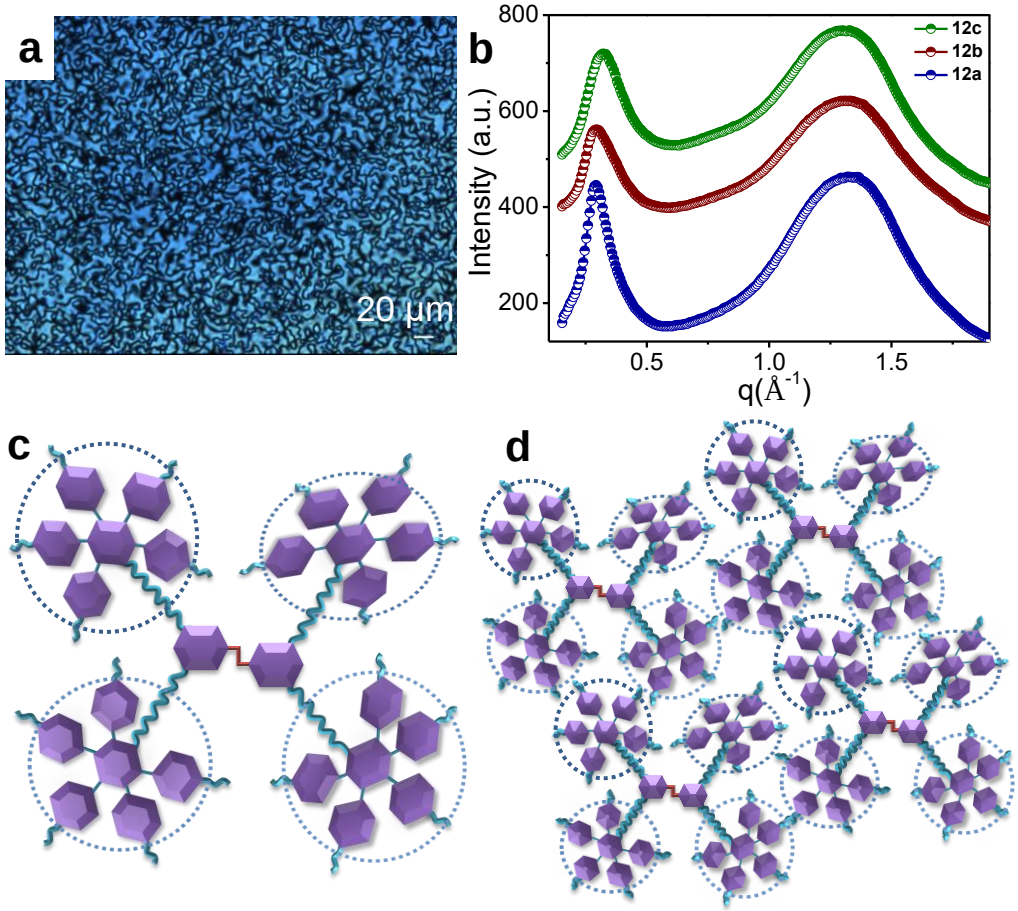

Figure 5.5 (a) Optical photomicrograph of compound **12a** at 30 °C (on cooling, crossed polarizers). (b) X-ray diffraction patterns of compound **12a**, **12b** & **12c** in their mesophase. Schematic of (c) the structure of compound **12**, modelled as four pentakis(phenylethynyl)benzene discs connected with flexible chains to azobenzene core. (d) Local arrangement of the model unit in the nematic phase.

The diffraction pattern corresponding to mesophase of **12a** showed one relatively strong reflection in the small angle region and one broad peak in wide angle regime, respectively. The calculated *d*-spacing of 21.40 Å for the signal in the small angle region correspond to intra and intermolecular correlation of the PA units and approximates the diameter of the

single PA disc (~19 Å). The spacing of the wide angle peak is calculated to be 4.74 Å which is mainly originated from the liquid-like correlation of the molten chains. The diffraction pattern corresponding to the nematic phases of the compounds **12b** and **12c** are very identical to **12a** and analysed in a similar way (Figure 5.5b). The *d*-spacing corresponding to first peak is found to deviate in a decreasing manner from **12a** to **12c** (Table 5.3). According to POM observation, compound **12d** exists as an isotropic liquid. To get further insights into this atypical behaviour of **12d**, we have recorded its diffraction pattern in the isotropic state. The diffraction pattern showed two peaks; one in the small angle and another in wide angle regime, similar to other compounds exhibiting mesophases (appendix IV, Figure A26). However, the calculated *d*-spacing for small angle peak is found to be 19.04 Å which is about 2 Å lesser as in compound **12a** and is almost comparable to compound **12c**. The spacing of the wide angle peak is calculated to be 4.80 Å which is nearly same as observed in other compounds.

The correlation length, i.e., the degree of order within the mesophase, was calculated using $\xi = [k\ 2\pi]/[(\Delta q)]$; equivalent to Scherrer's equation. The Δq is obtained by Lorentzian fitting of the peaks obtained in the diffraction pattern (appendix IV, Figure A27-A28). For compound **12a**, the correlation lengths for the reflections at 21.40 Å and 4.74 Å are calculated to be 32.66 Å and 8.64 Å, respectively. For effective comparison, the correlation length was divided by the *d*-spacing values, which results in a measure for the spatial order in terms of the molecular length scale. The respective correlation lengths for compounds **12** were found to decrease with increasing chain length of the alkyl spacer. The decrease in correlation length is significant for the reflection corresponding to the small angle region (Table 5.3). Variation of correlation length (ξ) (corresponding to reflection at small angle) with respect to number of methylene groups of alkyl spacer (m) for compounds **12a-d** is shown in the Figure 5.6 which follows an exponential decay ($\xi = a + \xi_0 \exp(-m/m_c)$). The characteristic number of methylene groups in alkyl spacer (m_c) is 4.11±0.89 which describes that the correlation length decreases moderately with m. The decrease in correlation length can be explained as follows. As compounds **12** are discotic mesogenic quadric based on pentakis(phenylethynyl)benzene linked *via* flexible alkyl spacers, they could be modelled as four PA discs linked with flexible chains to an azobenzene core (Figure 5.5c).

Table 5.3 X-ray reflections and corresponding correlation lengths obtained after fitting the peak profiles with Lorentzian profiles in the nematic phase of compounds **12a-c** and in the isotropic phase of compound **12d**.

Compound	Properties	Small angle peak	Wide angle peak
12a	*d*-spacing (Å)	21.40 ± 0.20	4.74 ± 0.30
	Correlation Length (ξ) (Å)	32.66 ± 2.52	8.64 ± 1.75
	ξ/d	1.53 ± 0.13	1.82 ± 0.48
12b	*d*-spacing (Å)	20.86 ± 0.25	4.79 ± 0.35
	Correlation Length (ξ) (Å)	27.04 ± 2.52	8.41 ± 1.75
	ξ/d	1.30 ± 0.14	1.76 ± 0.49
12c	*d*-spacing (Å)	19.24 ± 0.30	4.80 ± 0.35
	Correlation Length (ξ) (Å)	24.17 ± 2.52	8.35 ± 1.75
	ξ/d	1.26 ± 0.15	1.74 ± 0.49
12d	*d*-spacing (Å)	19.04 ± 0.30	4.81 ± 0.35
	Correlation Length (ξ) (Å)	21.76 ± 2.86	8.23 ± 1.75
	ξ/d	1.14 ± 0.17	1.71 ± 0.49

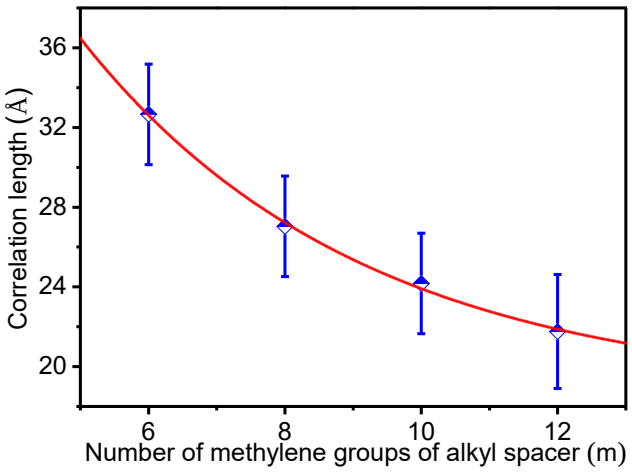

Figure 5.6 Variation of correlation lengths corresponding to reflection at small angle of compounds **12a-d** with respect to the varying number of methylene groups of alkyl spacer (*m*). Half-filled blue diamonds show the correlation length (ξ) data with error bar. Red line shows fit to the data which follows an exponential decay ($\xi = a + \xi_0 \exp(-m/m_c)$). The characteristic number of methylene groups in alkyl spacer (m_c) is 4.11 ± 0.89 which describes that the correlation length decreases moderately with *m*.

In case of PA, the phenyl rings are generally not in plane because of rotational freedom provided by ethynyl linkers which prevents columnar stacking. In addition, orientational freedom of PA group increases on increasing the spacer length which is reflected in the decreasing value of corresponding correlation lengths. However, the decrease in correlation length for the compound **12d** is large enough to avoid mesophase formation at room temperature and thus, it is found to exhibit an isotropic phase.

5.1.4.4 Dielectric and Birefringence Studies

The physical properties (e.g. elastic constants, birefringence, dielectric anisotropy) of the nematic mesogens strongly affects the electro-optical characteristics of the LC displays and thus are the main important factors to be considered. Therefore, to further explore the behaviour of the N_D phase of compounds **12a-c**, we measured some physical properties such as birefringence and dielectric constant as a function of voltage and temperature. We have used a phase modulation technique to measure the birefringence and an impedance analyser for measuring the dielectric constant simultaneously.[35, 40, 41] Compounds **12a**-**12c** could not be aligned homogeneously and thus it was impossible to conduct direct measurements of birefringence. However, the samples showed good homeotropic alignment on AL-1254 polyimide coated cells. Hence, we first measured the birefringence at a fixed temperature as a function of voltage. To study the temperature dependence of birefringence, we applied higher voltage than the Fréedericksz threshold voltage to get voltage induced homogeneous alignment. The dielectric constant of the samples was also first measured as a function of voltage at a fixed frequency (2 KHz) using an impedance analyser.[42]

The insets of Figure 5.7a-c show the variation of voltage dependent birefringence. The birefringence is zero at a zero voltage as expected due to the homeotropic state. It increases beyond a particular voltage and finally leads to saturation. The Fréedericksz threshold voltage (V_{th}) at a relative voltage is slightly higher in compound **12c** than **12a** and **12b**. For example, V_{th} for compounds **12a** and **12b** is about 2.5 V whereas it is about 5 V for **12c**. For measuring temperature dependent birefringence, a voltage of 20 V was applied for all the samples. At a relative temperature, the birefringence of compound **12a** is slightly lower than **12b** and **12c**. For example, at $T-T_{NI}$ = -12 °C, Δn for **12a** is 0.055 whereas in case of **12b** and

12c, it is about 0.08. This is expected because the polarizability anisotropy and hence the birefringence increases with increasing length of flexible alkyl spacer.

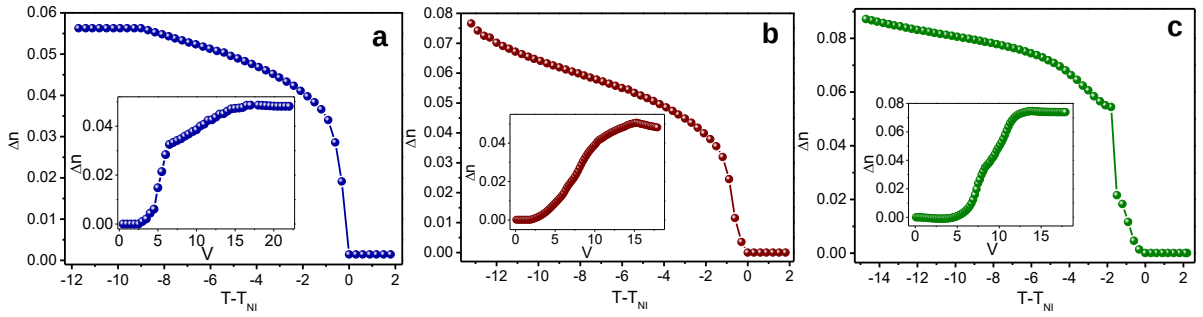

Figure 5.7 Temperature dependent birefringence (Δn) of (a) **12a** at a fixed voltage of 20 V and frequency of 4 kHz, Inset: voltage dependent birefringence (Δn) at a fixed temperature, $T\text{-}T_{NI}$ = -4.89 °C; (b) **12b** at a fixed voltage of 15 V and frequency of 2 kHz, Inset: Voltage dependent birefringence (Δn) at a fixed temperature, $T\text{-}T_{NI}$ = -5 °C and (c) **12c** at a fixed Voltage of 15 V and frequency of 2 kHz, Inset: Voltage dependent birefringence (Δn) at a fixed temperature, $T\text{-}T_{NI}$ = -6 °C.

The temperature and voltage dependent variation of dielectric constants of compounds **12b** and **12c** are shown in Figure 5.8 (due to very high ionic conductivity of **12a** and difficulty in alignment of the sample, its measurement was not carried out). The insets show that beyond the Fréedericksz threshold voltage, the dielectric constant increases and tend to saturate. The approximate dielectric anisotropy (Δε), i.e., the difference between the dielectric constant measured at zero voltage and at 20 V is much smaller in **12b** than **12c**. For example, for **12b**, Δε≈0.07 whereas for **12c**, Δε≈0.2. The temperature dependent dielectric constant was studied at 20 V simultaneously. Although absolute values of the dielectric constants of compounds **12b** and **12c** are slightly different, their temperature dependent behavior is almost similar.

Further, the bend elastic constant (K_{33}) of the samples can also be estimated from the Fréedericksz threshold voltage,$\left(V_{th} = \pi\sqrt{K_{33}/\epsilon_o\Delta\varepsilon}\right)$ of the voltage dependent dielectric data. For example, the Fréedericksz threshold voltages for **12b** and **12c** are 3.7 V and 4.9 V, respectively. The corresponding bend elastic constants at those temperatures are calculated to be 0.1 pN and 0.42 pN, respectively. There are a few reports which describe the detailed

physical properties of room temperature N_D compounds.[35] We observed that the birefringence and dielectric anisotropies of the synthesized compounds are significantly lower in comparison to those reported in the literature. The low birefringence of these compounds could be advantageous for employing them as compensating film in LC devices where the difference in the value of birefringence between the device material and the compensating film has to be lower.

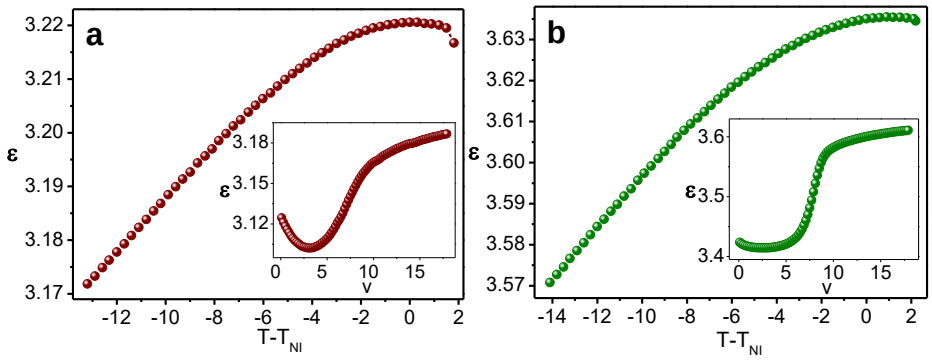

Figure 5.8 Temperature dependent dielectric (Ɛ) of compound (a) **12b** at a fixed voltage of 15 V and frequency of 2 kHz, Inset: Voltage dependence of dielectric (Ɛ) at a fixed temperature, $T-T_{NI}$ = -5 °C; and (b) **12c** at a fixed voltage of 15 V and frequency of 2 kHz, Inset: Voltage dependence of dielectric (Ɛ) at a fixed temperature, $T-T_{NI}$ = -6 °C.

Overall, we observed that combination of four PA units linked with the azo group sufficiently perturbed the system to yield a room-temperature N_D phase. In the assembly of PA units of monomeric derivatives, efficient packing of the discs is forbidden due to free rotation of phenyl rings provided by the ethynyl linkers. However, in most of the cases, the packing is not disordered enough to exhibit the nematic phase at room-temperature. Earlier, room-temperature N_D mesophase has been obtained by perturbing the symmetry of the PA unit leading to more disordered system.[26, 27] Here, we reveal that grouping of PA units by connecting them with a short azobenzene linking unit *via* flexible spacer could show room temperature N_D phase. In general, several other factors involved such as molecular topology, micro-segregation etc. might also be involved in the mesophase formation, however, conformational flexibility plays a main role here. This is also evident from the X-ray studies which show decrease in correlation length with increasing number of alkyl spacers. Infact,

we found that the compound **12d** with longest alkyl spacer displays isotropic behaviour at room-temperature. This observation can be explained on the basis that PA discs within each oligomer are randomly oriented and so the oligomer too. Hence, the doubly disordered effect due to random orientation of (i) individual PA unit of each oligomer and thus (ii) oligomers composed of PA discs, reduces down the packing efficiency enough to result into a room-temperature N_D phase. However, in compound **12d**, the disorderness was high enough to avoid the emergence of N_D phase.

5.1.5 Conclusions

In conclusion, we have successfully designed and synthesized two new series of compounds which could show room-temperature N_D phases. In the first series, two new discotic dyads which show N_D phases at room temperature due to folding of the two discs (*i.e.* TP & PA) of the dimer due to π-π interactions are reported. XRD analysis, DFT calculations as well as the lower values of birefringence and dielectric anisotropy are fully consistent with the prescribed model of the compounds. In the second series, design and synthesis of three room-temperature N_D LCs is presented consisting of an azobenzene core attached to which are four pentaalkynylbenzene (PA) units *via* flexible alkyl spacers. The presence of short azo linking group provides more disorder in the system, thereby reducing the packing efficiency among the PA units and resulting into the formation of a room-temperature N_D phase over a wide temperature range. Dielectric constant and birefringence studies were performed to gain further insights into the physical properties of the mesophase. Overall, all these compounds are promising materials for display device applications and also points the way towards development of new anisotropic soft materials.

5.2 Part B: Room-temperature Discotic Nematic Gold Nanoparticles decorated with pentaalkynylbenzene units

5.2.1 Introduction

Grafting LCs on a metal cluster such as gold nano-particles (GNPs) offers a combination of the properties of LCs with the size-dependent characteristics of GNPs. The inherent property of LCs to form mesophases due to their shape and polarizability anisotropy also influences the self-assembly of GNPs whereas the GNPs affects the electro-optic and alignment properties of LCs in devices which leads to collective advantages for both the components.[43-48] Coating the GNPs with LC molecules also provides a way to tune the properties of GNPs through variation in the localized surface plasmon resonance.[49] Not only that, decoration of GNPs with LC molecules serves as one of the best approach to avoid the micro- and macroscopic phase separation and thus GNP aggregation.[50, 51] These composite materials have shown enhanced processability and interesting applications such as in opto-electronics, catalysis, electrically controlled light-scattering properties as well as enhanced plasma-emitting properties etc.[52-72] In fact, this approach has led to manipulation of various LC display characteristics e.g. threshold voltage, birefringence, dielectric behavior, pretilt angle, contrast ratio etc.[73-83] It has been observed that these GNP- LC nanocomposites have also shown a drastic enhancement in the dielectric behaviour resulting into their remarkably enhanced switching speeds as compared to the pure LCs.[84-89]

However, achieving LC phase in the GNP systems is quite a challenging task. Mainly to obtain mesophase in such a system, the size of GNPs has to be controlled. Generally, GNPs should be sufficiently small (mostly in the range of 1.7 to 2 nm) so as to minimize the surface–anchoring effect of LCs, so that they can behave same as in bulk.[90] In addition, it is possible to control the polydispersity of these smaller GNPs and the variations in the size of these GNPs are smaller than the size of typical LCs.[91-94] Further, the crowding of LC molecules at the surface of GNPs should also be avoided as that can lead to reduced mobility in the composite system and thus loss of LC behavior.[95-103] For this purpose, dendritic kind of molecules can be employed which will direct the LC molecules to position themselves at a

distance from each other. The dendrimers are fluidic in LC phase and can balance the GNP system in the mesophase.

Moreover, for practical applications, a key challenge is to obtain the GNP-LC systems in which LC phase can be made stable over a suitable temperature interval (including room temperature). Investigation of a low ordered nematic phase where only orientational order is present provides a promising approach if we take into account the design challenges imposed for a GNP-LC system. However, the coordination between the shape of GNPs with that of the nematic phase which has only orientational order present in the mesophase is a challenging task. Only three reports are available in the literature which has shown the synthesis of nematic LC GNPs.[90, 104, 105] Among them, only one report describes the LC GNPs where nematic mesophase was stable at room-temperature.[25] All these reports are based-on laterally connected mesogen to the GNPs (**21**, **22**). This lateral connection not only provides a control over the size of GNPs but also prevents the crowding of mesogens at the gold surface which contribute to the formation of a room-temperature mesophase.

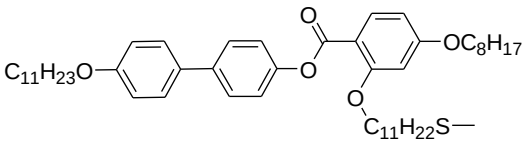

21

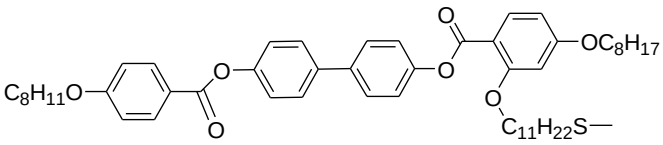

22

5.2.2 Objective

In this study, we have aimed to synthesize GNPs decorated with thiol terminated pentaalkynylbenzene units. The pentaalkynylbenzene derivatives generally form discotic nematic mesophase due to rotational freedom provided by the ethynyl linkers which avoids the column formation. It has been observed in the earlier reports that GNPs coated with triphenylene, cyanobiphenyls etc. were found to be non-LC. In our approach, we have chosen the conformationally flexible pentaalkynylbenzene units for coating GNPs whose size was regulated to be in the range of 2.5-3.1 nm. These conformationally flexible PA units when attached to smaller sized GNPs can induce a N_D LC phase by avoiding crowding on the surface of GNP due to their dendritic structure. In addition, these PA derivatives are optically negative birefringent and are thus very important for use in compensation foils to obtain

wide-viewing angle displays. Therefore, these LC GNPs will not only show the enhanced dielectric response but will also serve as compensation foils in the LCD display.

5.2.3 Results and Discussion

5.2.3.1 Synthesis and characterization

Thiol terminated compounds **25** were prepared by the synthetic route outlined in Scheme 5.3. Synthesis of compounds **14**, **23** and **24** was carried out following earlier reported procedures. For the synthesis of final compound, compound **24** was dissolved in a 1:1 mixture of dichloromethane and methanol.

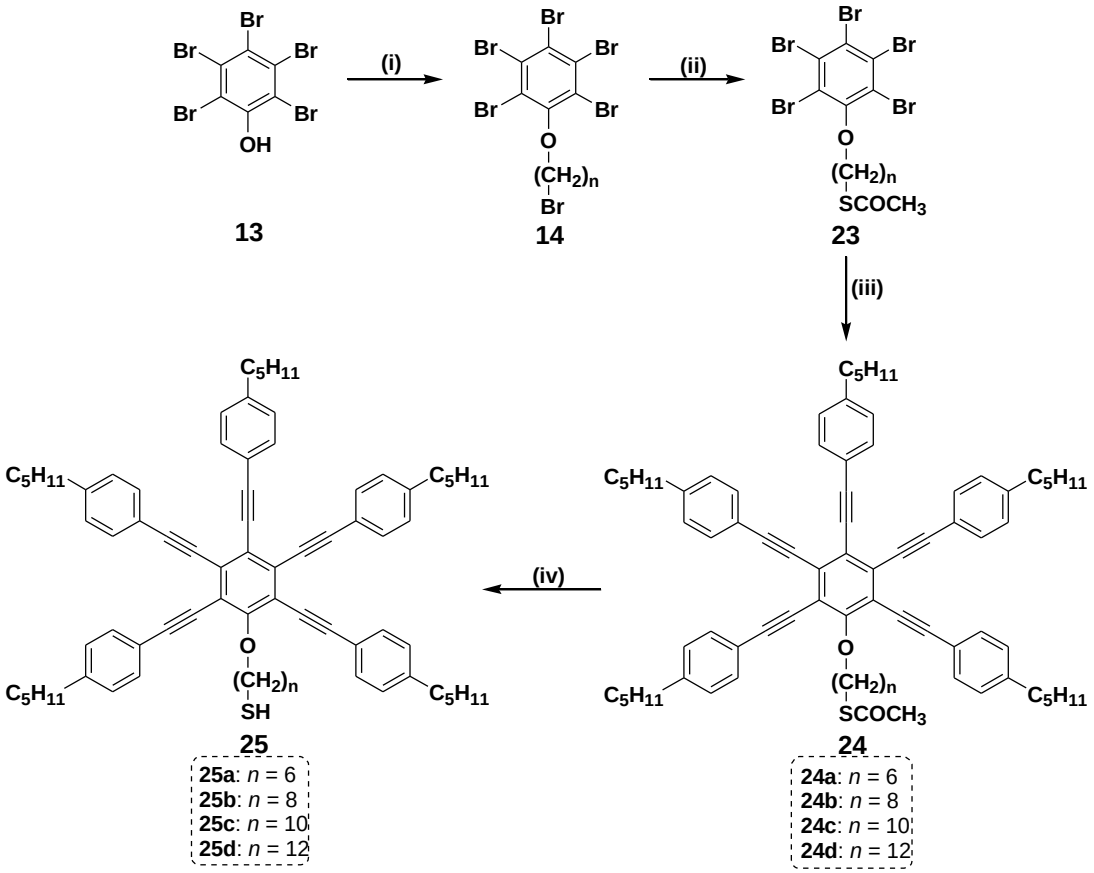

Scheme 5.3 Synthesis of the target compounds **25**. Reagents and conditions: (i) K_2CO_3, KI, Br-$(CH_2)_n$-Br, butanone, 80 °C, 18h, 88%; (ii) $KSCOCH_3$, DMF, RT, 8h, 80%; (iii) $Pd(PPh_3)_2Cl_2$, 4-pentylphenylacetylene, PPh_3, CuI, Et_3N,100 °C, 15h, 85%; (iv) K_2CO_3, MeOH: CH_2Cl_2 (1:1), 5h, 50%.

To that mixture, a few mg of potassium carbonate was added and it was stirred for around 5 hours at room temperature to obtain the crude product which was further purified by column chromatography to yield the pure compound **25** (see experimental section for details). All the synthesized compounds **24a-d** and **25a-d** were characterized by ^{1}H NMR, ^{13}C NMR, IR, UV-vis and mass spectrometry (appendix IV, Figure A29-A47).

5.2.3.2 Thermal Behavior

The thermal behavior of the compounds **25** (precise transition temperatures and respective enthalpy changes) was examined by differential scanning calorimetry (DSC) and the mesophase behavior was explored by polarized optical microscopy (POM) and X-ray scattering studies. The compounds of series **24** also exhibited mesomorphic behaviour. Interestingly, two of the compounds **24c** and **24d** displayed N_D phase even at room temperature on cooling from the isotropic phase (appendix IV, Table A1, Figure A48-49).

Table 5.4 Thermal behavior of the synthesized compounds **25** [a, b]

Compound	Heating Scan	Cooling Scan
25a	Cr 58.15 (0.51) N_D 110 I	I 104 N_D -10.15 (4.72) Cr
25b	Cr 59.84 (4.34) N_D 68.93 (0.18) I	I 41 N_D -29.67 (1.38) Cr
25c	Cr 65.96 (4.0) N_D 83.78 (0.58) I	I 47 N_D -15.74 (1.70) Cr
25d	N_D 50 (0.49) I	I 43 N_D -27.19 (3.70) Cr

[a]Phase transition temperatures (peak) in °C and transition enthalpies in kJ mol^{-1} (in parentheses). [b]Phase assignments: Cr = Crystalline, N_D = discotic nematic, I = isotropic. Some of the transitions were not observed in DSC scan, however, they were confirmed from POM studies.

The compounds of series **25** displayed a distinct behaviour as compared to their series 2**4** counterparts. Compound **25a** was solid at room temperature and displayed a crystal to N_D mesophase transition at 58 °C followed by isotropization at 110 °C (Table 5.4). On further cooling, the mesophase appeared at 104 °C and existed till -10 °C after which it transformed to a crystalline state. Similarly, compounds **25b** and **25c** melted at 59 and 66 °C to form the

N_D mesophase, followed by isotropization at 69 and 84 °C, respectively. On cooling, the mesophase for **25b** and **25c** appeared at 41 and 47 °C which crystallized at -28 and -14 °C respectively. Interestingly, compound **25d** existed in LC state even at room temperature and becomes isotropic at 50 °C on heating the sample. On cooling back from the isotropic state, a Schieleren texture typical of N_D phase appears at 43 °C which crystallizes at -27 °C (Figure 5.8, appendix IV Figure A50-51).

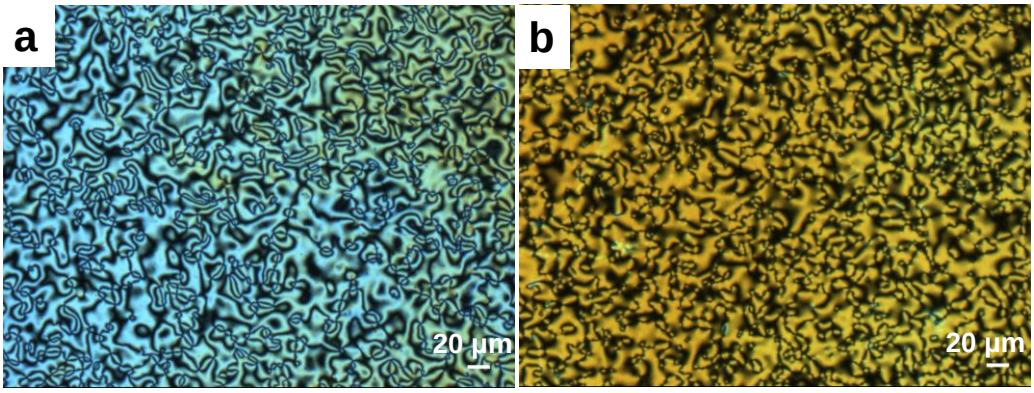

Figure 5.8 Optical photomicrograph of compound: (a) **25c** at 36.6 °C and (b) **25d** at 41.8 °C representing N_D phase (on cooling from isotropic, crossed polarizers).

5.2.3.3 X-ray Diffraction Studies

The quantitative study of the nematic phases of all the compounds of series **25** was detailed by SAXS/WAXS investigations (Figure 5.9a, appendix IV, Figure A52). The compounds of series **24** displayed similar diffractograms to those of series **25** in their mesophase (appendix IV, Table A2). All the compounds of series **25** in their mesophase displayed one relatively strong reflection in the small angle region and one broad peak in wide angle regime, respectively. For compound **25a**, the calculated *d*-spacing of around 19.95 Å for the signal in the small angle region corresponds to the intermolecular correlation of the PA units and thus approximates the diameter of a single PA disc (~19 Å). The spacing of the wide angle peak at 4.93 Å originates from the liquid-like correlation of the molten chains. The diffraction pattern corresponding to the nematic phases of the compounds **25b**, **25c** and **25d** are very identical to **25a** and analyzed in a similar way (Figure 5.9b). The *d*-spacing corresponding to the two peaks at small and wide-angle was found to be nearly same for **25a-d**. The peak for

alkyl chain-chain correlation shows slight deviation in a decreasing manner from **25a** to **25d** (Table 5.5). For compound **25a**, the correlation lengths for the reflections at 19.95 Å and 4.93 Å are calculated to be 39.18 Å and 9.22 Å, respectively. For an effectual comparison, the correlation length was divided by the *d*-spacing values, which results in a measure for the spatial order in terms of the molecular length scale.

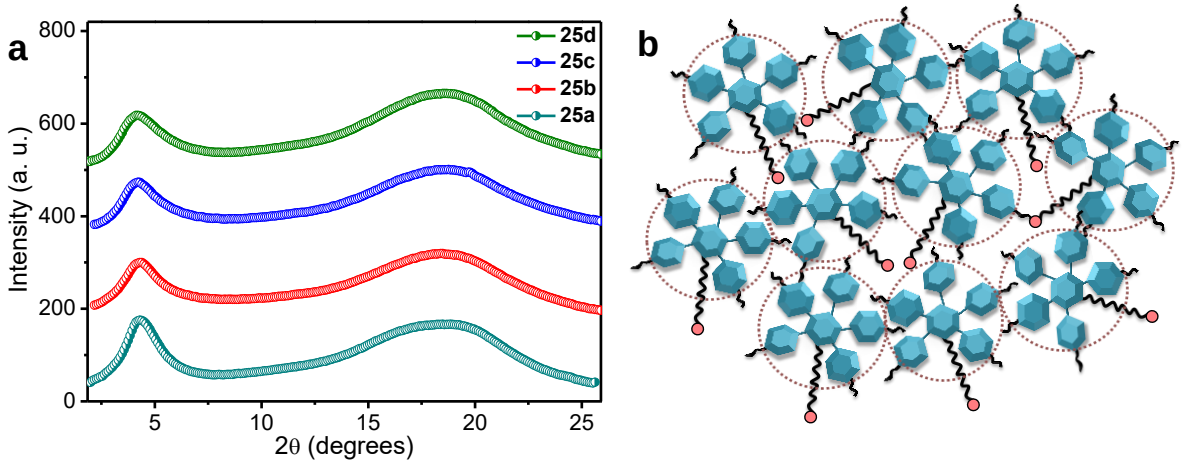

Figure 5.9 (a) X-ray diffraction pattern of compounds **25a-d** in the nematic phase. (b) The schematic representation of the arrangement of PA units in the mesophase.

Table 5.5 X-ray reflections and corresponding correlation lengths in the nematic phases of compound **25a-d**.

Compound	Properties	Small angle peak	Wide angle peak
25a	*d*-spacing (Å)	19.95 ± 0.06	4.93 ± 0.008
	Correlation Length (ξ) (Å)	39.18 ± 1.30	9.22 ± 0.23
	ξ/d	1.96 ± 0.06	1.87 ± 0.04
25b	*d*-spacing (Å)	19.96 ± 0.09	4.89 ± 0.008
	Correlation Length (ξ) (Å)	36.60 ± 1.45	10.58 ± 0.26
	ξ/d	1.83 ± 0.06	2.16 ± 0.05
25c	*d*-spacing (Å)	19.93 ± 0.08	4.87 ± 0.007
	Correlation Length (ξ) (Å)	34.97 ± 0.93	9.78 ± 0.15
	ξ/d	1.75 ± 0.04	2.00 ± 0.03
25d	*d*-spacing (Å)	19.99 ± 0.07	4.85 ± 0.004
	Correlation Length (ξ) (Å)	30.81 ± 0.76	9.17 ± 0.12
	ξ/d	1.54 ± 0.03	1.89 ± 0.02

The respective correlation lengths for compounds **25** were found to decrease with increasing chain length of the alkyl spacer. The decrease in correlation length is significant for the reflection corresponding to the small angle region (Table 5.5). This can be due to the fact that compounds **25** are discotic mesogens based on pentakis(phenylethynyl)benzene composed of flexible alkyl chains and a terminal thiol group. In case of PA, the phenyl rings are generally not in plane because of rotational freedom provided by ethynyl linkers which prevents columnar stacking. In addition, orientational freedom of PA group increases on increasing the alkyl chain length which is also reflected in the decreasing value of corresponding correlation lengths.

5.2.3.4 Preparation of GNPs decorated with thiol terminated PA units

Our next goal was to synthesize and characterize the GNPs coated with PA units. The preparation of GNPs was carried out by closely following the earlier reported Brust Schiffrin method. A solution of tetraoctylammonium bromide (0.124 mmol) in toluene (5 ml) was prepared and added to an aqueous solution of $HAuCl_4.3H_2O$ (0.028 mmol). The resulting solution was stirred for 20 minutes to ensure a complete transfer of gold chloride from aqueous to organic layer. The organic layer was separated and washed with distilled water. A solution of thiol (0.038 mmol) in toluene (2 ml) was added to the above solution and the resulting mixture was stirred for 30 minutes. An aqueous solution of $NaBH_4$ (0.28 mmol) was added dropwise to the above solution and the mixture is stirred for a further period of 6h. The toluene layer was washed with distilled water, diluted with methanol (250 ml) and kept in refrigerator for overnight. The precipitate obtained was purified by re-suspending in toluene and then centrifugation after the addition of methanol (10 ml). This purification step was repeated several times to ensure the complete removal of non-covalently bound organic material. All the synthesized GNPs were characterised by ^{1}H NMR, UV-vis and transmission electron microscopy (TEM) techniques. Their thermotropic behaviour was analysed by POM, DSC and SAXS/WAXS techniques. The ^{1}H NMR spectra of the synthesized nanoparticles displayed broadened peaks as compared to those obtained for thiols and thus indicates that thiols are attached to the surface of gold nano-particles and are not present in their free form (Figure 5.10a-b). Further, a characteristic peak at 517 nm in the UV-vis spectra typically represents the formation of spherical GNPs (Figure 5.10c).

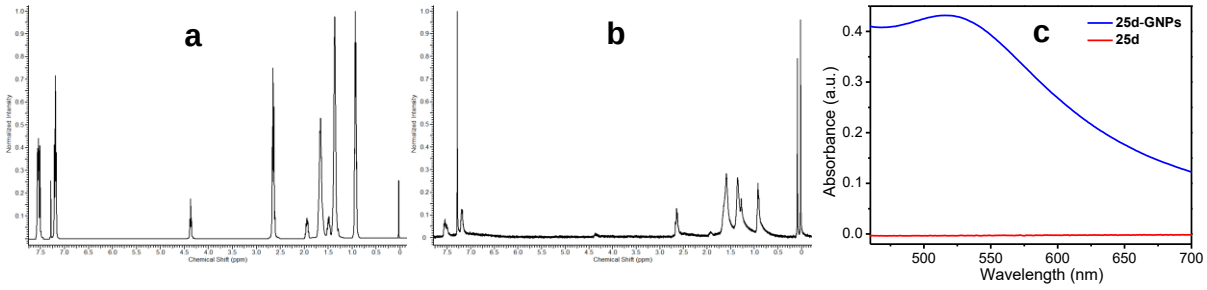

Figure 5.10 The 1H NMR spectrum of (a) compound **25d** and (b) **25d**-GNPs (i.e. GNPs coated with **25d**). (c) The UV-vis spectra of **25d**-GNPs showing characteristic peak at 517 nm for the formation of spherical GNPs which was absent in **25d**.

We have found that GNPs with lower chain lengths *i.e.* **25a**-**25c** exhibited variable results under POM studies. They were sticky solids at room temperature and displayed an increase in birefringence with some phase separation occurring on heating. On cooling, they did not display any birefringence till room temperature. The variable results in subsequent heating and cooling cycles for these compounds could be because of the non-uniform coverage of the capping agent on the Au cluster due to steric hinderance arising from the lower chain length of the spacer unit. Interestingly, in contrast to the above observations, **25d**-GNPs were very stable and displayed an enantiotropic mesophase which existed even at room-temperature. Therefore we have discussed **25d**-GNPs in details in the next section.

The **25d**-GNPs were displaying birefringence with shearability of textures at room-temperature which confirms the presence of LC phase which on heating converted to isotropic liquid at 60 °C (Figure 5.11a). On further cooling, a Schlieren texture typical of nematic mesophase was observed at 57 °C which remained stable upto -12.95 °C (Figure 5.11b, appendix IV Figure A53). It can be thus inferred that the room-temperature N_D phase of **25d** remained unaffected even after coating **25d** on GNPs. However, the mesophase range was found to vary from pure thiol **25d**. The size of the **25d**-GNPs was found to be in the range of 2.5-3.1 nm from TEM observations (Figure 5.11c). DLS measurements also indicated the formation of GNPs of size of ~2.76 nm with a polydispersity index of 0.348. The number of mesogens attached to a single GNP was found to be around 263 from TGA analysis (appendix IV, Figure A54). The mean formula for **25d**-GNPs is found to be $Au_{574}(PA)_{263}$.

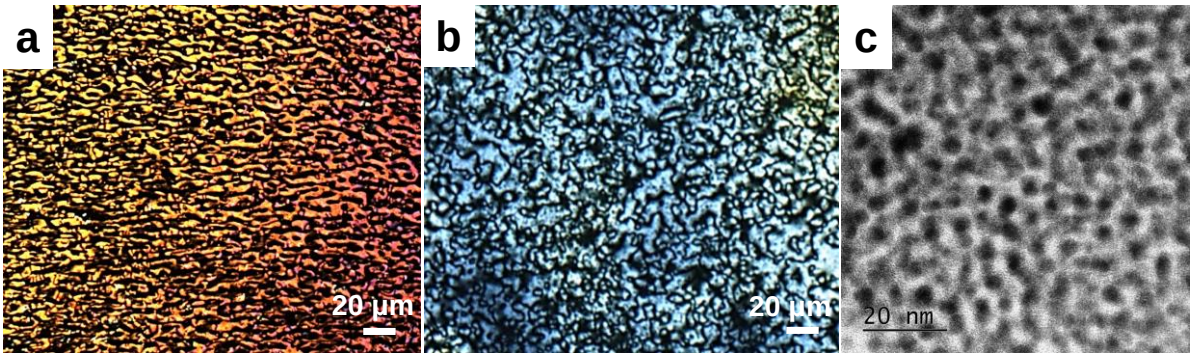

Figure 5.11 The POM textures of **25d**-GNPs (a) on heating at 45 °C and (b) on cooling from the isotropic at 40 °C (Crossed polarizers, Magnification: 200 X). (c) TEM image of **25d**-GNPs obtained by dispersing their dilute solution in toluene on a carbon coated copper grid.

The nematic mesophase exhibited by **25d**-GNPs was further characterised by SAXS/WAXS studies. The XRD pattern exhibited two peaks: one sharp peak at small-angle and other diffuse peak in wide-angle region (Figure 5.12a-b). A broad diffuse band was also observed at small-angle which could be ascribed to the distribution of the GNPs between the domain gaps in a random disordered manner. The calculated *d*-spacing of 42.68 Å at small-angle correspond to side-by-side separation of the **25d**-GNPs and thus approximates the diameter of a single **25d**-GNP i.e. ~41-42 Å. Whereas, the peak in the wide angle regime observed at 4.86 Å correspond to liquid like correlation of molten alkyl chains. Figure 5.12c shows the **25d**-GNP modelled as a gold cluster surrounded by PA units. The arrangement of model units in the nematic mesophase is shown in Figure 5.12d. The correlation lengths for the reflections at 42.68 Å and 4.86 Å are calculated to be 135.16 Å and 14.72 Å, respectively. For measuring the spatial order in terms of the molecular length scale, the correlation length was divided by the *d*-spacing values which were around 3.16 and 0.34 respectively for the peak at small- and wide-angle and is about double of the values as observed for the compound **25d**. The correlation lengths for the reflections at 42.68 Å and 4.86 Å are calculated to be 135.16 Å and 14.72 Å, respectively. For measuring the spatial order in terms of the molecular length scale, the correlation length was divided by the *d*-spacing values. These values were found to be around 3.16 and 0.34 respectively for the peak at small- and wide-angle which is about double of the values as observed for the compound **25d**. A reason for the stabilization of mesophase in case of **25d**-GNPs could be due to longer terminal alkyl

spacer length of thiol **25d** which avoids crowding of the mesogens on gold surface and thus ensures a uniform coating of mesogens on GNPs which may not be feasible in case of shorter spacer length of thiols **25a**-**5c**.

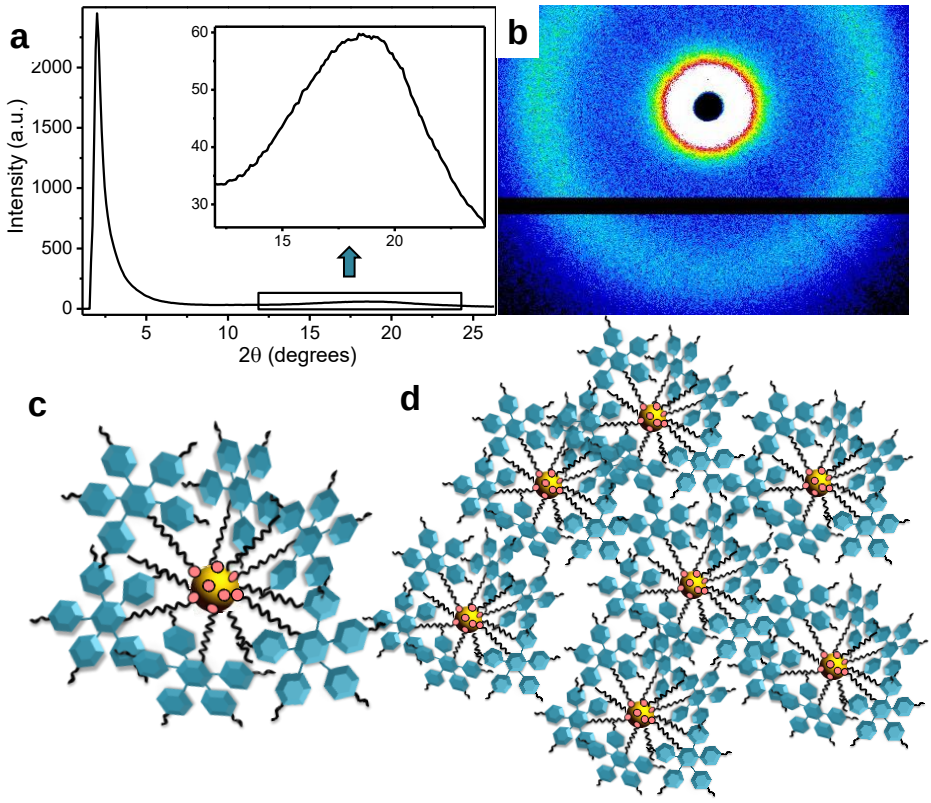

Figure 5.12 (a) The X-ray diffraction pattern of **25d**-GNPS in N_D phase at room-temperature and (b) corresponding 2D diffraction pattern. (c) A model unit of **25d**-GNPs and (d) their arrangement in N_D mesophase.

To investigate the physical properties and bring out the effect of the GNPs, we conducted birefringence and dielectric measurements. We used polyimide (AL-1254) coated cells with antiparallel rubbing. Such cells provide planar alignment of the calamitic nematic LCs. In case of N_D LCs, it provides homeotropic alignment of the director (i.e. the plane of discs is parallel to the substrates). Figure 5.13a shows the voltage dependent effective dielectric constant (ε_{eff}) for the compounds **25d** and **25d**-GNPs. ε_{eff} is larger for **25d**-GNPs as compared to **25d**. It shows a slight increase beyond a particular voltage and gets saturated at much higher voltage which are termed as the threshold voltages (V_{th}) for the Fréedericksz transition from the homeotropic to planar state. For example, the threshold voltages are

nearly about 3 V for **25d** and **25d**-GNPs. This transition is observed under POM. Hence, both the samples have negative dielectric anisotropy and their values are very small ($\Delta\varepsilon \approx -0.1$). Figure 5.13b shows the variation of ε_{II} in the nematic phase measured at a fixed voltage of 18 V.

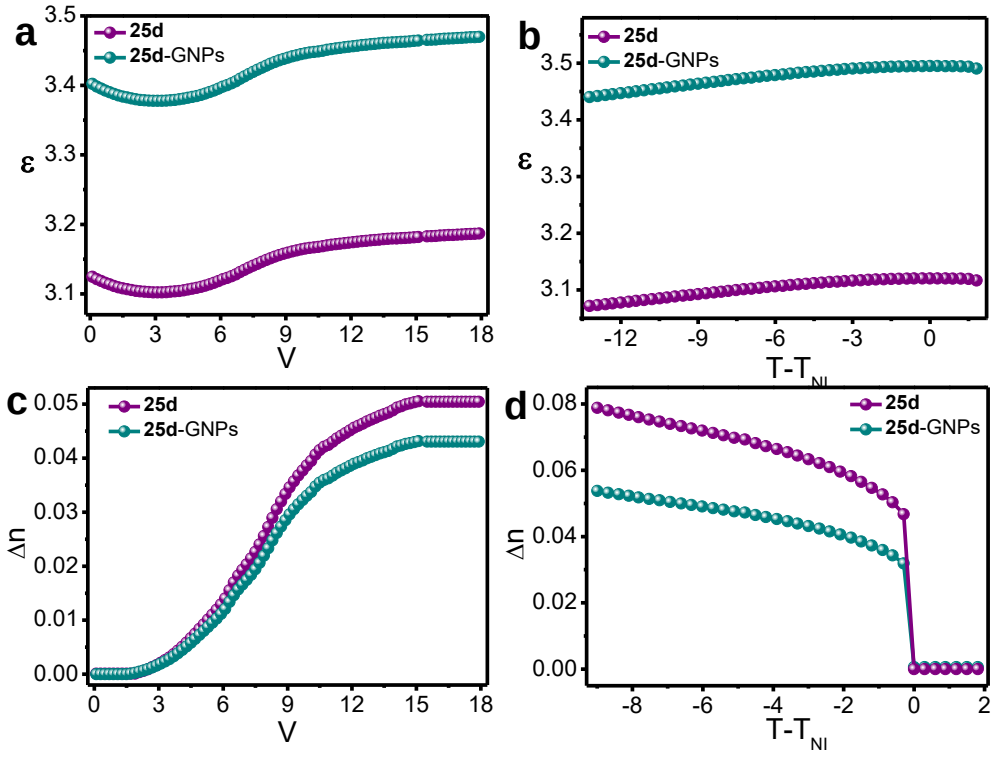

Figure 5.13 (a) Voltage dependent dielectric of compound **25d** at a fixed temperature $T-T_{NI}$ = -3.59 °C and **25d**-GNPs at a fixed temperature $T-T_{NI}$ = -4.0 °C. (b) Temperature dependent dielectric of compound **25d** and **25d**-GNPs at a fixed voltage of 18 V and frequency of 2KHz. (c) Voltage dependent birefringence (Δn) of **25d** at fixed temperature of $T-T_{NI}$ = -3.78 °C and of **25d**-GNPs at fixed temperature of $T-T_{NI}$ = -6.20 °C . (d) Temperature dependent birefringence (Δn) of **25d** and **25d**-GNPs at a fixed voltage of 20 V and frequency of 2 KHz.

It shows that ε_{II} is almost constant in the nematic phase and it is higher by about 10% in **25d** than in **25d**-GNPs. Figure 5.13c shows the variation of birefringence (Δn) with applied voltage. We observed that beyond the Fréedericksz threshold voltage (V_{th} = 3 V) Δn increases and saturates beyond 15 V. This means that the director of the N_D mesogens is completely re-orientated to the planar state. Figure 5.13d shows the temperature variation of

the birefringence measured at a fixed voltage of 18 V. It is observed that Δn in the compound **25d**-GNPs is significantly lower than in compound **25d**. For example, at $T-T_{NI}$ = -9 °C, Δn in **25d**-GNPs is about 38% smaller than that of **25d**. Since Δn is proportional to the orientational order parameter S, we conclude that inclusion of gold nanoparticle has reduced the order parameter significantly and this is consistent with our proposed model presented in Figure 5.12d where the GNPs are surrounded by PA units.

We further measured the effective electrical conductivity (σ_{eff}) of the sample as function of voltage and temperature. Figure 5.14a shows that **25d**-GNPs have larger conductivity than that of **25d**. With increasing field, it slightly increases beyond the Fréedericksz threshold voltage (3 V) since the conductivity along the director is expected to be larger than the perpendicular direction. The increase in σ_{eff} at higher voltage in both the compounds could be due to the increase in the mobility of the charges at higher voltage.

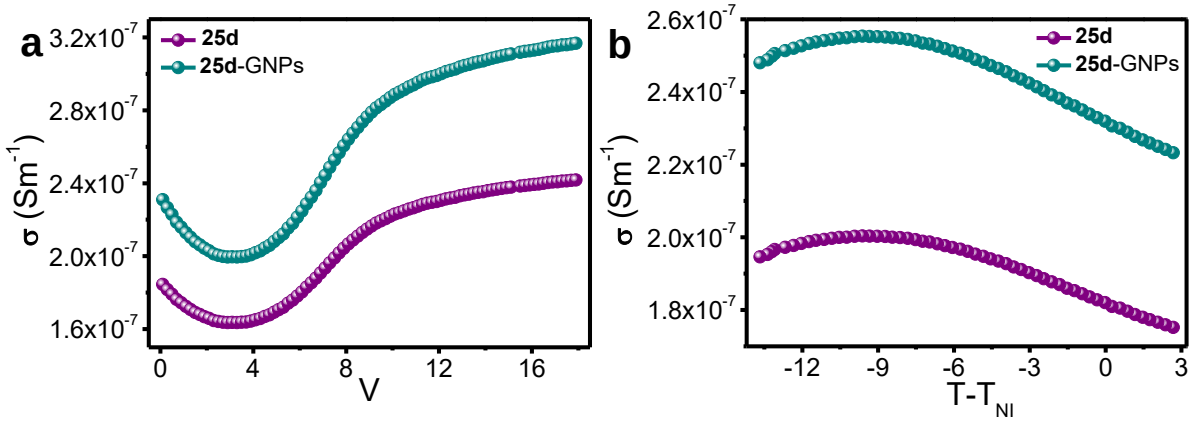

Figure 5.14 (a) Variance of conductivity of **25d** and **25d**-GNPs at a fixed temperature (-2.50 °C) (b) Temperature variation of conductivity of **25d** and **25d**-GNPs at fixed voltage of 18 V and a frequency of 2 KHz.

Figure 5.14b shows the temperature variation of σ_{II} for both the compounds measured at a frequency 2 kHz. σ_{II} in **25d**-GNPs is about 30% larger than that of **25d**. Therefore incorporation of gold nanoparticles has reduced the orientational order parameter and enhanced the electrical conductivity significantly.

Till now, only one report has been reported in the literature which shows the room-temperature thermotropic nematic GNPs by employing calamitic mesogens with thiols present at a lateral position. This report describes for the first time, the synthesis of GNPs decorated with thiol functionalized PA units which exhibits N_D phase at room-temperature. These N_D GNPs have shown enhanced dielectric response and increased conductivity values as compared to the thiols. Therefore, these GNPs exhibiting N_D mesophase at room-temperature are very interesting materials for display applications also points the way towards development of new anisotropic soft materials for display applications.

5.3 Experimental Section

5.3.1 Synthesis of compound 11a The synthesis of compounds **14**, **15**, **17** and **18** has been described in the earlier reports. For the synthesis of the target compounds **11a**, monohydroxytriphenylene **18** (1 equivalent) was dissolved in *n*-butanone. To that solution, cesium carbonate (3 equivalents) was added & the mixture was stirred for 15 min followed by the addition of compound **15** & a catalytic amount of KI. The mixture was refluxed for 18 h. The solvent was evaporated & the crude was purified through column chromatography to obtain the final compound **11a**. ^{1}H NMR (400 MHz, $CDCl_3$, δ in ppm): 7.89 (s, 6H), 7.56 (m, 10H), 7.23 (m, 10H), 4.41 (m, 2H), 4.28 (t, 12H, J = 8, 4 Hz), 2.67 (m, 10H), 2.00 (m, 14H), 1.66 (m, 16H), 1.40 (m, 50H), 0.97 (m, 30H). ^{13}C NMR (400 MHz, $CDCl_3$, δ in ppm): 160.14, 149.01, 148.94, 148.94, 148.92, 144.03, 143.98, 143.74, 131.78, 131.67, 131.54, 128.78, 128.55, 128.54, 123.62, 123.55, 120.71, 120.48, 120.45, 120.11, 107.29, 99.51, 99.41, 97.34, 87.08, 84.05, 71.92, 69.73, 69.69, 69.53, 50.56, 37.87, 36.01, 35.99, 35.88, 34.67, 31.77, 31.73, 31.70, 31.63, 31.50, 31.47, 31.01, 30.98, 30.89, 30.63, 29.45, 26.94, 26.29, 26.21, 25.89, 22.70, 22.57, 22.52, 14.16, 14.10, 14.08, 14.05, 8.35, 7.46. FT-IR (cm^{-1}): 3026, 2955, 2930, 2858, 2209, 1616, 1512, 1467, 1433, 1387, 1381, 1347, 1262, 1170, 1115, 1081, 1041, 1021, 986, 929, 866, 839, 769, 658, 645, 625. UV-vis (nm): 237, 263, 280, 338, 381, 418. MS (MALDI): *m/z* for $C_{125}H_{158}O_7$ 1772.2041; Found 1772.2258.

5.3.2 Synthesis of compound 11b Compound was synthesized according to a similar procedure to **11a**. ^{1}H NMR (400 MHz, $CDCl_3$, δ in ppm): 7.88 (s, 6H), 7.58 (m, 10H), 7.21 (m, 10H), 4.41 (t, 2H, J = 8, 4Hz), 4.26 (m, 12H), 2.64 (m, 10H), 1.98 (m, 14H), 1.66 (m,

20H), 1.40 (m, 50H), 0.94 (m, 30H). ^{13}C NMR (400 MHz, $CDCl_3$, δ in ppm): 160.22, 149.00, 148.96, 144.04, 143.96, 143.73, 131.80, 131.68, 131.60, 128.79, 128.57, 128.55, 124.11, 123.65, 123.63, 120.73, 120.54, 120.50, 120.13, 107.31, 99.55, 99.39, 97.33, 87.11, 86.63, 84.11, 74.73, 69.70, 36.02, 35.96, 31.74, 31.52, 31.49, 31.01, 30.98, 30.68, 29.71, 29.59, 29.56, 29.47, 26.42, 26.25, 25.92, 25.90, 22.73, 22.72, 22.59, 22.56, 14.11, 14.07. FT-IR (cm^{-1}): 3026, 2955, 2929, 2858, 2208, 1616, 1512, 1467, 1434, 1385, 1347, 1262, 1170, 1115, 1082, 1041, 1021, 976, 963, 929, 898, 769, 752, 727, 667, 645, 625. UV-vis (nm): 237, 264, 280, 338, 380, 416. MS (MALDI): *m/z* for $C_{127}H_{162}O_7$ 1800.2354; Found 1800.2162.

5.3.3 Synthesis of compound 11c Compound was synthesized according to a similar procedure to **11a**. ^{1}H NMR (400 MHz, $CDCl_3$, δ in ppm): 7.88 (s, 6H), 7.56 (m, 10H), 7.21 (m, 10H), 4.41 (t, 2H, J = 4, 8 Hz), 4.27 (t, 12H, J = 8, 4 Hz), 2.66 (m, 10H), 1.98 (m, 14H), 1.65 (m, 24H), 1.42 (m, 50H), 0.96 (m, 30H). ^{13}C NMR (400 MHz, $CDCl_3$, δ in ppm): 160.25, 148.97, 144.03, 143.92, 143.73, 131.81, 131.70, 131.69, 131.62, 131.58, 131.52, 128.77, 128.56, 128.55, 124.09, 123.63, 120.75, 120.58, 120.51, 120.13, 107.32, 99.54, 99.38, 87.13, 84.12, 74.78, 69.71, 36.02, 36.00, 31.75, 31.52, 31.50, 31.02, 31.00, 30.69, 29.74, 29.72, 29.64, 29.59, 29.47, 26.95, 26.46, 26.29, 25.91, 22.74, 22.72, 22.59, 14.12, 14.10, 14.08. FT-IR (cm^{-1}): 3026, 2955, 2929, 2857, 2208, 1617, 1512, 1467, 1435, 1386, 1348, 1262, 1171, 1114, 1082, 1042, 1021, 979, 929, 838, 726. UV-vis (nm): 239, 262, 280, 335, 370, 414. MS (MALDI): *m/z* for $C_{129}H_{166}O_7$1828.2667; Found 1828.2506.

5.3.4 Synthesis of compound 11d Compound was synthesized according to a similar procedure to **11a**. ^{1}H NMR (400 MHz, $CDCl_3$, δ in ppm): 7.85 (s, 6H), 7.53 (m, 10H), 7.19 (m, 10H), 4.37 (t, 2H, J = 8 Hz), 4.25 (t, 12H, J = 4, 8 Hz), 2.65 (m, 10H), 1.96 (m, 14H), 1.61 (m, 28H), 1.36 (m, 50H), 0.94 (m, 30H). ^{13}C NMR (400 MHz, $CDCl_3$, δ in ppm): 148.96, 131.79, 131.69, 131.67, 131.61, 131.59, 131.57, 128.55, 123.61, 107.31, 69.71, 35.90, 31.71, 31.48, 30.96, 29.76, 29.74, 29.70, 29.64, 29.56, 29.44, 25.87, 22.69, 22.55, 14.09, 14.06. FT-IR (cm^{-1}): 3027, 2955, 2929, 2857, 2209, 1617, 1512, 1467, 1456, 1435, 1387, 1381, 1349, 1300, 1262, 1171, 1115, 1042, 1021, 929, 867, 838, 726. UV-vis (nm): 238, 261, 280, 336, 380, 417. MS (MALDI): *m/z* for $C_{131}H_{170}O_7$1856.2980; Found 1856.2778.

5.3.5 Synthesis of compound 12a For the synthesis of the target compound **12a**, compound **20** (1 equivalent) was dissolved in aqueous KOH (1.1 equivalent) solution. To that solution, compound **15** (6 equivalents) was added followed by the addition of tetraoctylammonium bromide in catalytic amounts. The reaction mixture was refluxed under vigorous stirring for 5 hours & was then cooled to room temperature. The compound was extracted with chloroform. The organic layer was washed with brine & dried over anhydrous sodium sulphate. The chloroform was removed by rotary evaporation and the resulting residue was purified by column chromatography over silica gel using hexane & ethyl acetate as eluent to yield pure compound **12a**. ^{1}H NMR (400 MHz, $CDCl_3$, δ in ppm): 8.79 (t, 2H, J = 1.6 Hz), 8.77 (d, 4H, J = 1.6 Hz), 7.53 (m, 40H), 7.17 (m, 40H), 4.41 (t, 8H, J = 4, 8 Hz), 4.28 (t, 8H, J = 8, 4 Hz), 2.63 (m, 40H), 1.98 (m, 8H), 1.66 (m, 48H), 1.31 (m, 96H), 0.96 (m, 60H). ^{13}C NMR (400 MHz, $CDCl_3$, δ in ppm): 165.0, 160.08, 143.92, 143.62, 132.08, 131.79, 131.69, 131.54, 128.77, 128.51, 124.12, 120.78, 120.50, 120.04, 99.51, 99.33, 97.32, 87.11, 86.66, 84.13, 36.10, 36.01, 35.94, 34.69, 31.97, 31.63, 31.53, 30.98, 30.94, 29.75, 29.41, 26.17, 22.72, 22.58, 22.54, 18.79, 14.16, 14.08, 11.47. FT-IR (cm^{-1}): 3026.95, 2953.43, 2926.12, 2855.35, 2206.00, 1903.38, 1725.69, 1606.06, 1511.33, 1463.68, 1423.25, 1377.33, 1345.33, 1311.38, 1233.90, 1191.62, 1112.20, 1083.02, 1019.30, 982.59, 923.47, 896.19, 837.22, 810.58, 757.83, 726.77, 686.28. UV-vis (nm): 237, 263, 338, 381, 418. Elemental analysis (%): Calculated C 87.09 H 7.99 N 0.63. Found C 87.17 H 8.19 N 0.98.

5.3.6 Synthesis of compound 12b Compound was synthesized according to a similar procedure to **12a**. ^{1}H NMR (400 MHz, $CDCl_3$, δ in ppm): 8.85 (t, 2H, J = 1.2 Hz), 8.82 (d, 4H, J = 1.6 Hz), 7.56 (m, 40H), 7.21 (d, 40H, J = 8 Hz), 4.42 (t, 8H, J = 8, 4Hz), 4.35 (t, 8H, J = 8, 4 Hz), 2.67 (m, 40H), 1.98 (m, 8H), 1.77 (m, 8H), 1.68 (m, 40H), 1.37 (m, 112H), 0.95 (m, 60H). ^{13}C NMR (400 MHz, $CDCl_3$, δ in ppm): 165.13, 160.20, 152.22, 143.98, 143.90, 143.68, 132.17, 131.81, 131.71, 131.60, 128.79, 128.54, 124.11, 120.80, 120.56, 120.08, 99.58, 99.36, 97.35, 87.17, 86.70, 84.18, 65.91, 36.00, 32.00, 31.56, 31.04, 31.00, 30.66, 29.78, 29.58, 29.45, 29.32, 26.39, 25.99, 22.62, 22.60, 14.20,14.12. FT-IR (cm^{-1}): 3026.02, 2953.93, 2925.79, 2854.69, 2206.52, 1903.12, 1725.88, 1606.39, 1511.43, 1464.10, 1423.79, 1377.45, 1345.64, 1311.20, 1234.33, 1189.35, 1112.49, 1084.02, 1019.44, 922.22, 836.38,

813.59, 758.63, 725.59, 684.96. UV-vis (nm): 237, 264, 338, 380, 416. Elemental analysis (%): Calculated C 87.06 H 8.14 N 0.61. Found C 86.76 H 8.23 N 0.85.

5.3.7 Synthesis of compound 12c Compound was synthesized according to a similar procedure to **12a**. ^{1}H NMR (400 MHz, $CDCl_3$, δ in ppm): 8.82 (t, 2H, J = 1.6 Hz), 8.79 (d, 4H, J = 1.6 Hz), 7.54 (m, 40H), 7.17 (dd, 40H, J = 2 Hz), 4.37 (m, 16H), 2.63 (m, 40H), 1.93 (m, 8H), 1.81 (m, 8H), 1.63 (m, 40H), 1.345 (m, 128H), 0.92 (m, 60H). ^{13}C NMR (400 MHz, $CDCl_3$, δ in ppm): 165.19, 160.02, 143.98, 143.67, 143.64, 131.76, 131.65, 131.57, 128.73, 128.53, 128.51, 120.53, 99.51, 99.34, 87.01, 86.62, 84.09, 35.97, 31.05, 30.99, 29.59, 29.35, 28.73, 25.99, 22.56, 14.07. FT-IR (cm^{-1}): 3025.98, 2953.99, 2925.09, 2854.12, 2206.40, 1725.89, 1606.37, 1511.28, 1464.25, 1423.46, 1377.41, 1345.81, 1311.47, 1234.01, 1188.43, 1112.10, 1084.19, 1019.54, 976.86, 921.69, 836.03, 812.88, 758.38, 724.27, 684.82. UV-vis (nm): 238, 261, 338, 380, 420. Elemental analysis (%): Calculated C 87.02 H 8.29 N 0.60. Found C 87.48 H 8.42 N 0.99.

5.3.8 Synthesis of compound 12d Compound was synthesized according to a similar procedure to **12a**. ^{1}H NMR (400 MHz, $CDCl_3$, δ in ppm): 8.83 (s, 2H), 8.79 (d, 4H, J = 1.6 Hz), 7.53 (m, 40H), 7.18 (d, 40H, J = 8 Hz), 4.38 (m, 16H), 2.63 (t, 40H, J = 8 Hz), 1.93 (m, 8H), 1.83 (m, 8H), 1.61 (m, 40H), 1.35 (m, 144H), 0.91 (m, 60H). ^{13}C NMR (400 MHz, $CDCl_3$, δ in ppm): 166.32, 159.99, 152.22, 143.93, 131.79, 131.70, 131.61, 131.52, 131.47, 128.80, 128.54, 127.94, 126.59, 120.46, 120.08, 99.42, 97.32, 87.09, 84.07, 77.38, 77.07, 76.75, 74.13, 69.81, 67.38, 65.76, 53.18, 42.05, 35.98, 35.93, 31.53, 30.97, 30.92, 30.29, 29.75, 28.65, 22.58, 14.09. FT-IR (cm^{-1}): 3027.97, 2926.58, 2855.81, 2208.45, 1727.61, 1606.86, 1568.42, 1512.53, 1463.93, 1423.93, 1378.28, 1347.63, 1316.54, 1235.62, 1189.17, 1111.48, 1084.39, 1020.08, 981.52, 923.60, 886.78, 838.50, 759.05, 738.17, 685.58. UV-vis (nm): 238, 262, 338, 380, 418.

5.3.9 Synthesis of compound 24a For the synthesis of compound **24a**, compound **14** (1 equivalent) was dissolved in DMF followed by the addition of potassium thioacetate (3 equivalents). The reaction mixture was stirred at room-temperature for 8 hours. After completion of reaction, the mixture was poured into water and the organic layer was extracted with dichloromethane. The compound was then purified through column

chromatography over silica gel to get the pure product **24a**. ^{1}H NMR (400 MHz, $CDCl_3$, δ in ppm): 7.55 (m, 10H), 7.21 (m, 10H), 4.38 (t, 2H, J = 4, 8 Hz), 2.83 (t, 2H, J = 8, 4 Hz), 2.66 (m, 10H), 2.34 (s, 3H), 1.94 (p, 2H, J = 8, 8, 8, 4 Hz), 1.64 (m, 14H), 1.42 (m, 24H), 0.94 (m, 15H). ^{13}C NMR (400 MHz, $CDCl_3$, δ in ppm): 196.00, 160.16, 144.05, 143.97, 143.74, 131.79, 131.67, 131.58, 128.77, 128.60, 124.13, 120.69, 120.46, 120.09, 99.58, 99.39, 97.35, 87.07, 86.59, 84.04, 74.51, 36.00, 31.52, 30.99, 30.66, 30.45, 29.49, 29.12, 28.80, 25.96, 22.58, 14.08. FT-IR (cm^{-1}): 3079.7, 3031.3, 2958.8, 2929.1, 2857.5, 2206.1, 1690.7, 1606.1, 1512.4, 1463.7, 1423.9, 1377.2, 1348.0, 1308.1, 1262.0, 1200.0, 1177.0, 1139.0, 1107.9, 1082.8, 1019.4, 961.7, 852.3, 812.9, 728.0, 629.4, 530.2. UV-vis (nm): 236, 263, 338, 380, 418. MS (MALDI): *m/z* for $C_{79}H_{90}O_2S$ 1102.6662; Found 1102.7709.

5.3.10 Synthesis of compound 24b Compound was synthesized according to a similar procedure to **24a**. ^{1}H NMR (400 MHz, $CDCl_3$, δ in ppm): 7.56 (m, 10H), 7.20 (m, 10H), 4.38 (t, 2H, J = 4, 8 Hz), 2.85 (t, 2H, J = 8 Hz), 2.66 (m, 10H), 2.34 (s, 3H), 1.94 (p, 2H, J = 4, 8, 8, 8 Hz), 1.66 (p, 12H, J = 8, 8, 4, 8 Hz), 1.54 (p, 2H, J = 4, 8, 8, 8 Hz), 1.35 (m, 26H), 0.93 (t, 15H, J = 8, 4 Hz). ^{13}C NMR (400 MHz, $CDCl_3$, δ in ppm): 196.07, 160.22, 144.04, 143.94, 143.73, 131.78, 131.67, 131.59, 128.75, 128.56, 124.08, 120.69, 120.51, 120.10, 99.54, 99.38, 97.31, 87.08, 86.60, 84.07, 74.72, 35.99, 31.52, 31.01, 30.98, 30.67, 30.57, 29.17, 29.14, 28.84, 26.32, 22.58, 14.09. FT-IR (cm^{-1}): 3029.6, 2929.1, 2856.9, 2206.5, 1692.9, 1606.2, 1512.3, 1463.7, 1423.6, 1377.6, 1348.2, 1301.2, 1262.7, 1200.6, 1179.1, 1134.6, 1111.7, 1082.8, 1019.4, 957.3, 845.8, 814.4, 729.8, 627.8, 530.6. UV-vis (nm): 236, 263, 338, 381, 418. MS (MALDI): *m/z* for $C_{81}H_{94}O_2S$ 1130.6975; Found 1130.7202.

5.3.11 Synthesis of compound 24c Compound was synthesized according to a similar procedure to **24a**. ^{1}H NMR (400 MHz, $CDCl_3$, δ in ppm): 7.54 (m, 10H), 7.20 (t, 10H, J = 8 Hz), 4.38 (t, 2H, J = 4, 8 Hz), 2.87 (t, 2H, J = 8 Hz), 2.65 (t, 10H, J = 8, 4 Hz), 2.34 (s, 3H), 1.94 (p, 2H, J = 4, 8, 8, 4 Hz), 1.66 (m, 12H), 1.54 (m, 2H), 1.31 (m, 28H), 0.93 (t, 15H, J = 8 Hz). ^{13}C NMR (400 MHz, $CDCl_3$, δ in ppm): 196.12, 166.66, 144.03, 143.92, 131.78, 131.66, 131.60, 128.74, 128.56, 124.06, 120.46, 120.11, 99.53, 87.07, 84.07, 74.79, 35.99, 31.50, 31.01, 30.66, 29.53, 29.49, 29.19, 28.87, 26.36, 22.58, 14.08. FT-IR (cm^{-1}): 3083.1, 3026.9, 2958.8, 2928.4, 2856.0, 2207.8, 1693.2, 1601.7, 1512.2, 1463.8, 1424.6, 1380.7, 1348.2, 1262.4, 1202.6, 1180.4, 1134.0, 1084.5, 1019.7, 965.8, 837.9, 817.7, 731.4, 626.6,

550.8, 534.6. UV-vis (nm): 236, 260, 338, 382, 419. MS (MALDI): *m/z* for $C_{83}H_{98}O_2S$ 1158.7288; Found 1158.7325.

5.3.12 Synthesis of compound 24d Compound was synthesized according to a similar procedure to **24a**. ^{1}H NMR (400 MHz, $CDCl_3$, δ in ppm): 7.56 (m, 10H), 7.21 (m, 10H), 4.39 (t, 2H, *J* = 4, 8 Hz), 2.88 (t, 2H, *J* = 8, 4 Hz), 2.66 (t, 10H, *J* = 8 Hz), 2.34 (s, 3H), 1.95 (p, 2H, *J* = 4, 8, 8, 8 Hz), 1.63 (m, 14H), 1.33 (m, 30H), 0.94 (t, 15H, *J* = 4, 8 Hz). ^{13}C NMR (400 MHz, $CDCl_3$, δ in ppm): 196.12, 160.26, 144.03, 143.91, 131.79, 131.67, 131.61, 128.74, 128.57, 128.55, 124.08, 120.71, 120.54, 120.13, 99.53, 99.38, 97.31, 87.10, 86.62, 84.10, 74.81, 36.01, 31.52, 31.01, 30.98, 29.67, 29.55, 29.20, 28.90, 26.41, 22.59, 140.09. FT-IR (cm^{-1}): 3027.0, 2958.8, 2928.0, 2855.6, 2207.8, 1693.6, 1608.6, 1512.3, 1463.7, 1424.6, 1377.2, 1348.5, 1261.7, 1202.6, 1177.0, 1134.0, 1107.9, 1085.6, 1019.8, 954.3, 837.9, 724.5, 626.6, 531.6. UV-vis (nm): 236, 263, 338, 381, 419. MS (MALDI): *m/z* for $C_{85}H_{102}O_2S$ 1186.7601; Found 1186.7948.

5.3.13 Synthesis of compound 25a For the synthesis of thiol **25a**, compound **24** was dissolved in 1:1 mixture of methanol and dichloromethane. To the above solution, a pinch of potassium carbonate was added. The reaction mixture was stirred at room-temperature for 4-5 hours. The mixture was then poured into water and extracted with dichloromethane. The organic layer was washed with brine & dried over anhydrous sodium sulphate. The dichloromethane was removed by rotary evaporation and the resulting residue was purified by column chromatography over silica gel (230-400) using hexane & ethyl acetate as eluent to yield compound **25a**. ^{1}H NMR (400 MHz, $CDCl_3$, δ in ppm): 7.53 (m, 10H), 7.19 (t, 10H, *J* = 8 Hz), 4.37 (t, 2H, *J* = 4, 8 Hz), 2.64 (m, 12H), 1.94 (p, 2H, *J* = 4, 8, 8, 4), 1.65 (m, 14H), 1.49 (q, 2H, *J* = 8 Hz), 1.36 (m, 20H), 0.92 (m, 15H). ^{13}C NMR (400 MHz, $CDCl_3$, δ in ppm): 160.14, 143.98, 131.79, 131.67, 131.57, 128.77, 128.58, 128.50, 120.49, 120.08, 99.59, 99.36, 97.32, 87.09, 84.05, 38.97, 35.99, 31.50, 30.96, 29.21, 28.54, 26.09, 22.51, 14.07. FT-IR (cm^{-1}): 3031.3, 2955.4, 2928.6, 2856.9, 2207.8, 1605.1, 1512.4, 1463.5, 1424.9, 1377.2, 1347.2, 1304.7, 1266.7, 1204.5, 1177, 1114.8, 1084.1, 1019.8, 966.2, 838.0, 821.2, 731.4, 552.1, 531.1. UV-vis (nm): 237, 263, 338, 382, 417. MS (MALDI): *m/z* for $C_{77}H_{88}OS$ 1060.6556; Found 1060.6500.

5.3.14 Synthesis of compound 25b Compound was synthesized according to a similar procedure to **25a**. ^{1}H NMR (400 MHz, $CDCl_3$, δ in ppm): 7.54 (m, 10H), 7.20 (m, 10H), 4.38 (t, 2H, J = 8, 4 Hz), 2.64 (m, 12H), 1.94 (m, 2H), 1.66 (m, 14H), 1.37 (m, 26H), 0.93 (m, 15H). ^{13}C NMR (400 MHz, $CDCl_3$, δ in ppm): 162.18, 143.92, 143.69, 131.79, 131.67, 131.59, 128.77, 128.55, 124.09, 120.54, 120.49, 120.10, 99.51, 99.37, 87.11, 86.64, 84.10, 52.62, 39.11, 36.00, 31.50, 30.99, 30.96, 30.61, 29.55, 29.29, 28.59, 26.37, 22.57, 14.07. FT-IR (cm^{-1}): 3031.3, 2928.1, 2856.3, 2208.2, 1605.1, 1512.5, 1463.5, 1424.4, 1379.5, 1347.5, 1302.5, 1262.1, 1203.4, 1181.4, 1115.4, 1082.6, 1019.9, 975.9, 837.7, 816.4, 726.5, 551.8, 530.2. UV-vis (nm): 236, 262, 335, 382, 419. MS (MALDI): *m/z* for $C_{79}H_{92}OS$ 1088.6869; Found 1088.6685.

5.3.15 Synthesis of compound 25c Compound was synthesized according to a similar procedure to **25a**. ^{1}H NMR (400 MHz, $CDCl_3$, δ in ppm): 7.53 (m, 10H), 7.19 (t, 10H, J = 8, 4 Hz), 4.37 (t, 2H, J = 4, 8 Hz), 2.66 (m, 12H), 1.93 (p, 2H, J = 8, 8, 4, 8 Hz), 1.65 (m, 14H), 1.31 (m, 30H), 0.93 (t, 15H, J = 4, 8 Hz). ^{13}C NMR (400 MHz, $CDCl_3$, δ in ppm): 160.23, 144.02, 143.91, 131.78, 131.66, 131.60, 128.74, 128.55, 124.07, 120.70, 120.11, 99.52, 87.08, 84.08, 74.78, 39.13, 36.01, 31.50, 31.01, 30.98, 29.64, 26.40, 22.57, 14.08. FT-IR (cm^{-1}): 3027.0, 2955.1, 2928.0, 2855.7, 2207.9, 1606.5, 1512.4, 1463.7, 1424.2, 1380.7, 1347.4, 1300.6, 1262.8, 1202.8, 1180.4, 1111.3, 1082.9, 1019.7, 968.9, 837.4, 821.2, 728.0, 552.0, 531.1. UV-vis (nm): 234, 263, 328, 379, 420. MS (MALDI): *m/z* for $C_{81}H_{96}OS$ 1116.7182; Found 1116.7401.

5.3.16 Synthesis of compound 25d Compound was synthesized according to a similar procedure to **25a**. ^{1}H NMR (400 MHz, $CDCl_3$, δ in ppm): 7.56 (t, 10H, J = 8 Hz), 7.20 (t, 10H, J = 8, 4 Hz), 4.39 (t, 2H, J = 4, 8 Hz), 2.68 (m, 12H), 1.95 (p, 2H, J = 4, 8, 8, 4), 1.68 (m, 14H), 1.32 (m, 34H), 0.94 (t, 15H, J = 4, 8 Hz). ^{13}C NMR (400 MHz, $CDCl_3$, δ in ppm): 160.26, 144.01, 143.89, 143.71, 132.33, 132.22, 131.79, 131.67, 131.60, 129.09, 128.75, 128.55, 128.52, 124.07, 120.73, 120.55, 120.50, 120.11, 99.53, 99.38, 97.30, 87.12, 86.64, 84.11, 74.79, 39.17, 36.01, 31.50, 30.99, 30.64, 29.69, 29.29, 28.62, 26.42, 26.19, 22.57, 14.08. FT-IR (cm^{-1}): 3026.8, 2955.2, 2927.6, 2855.3, 2207.8, 1606.5, 1512.3, 1463.7, 1424.6, 1377.2, 1347.2, 1258.1, 1203.0, 1179.5, 1084.1, 1019.9, 978.7, 837.7, 817.7, 721.9, 552.04.

UV-vis (nm): 235, 263, 338, 381, 418. MS (MALDI): *m/z* for $C_{83}H_{100}OS$ 1144.7495; Found 1144.7487.

References

(1) Kumar, S. *Chem. Soc. Rev.* **2006**, *35*, 83-109.

(2) Wöhrle, T.; Wurzbach, I.; Kirres, J.; Kostidou, A.; Kapernaum, N.; Litterscheidt, J.; Haenle, J. C.; Staffeld, P.; Baro, A.; Giesselmann, F.; Laschat, S. *Chem. Rev*. **2016**, *116*, 1139-1241.

(3) Kumar, S. in Chemistry Of Discotic Liquid Crystals: From Monomers to Polymers, CRS Press, Taylor & Francis Group: Boca Raton, **2011**.

(4) Lu, M.; Yang, K. H. *Jpn. J. Appl. Phys.* **2000**, *36*, L412-L415.

(5) Mori, H.; Itoh, Y.; Nishuira, Y.; Nakamura, T.; Shinagawa, Y. *Jpn. J. Appl. Phys*. **1997**, *36*, 143-147.

(6) Bisoyi, H. K.; Kumar, S. *Chem. Soc. Rev.* **2010**, *39*, 264-285.

(7) Phillips, T. J.; Jones, J. C.; McDonnell, D. G. *Liq. Cryst.* **1993**, *15*, 203-215.

(8) Hindmarsh, P.; Watson, M. J.; Hird, M.; Goodby, J. W. *J. Mater. Chem.* **1995**, *5*, 2111-2123.

(9) Praefcke, K.; Kohne, B.; Singer, D. *Angew. Chem. Int. Ed. Engl*. **1990**, *29*, 177-179.

(10) Destrade, C.; Gasparoux, H.; Babeau, A.; Tinh, N. H. *Mol. Cryst. Liq. Cryst.* **1981**, *67*, 37-47.

(11) Lee, W. K.; Wintner, B. A.; Fontes, E.; Heiney, P. A.; Ohba, M.; Haseltine, J. N.; Smith, A. B. *Liq. Cryst.* **1989**, *4*, 87-102.

(12) Mamlock, L.; Malthete, J.; Tinh, N. H.; Destrade, C.; Levelut, A. M. *J. Phys. Lett.* **1982**, *43*, 641-647.

(13) Praefcke, K.; Kohne, B.; Gutbier, K.; Johnen, N.; Singer, D. *Liq. Cryst.* **1989**, *5*, 233-249.

(14) Imrie, C. T.; Lu, Z.; Picken, S. J.; Yildirim, Z. *Chem. Commun*. **2007**, 1245-1247.

(15) Kim, B. G.; Kim, S.; Park, S. Y. *Tetrahedron Lett.* **2001**, *42*, 2697-2699.

(16) Kumar, S.; Varshney, S. K. *Org. Lett.* **2002**, *4*, 157-159.

(17) Kumar, S.; Varshney, S. K. *Liq. Cryst*. **2001**, *28*, 161-163.

(18) Zhang, L.; Hughes, D. L.; Cammidge, A. N. *J. Org. Chem.* **2012**, *77*, 4288-4297.

(19) Zhang, L.; Gopee, H.; Hughes, D. L.; Cammidge, A. N. *Chem. Commun.* **2010**, *46*, 4255-4257.

(20) Lee, J. H.; Jang, I.; Hwang, S. H.; Lee, S. J.; Yoo, S. H.; Jho, J. Y. *Liq. Cryst.* **2012**, *39*, 973-981.

(21) Lee, J. H.; Han, M.-J.; Hwang, S. H.; Jang, I.; Lee, S. J.; Yoo, S. H.; Jho, J. Y.; Park, S.-Y. *Tetrahedron Lett.* **2005**, *46*, 7143-7146.

(22) Kumar, S.; Varshney, S. K. *Angew. Chem. Int. Ed*. **2000**, *112*, 3270-3272.

(23) Kumar, S.; Varshney, S. K.; Chauhan, D. *Mol. Cryst. Liq. Cryst*. **2003**, *396*, 241-250.

(24) Varshney, S. K.; Prasad, V.; Takezoe, H. *Liq. Cryst.* **2011**, *38*, 53-60.

(25) Kohmoto, S.; Mori, E.; Kishikawa, K. *J. Am. Chem. Soc.* **2007**, *129*, 13364-13365.

(26) Chien, S. C.; Chen, H. H.; Chen, H. C.; Yang, Y. L.; Hsu, H. F.; Shih, T. L.; Lee, J. J. *Adv. Funct. Mater*. **2007**, *17*, 1896-1902.

(27) Chen, H. H.; Lin, H. A.; Chien, S. C.; Wang, T.-H.; Hsu, H.-F.; Shih, T.-L.; Wu, C. *J. Mater. Chem.* **2012**, *22*, 12718-12722.

(28) Praefcke, K.; Kohne, B.; Singer, D.; Demus, D.; Pelzl, G.; Diele, S. *Liq. Cryst.* **1990**, *7*, 589-594.

(29) Gupta, M.; Bala, I.; Pal, S. K. *Tetrahedron Lett.* **2014**, *55*, 5836-5840.

(30) Gupta, M.; Pal, S. K. *Liq. Cryst.* **2015**, *42*, 1250-1256.

(31) Gupta, M.; Pal, S. K. *Langmuir* **2016**, *32*, 1120-1126.

(32) Becke, A. D. *J. Chem. Phys.* **1993**, *98*, 5648-5652.

(33) Grimme, S.; Antony, J.; Ehrlich, S.; Krieg, H. *J. Chem. Phys.* **2010**, *132*, 154104-154119.

(34) Zhao, Y.; Truhlar, D. *Theor. Chem. Acc.* **2008**, *120*, 215-241.

(35) VenkataSai, D.; Mirri, G.; Kouwer, P.; Sahoo, R.; Musevic, I.; Dhara, I. *Soft Matt.* **2016**, *12*, 2960-2964.

(36) Bozek, K. J. A.; Williams, V. E. *Soft Matt.* **2014**, *10*, 5749-5754.

(37) Boden, N.; Bushby, R. J.; Cammidge, A. N.; El-Mansoury, A.; Martin, P. S.; Lu, Z. *J. Mater. Chem.* **1999**, *9*, 1391-1402.

(38) Tzeng, M. C.; Liao, S. C.; Chang, T. H.; Yang, S. C.; Weng, M. W.; Yang, H. C.; Chiang, M. Y.; Kai, Z.; Wu, J.; Ong, C. W. *J. Mater. Chem.* **2011**, *21*, 1704-1712.

(39) Gupta, M.; Agarwal, N.; Arora, A.; Kumar, S.; Kumar, B.; Sheet, G.; Pal, S. K. *RSC Adv.* **2014**, *4*, 41371-41377.

(40) Sathyanarayana, P.; Varia, M. C.; Prajapati, A. K.; Kundu, B.; Sastry, V. S. S.; Dhara, S. *Phys. Rev. E* **2010**, *82*, 05070-1-4.

(41) Sathyanarayana, P.; Mathews, M.; Li, Q.; Sastry, V. S. S.; Takezoe, H.; Dhara, S. *Phys. Rev. E* **2010**, *81*, 010702-1-4.

(42) Sathyanarayana, P.; Jampani, V. S. R.; Skarabot, M.; Musevic, I.; Le, K. V.; Takezoe, H.; Dhara, S. *Phys. Rev. E* **2012**, *85***,** 011702-1-9.

(43) Goodby, J. W.; Saez, I. M.; Cowling, S. J.; Gortz, V.; Draper, M.; Hall, A. W.; Sia, S.; Cosquer, G.; Lee, S. E.; Raynes, E. P. *Angew. Chem. Int. Ed*. **2008**, *47*, 2754 – 2787.

(44) Hegmann, T.; Qi, H.; Marx, V. M. *J. Inorg. Organomet. Polym. Mater*. **2007**, *17*, 483–508.

(45) Giljohann, D. A.; Seferos, D. S.; Patel, P. C.; Millstone, J. E.; Rosi, N. L.; Mirkin, C. A. *Nano Lett*. **2007**, *7*, 3818 –3821.

(46) Huang, W. Y.; Qian, W.; Jain, P. K.; El-Sayed, M. A. *Nano Lett*. **2007**, *7*, 3227–3234.

(47) Prasad, S. K.; Sandhya, K. L.; Nair, G. G.; Hiremath, U. S.; Yelamaggad, C. V.; Sampath, S. *Liq. Cryst*. **2006**, *33*, 1121–1125.

(48) Qi, H.; Kinkead, B.; Hegmann, T. *Adv. Funct. Mater*. **2008**, *18*, 212–221.

(49) Koenig, G. M.; Meli, M. V.; Park, J. S.; de Pablo, J. J.; Abbott, N. L. *Chem. Mater*. **2007**, *19*, 1053–1061.

(50) Qi, H.; Hegmann, T. *J. Mater. Chem*. **2008**, *18*, 3288–3294.

(51) Goodby, J. W.; Saez, I. M.; Cowling, S. J.; Gçrtz, V.; Draper, M.; Hall, A. W.; Sia, S.; Cosquer, G.; Lee, S.-E.; Raynes, E. P. *Angew. Chem. Int. Ed*. **2008**, *47*, 2754–2787.

(52) Daniel, M. C.; Astruc, D. *Chem. Rev*. **2004**, *104*, 293–346.

(53) Antonietti, M.; Ozin, G. O. *Chem. Eur. J*. **2004**, *10*, 29–41.

(54) Xia, Y.; Yang, P.; Wu, S. Y.; Mayers, B.; Gates, B.; Yn, Y.; Kim, F.; Yan, H. *Adv. Mater*. **2003**, *15*, 353–389.

(55) Wirtz, M.; Martin, C. R. *Adv. Mater*. **2003**, *15*, 455–458.

(56) Brust, M.; Kiely, C. J. *Colloids Surf. A* **2002**, *202*, 175–186.

(57) Bönnemann, H.; Richards, R. M. *Eur. J. Inorg. Chem*. **2001**, 2455–2480.

(58) Burda, C.; Chen, X.; Narayanan, R.; El-Sayed, M. A. *Chem. Rev*. **2005**, *115*, 1025–1102.

(59) Ipe, B. I.; Mehima, S.; Thomas, K. G. *J. Am. Chem. Soc*. **2003**, *125*, 7174–7175.

(60) Dubertret, B.; Skourides, P.; Norris, D. J.; Noireaux, V.; Brivanlou, A. H.; Libchaber, A. *Science* **2002**, *298*, 1759–1762.

(61) Stellaci, F.; Bauer, C. A.; Meyer-Friedrichsen, T.; Wenseleers, W.; Marder, S. R.; Perry, J. W. *J. Am. Chem. Soc*. **2003**, *125*, 328–329.

(62) Lim, W. P.; Zhang, Z.; Low, H. Y.; Chin, W. S. *Angew. Chem. Int. Ed*. **2004**, *43*, 5685–5689.

(63) Fukumi, K.; Chayahara, A.; Kadono, K.; Sakaguchi, T.; Horino, Y.; Miya, M.; Fujji, K.; Hayakawa, J.; Satou, M. *J. Appl. Phys*. **1994**, *75*, 3075–3080.

(64) Rockstuhl, C.; Lederer, F.; Etrich, C.; Pertsch, T.; Scharf, T. *Phys. Rev. Lett*. **2007**, *99*, 017401-4.

(65) Donnio, B.; García-Vazquez, P.; Gallani, J.-L.; Guillon, D.; Terazzi, E. *Adv. Mater*. **2007**, *19*, 3534−3539.

(66) Draper, M.; Saez, I. M.; Cowling, S. J.; Gai, P.; Heinrich, B.; Donnio, B.; Guillon, D.; Goodby, J. W. *Adv. Funct. Mater*. **2011**, *21*, 1260−1278.

(67) Cseh, L.; Mehl, G. H. *J. Am. Chem. Soc*. **2006**, *128*, 13376− 13377.

(68) Cseh, L.; Mehl, G. H. *J. Mater. Chem*. **2007**, *17*, 311−315.

(69) Zeng, X. B.; Liu, F.; Fowler, A. G.; Ungar, G.; Cseh, L.; Mehl, G. H.; Macdonald, J. E. *Adv. Mater*. **2009**, *21*, 1746−1750.

(70) Qi, H.; Hegmann, T. *J. Mater. Chem*. **2006**, *16*, 4197−4205.

(71) Marx, V. M.; Girgis, H.; Heiney, P. A.; Hegmann, T. *J. Mater. Chem*. **2008**, *18*, 2983−2994.

(72) Frein, S.; Boudon, J.; Vonlanthen, M.; Scharf, T.; Barbera, J.; Suss-Fink, G.; Burgi, T.; Deschenaux, R. *Helv. Chim. Acta* **2008**, *91*, 2321−2337.

(73) Jeng, S. C.; Hwang, S. J.; Yang, C. Y. *Opt. Lett*. **2009**, *34*, 455– 457.

(74) Hwang, S. J.; Jeng, S. C.; Yang, C. Y.; Kuo, C. W.; Liao, C. C. *J. Phys. D: Appl. Phys.* **2009**, *42*, 025102(1)-025102(6).

(75) Teng, W. Y.; Jeng, S. C.; Kuo, C. W.; Lin, Y. R.; Liao, C. C.; Chin, W. K. *Opt. Lett*. **2008**, *33*, 1663–1665.

(76) Qi, H.; Hegmann, T. *J. Mater. Chem*. **2008**, *18*, 3288 –3294.

(77) Kundu, S.; Akimoto, M.; Hirayama, I.; Inoue, M.; Kobayashi, S.; Takatoh, K. *Jpn. J. Appl. Phys*. **2008**, *47*, 4751–4754.

(78) Qi, H.; Kinkead, B.; Hegmann, T. *Adv. Funct. Mater*. **2008**, *18*, 212–221.

(79) Kuo, C. W.; Jeng, S. C.; Wang, H. L.; Liao, C. C. *Appl. Phys. Lett*. **2007**, *91*, 141103-3.

(80) Qi, H.; Hegmann, T. *J. Mater. Chem*. **2006**, *16*, 4197–4205.

(81) Qi, H.; Kinkead, B.; Marx, V. M.; Zhang, H. R.; Hegmann, T. *ChemPhysChem*. **2009**, *10*, 1211–1218.

(82) Qi, H.; ÓNeil, J.; Hegmann, T. *J. Mater. Chem*. **2008**, *18*, 374–380.

(83) Qi, H.; Kinkead, B.; Hegmann, *T. Proc. SPIE* **2008**, *6911*, 691106(1)-691106(11).

(84) Yoshikawa, H.; Maeda, K.; Shiraishi, Y.; Xu, J.; Shiraiki, Y.; Toshima, N.; Kobayashi, S. *Jpn. J. Appl. Phys*. **2002**, *41*, L1315–L1317.

(85) Buchnev, O.; Ouskova, E.; Reznikov, Y.; Kresse, H.; Grabar, A. *Mol. Cryst. Liq. Cryst*. **2004**, *422*, 47–55.

(86) Reznikov, Y.; Buchnev, O.; Tereshchenko, O.; Reshetnyak, V.; Glushchenko, A.; West, J. *Appl. Phys. Lett*. **2003**, *82*, 1917–1919.

(87) Barmatov, E. B.; Pebalk, D. A.; Barmakova, M. V. *Langmuir*, **2004**, *20*, 10868–10871.

(88) In, I.; Jim, Y.-W.; Kim, Y. J.; Kim, S. Y. *Chem. Commun*. **2005**, 800–801.

(89) Qi, H.; Hegmann, T. *J. Mater. Chem*. **2006**, *16*, 4197–4205.

(90) Cseh, L.; Mehl, G. H. *J. Mater. Chem*. **2007**, *17*, 311-315.

(91) Kanayama, N.; Tsutsumi, O.; Kanazawa, A.; Ikeda, T. *Chem. Commun*. **2001**, 2640–2641.

(92) Kanie, K.; Sugimoto, T. *J. Am. Chem. Soc*. **2003**, *125*, 10518–10519.

(93) Jana, N. R.; Gearheart, L. A.; Obare, S. O.; Johnson, C. J.; Mann, K. J. S.; Murphy, C. J. *J. Mater. Chem*. **2002**, *12*, 2909–2912.

(94) Brust, M.; Walker, M.; Bethell, D.; Schiffrin, D. J.; Whyman, R. *J. Chem. Soc., Chem. Commun*. **1994**, 801–802.

(95) Richardson, R. M.; Ponomarenko, S. A.; Boiko, N. I.; Shibaev, V. P. *Liq. Cryst*. **1999**, *26*, 101–108.

(96) Marcos, M.; Giménez, R.; Serrano, J. L.; Donnio, B.; Heinrich, B.; Guillon, D. *Chem. Eur. J.* **2001**, *7*, 1006–1013.

(97) Donnio, B.; Barberá, J.; Gime´nez, R.; Guillon, D.; Marcos, M.; Serrano, J. L. *Macromolecules* **2002**, *35*, 370–381.

(98) Rueff, J. M.; Barberá, J.; Donnio, B.; Guillon, D.; Marcos, M.; Serrano, J. L. *Macromolecules* **2003**, *36*, 8368–8375.

(99) Kato, T.; Mizohita, N.; Kishimoto, K. *Angew. Chem. Int. Ed.* **2006**, *45*, 38–68.

(100) Donnio, B.; Guillon, D. *Adv. Polym. Sci*. **2006**, *201*, 45–155.

(101) Christopolous, D. K.; Photinos, D. J.; Stimson, L. M.; Terzis, A. F.; Vanakaras, A. G. *J. Mater. Chem*. **2003**, *13*, 2756–2764.

(102) Wilson, M. R.; Ilnytskyi, J. M.; Simson, L. M. *J. Chem. Phys*. **2003**, *119*, 3509–3515.

(103) Vanakaras, A. G.; Photinos, D. J. *J. Mater. Chem*. **2005**, *15*, 2002–2012.

(104) Cseh, L.; Mehl, G. H. *J. Am. Chem. Soc*. **2006**, *128*, 13376-13377.

(105) Yu, C. H.; Schubert, C. P. J.; Welch, C.; Tang, B. J.; Tamba, M. G.; Mehl, G. H. *J. Am. Chem. Soc*. **2012**, *134*, 5076-5079.

Appendix IV

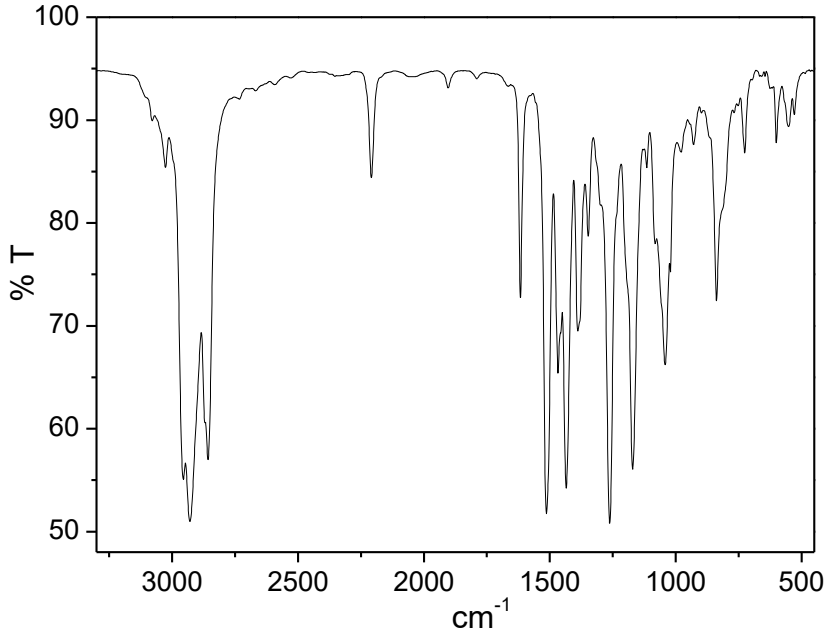

Figure A1 FT-IR spectrum of compound **11c**. Other Compounds show similar spectra**.**

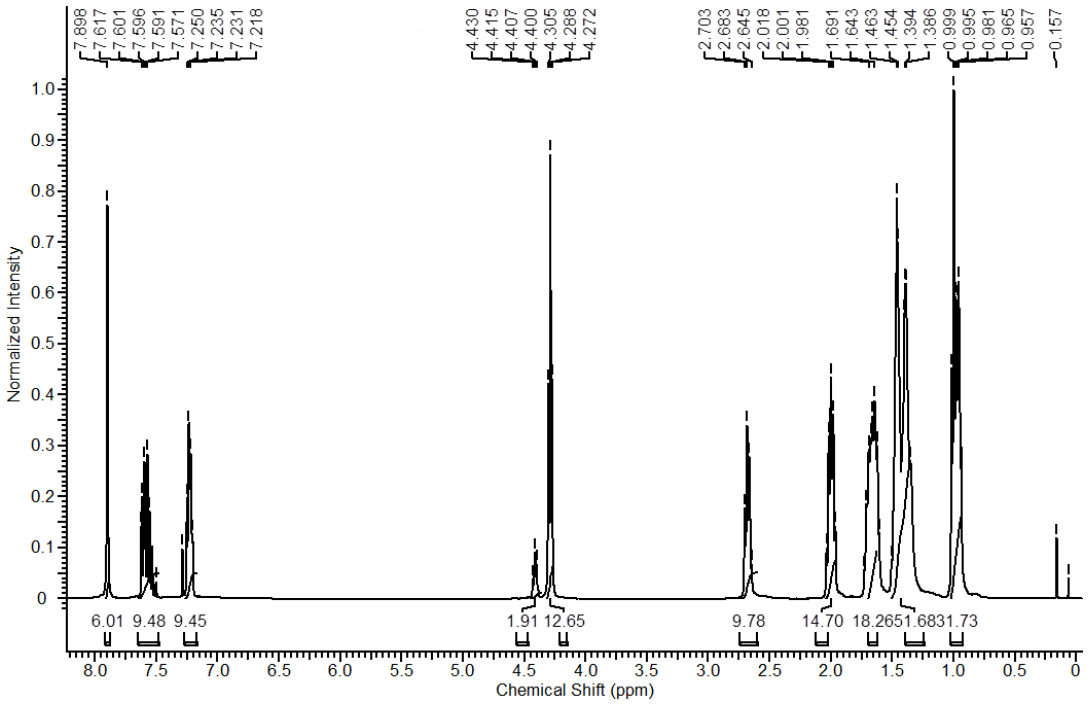

Figure A2 ^{1}H NMR spectrum of compound **11a**.

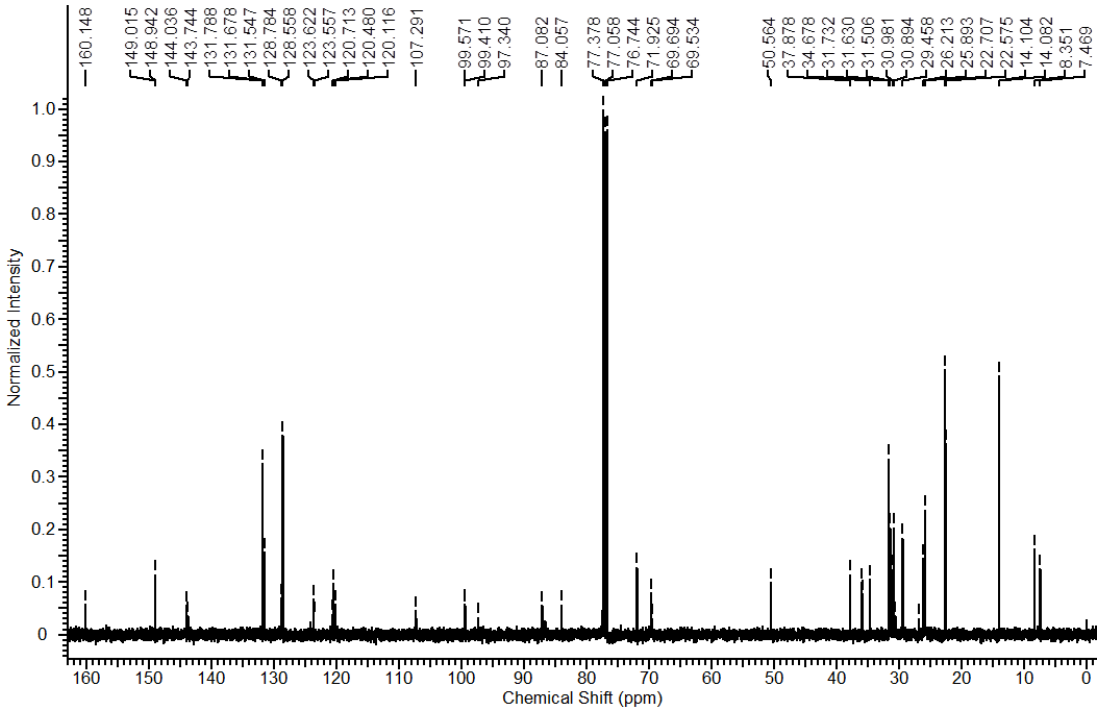

Figure A3 ^{13}C NMR spectrum of compound **11a**.

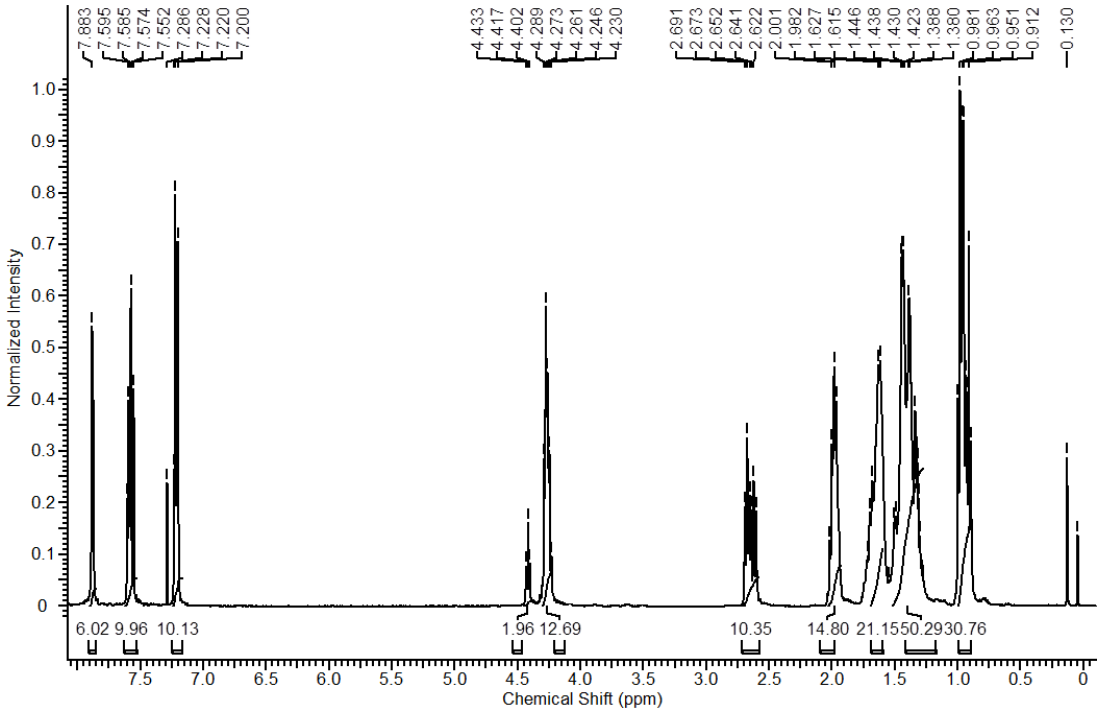

Figure A4 ^{1}H NMR spectrum of compound **11b**.

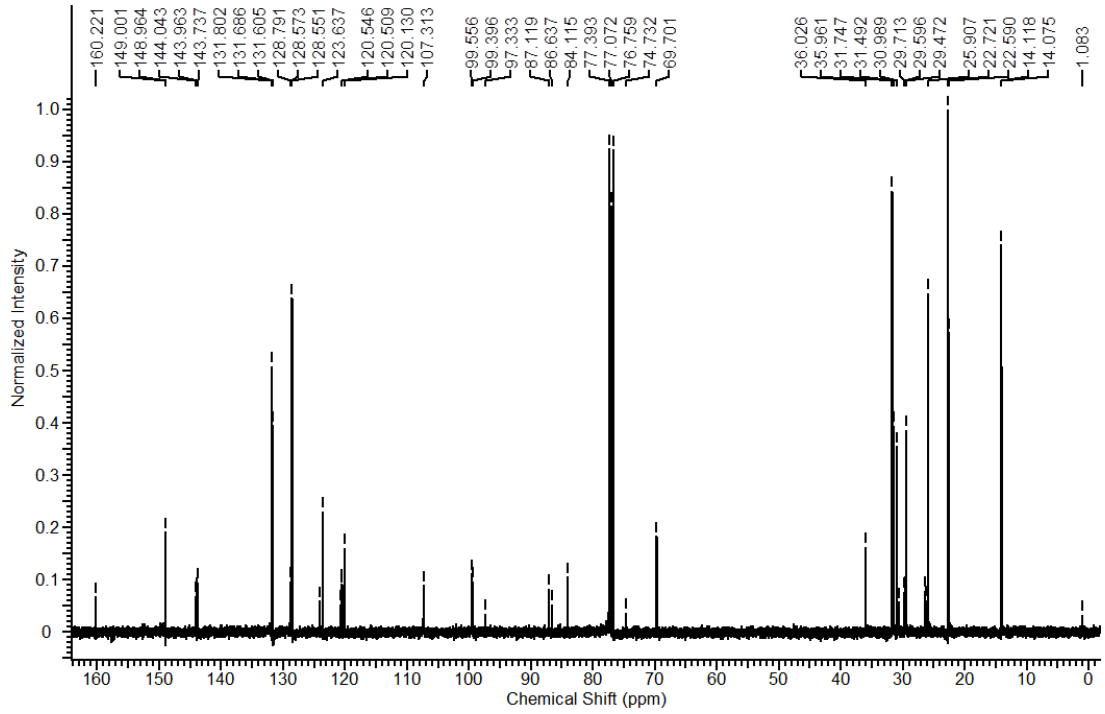

Figure A5 ^{13}C NMR spectrum of compound **11b**.

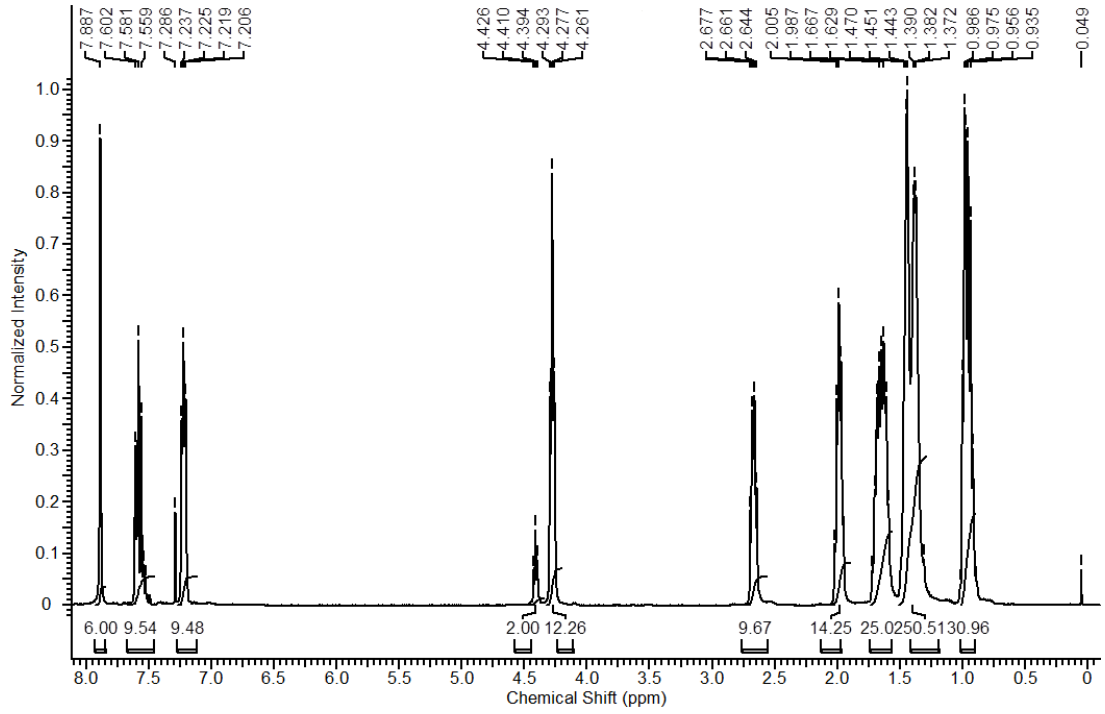

Figure A6 ^{1}H NMR spectrum of compound **11c**.

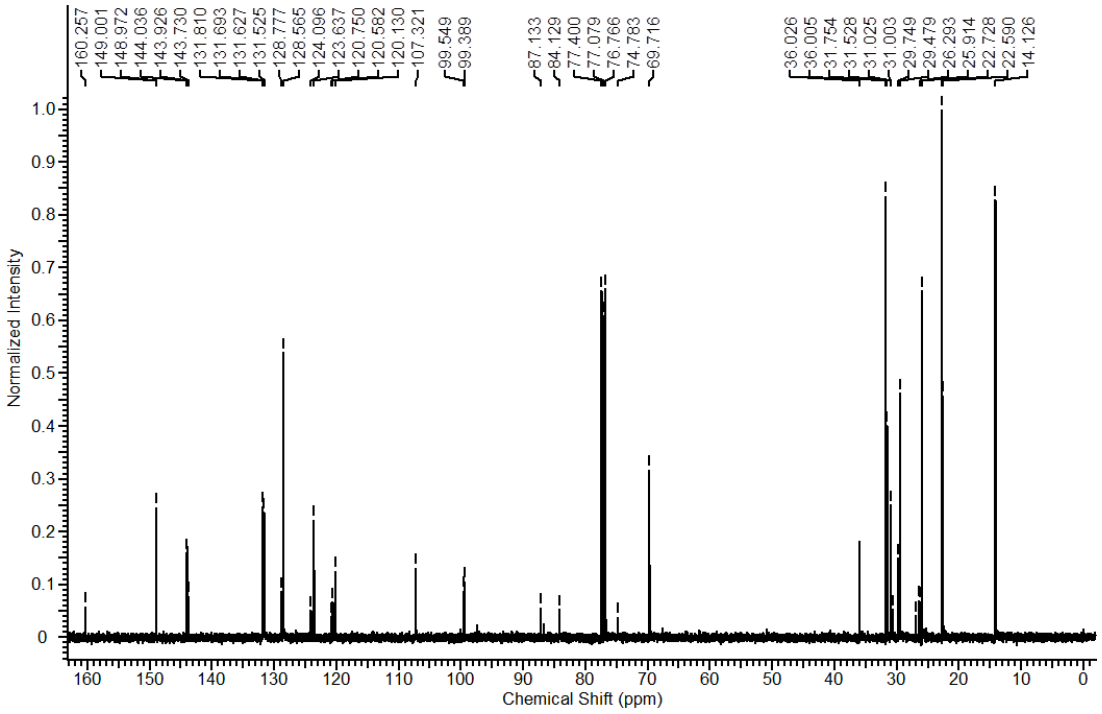

Figure A7 ^{13}C NMR spectrum of compound **11c**.

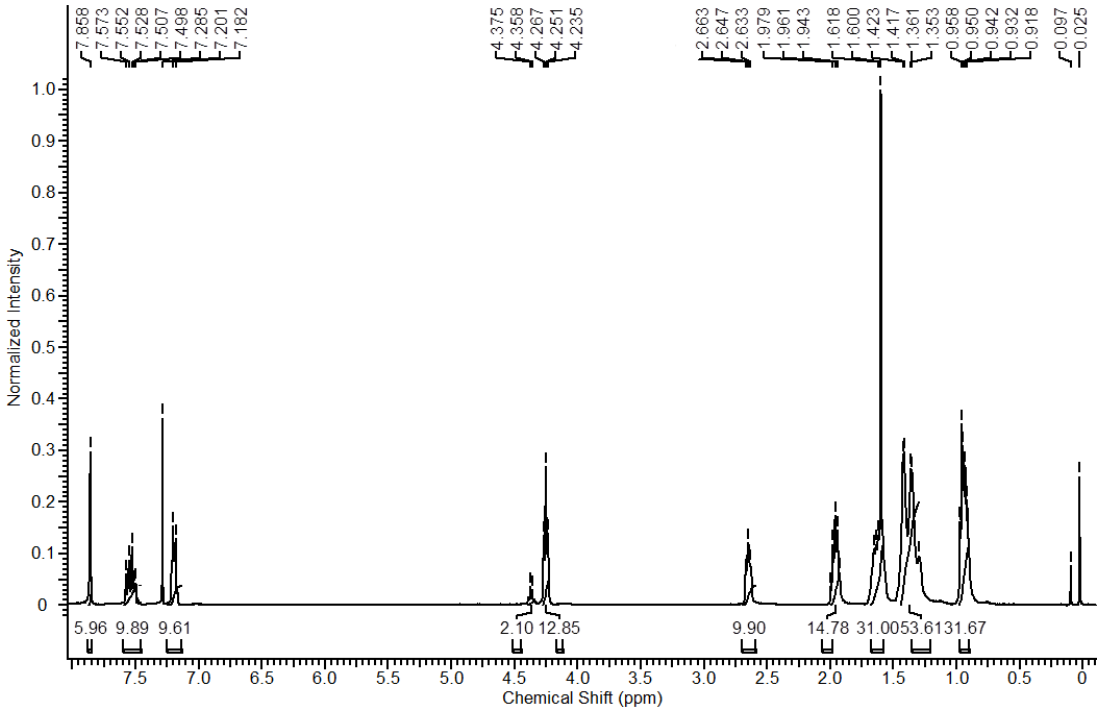

Figure A8 ^{1}H NMR spectrum of compound **11d**.

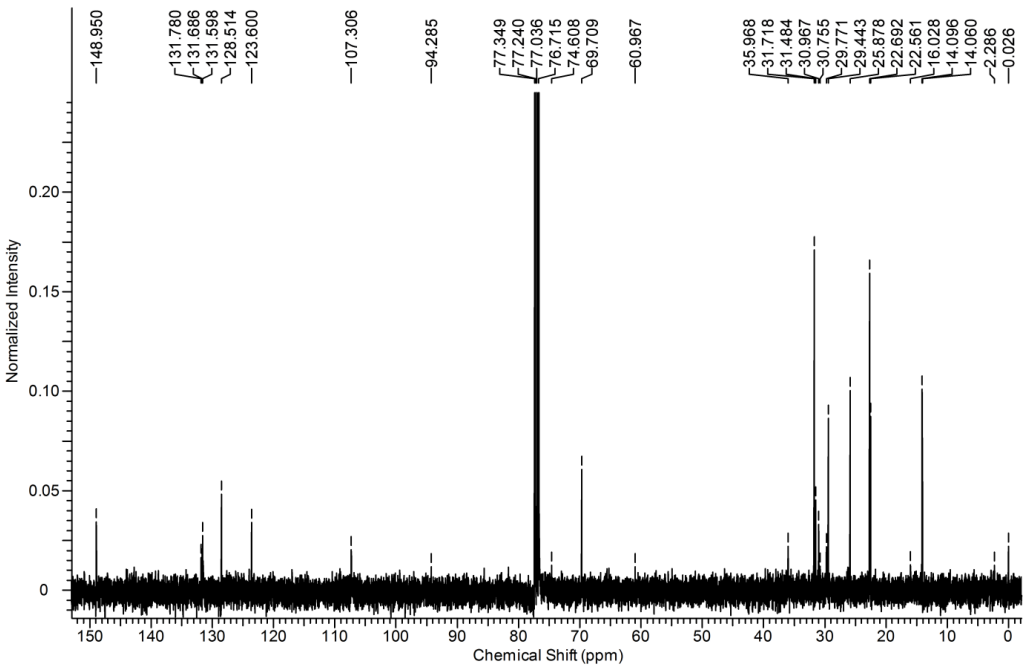

Figure A9 ^{13}C NMR spectrum of compound **11d**.

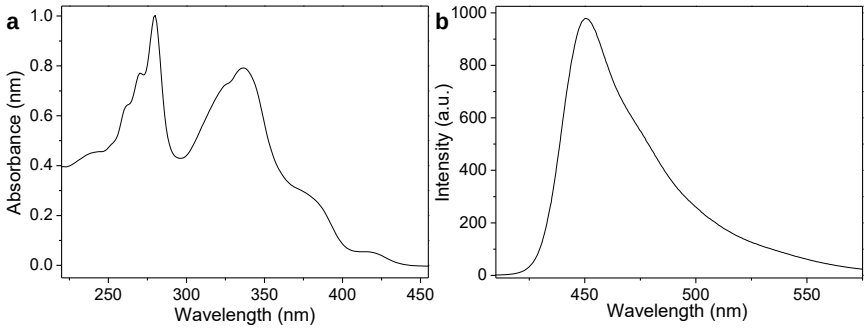

Figure A10 (a) UV-vis absorption & (b) emission spectra of compound **11b** in solution (5 μM in dichloromethane)

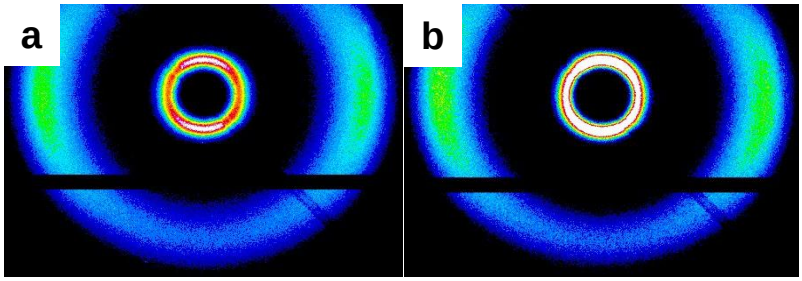

Figure A11 2D diffraction patterns obtained for (a) **11b** and (b) **11c** at room temperature, on cooling from the isotropic melt.

Coordinates for computationally optimized structures

11b_folded

C	-1.39051300	-4.62116900	-1.62512100
C	0.09786900	-5.00647400	-1.65216400
C	0.93263800	-3.75597100	-1.87493800
O	2.32540500	-4.08691300	-1.82847800
C	3.20899700	-3.05781700	-1.70143400
C	2.85705500	-1.71779000	-1.74877500
C	3.78055700	-0.67709400	-1.50697200
C	5.12724000	-1.01569400	-1.22612100
C	5.48234800	-2.38392600	-1.23963600
C	4.56894900	-3.39326900	-1.47122900
C	3.36746500	0.72536300	-1.52468900
C	4.32402400	1.74624500	-1.29615100
C	5.71157200	1.39718700	-1.00391000
C	6.09972300	0.03494500	-0.94305400
C	2.01917900	1.08940600	-1.73831900
C	1.59935700	2.40783400	-1.72107800
C	2.56046100	3.42974200	-1.52123900
C	3.87981300	3.08685100	-1.32067600
C	6.67740900	2.39289700	-0.72924200
C	7.97951800	2.07922400	-0.37927200
C	8.36627400	0.71652900	-0.31226000
C	7.43687600	-0.26216600	-0.59561000
O	0.30485600	2.81404900	-1.85620800
C	-0.69899200	1.81965300	-2.03841700
O	2.20298100	4.75776300	-1.42850200
O	8.94433200	2.99223800	-0.05379000
C	8.61947300	4.37082200	-0.14674900
O	9.62651100	0.34510900	0.09088400
C	10.67884600	0.66174200	-0.82422600
O	5.00670100	-4.69012100	-1.35977700
C	4.77376500	-5.55368600	-2.47705200
H	-1.50300300	-3.72451800	-1.00505600
H	-1.71171100	-4.34164800	-2.63862200
H	0.30309800	-5.74969500	-2.43346600
H	0.40564800	-5.44486300	-0.69755700
H	0.70661800	-3.03578000	-1.08007700
H	0.69752300	-3.28685500	-2.84278500
H	1.82775200	-1.46971100	-1.95463300
H	6.50124400	-2.70263900	-1.05516300
H	1.27410700	0.31963800	-1.86917800
H	4.55819200	3.91237300	-1.14531200
H	6.38571700	3.43251500	-0.75831500
H	7.78533400	-1.28505200	-0.51895900
H	-0.70311000	1.10487900	-1.21012700
H	-0.55679800	1.28797000	-2.98903700
H	10.77877100	1.74310000	-0.96340700
H	10.50652700	0.18090000	-1.79723300
H	5.18774700	-5.11839500	-3.39663500
H	3.70862800	-5.75512400	-2.61372300
C	-2.34849500	-5.67848000	-1.05980900
C	-1.98349100	-6.15480700	0.36296900
H	-1.44076400	-5.35600600	0.87732100
H	-1.29002000	-7.00189800	0.28935800
C	-3.20191400	-6.55847200	1.22555800
H	-2.94104800	-7.42176400	1.85136000
H	-4.02302200	-6.89732900	0.57689900
H	-3.35019100	-5.23149200	-1.04776100
H	-2.40860000	-6.54566600	-1.73301000
C	-3.72007800	-5.46133300	2.17558500
H	-4.54602900	-5.87275200	2.77327300

H	-2.92600200	-5.18375300	2.88099500
C	-4.23977400	-4.17952000	1.53230200
H	-4.70183400	-3.53191200	2.28549500
H	-4.98750900	-4.38978400	0.76011000
O	-3.12623200	-3.48924300	0.92862600
C	-2.99720500	-2.14083100	0.98286100
C	-1.41772100	-0.27252400	1.20564100
C	-2.48185800	0.64656700	1.00246900
C	-3.79235700	0.16223400	0.77025300
C	-4.05406500	-1.24025100	0.73832800
C	-1.68478300	-1.66867000	1.21922100
C	-0.62558300	-2.58072800	1.44088900
C	0.33285700	-3.31088200	1.60820500
C	-0.10638500	0.21611700	1.41483600
C	0.99864800	0.69563500	1.58976300
C	-5.35206600	-1.67051400	0.36642500
C	-6.48799600	-1.92983900	0.01877600
C	-4.83740600	1.08803600	0.54371400
C	-5.70026900	1.92368200	0.35561700
C	-2.22992600	2.04130600	0.98995300
C	-2.01242100	3.23633300	0.94904300
C	-7.82083800	-2.17343700	-0.40958700
C	-8.55655800	-1.14466800	-1.03322600
C	-8.44094100	-3.42260300	-0.21802900
C	-9.86672600	-1.36570400	-1.44215300
H	-8.08463900	-0.17980000	-1.19137700
C	-9.75214600	-3.62859400	-0.63507200
H	-7.88793400	-4.22239400	0.26588700
H	-10.41902500	-0.55885300	-1.91878700
H	-10.21591700	-4.59933800	-0.47512700
C	1.51105800	-4.09770500	1.71190900
C	2.76709600	-3.48148400	1.53771900
C	1.46557700	-5.48711400	1.92849100
C	3.92907000	-4.23702400	1.55994400
H	2.80653500	-2.41749900	1.33338200
C	2.64139400	-6.23346400	1.93528500
H	0.50621700	-5.97405300	2.07054800
H	4.88364000	-3.74816200	1.38954200
H	2.58790200	-7.31000700	2.08030800
C	-1.73542000	4.63058300	0.89342300
C	-0.49339700	5.08788700	0.41155600
C	-2.68632700	5.57779800	1.32116700
C	-0.21487400	6.44930500	0.37340000
H	0.23642500	4.37838900	0.04419900
C	-2.39329700	6.93744100	1.26984700
H	-3.64413300	5.23550100	1.70242300
H	0.75677200	6.77139600	0.00649100
H	-3.13648900	7.65581900	1.60908600
C	2.25190000	1.32124700	1.82840700
C	2.32628800	2.72462700	1.92068300
C	3.43538200	0.57131900	1.97960400
C	3.54498200	3.34703300	2.16756400
H	1.42410500	3.31409400	1.79411600
C	4.64564700	1.20781300	2.22264300
H	3.39473700	-0.50908900	1.90200100
H	3.58267900	4.43215300	2.22856700
H	5.55211800	0.61482500	2.31278700
C	-6.67361700	2.93488800	0.13875900
C	-6.27119400	4.26599700	-0.09547800
C	-8.05066100	2.63807400	0.15011600
C	-7.22063600	5.25821600	-0.31120400
H	-5.21164200	4.50415700	-0.11074700
C	-8.98744300	3.64303700	-0.06823800
H	-8.37264000	1.61754300	0.33424100
H	-6.89208300	6.27889500	-0.49423000
H	-10.04660800	3.39564300	-0.05763100
H	7.81387000	4.64265600	0.54770300
H	5.30171900	-6.48265200	-2.24855200

H	11.59498400	0.26338400	-0.38146100
H	-1.64802400	2.35564600	-2.04706900
H	9.52820400	4.91028200	0.12687800
H	8.32341300	4.64758900	-1.16793600
C	-1.15548300	7.39862800	0.79792600
C	-10.48871200	-2.60894600	-1.25424000
C	-8.59335000	4.96856200	-0.29991600
C	3.88849100	-5.62740700	1.73893400
C	4.72211000	2.60447300	2.32984200
C	-0.85559200	8.87652100	0.71971000
H	0.21218800	9.07637600	0.86106600
H	-1.13532500	9.28577200	-0.26074500
H	-1.41002600	9.44112800	1.47715100
C	6.03527800	3.28189000	2.63706800
H	6.23854300	3.27587900	3.71648500
H	6.87133300	2.77689500	2.14333000
H	6.02866200	4.32941200	2.31493300
C	5.16373300	-6.42921400	1.67452700
H	4.97603800	-7.50263000	1.78014000
H	5.66073600	-6.25500900	0.71275700
H	5.86581000	-6.13063600	2.46342000
C	-11.90002900	-2.85024200	-1.73324200
H	-11.90936100	-3.19059900	-2.77755000
H	-12.40153800	-3.61936900	-1.13618200
H	-12.50216500	-1.93642400	-1.68504400
C	-9.61671700	6.06020800	-0.50110900
H	-9.86705600	6.54639500	0.45153700
H	-9.24492900	6.83999600	-1.17472700
H	-10.54889100	5.66579800	-0.91948300
C	1.66504900	5.33953900	-2.62180400
H	1.50661800	6.39677200	-2.39702200
H	2.37829200	5.24461600	-3.45159100
H	0.71292200	4.87817300	-2.89743900

11b_linear

C	2.19062400	-3.65475700	-1.07516700
C	1.16131600	-3.37261900	-2.17556800
C	-0.27886000	-3.69673700	-1.75621600
C	-1.31551600	-2.96090600	-2.61097600
C	-2.75392000	-3.13050100	-2.11032900
C	-3.71617600	-2.14701800	-2.78401500
C	-5.09700900	-2.14535700	-2.14723300
O	-5.80118100	-1.01373600	-2.66369000
C	-6.92281300	-0.58600600	-2.01599300
C	-7.66436300	-1.34912800	-1.13104100
C	-8.80356200	-0.83646100	-0.46582500
C	-9.19227000	0.50482000	-0.71574300
C	-8.42385200	1.26344300	-1.62837000
C	-7.31604400	0.75181300	-2.26895900
C	-9.57270300	-1.65230800	0.47363200
C	-10.69260000	-1.09450800	1.14203000
C	-11.09385600	0.28614100	0.88088500
C	-10.35590500	1.07062100	-0.03993100
C	-9.22546000	-2.99963700	0.73548700
C	-9.93497400	-3.78580000	1.62699200
C	-11.03988900	-3.22021600	2.31342900
C	-11.39081700	-1.91173800	2.06043200
C	-12.21119300	0.86462000	1.52894200
C	-12.60526100	2.17015900	1.28984000
C	-11.87690800	2.94936100	0.35409100
C	-10.78663200	2.39511600	-0.28141300
O	-9.66569900	-5.09549000	1.90465500
C	-8.58869600	-5.71801400	1.22250900

O	-11.81022600	-3.96140300	3.17550800
C	-11.16679100	-4.35423000	4.39147100
O	-13.65690300	2.79501300	1.89624200
C	-14.40227700	2.06865100	2.86112700
O	-12.19418200	4.26317000	0.11005100
C	-13.43064300	4.47822500	-0.57617600
O	-6.56302400	1.57954700	-3.06842300
C	-6.54742400	1.24652000	-4.46098200
H	1.88796600	-3.12235600	-0.16791700
H	2.22605000	-4.72293400	-0.82565200
H	1.41810200	-3.91034600	-3.09949300
H	1.21748400	-2.30189000	-2.41526200
H	-0.41838500	-3.38610200	-0.71145700
H	-0.45395000	-4.78169500	-1.78150800
H	-1.24066100	-3.27877100	-3.66101600
H	-1.07021700	-1.88994500	-2.59289500
H	-2.76678600	-2.94520700	-1.02695400
H	-3.09142100	-4.16698100	-2.25488700
H	-3.80378700	-2.35636200	-3.85781300
H	-3.31044000	-1.13345900	-2.68876900
H	-5.01419400	-2.05232800	-1.05481400
H	-5.64787300	-3.07186700	-2.36726600
H	-7.34681900	-2.36618400	-0.94861000
H	-8.66363600	2.29713300	-1.84468300
H	-8.38770200	-3.44141400	0.21570200
H	-12.25002000	-1.54325300	2.60724200
H	-12.77456300	0.27588100	2.23829500
H	-10.26734800	3.04020500	-0.97940500
H	-7.63038900	-5.22966600	1.44771200
H	-8.74685700	-5.71666600	0.13550500
H	-10.82617700	-3.47343300	4.95333400
H	-10.31718300	-5.01758000	4.20102900
H	-13.77108600	1.75519700	3.70358500
H	-14.88055400	1.18301600	2.42069700
H	-14.28439200	4.13109100	0.01457200
H	-13.42798300	3.97069700	-1.55086100
H	-5.95030700	2.02056600	-4.94893100
H	-7.56561800	1.25901300	-4.87285100
H	-11.92269200	-4.88525400	4.97493200
H	-8.56256900	-6.74814700	1.58253300
H	-15.17185800	2.75389300	3.22129200
H	-13.50648500	5.55722200	-0.73076600
H	-6.09282400	0.26630800	-4.63361800
C	3.57966700	-3.14537000	-1.45229400
H	3.50093000	-2.22829600	-2.04514000
H	4.14264700	-3.87983900	-2.04088600
O	4.35614200	-2.88056200	-0.26014100
C	4.94065500	-1.65867900	-0.13782200
C	4.19545500	-0.45977300	-0.15146600
C	6.33975800	-1.63421000	0.03994700
C	4.87367700	0.78657500	-0.01725600
C	7.00907600	-0.39266900	0.22414100
C	6.27823400	0.82098500	0.16758900
C	7.08821900	-2.83677800	0.01637400
C	7.81241800	-3.81243700	-0.01399900
C	8.40322900	-0.36390300	0.45946000
C	9.59521700	-0.32675100	0.69588300
C	6.93893300	2.06570400	0.31223800
C	7.48512500	3.14515200	0.42511000
C	4.13823500	1.99364200	-0.06953400
C	3.49530700	3.02390900	-0.12455600
C	2.77913400	-0.44106900	-0.26752600
C	1.57477800	-0.29157600	-0.35063800
C	8.70531300	-4.91763500	-0.05651700
C	8.28115700	-6.21873800	0.27484900
C	10.05229100	-4.72313300	-0.42497200
C	9.17895500	-7.28097300	0.24259500
H	7.24740900	-6.38069400	0.56458400

C	10.93790300	-5.79501000	-0.45152100
H	10.38687800	-3.72545500	-0.69248800
H	8.83418600	-8.27806600	0.50751200
H	11.97378600	-5.62376300	-0.73605200
C	10.98522100	-0.26721200	0.98044600
C	11.74485900	-1.44482300	1.12931400
C	11.63185500	0.97595400	1.13197700
C	13.10537300	-1.37233700	1.40768600
H	11.25373500	-2.40854100	1.03644100
C	12.99277000	1.03093500	1.41103900
H	11.05029800	1.88857300	1.04161500
H	13.67505800	-2.29172700	1.52335500
H	13.47434500	1.99913400	1.52880400
C	8.10561500	4.41620300	0.56202900
C	9.46458400	4.59797900	0.23911800
C	7.36831200	5.52746600	1.01771900
C	10.05901900	5.84854100	0.37241400
H	10.03782900	3.75293200	-0.13075600
C	7.97671400	6.77161500	1.14474300
H	6.32082300	5.39764200	1.27331700
H	11.10855800	5.97029800	0.11383000
H	7.39091700	7.61792100	1.49670200
C	2.73501800	4.22139300	-0.19434800
C	1.32622300	4.17771300	-0.17391500
C	3.37116200	5.47558100	-0.28364000
C	0.58727900	5.35350700	-0.24050000
H	0.82534200	3.21709200	-0.10079100
C	2.61664500	6.64201300	-0.34976900
H	4.45618100	5.51939100	-0.30383400
H	-0.49903900	5.30100300	-0.21956000
H	3.12378500	7.60199300	-0.41645500
C	0.17406700	-0.04755600	-0.44694500
C	-0.75027800	-0.72514400	0.36952200
C	-0.31485500	0.92303900	-1.34722200
C	-2.10866800	-0.42257900	0.30053200
H	-0.39111100	-1.47458900	1.06812000
C	-1.67410600	1.21271600	-1.40487100
H	0.38681500	1.44920900	-1.98749600
H	-2.80349900	-0.94802400	0.95162500
H	-2.02904800	1.96942500	-2.10080500
C	10.52002600	-7.09217400	-0.12075500
C	13.75586100	-0.13789900	1.54822400
C	9.33069700	6.95619700	0.82920400
C	1.21477200	6.60472600	-0.33192100
C	-2.59816500	0.55762800	-0.57426400
C	9.99183400	8.30234200	1.00426900
H	10.39964200	8.41308800	2.01819500
H	10.82292000	8.43629700	0.30346700
H	9.28173500	9.12192700	0.84938600
C	15.24022900	-0.06840000	1.81505400
H	15.58961400	-0.94369700	2.37321700
H	15.80887200	-0.03298800	0.87582700
H	15.50402300	0.82725500	2.38783000
C	0.40273400	7.87309300	-0.43855400
H	0.17318300	8.10763600	-1.48687900
H	-0.55239100	7.78419800	0.09029100
H	0.94193500	8.73183900	-0.02439100
C	-4.05997900	0.93296100	-0.60439300
H	-4.21774200	1.91141000	-0.13225500
H	-4.45012700	1.00286100	-1.62448000
H	-4.67572900	0.20875500	-0.06181600
C	11.47870100	-8.25697700	-0.18446100
H	11.21330800	-9.03593400	0.53848800
H	11.47101300	-8.72097600	-1.18010400
H	12.50797500	-7.94187600	0.0184830

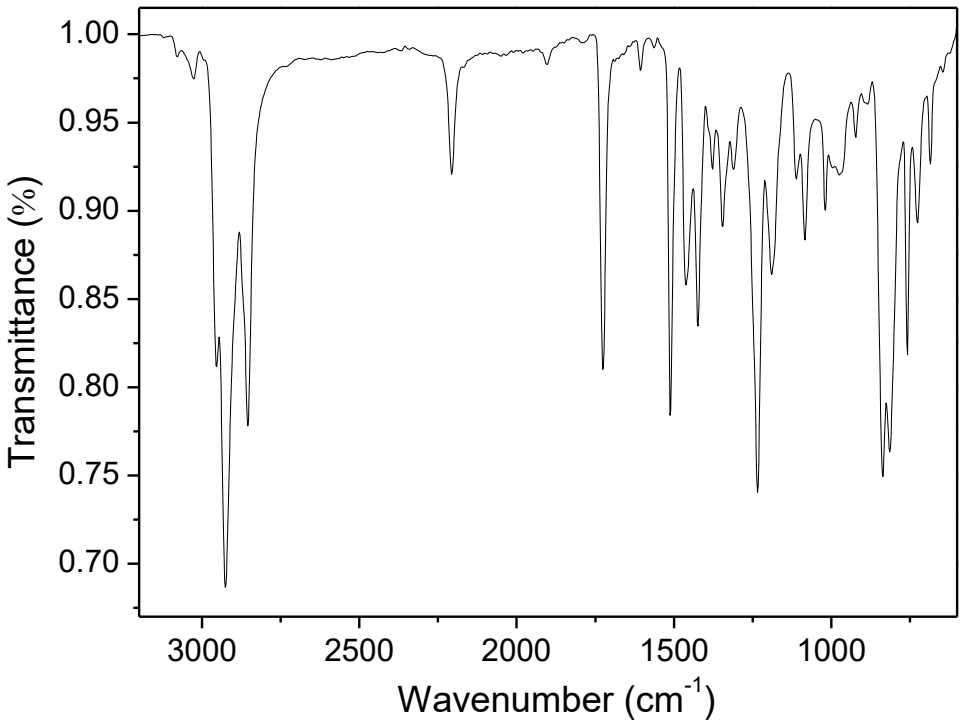

Figure A12 FT-IR spectrum of the compound **12b**.

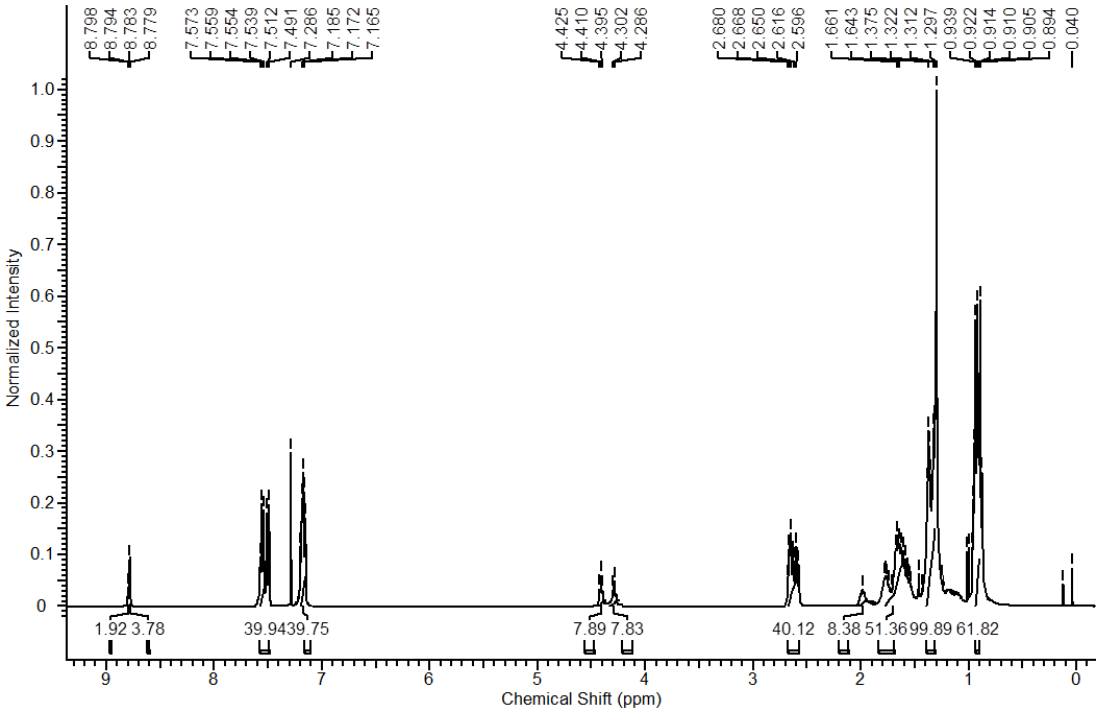

Figure A13 ^{1}H NMR spectrum of compound **12a**.

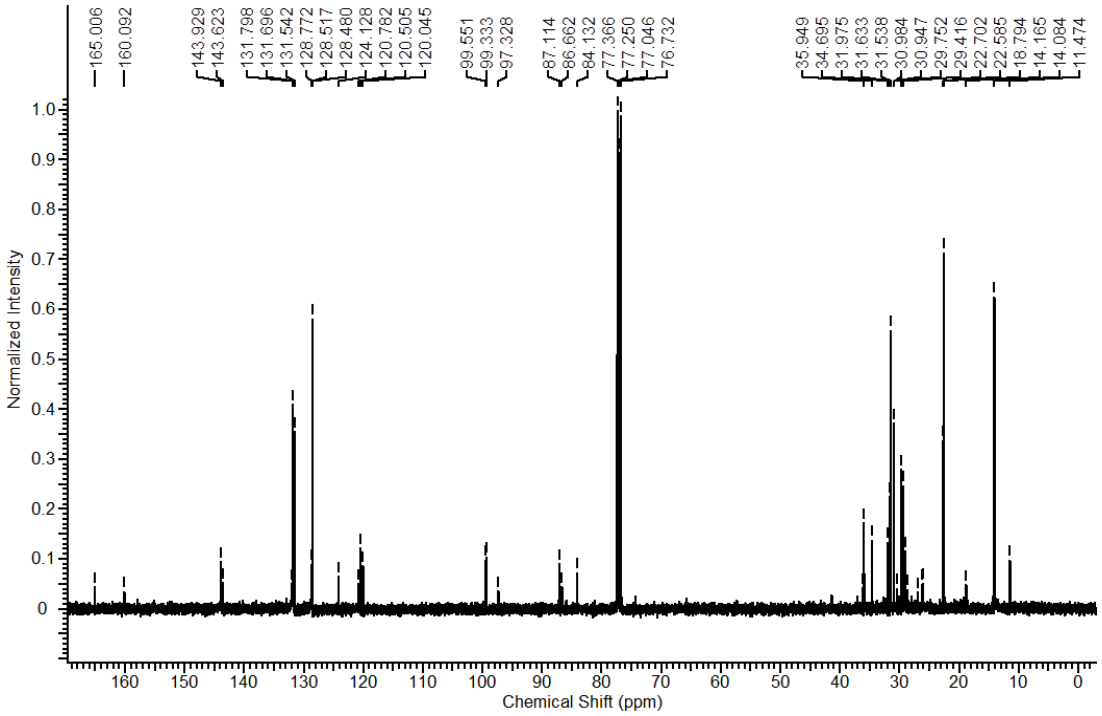

Figure A14 ^{13}C NMR spectrum of compound **12a**.

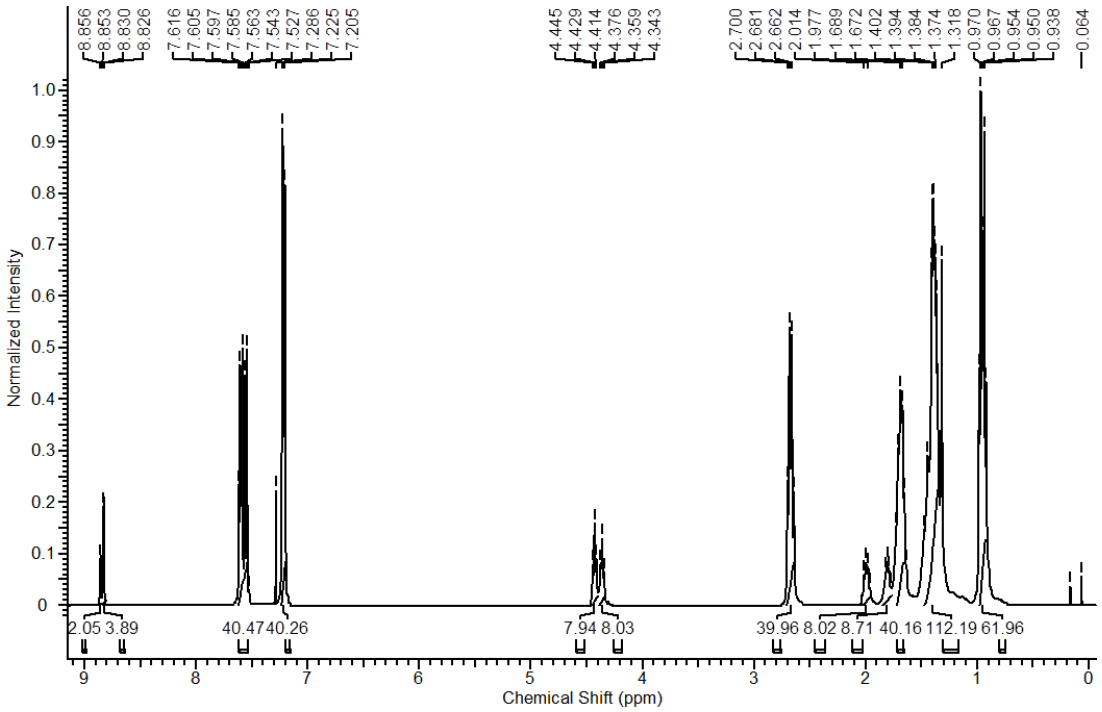

Figure A15 ^{1}H NMR spectrum of compound **12b**.

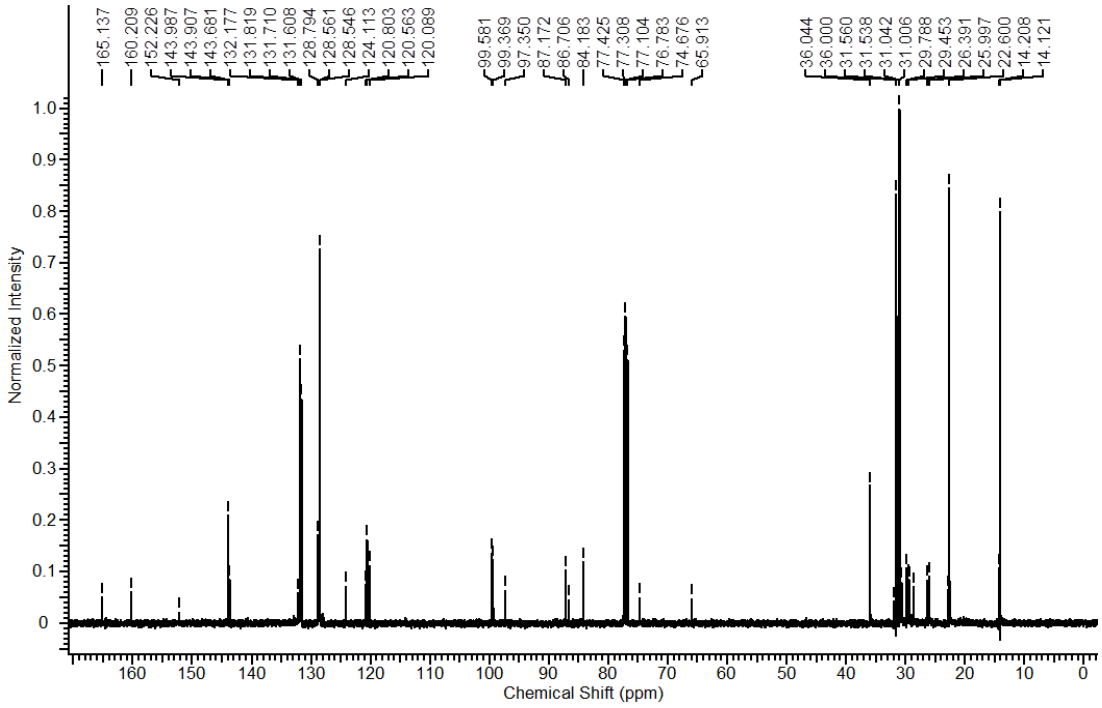

Figure A16 ^{13}C NMR spectrum of compound **12b**

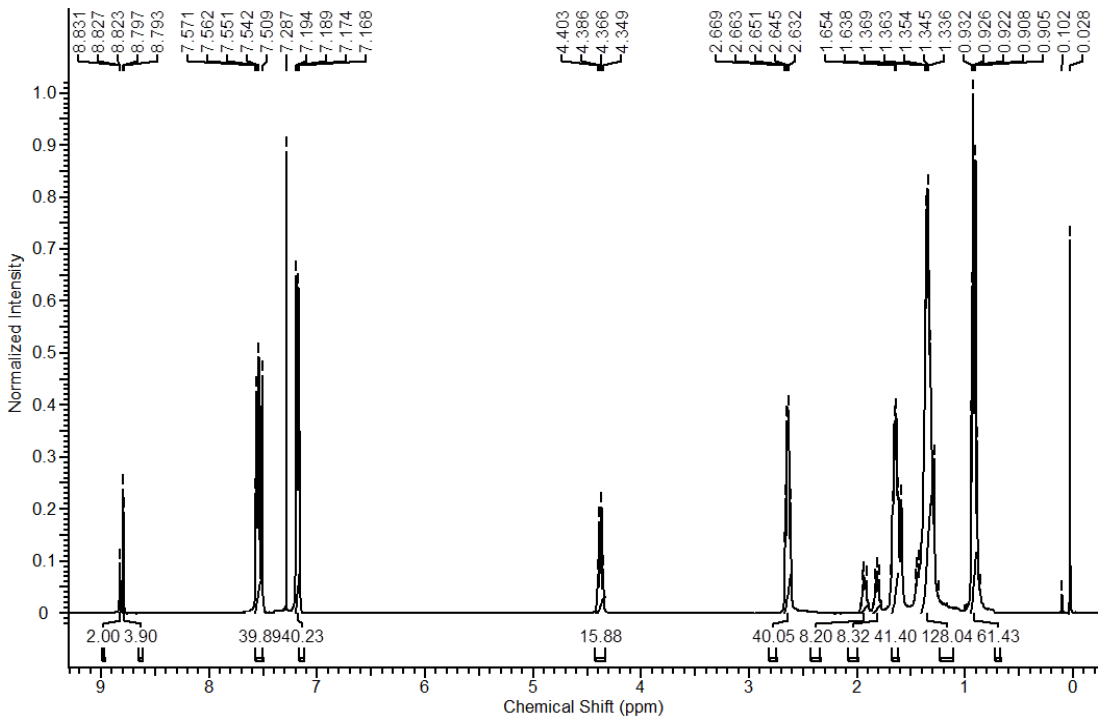

Figure A17 ^{1}H NMR spectrum of compound **12c**.

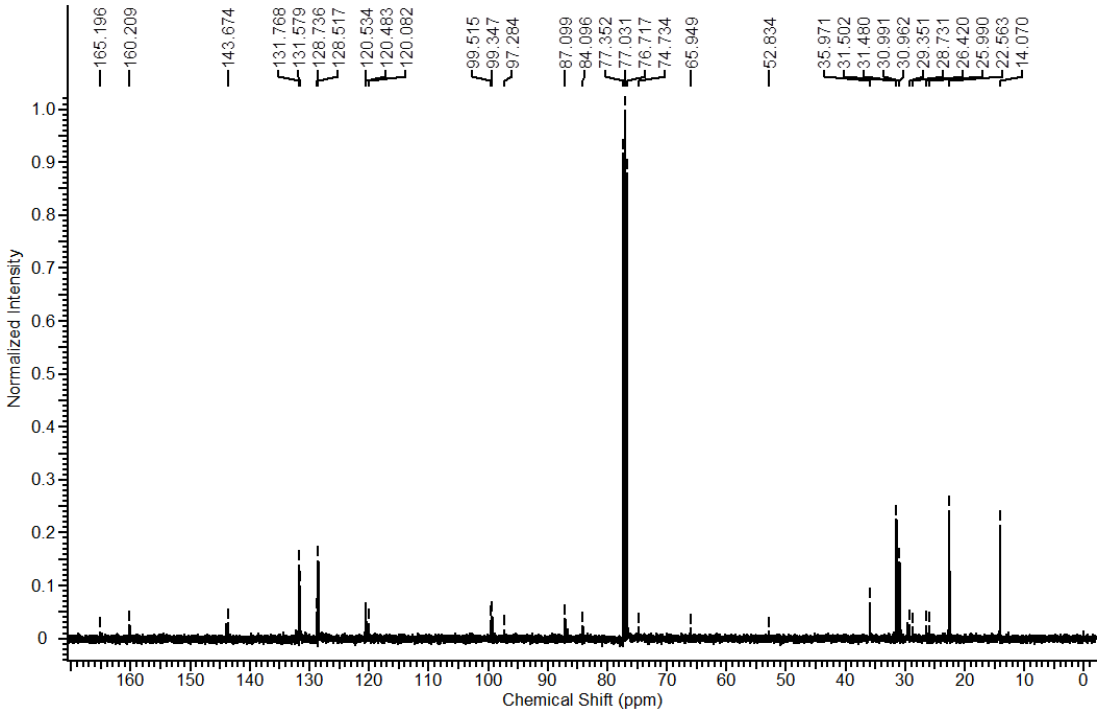

Figure A18 ^{13}C NMR spectrum of compound **12c**.

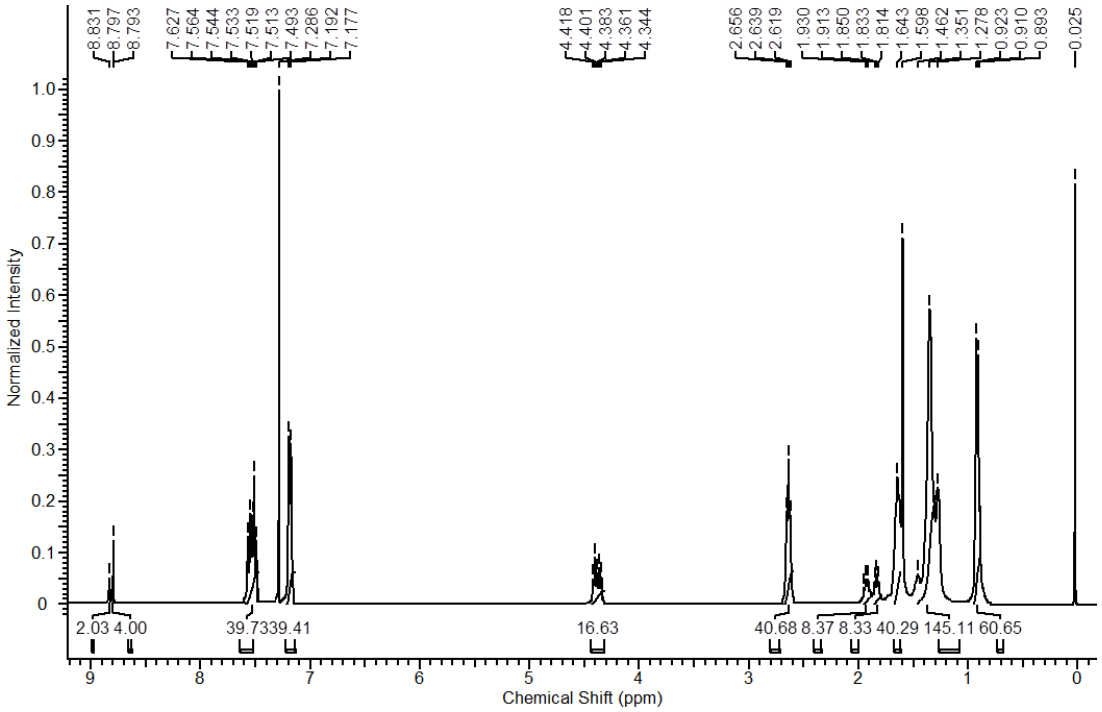

Figure A19 ^{1}H NMR spectrum of compound **12d**.

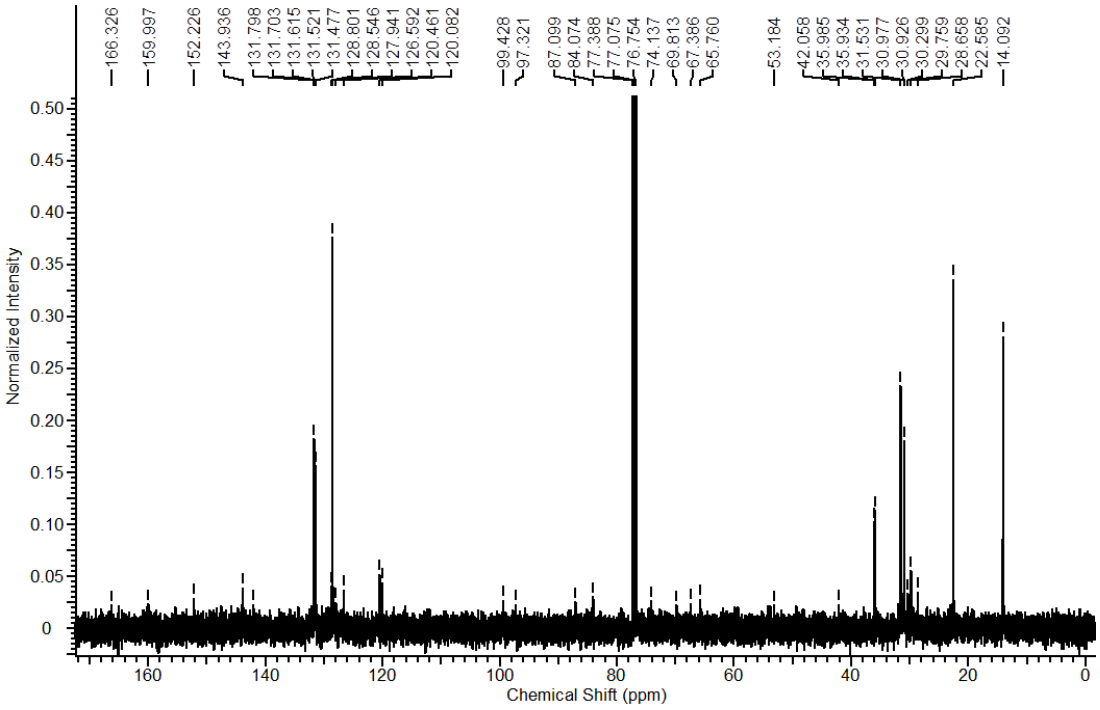

Figure A20 ^{13}C NMR spectrum of compound **12d**.

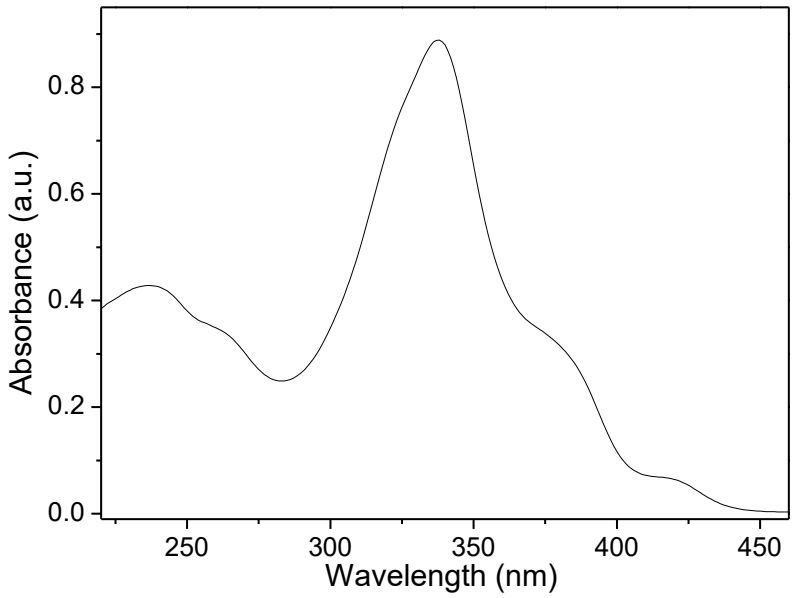

Figure A21 UV-vis absorption spectrum of compound **12a** in solution (5 μM in dichloromethane)

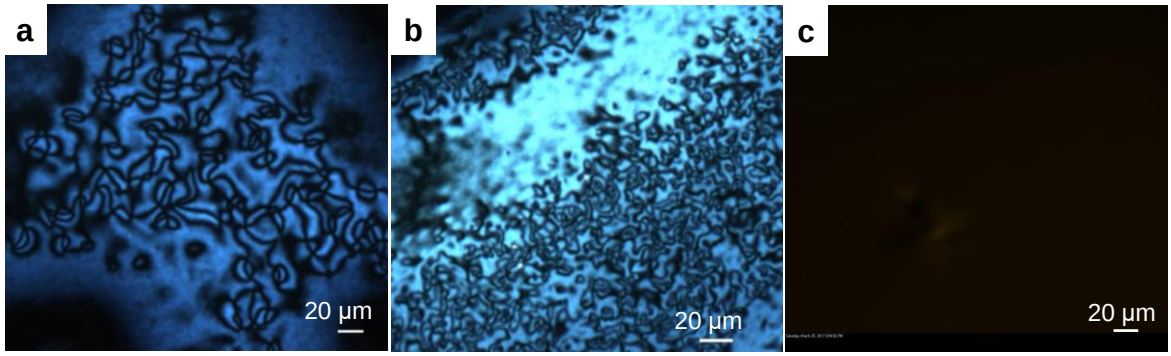

Figure A22 Polarizing optical micrograph of compound (a) **12b** at 44 °C and (b) **12c** at 54.6 °C, on cooling from the isotropic melt (between crossed polarizers). Figure (c) shows the micrograph of compound **12d** at room temperature.

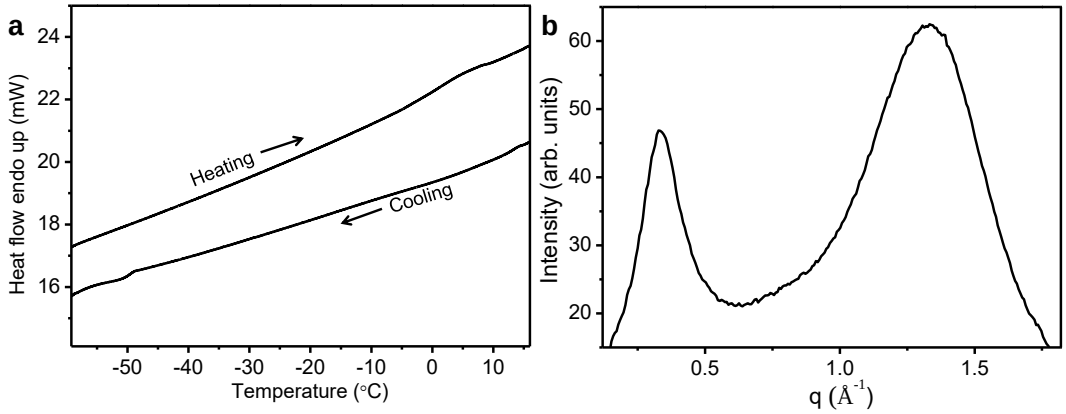

Figure A23 (a) DSC thermogram of compound **12d** on cooling below room-temperature upto -60 °C. (b) X-ray diffractogram of compound **12d** at -60 °C.

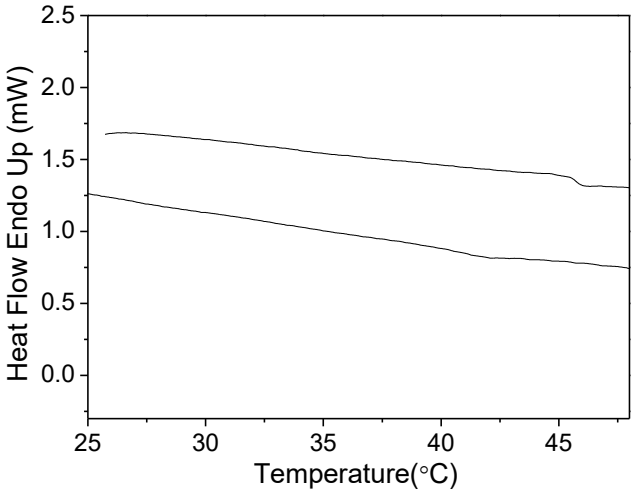

Figure A24 The DSC trace of compound **12a** on heating and cooling (scan rate 5 °C/min)

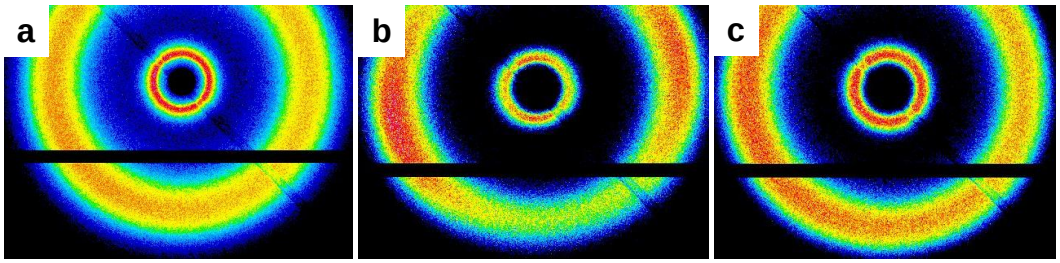

Figure A25 2D X-ray diffraction patterns corresponding to N_D mesophases of compound (a) **12a**, (b) **12b** and (c) **12c**.

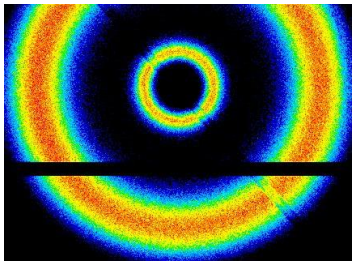

Figure A26 2D X-ray diffraction pattern corresponding to isotropic state of compound **12d**.

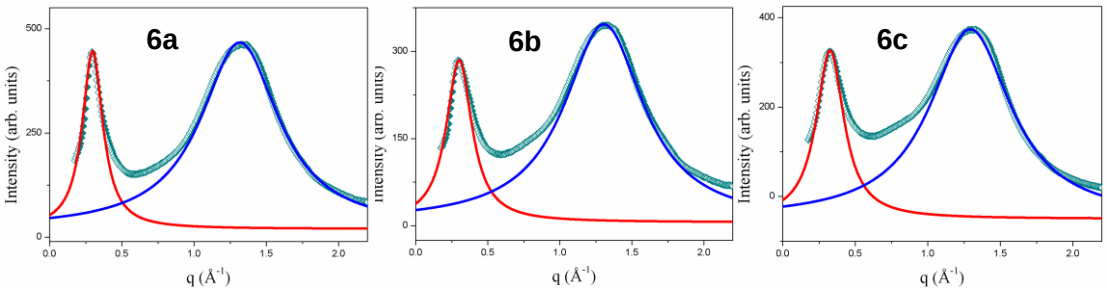

Figure A27 Fitting of diffraction peak profiles with Lorentzian profiles in the N_D phases of compounds **12a**, **12b** and **12c**.

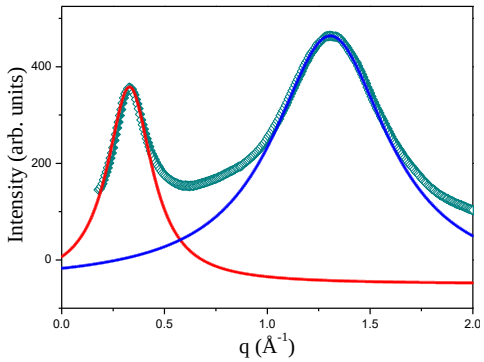

Figure A28 Fitting of diffraction peak profiles with Lorentzian profiles in the isotropic state of compounds **12d**.

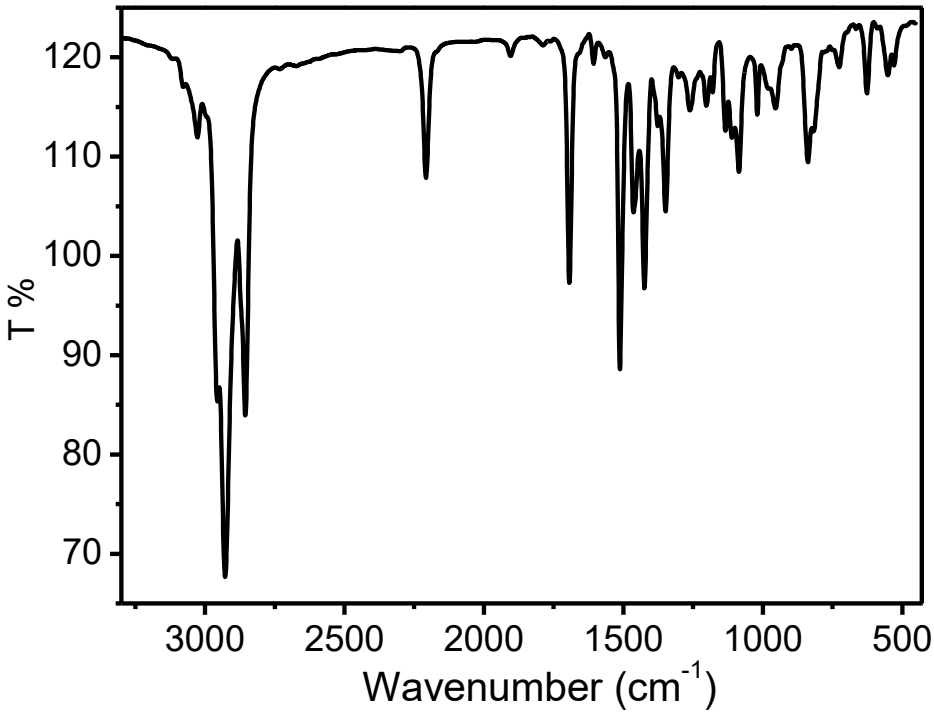

Figure A29 Representative FT-IR spectrum of compound **24d.** Other Compounds of this series show similar spectra**.**

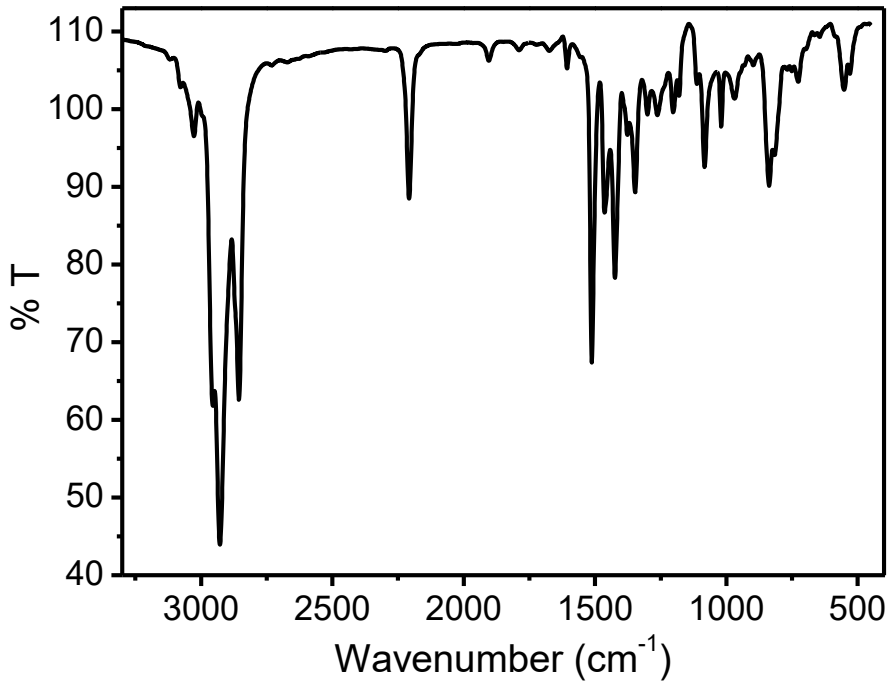

Figure A30 Representative FT-IR spectrum of compound **25c.** Other Compounds of this series show similar spectra**.**

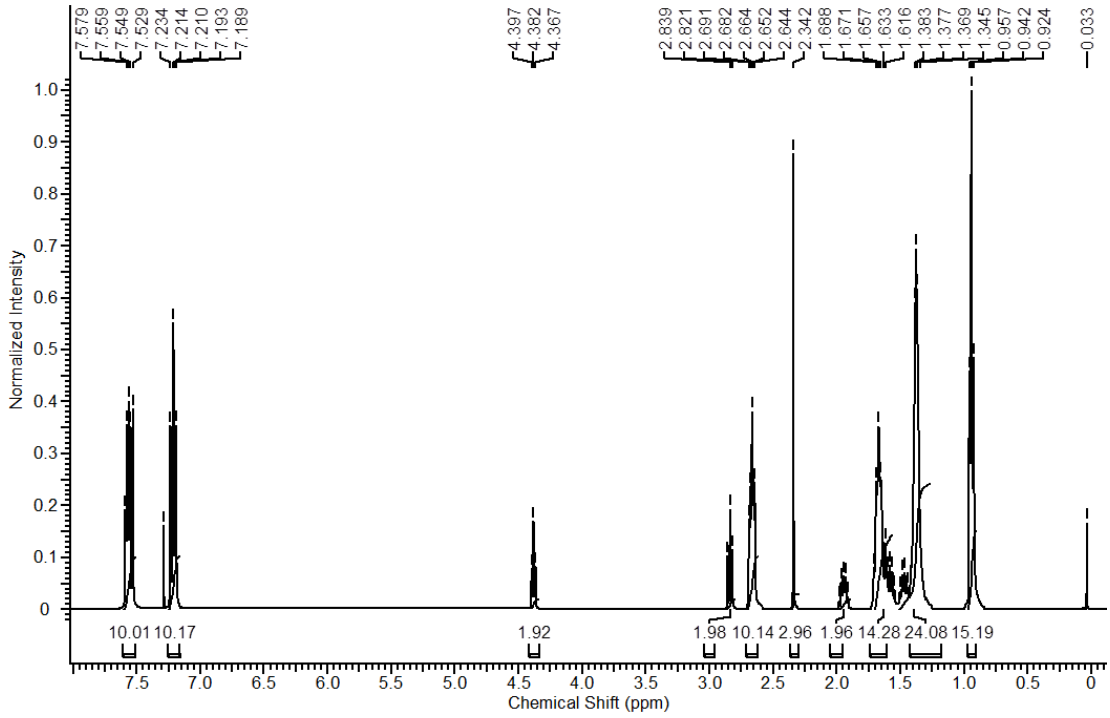

Figure A31 ^{1}H NMR spectrum of compound **24a**.

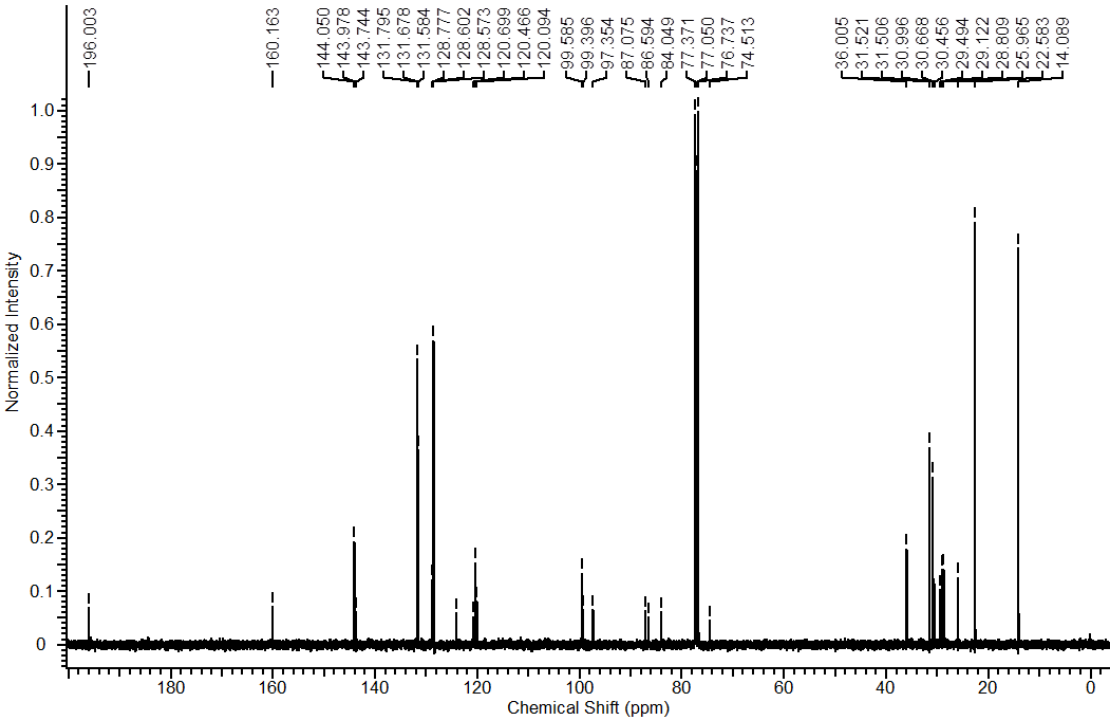

Figure A32 ^{13}C NMR spectrum of compound **24a**.

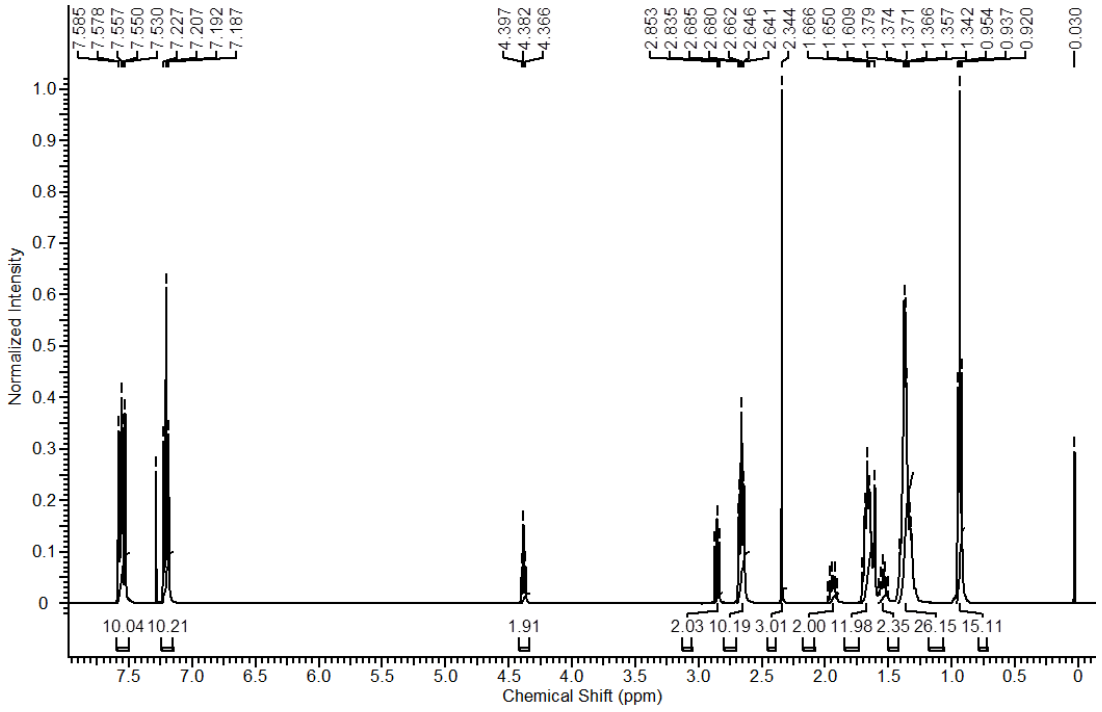

Figure A33 ^{1}H NMR spectrum of compound **24b**.

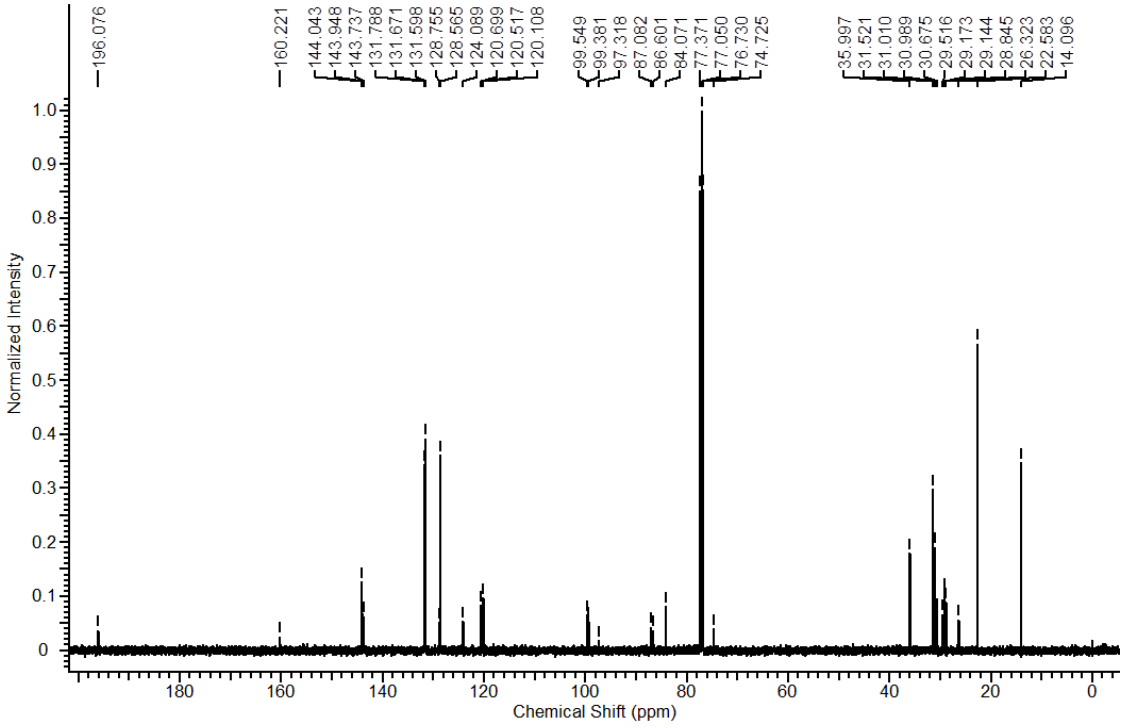

Figure A34 ^{13}C NMR spectrum of compound **24b**.

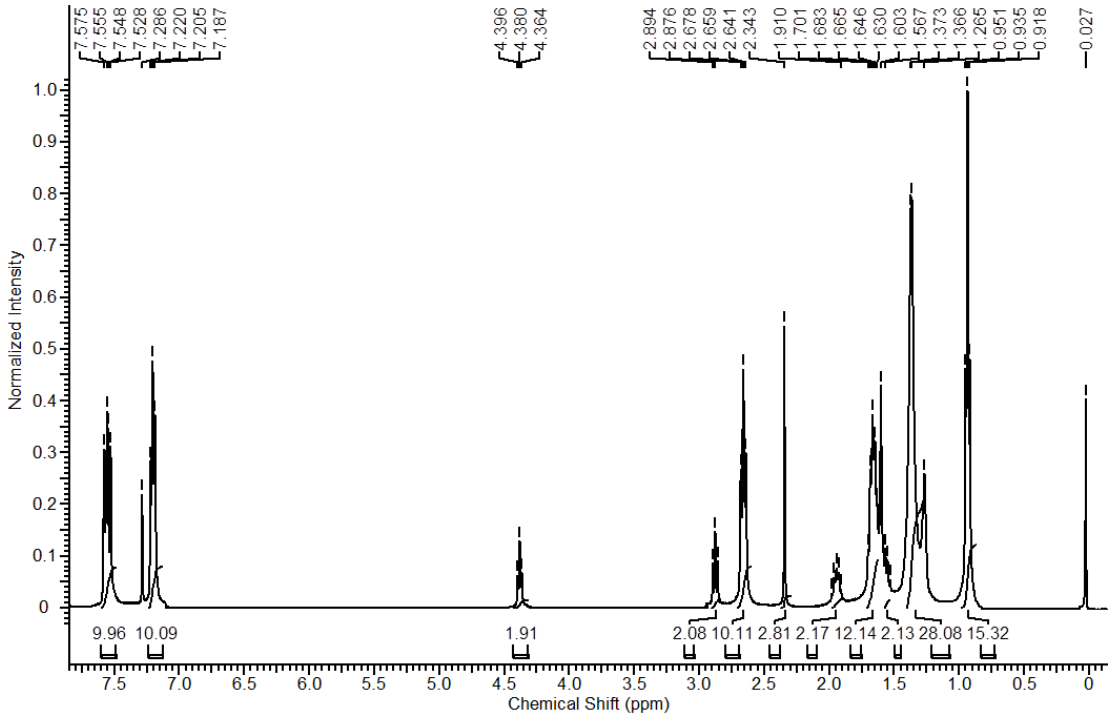

Figure A35 ^{1}H NMR spectrum of compound **24c**.

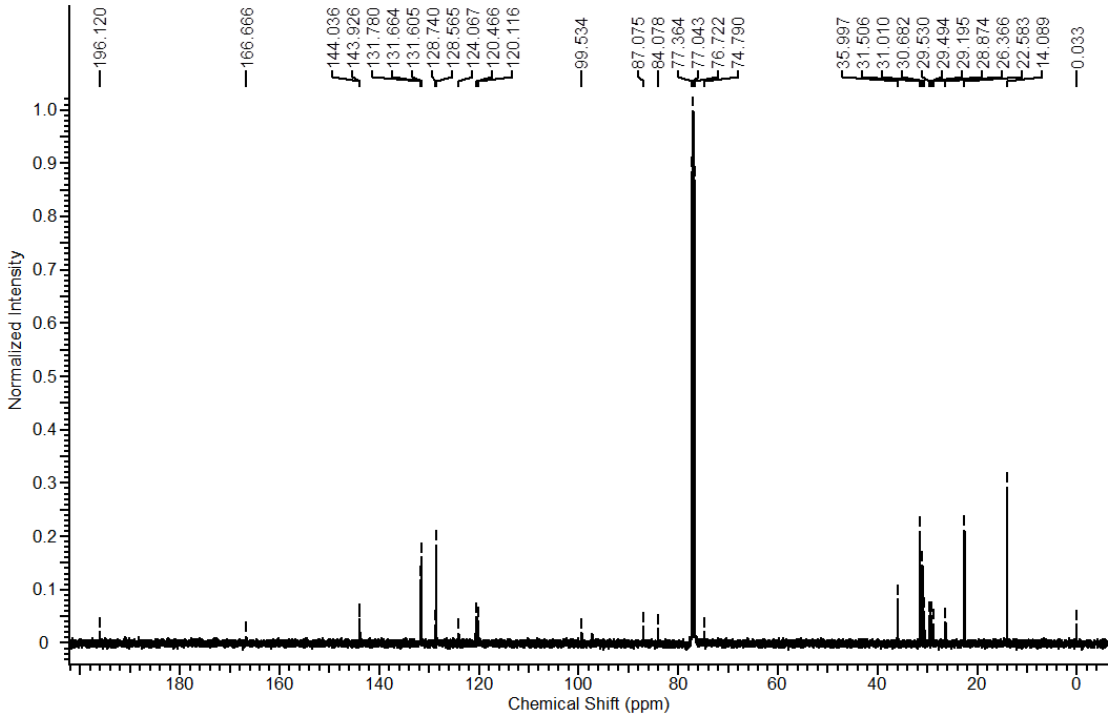

Figure A36 ^{13}C NMR spectrum of compound **24c**.

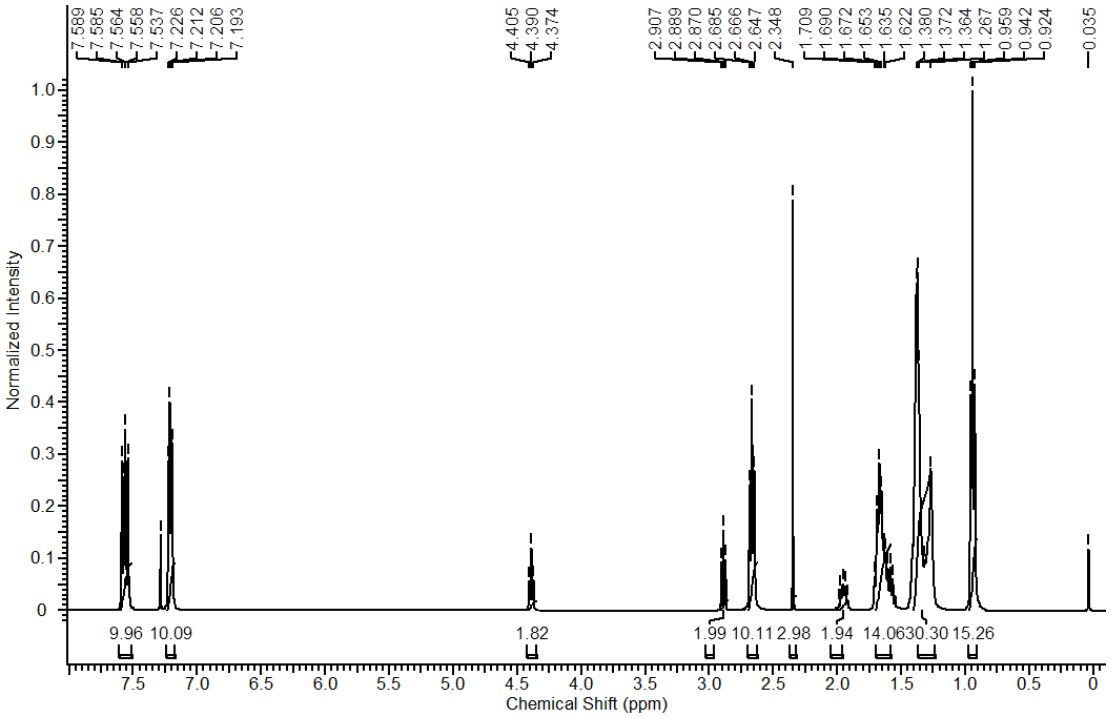

Figure A37 ^{1}H NMR spectrum of compound **24d**.

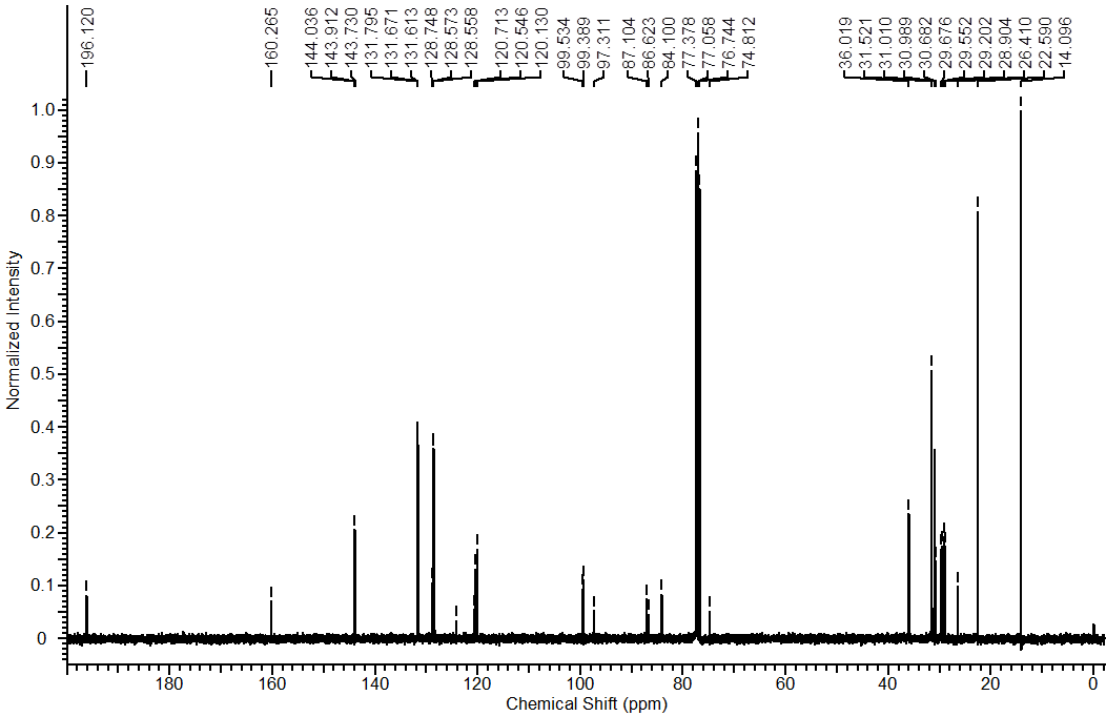

Figure A38 ^{13}C NMR spectrum of compound **24d**.

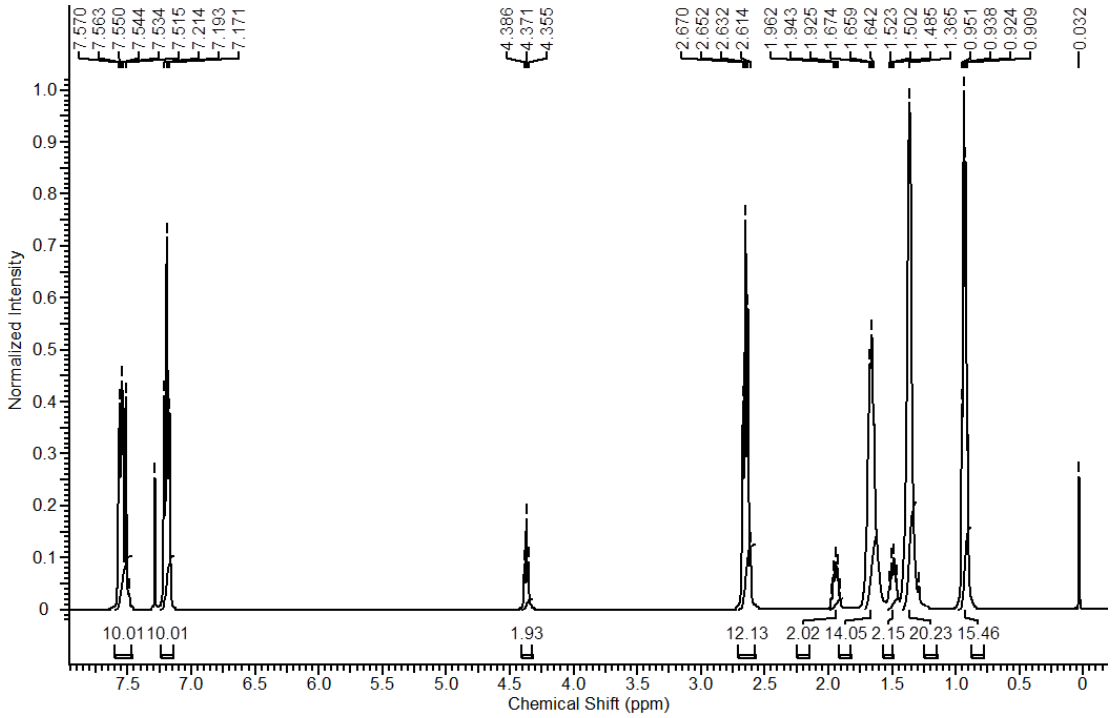

Figure A39 ^{1}H NMR spectrum of compound **25a**.

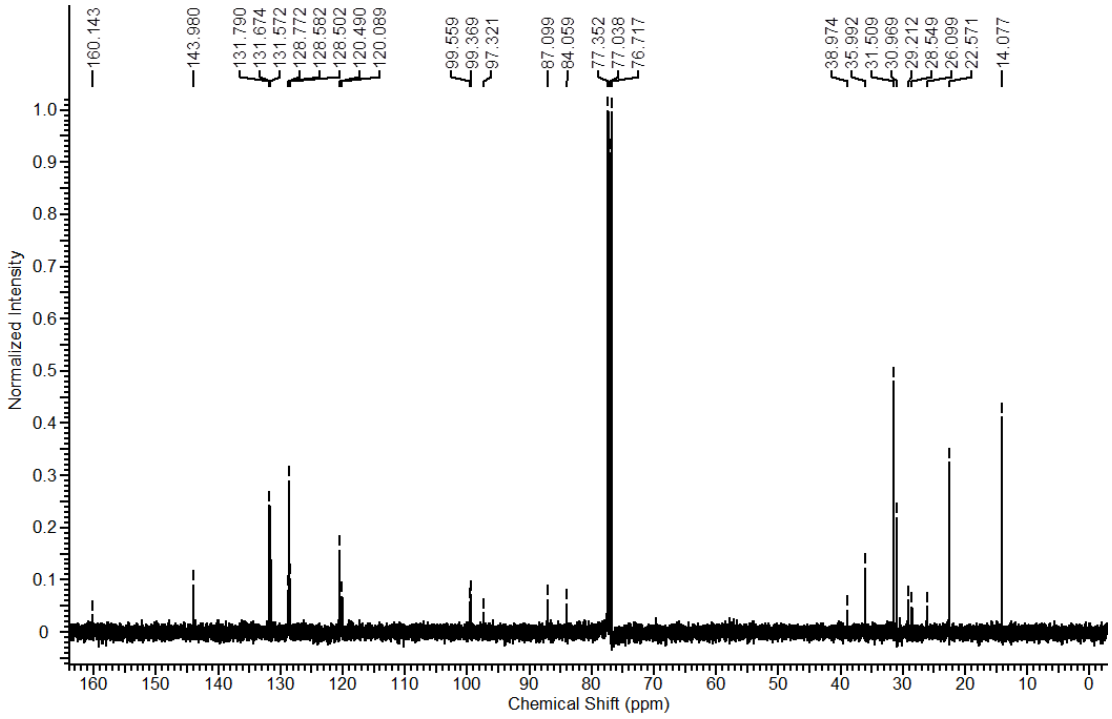

Figure A40 ^{13}C NMR spectrum of compound **25a**.

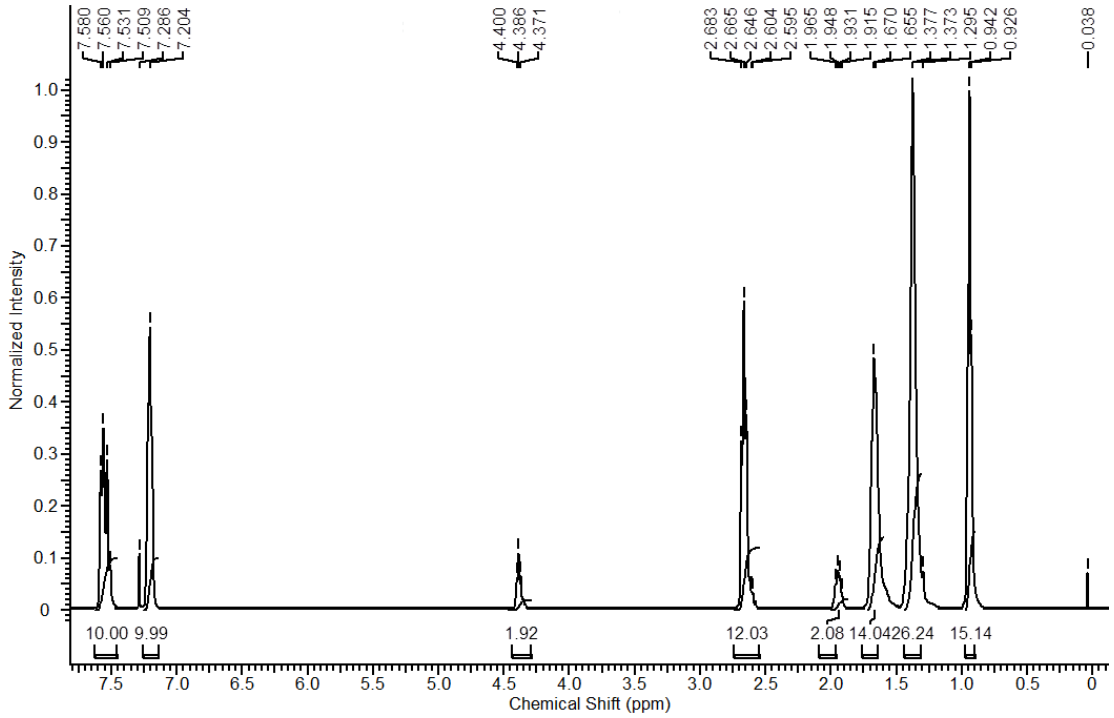

Figure A41 ^{1}H NMR spectrum of compound **25b**.

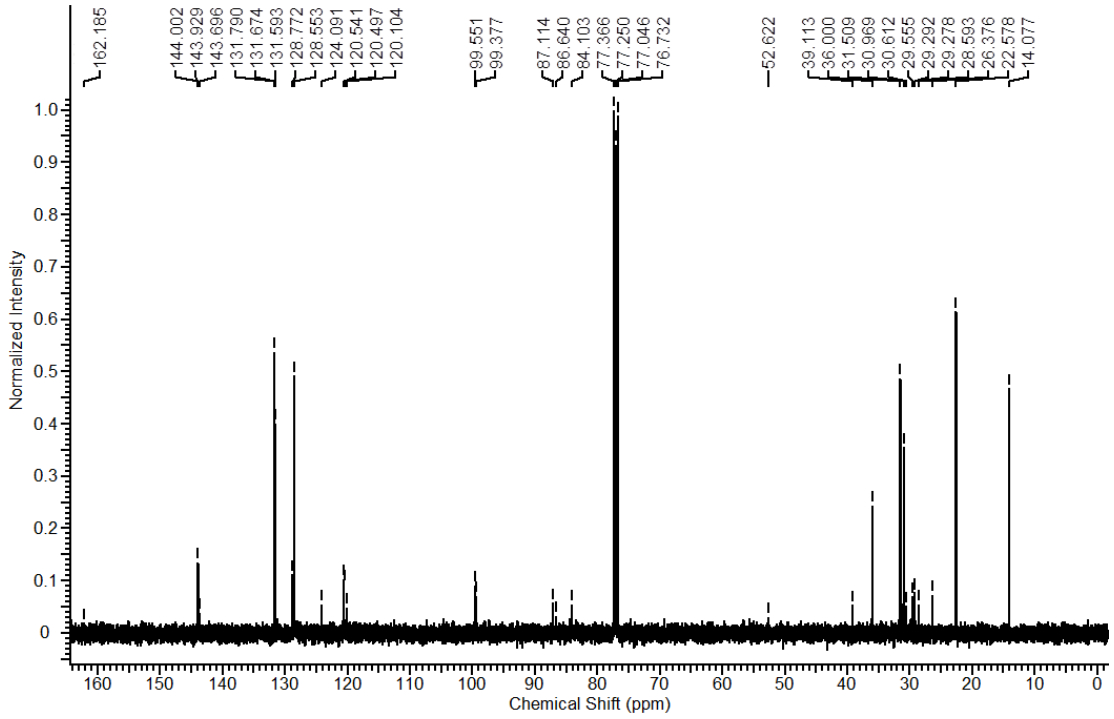

Figure A42 ^{13}C NMR spectrum of compound **25b**.

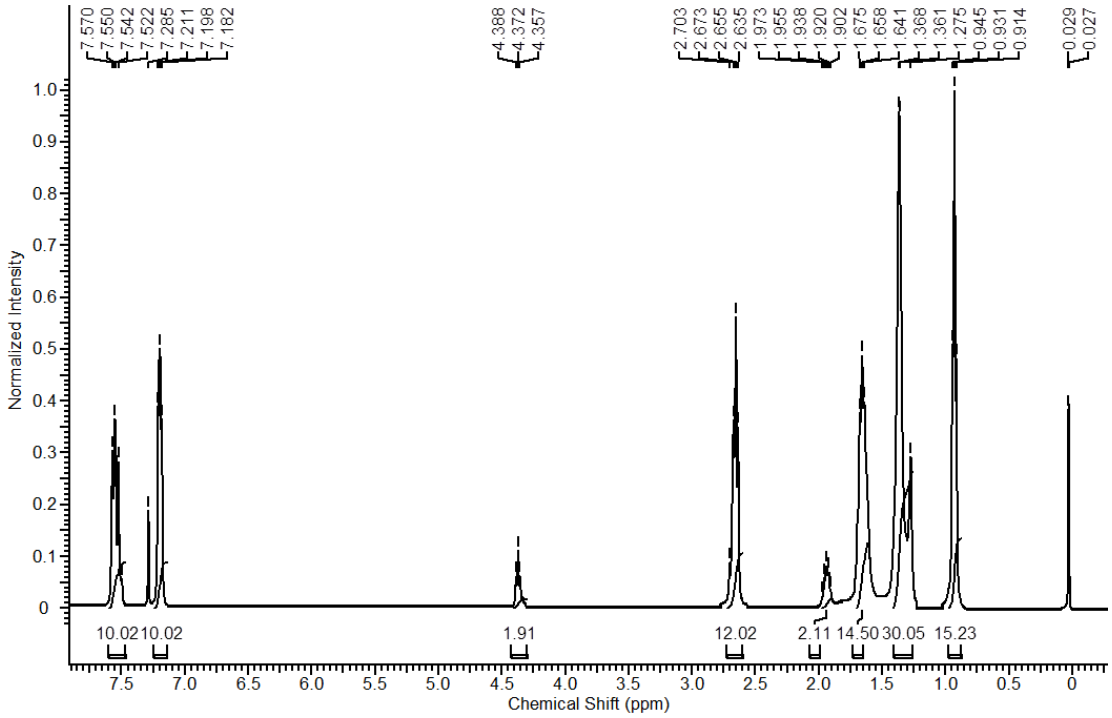

Figure A43 ^{1}H NMR spectrum of compound **25c**.

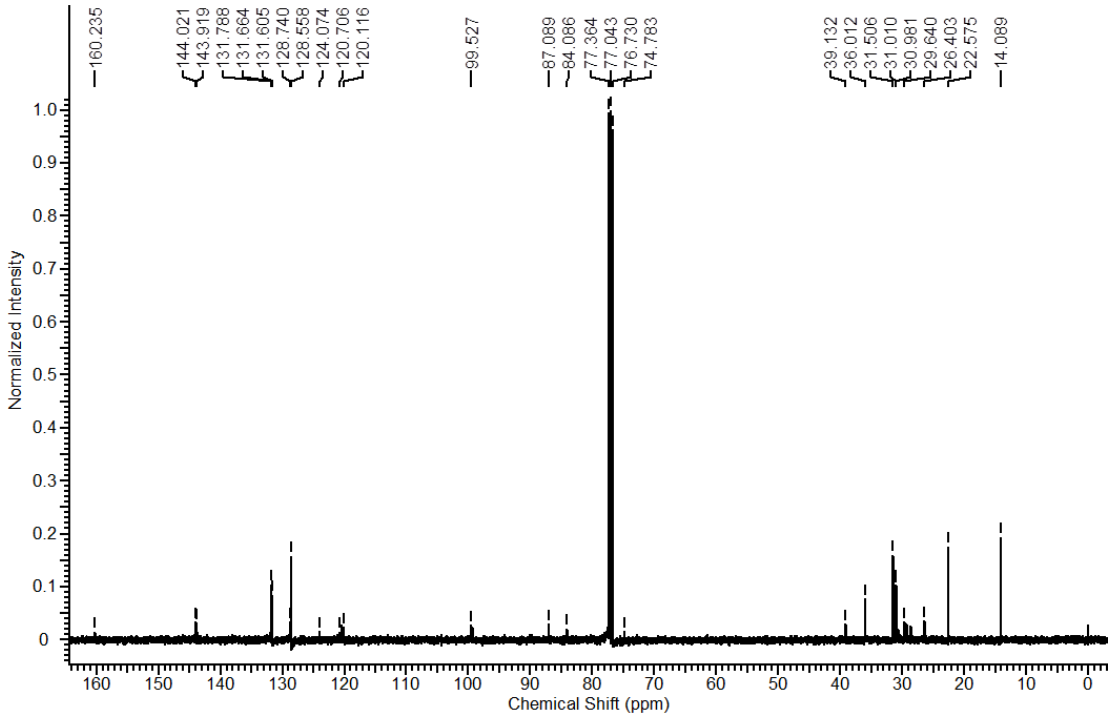

Figure A44 ^{13}C NMR spectrum of compound **25c**.

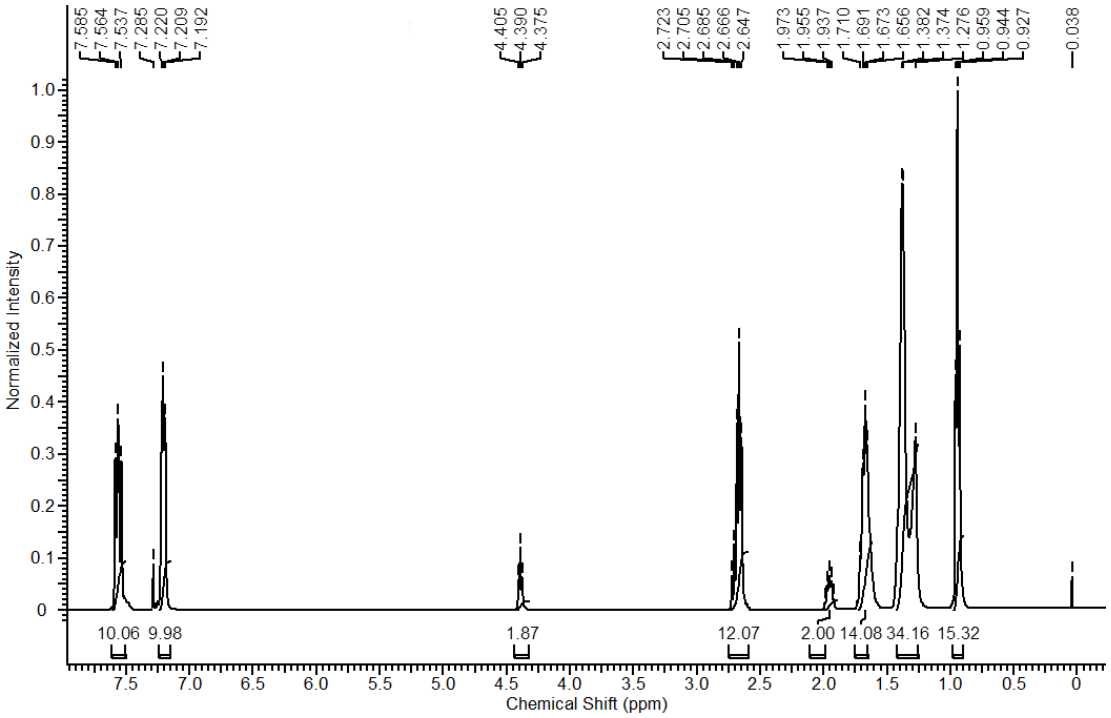

Figure A45 ^{1}H NMR spectrum of compound **25d**.

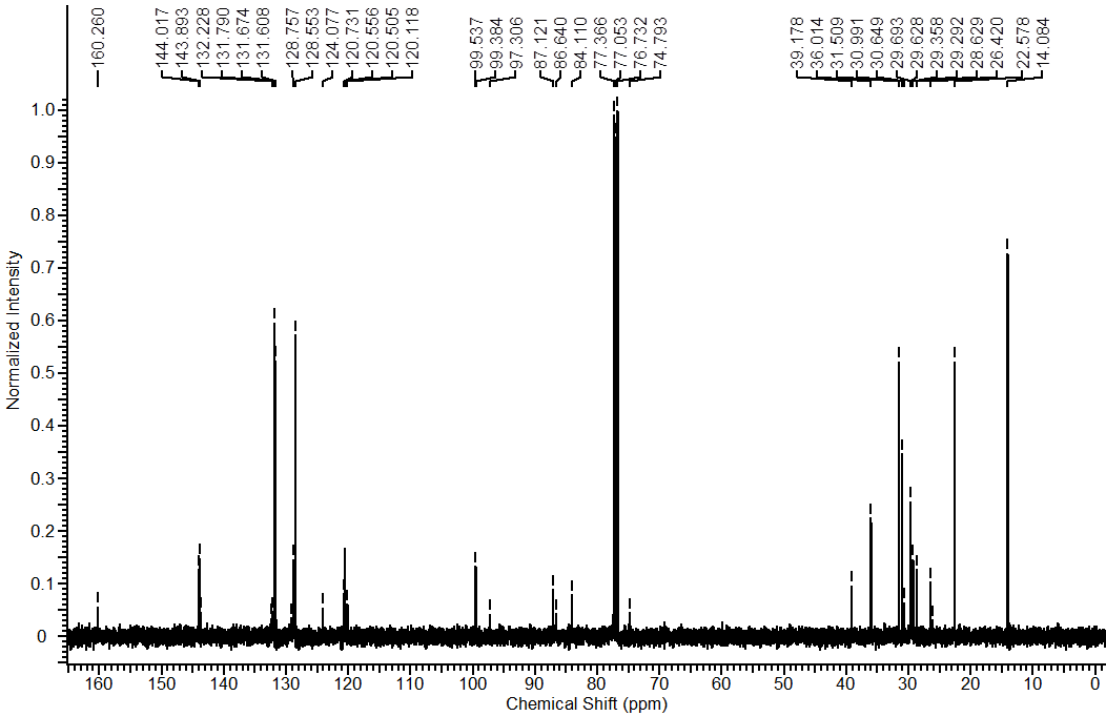

Figure A46 ^{13}C NMR spectrum of compound **25d**.

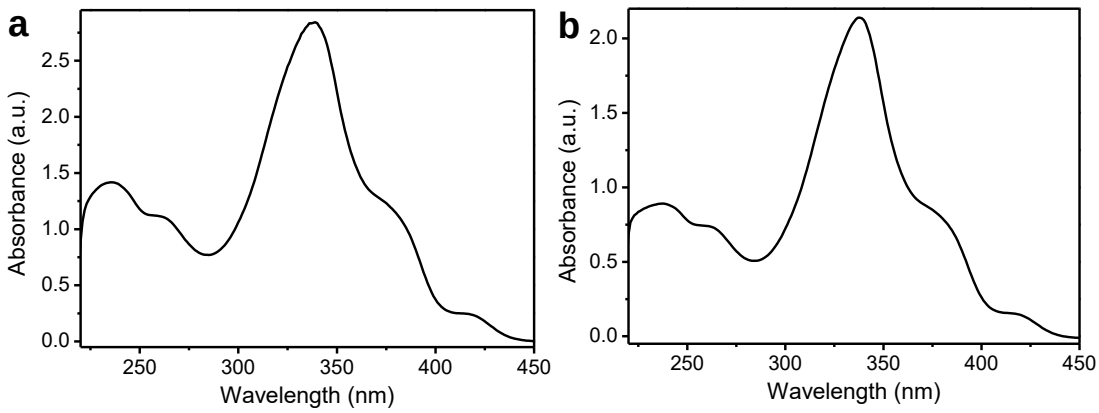

Figure A47 UV-vis absorption spectra of compound (a) **24b** and (b) **25d** in solution (5 μM in dichloromethane).

Table A1 Thermal behavior of the synthesized compounds **24**[a, b]

Compound	Heating Scan	Cooling Scan
24a	Cr 80.31 (17.95) N_D 87.37 (0.59) I	I 86.28 (1.91) N_D 54.23 (29.06) Cr
24b	Cr 69.45 (8.85) N_D 74.75 (5.47) I	I 73 N_D 50.61 (26.02) Cr
24c	Cr 33.56 (10.56) N_D 52 I	I 38 N_D -9.47 (7.25) Cr
24d	Cr 44.08 (13.26) N_D 53.14 (16.75) I	I 46 N_D -12.55 (3.48) Cr

[a] Phase transition temperatures (peak) in °C and transition enthalpies in $kJmol^{-1}$ (in parentheses). [b] Phase assignments: Cr = Crystalline, N_D = discotic nematic, I = isotropic.

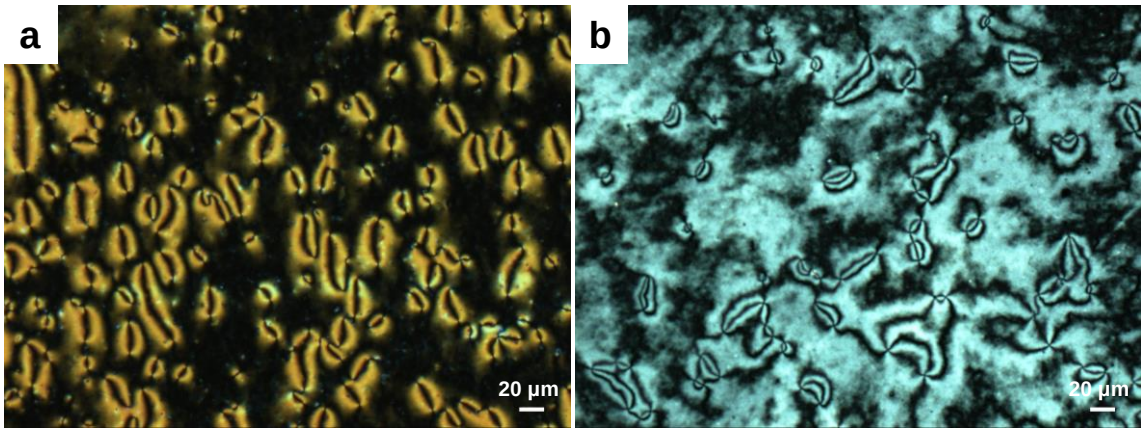

Figure A48 Optical photomicrograph of compound (a) **24c** at 34 °C and (b) **24d** at 43 °C (on cooling from isotropic, crossed polarizers).

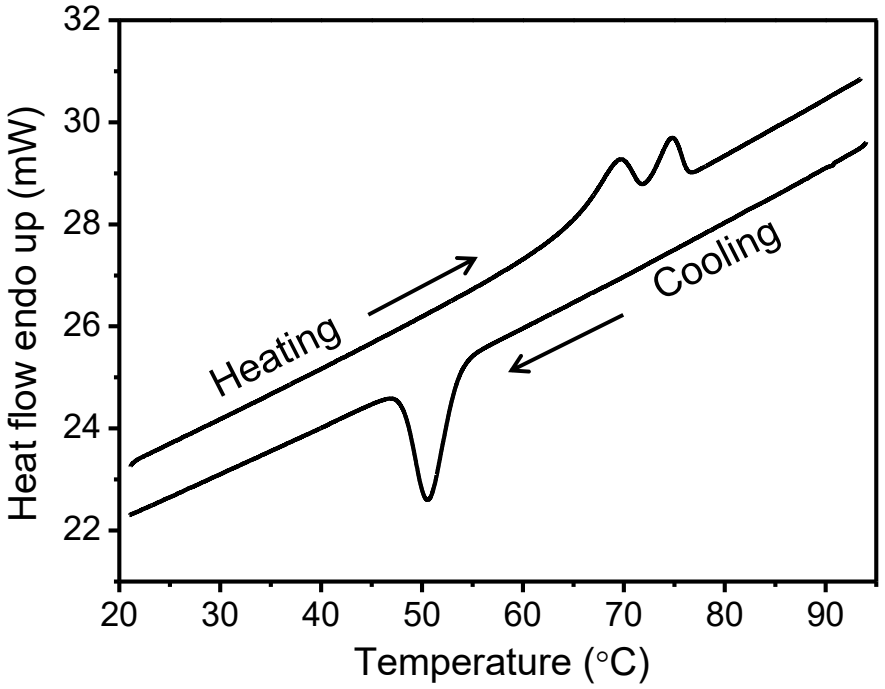

Figure A49 DSC thermogram of compound **24b** on heating and cooling cycles at the rate of 5 °C/min.

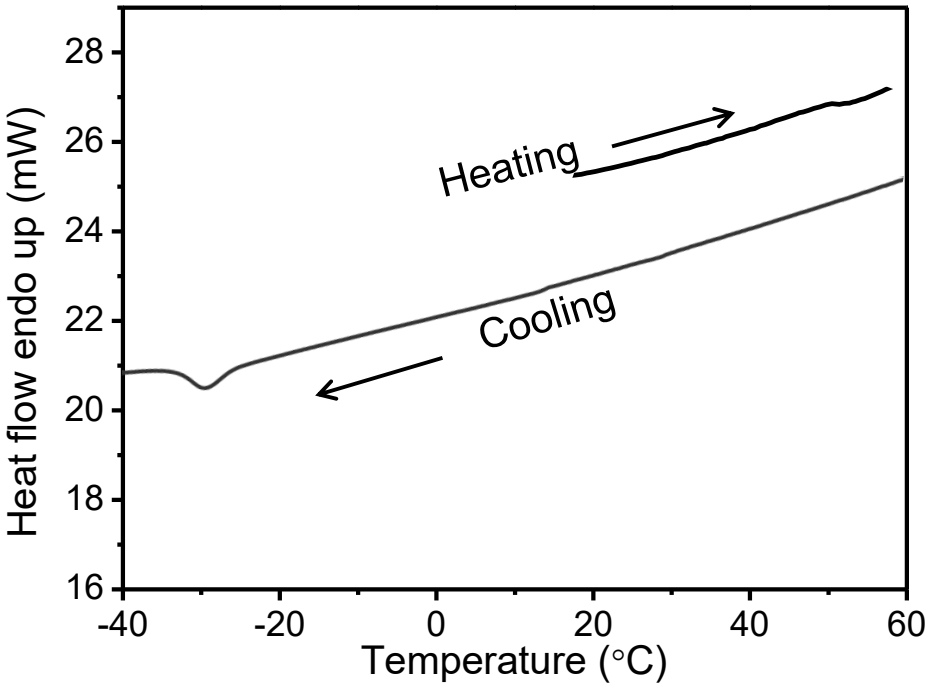

Figure A50 DSC thermogram of compound **25d** on heating and cooling cycles at the rate of 5 °C/min.

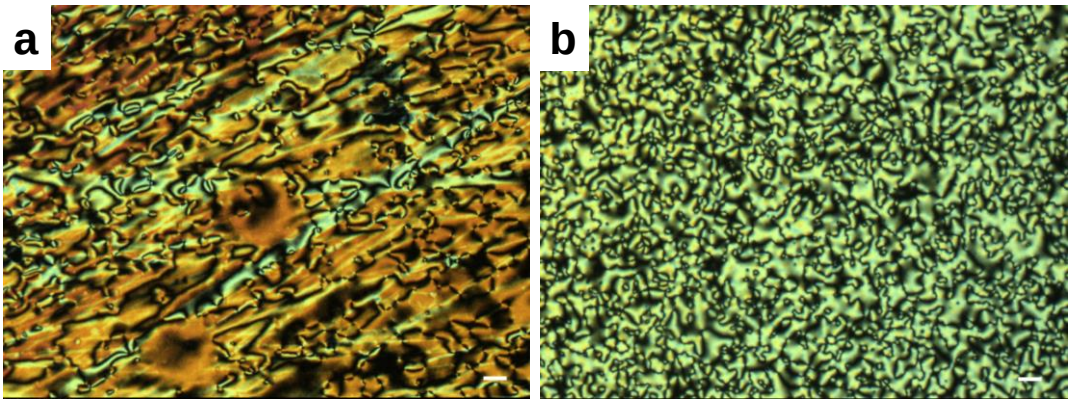

Figure A51 Optical photomicrograph of compound: (a) **25a** at 60 °C and (b) **25b** at 25 °C representing N_D phase (on cooling from isotropic, crossed polarizers, scale bar = 20 μm).

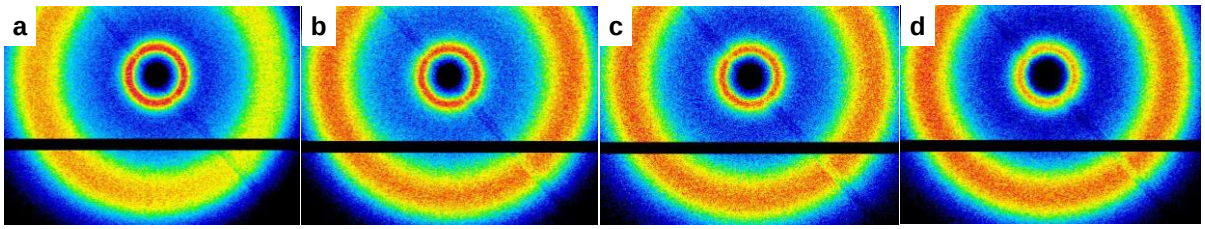

Figure A52 2D diffraction patterns of compound **25a-d** in the nematic mesophase.

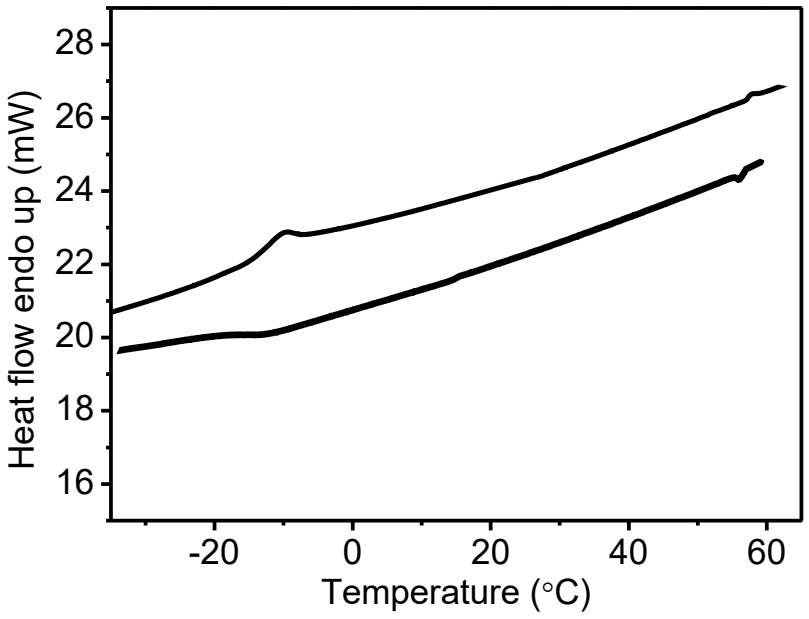

Figure A53 DSC thermogram of compound **25d**-GNPs on heating and cooling cycles at the rate of 5 °C/min.

Table A2 X-ray reflections and corresponding correlation lengths in the nematic phases of compound **24a-d**.

Compound	Properties	Small angle peak	Wide angle peak
24a	*d*-spacing (Å)	21.00 ± 0.03	4.93 ± 0.004
	Correlation Length (ξ) (Å)	45.47 ± 0.63	8.43 ± 0.10
	ξ/d	2.16 ± 0.03	1.70 ± 0.03
24b	*d*-spacing (Å)	21.04 ± 0.04	4.94 ± 0.005
	Correlation Length (ξ) (Å)	43.52 ± 0.83	8.83 ± 0.12
	ξ/d	2.06 ± 0.04	1.78 ± 0.03
24c	*d*-spacing (Å)	20.70 ± 0.05	4.92 ± 0.005
	Correlation Length (ξ) (Å)	37.49 ± 0.74	8.91 ± 0.11
	ξ/d	1.81 ± 0.03	1.81 ± 0.02
24d	*d*-spacing (Å)	20.30 ± 0.09	4.94 ± 0.007
	Correlation Length (ξ) (Å)	29.45 ± 0.94	8.96 ± 0.18
	ξ/d	1.45± 0.04	1.81 ± 0.03

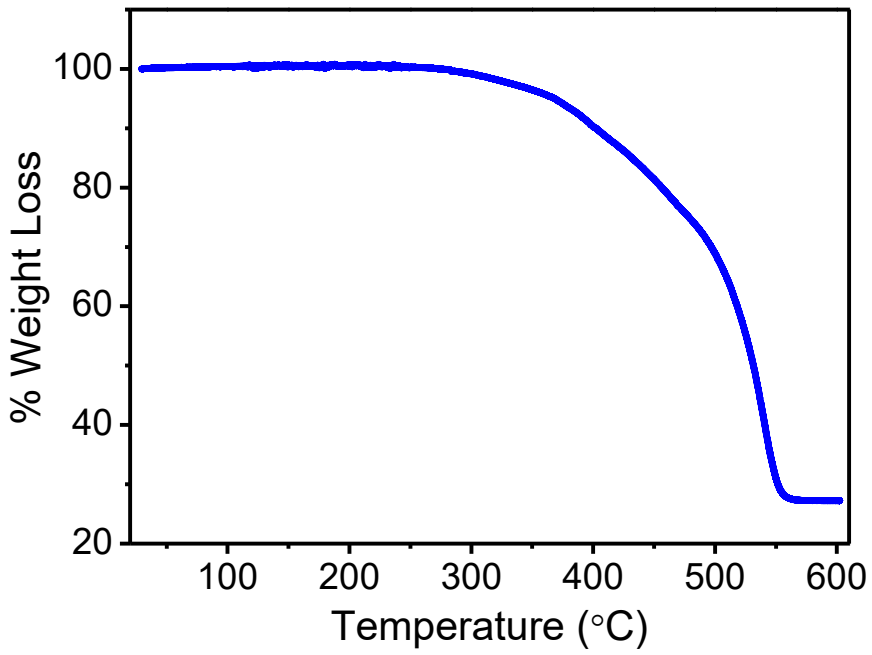

Figure A54 TGA curve of **25d**-GNPs. The measurements were performed under a nitrogen atmosphere, with heating and cooling rates of 10 °C/min.

Chapter 6

Conclusion

This thesis presents the work which was carried out to gain insights into the structure-property relationships in dimeric and oligomeric liquid crystals (LCs). These materials were synthesized from the point of view of application in opto-electronic devices as well as for obtaining materials with a combination of desirable properties for new applications in various devices. The work described in the thesis can be concluded as follows:

(1) Synthesis and characterization of new disc-rod oligomeric mesogens based on azobenzene core where the azobenzene tetracarboxylic acid disc was attached to four cyanobiphenyl rod-like moieties *via* flexible alkyl spacers has been carried out in order to study the structure-property relationship in disc-rod oligomers. Out of the eight compounds synthesized (n = 5-12), the oligomers containing n = 8 and n = 10 were found to exhibit a monotropic nematic phase. Surface manometry of the compound with n = 10 was explored which revealed the formation of a stable monolayer at the air-water interface. Interestingly, temperature dependent AFM topography carried out with the film deposited on a hydrophobic silicon substrate showed the reversible formation of aligned fibres (~20-40 µm) in the mesophase (Figure 6.1). This approach provides rational design and control over the anisotropic properties of the ordered phase for various applications.

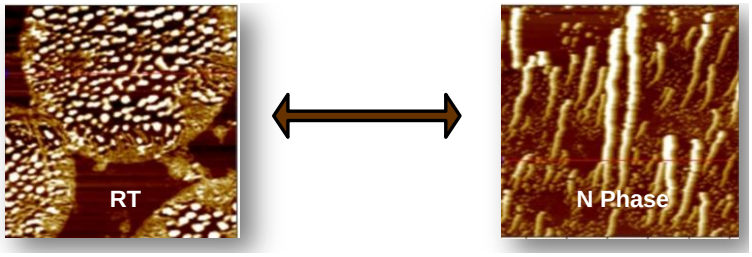

Figure 6.1 AFM topography showing the formation of nanodroplets at room-temperature and well aligned rod like structures in nematic phase at 115 °C for compound with n = 10. This process was found to be reversible in consecutive heating and cooling cycles.

(2) Synthesis and characterization of disc-disc oligomers in which the azobenzene tetracarboxylic acid disc was tethered to four triphenylene discotic moieties *via* flexible alkyl spacers was performed to obtain oligomeric LCs with photo-responsive behaviour. All the three synthesized compounds (*n* = 8, 10, 12) of this series were found to self-organize into room temperature columnar structures. The compounds with longer spacer length (*i.e.*, *n* = 10 and 12) exhibited columnar rectangular (Col_r) mesophase whereas the compound with *n* = 8 existed in glassy Col_r state. Interestingly we found that the Col_r self-assembly of these compounds switched to columnar hexagonal (Col_h) on doping the compounds with 2, 4, 7-trinitrofluorenone (TNF). The combination of the various properties such as LC phase at room-temperature, easy alignment by mechanical shearing, increased charge hopping expected from the donor-acceptor charge transfer complexes and the transition from Col_r to Col_h phase makes these oligomers very advantageous for new device applications (Figure 6.2).

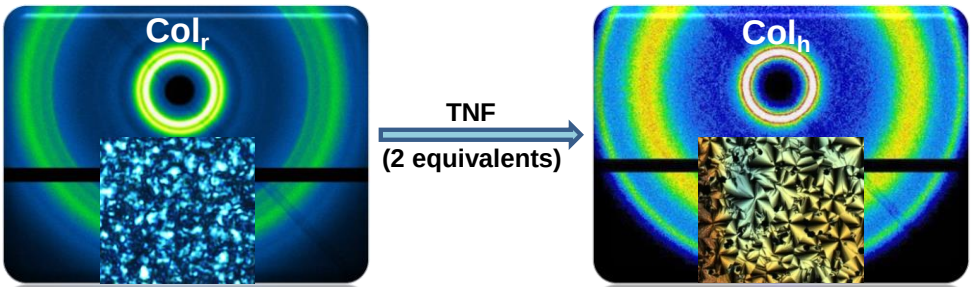

Figure 6.2 Schematic representation of change-over of columnar rectangular to hexagonal assemblies on doping the oligomers with TNF in the ratio of 1:2 (Compound: TNF).

(3) A facile synthesis of a new room-temperature discotic mesogenic dyad based on triphenylene and pentaalkynylbenzene linked *via* flexible alkyl spacer is described. This work was carried out to explore the self-organization of the system resulting from triphenylene and pentaalkynylbenzene units which can individually self-assemble into Col_h and nematic discotic (N_D) mesophase respectively. Interestingly, the dyad was found to self-assemble into a Col_h mesophase at room-temperature. This was due to the fact that strong π-π interactions between the triphenylene units overcame the rotational freedom provided by the side arms of pentaalkynylbenzene unit, however, due to the rotational freedom of pentaalkynylbenzene unit, the inter-disc interactions of triphenylene units in the dyad

ultimately led to mesophase even at room-temperature. The LC property of the dyad was further manipulated by preparing charge transfer complexes with TNF which led to improved mesophase range. In addition, the dyad also exhibited an excellent blue light emission property which makes it suitable for various opto-electronic applications (Figure 6.3).

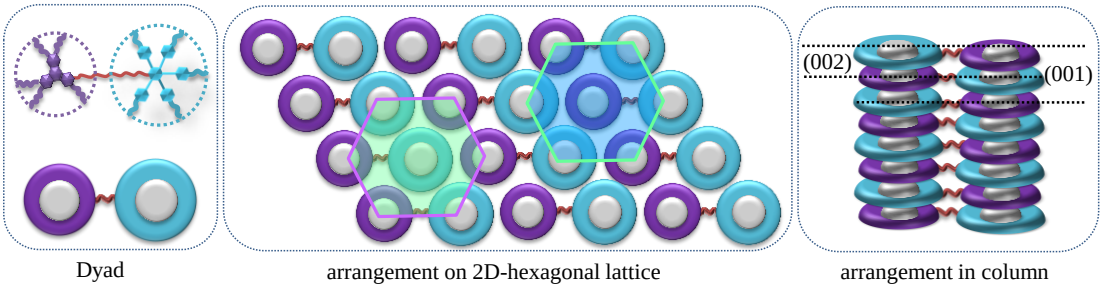

Figure 6.3 Figure illustrating the dyad based on pentaalkynylbenzene and triphenylene units and its arrangement in columnar hexagonal lattice.

(4) An attempt to look into the molecular interplay of the discotic cholesteric dimers obtained by linking a pentaalkynylbenzene core with the cholesterol group through flexible alkyl spacers was made. Two compounds were designed in this study where the length of the flexible spacer was varied remarkably to study the effect of length of the spacer on the twisting of the discs by the cholesterol units and thus on stabilisation of mesophase (Figure 6.4). Both the synthesized dimers displayed chiral nematic (N*) phase at room-temperature.

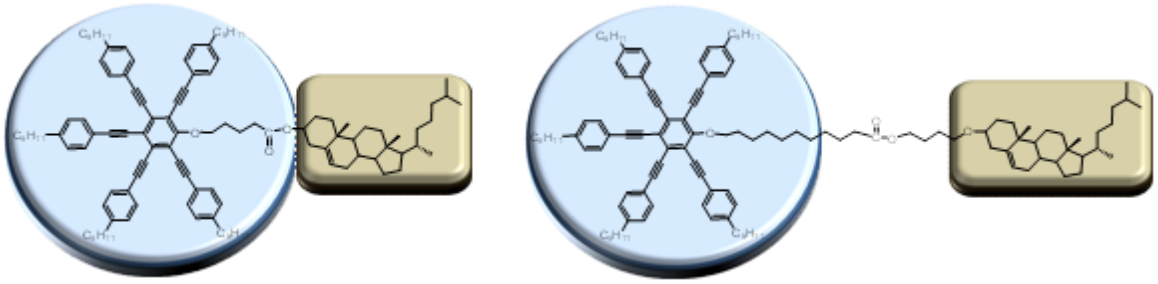

Figure 6.4 Design of the dimers based-on pentaalkynylbenzene and cholesterol synthesized in the study.

For the dimer with longer spacer, the mesophase range was much wider which can be assigned to uniform alignment of helices which was also predicted from POM studies and

increased steady state anisotropy. In addition, the mesogens exhibited excellent fluorescence emission properties making them suitable for various opto-electronic applications.

(5) A straightforward synthesis of multialkynylbenzene-bridged triphenylene based dyad systems (via flexible alkyl spacers) that self-organize into room-temperature columnar structures over a long range has been elaborated (Figure 6.5). The compounds with spacer lengths (*n*) of 8 and 10 exhibit a columnar oblique (Col_{ob}) mesophase whereas the compound with $n = 6$ shows a Col_{ob} plastic phase. Interestingly, the later compound ($n = 6$) shows the formation of well-nucleated spherulites of about several hundred micrometers which indicates the planar arrangement of columns over a long-range. All of these compounds show blue luminescence in solution and in the thin-film state under long wavelength (365 nm) UV light. The property of room-temperature columnar self-assembly over long range together with blue light emission in neat state make these compounds very promising for possible potential applications in semiconductor devices.

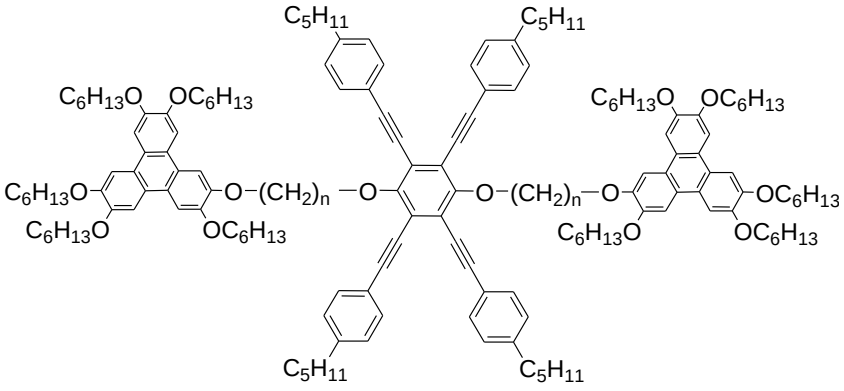

Figure 6.5 Design of the multialkynylbenzene bridged triphenylene triads exhibiting long range columnar self-assembly and blue light emission in neat state.

(6) Synthesis of lath-shaped symmetrical triads based on multialkynylbenzene linked *via* flexible alkyl spacers was performed in order to gain structure-property relationships in multialkynylbenzene systems (Figure 6.6). Four mesogens were synthesized in which multialkynylbenzene units were connected to each other in a side-by-side fashion with varying flexible alkyl spacers. The first three compounds were found to be non-mesomorphic, however, the compound with longest alkyl spacer i.e. $n = 12$ exhibited N_D

phase which has been characterized by POM and detailed X-ray scattering studies (SAXS/WAXS). The clearing temperatures in these triads were found to be reduced as compared to their dimeric homologues.

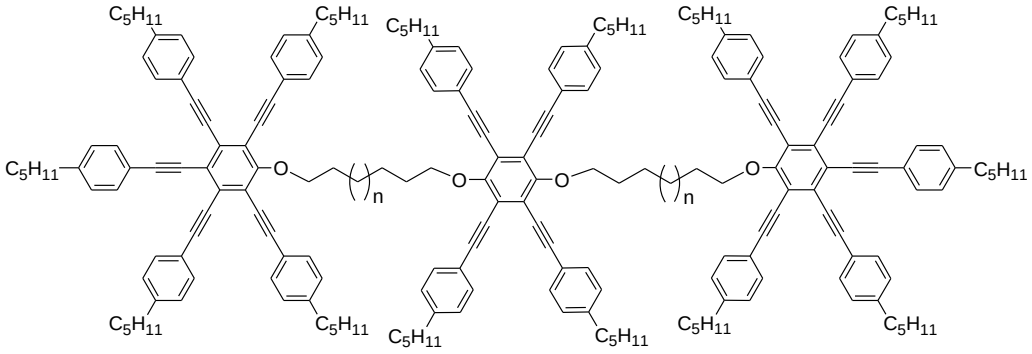

Figure 6.6 Lath-shaped symmetrical triads based on multialkynylbenzene.

(7) The discotic nematogens displaying discotic nematic (N_D) phase at room-temperature are very much in demand due to their usage in optical compensation films to widen the viewing angle of commonly used twisted nematic display. We have developed various new strategies to obtain room-temperature N_D phases. The first approach is based-on the N_D LC dimer consisting of a triphenylene and a pentaalkynylbenzene unit linked *via* flexible alkyl spacers (Figure 6.7). The formation of the N_D phase was realized most likely through folding of the dimeric molecule that prevented stacking between the triphenylene units, as suggested by modeling in the mesophase derived from X-ray scattering results and high-level DFT calculations. The second approach is based-on design and synthesis of three room-temperature oligomeric N_D LCs. These oligomeric LCs consists of an azobenzene core attached to which are four pentaalkynylbenzene units through flexible alkyl spacers (Figure 6.7). The presence of a short azo linking group provides more disorder in the system, thereby reducing the packing efficiency among the pentaalkynylbenzene units and resulting into the formation of a room-temperature N_D phase over a wide temperature range.

Further, to enhance the dielectric response and thus to lower switching time in these N_D LCs, we have carried out the synthesis and characterization of gold nano-particles (GNPs) coated with pentaalkynylbenzene units which displayed N_D phase even at room-temperature.

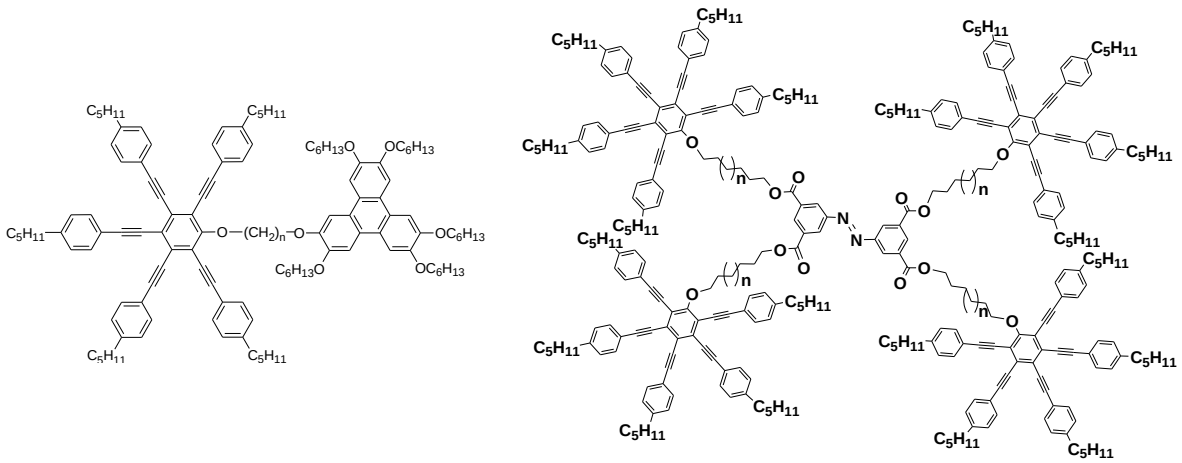

Figure 6.7 Design of the dimeric and oligomeric molecules exhibiting room-temperature N_D phase.

These gold nano-clusters are very interesting materials as inherent property of LCs to form mesophases due to their shape and polarizability anisotropy also influences the self-assembly of GNPs whereas the GNPs affects the electro-optic and alignment properties of LCs in devices which leads to collective advantages for both the components. Thus, these N_D GNPs are promising materials to exhibit the property of optical compensation (due to nematic discotic pentaalkynylbenzene units) with enhanced dielectric response (because of gold nano-particles).

Thus, LCs reported in this thesis are potential candidates for application in cost effective opto-electronic devices.

List of Publications

(1) **Gupta, M.**; Gupta, S. P.; Rasna, M. V.; Adhikari, D.; Dhara, S.; Pal, S. K. A new strategy towards the synthesis of a room-temperature discotic nematic liquid crystal employing triphenylene and pentaalkynylbenzene units. *Chemical Communications* **2017**, *53*, 3014-3017.

(2) **Gupta, M.**; Gupta, S. P.; Mohapatra, S. S.; Dhara, S.; Pal, S. K. Room-temperature oligomeric discotic nematic liquid crystals over a wide temperature range: Structure-property relationships. *Chemistry- A European Journal* **2017**, *23*, 10626–10631.

(3) **Gupta, M.**; Gupta, S. P.; Pal, S. K. TNF induced switching of columnar rectangular to hexagonal assemblies in a new class of triphenylene-based room temperature discotic liquid crystals. *Journal of Physical Chemistry B* **2017**, *121*, 8593-8602.

(4) Gupta, S. P.; **Gupta, M.**; Pal, S. K. Highly resolved morphology of room-temperature columnar liquid crystals derived from triphenylene and multialkynylbenzene using reconstructed electron density maps. *Chemistry Select* **2017**, *2*, 6070 – 6077.

(5) **Gupta, M.**; Pal, S. K. Triphenylene-based room-temperature discotic liquid crystals: A new class of blue-light-emitting materials with long-range columnar self-assembly. *Langmuir* **2016**, *32*, 1120-1126.

(6) **Gupta, M.**; Pal, S. K. The first examples of room temperature liquid crystal dimers based on cholesterol and pentaalkynylbenzene. *Liquid Crystals* **2015**, *42*, 1250-1256.

(7) **Gupta, M**.; Agarwal, N.; Arora, A.; Kumar, S.; Kumar, B.; Sheet, G.; Pal, S. K. Synthesis and characterization of novel azobenzene-based mesogens and their organization at the air-water and air-solid interfaces. *RSC Advances* **2014**, *4*, 41371-41377.

(8) **Gupta, M.**; Bala, I.; Pal, S. K. A room temperature discotic mesogenic dyad based-on triphenylene and pentaalkynylbenzene. *Tetrahedron Letters* **2014**, *55*, 5836-5840.

(9) Gupta, S. K.; Setia, S.; Sidiq, S.; **Gupta, M.**; Kumar, S.; Pal, S. K. New perylene-based non-conventional discotic liquid crystals. *RSC Advances* **2013**, *3*, 12060-12065.

(10) Setia, S.; Soni, A.; **Gupta, M.**; Sidiq, S.; Pal, S. K. Microwave-assisted synthesis of novel mixed tail rufigallol derivatives. *Liquid Crystals* **2013**, *40*, 1364-1372.

(11) **Gupta, M.**; Pal, S. K. Structure property relationships in lath-shaped triads based on multialkynylbenzene. *Communicated*.

(12) **Gupta, M.**; Mohapatra, S. S.; Dhara, S.; Pal, S. K. Room-temperature discotic nematogens derived from gold nanoparticles coated with pentaalkynylbenzene units. *Communicated*.

(13) **Gupta, M.**; Pal, V.; Pal, S. K. Photo-responsive liquid crystals derived from azobenzene centered cholesterol-based tetramers. *Manuscript under preparation*.

Honors, awards and recognitions

(1) International Union of Crystallography (IUCr) sponsored Young Scientist Award to attend 4th International Soft Matter Conference (ISMC 2016) held in Grenoble, France (12-16 September, 2016).

(2) Department of Science and Technology (DST) travel grant to attend 26th International Liquid Crystal Conference (ILCC 2016) held in Kent State University, Ohio, USA (31 July-5 August, 2016).

(3) "*A new strategy towards the synthesis of a room-temperature discotic nematic liquid crystal employing triphenylene and pentaalkynylbenzene units*'' was featured as inside back cover in *Chemical Communications*.

Conferences

(1) Oral presentation entitled "*A New Strategy Towards the Synthesis of Room-Temperature Discotic Nematic Liquid Crystals*" **Gupta, M.**; Pal, S. K. at the Inter-

IISER Chemistry Meet (IICM 2017) held in IISER Bhopal, Bhopal, India (20-22 January, 2017).

(2) Poster presentation entitled "*Triphenylene-Based Room-Temperature Discotic Liquid Crystals: A New Class of Blue-Light-Emitting Materials with Long-Range Columnar Self Assembly*" **Gupta, M**.; Pal, S. K. at the 4th International Soft Matter Conference (ISMC 2016) held in Grenoble, France (12-16 September, 2016).

(3) Poster presentation entitled "*Multialkynylbenzene-Bridged Triphenylene-based Room Temperature Discotic Liquid Crystals: New Blue Light-emitting Materials with Long Range Columnar Self-assembly*" **Gupta, M**.; Pal, S. K. at the 26th International Liquid Crystal Conference (ILCC 2016) held in Kent State University, Ohio, USA (31 July-5 August, 2016).

(4) Oral presentation entitled "*Discotic Triads Based-on Multialkynylbenzene Bridged Triphenylene Exhibiting Blue Light-Emission With Long Range Columnar Self-Assembly*" **Gupta, M**.; Pal, S. K. at the International Conference on Materials Science & Technology held in Conference Centre, University of Delhi, Delhi, India (1-4 March, 2016).

(5) Participated in "*Solid-state and Materials Chemistry"* workshop held at the Institute of Nano Science and Technology, Mohali, India (8 February, 2016).

(6) Poster presentation entitled "*Multialkynylbenzene-Bridged Triphenylene-based Room Temperature Discotic Liquid Crystals*" **Gupta, M.**; Pal, S. K. at the 22nd National Conference on Liquid Crystals (NCLC-22) held in DIT University, Dehradun, India (21-23 December, 2015).

(7) Participated in "*Inside Raman 2015"* workshop organized by Renishaw Metrology Systems at the Indian Institute of Science Education and Research Mohali (IISERM), S.A.S. Nagar Mohali, India (10-11 December, 2015).

(8) Poster presentation entitled "*A Room Temperature Discotic Mesogenic Dyad Based-on Triphenylene and Pentaalkynylbenzene*" **Gupta, M.**; Pal, S. K. at the 21st National Conference on Liquid Crystals (NCLC-21) held in Vikramajit Singh Sanatan Dharm (VSSD) College, Chhatrapati Shahu Ji Maharaj University, Kanpur, India (10-12 November, 2014).

(9) Participated in *National Seminar on Crystallography 43A* held at the Indian Institute of Science Education and Research Mohali (IISERM), S.A.S. Nagar Mohali, India (13-17 October, 2014).

(10) Poster presentation entiltled "*Synthesis and Characterization of Novel Azobenzene-based Mesogens and Their Organization at the Air–Water and Air–Solid Interfaces*" **Gupta, M.**; Pal, S. K. at the 20th National Conference on Liquid Crystals (NCLC-20) held in Manipal Institute of Technology, Manipal University, Manipal, India (16-18 December, 2013).